TAOFEEQ OLADAYO BELLO

Carbon Dioxide Conversion Technologies to Formic Acid and Methanol Promoted by Ionic Liquid

SÃO PAULO
2022

TAOFEEQ OLADAYO BELLO

Carbon Dioxide Conversion Technologies to Formic Acid and Methanol Promoted by Ionic Liquid

Revised Version
(The original version can be found in the unit that host the graduate program)

Thesis submitted to the Polytechnic School of the Universidade de São Paulo in partial fulfillment of the requirements for the degree of Doctor of Science
Area of Concentration: Chemical Engineering.
Advisor: Prof. Dr. Claudio Augusto Oller do Nascimento

São Paulo

2022

Este exemplar foi revisado e corrigido em relação à versão original, sob responsabilidade única do autor e com a anuência de seu orientador.

Assinatura do autor: _____

Assinatura do orientador: _____

Catalogação-na-publicação

Bello, Taofeeq Oladayo
Tecnologias de conversão de dióxido de carbono em ácido fórmico e metanol promovidas por líquidos iônico / T. O. Bello -- versão corr. -- São Paulo, 2022.
210 p.

Tese (Doutorado) - Escola Politécnica da Universidade de São Paulo. Departamento de Engenharia Química.

1.Dioxido do carbono 2.Liquidos ionico 3.Acido formico 4.Metanol 5.Termodinamica I.Universidade de São Paulo. Escola Politécnica. Departamento de Engenharia Química II.t.

Nome: Taofeeq Oladayo Bello

Título: Carbon Dioxide Conversion Technologies to Formic Acid and Methanol Promoted by Ionic Liquid

Thesis presented to Escola Politecnica da Universidade de São Paulo to obtain the the degree of Doctor of Science

Aprovado em:

Banca Examinadora

Prof. Dr. Cláudio Augusto Oller do Nascimento

Instituição: Escola Politecnica da Universidade de São Paulo

Julgamento _____

Prof. Dr. Caetano Rodrigues Miranda

Instituição: Escola Politecnica da Universidade de São Paulo

Julgamento: _____

Prof.(a)Dr.(a) Ofélia de Queiroz Fernandes Araujo.

Instituição: Universidade Federal do Rio de Janeiro

Julgamento: _____

Prof.(a)Dr.(a) Joan Frances Brennecke.

Instituição: University of Texas Austin

Julgamento: _____

Prof. Dr. Rafael Mattos dos Santos.

Instituição: University of Guelph

Julgamento: _____

ABSTRACT

Carbon dioxide (CO_2) can be recycled as a carbon building block to produce organic chemicals as a waste product. However, CO_2 is thermodynamically and kinetically difficult to transform because of its stability. The conditions and parameters must be viable to circumvent the bottleneck of the process conditions and performance parameters. Hence, the proposed study aims to find innovative methods in terms of improving the yield and reducing the energy requirement for the favourable production of formic acid and methanol simultaneously from CO_2, subsequently improving its economic value and finally reducing its impact on the environment.

Ionic liquids have been used as a suitable solvent for the conversion of CO_2 to various organic products. Their excellent characteristics, such as low pressure, high turnability, and stability, have allowed them to be used in many fields. A series of cations and anions were randomly paired through a theoretical approach. The conductor-like screening model for real solvent (COSMO-RS) was employed to predict thermodynamic, physical, and toxicity properties. From 240 ionic liquids (ILs), four ILs were finally selected for a continuous process evaluation by Aspen Plus. The result showed a high tendency for CO_2 absorption capacity and lower energy consumption.

The process simulation through Aspen simulator shows the reaction's feasibility with the selected ionic liquid. The results revealed a high CO_2 conversion of up to 80% conversion of CO_2 per pass and improved yield of formic acid at low temperature and moderate pressure. Economic metrics of the plant showed that the process profitability largely depends on the source (cost) of H_2 and the selling price of formic acid. A profitable process plant is achievable at a hydrogen price of 1.5USD/Kg and a minimum selling price of 0.935USD/Kg of formic acid.

A mechanistic approach through quantum chemical calculation (DFT) was conducted to further understand the reaction's insight. Thermochemical and kinetic data were also evaluated. The results showed that a negative Gibbs energy was achieved when the reaction is promoted by an IL, which affirmed the process simulation results. However, since the ionic liquid is not yet available commercially, further experimental work is needed to get insight into the kinetic behaviour of the IL in the reaction in terms of the breakage of H_2 bond and formation of intermediates reaction.

Keywords: Carbon Dioxide Utilization; CO_2 Chemical Conversion; Ionic Liquid, COSMO-RS; Density functional Theory; Thermodynamics; Formic acid; Methanol; Systematic Screening;

DEDICATION

This piece of work is dedicated to Almighty Allah, the most beneficient and the merciful.

To the blessed memory of my late and beloved parents, Prince Ganiyu Babatunde Bello and Mistura Bolanle Bello.

ACKNOWLEDGMENTS

The biggest form of ingratitude is appreciation unexpressed. Therefore, the successful and timely completion of this work was as a result of several contributory efforts from individuals whose names I must not fail to mention with thanks.

My profound gratitude goes to Almighty ALLAH, the beneficent and most merciful for his guidance, provision, and sustenance right from the onset I set my foot into this world.

My sincere gratitude also goes to my supervisor Professor Claudio Oller do Nascimento for his continuous guidance and supervisory efforts throughout the phases of this work. My utmost appreciation also goes to Professor Rita Maria de Brito Alves and Professor Esio Bresciani for the efforts expended, guidance, and support beyond an official relationship, and for their invaluable contributions towards a smooth and successful academic career.I must also appreciate Professor Pedro de Alcantara Pessoa Filho for his advice at the start of this work and while taking his course on thermodynamics.

My appreciation also goes to Professor Rafael Santos for his prompt response during my search for an internship position, his supervision, guidance, supervision and advice for my professional and academic development throughout my research internship in Canada.

My deepest appreciation goes to my boss, Demola Onanuga for his moral, and financial support towards achieving this academic feat. Also to the family of Ibharebhor, I appreciate your moral support and advice all through this period. To my siblings, Sadeeq, Ahmed and Sheriff Bello, I appreciate your moral support and understanding throughout my period away from you.

I owe profound gratitude to my adorable wife Aisha for her support, understanding, constant encouragement and great sacrifice for the completion of my degree. To my son Mubashir-Zayd, I appreciate your coming to this world with loads of blessing and the sacrifice you paid while I was away on internship

Also, this list is not completed without friends and associate whose effort cannot be over emphasized, amongst these are Adukwu's family, Kolawole's family, Michael, Patience, Basheer, Ahmad, Amir Kelvin, Joao, Caroline, Maria Clara, Igour, and those whose our paths have crossed during this journey.

Contents

LIST OF FIGURES

LIST OF TABLES

CHAPTER I

I.1 Introduction

I.1.1 Increase in the Concentration of Greenhouse Gases

Energy is an essential component of our contemporary daily lives. The current global demand for energy is mainly provided by fossil fuels (OLAH; GOEPPERT; PRAKASH, 2009a). However, relying on fossil fuels as the dominant energy source has resulted in the atmosphere's present alarming carbon dioxide rate(INTERGOVERNMENTAL PANEL ON CLIMATE CHANGE(IPCC), 2014). As a result, total anthropogenic greenhouse (GHG) gases increased significantly between 2000 and 2010 compared to the past three centuries. Total anthropogenic emissions were the highest in mankind history from 2000 to 2010, reaching 49 (±4.5) gigatons of CO_2 equivalent annually in 2010(INTERGOVERNMENTAL PANEL ON CLIMATE CHANGE(IPCC), 2014). Despite the existence of a broad range of multilateral institutions and domestic mitigation measures, GHG emissions have continued to grow at an alarming rate.

As shown in Figure I.1, from 2000 to 2010, the average annual increase in GHG emissions was 1.0 $GtCO_2eq/yr$ (2.2%), opposed to 0.4$GtCO_2eq/yr$ (1.3%) per year from 1970 to 2000 over the full era (INTERGOVERNMENTAL PANEL ON CLIMATE CHANGE(IPCC), 2014). From the overall GHG emissions of 49 $GtCO_2eq/yr$ in 2010, CO_2 emissions from fossil fuel combustion and industrial processes and forestry and other land use (FOLU) contributed approximately 78 % to the overall rise in GHG emissions from 1970 to 2010, with comparable percentage contributions for the period of 2000–2010. CO_2 emissions from fossil fuels reached 32 (±2,7) $GtCO_2/yr$ in 2010 and rose further between 2010 and 2011 by approximately 3% and between 2011 and 2012 by approximately 1–2% (Fig. I.2). CO_2 continues the significant GHG of a total of 49 (±4.5) $GtCO_2eq$ per year for 2010 anthropogenic GHG emissions, of which it represents 76% of the complete GHG anthropogenic emissions (38±3.8 $GtCO_2eq/yr$, 16% (7.8±1.6 $GtCO_2eq/yr$) from methane (CH_4), 6.2% (3.1±1.9 $GtCO_2eq/yr$) from nitrous oxide (N_2O), and 2.0% (1.0±0.2 $GtCO_2eq/yr$) from fluorinated gases(INTERGOVERNMENTAL PANEL ON CLIMATE CHANGE(IPCC), 2014).

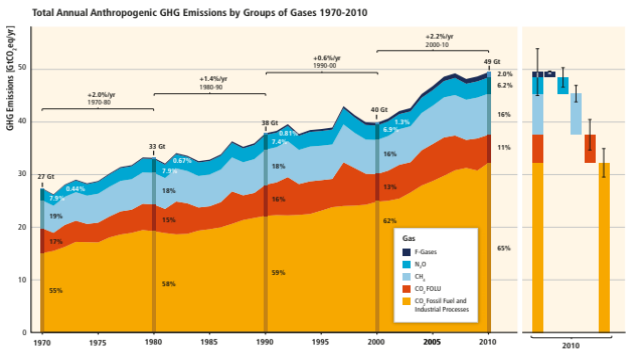

Figure I.1. Total GHG emission by group of gases 1970-2010 (INTERGOVERNMENTAL PANEL ON CLIMATE CHANGE(IPCC), 2014)

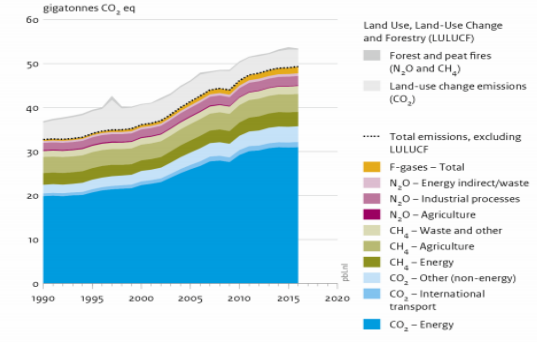

Figure I.2. Total GHG emission by sector from 1990-2015(INTERGOVERNMENTAL PANEL ON CLIMATE CHANGE(IPCC), 2014)

According to a 2018 British Petroleum statistical report(BRITISH PETROLEUM, 2018), Brazil is ranked ninth-largest consumer of energy and the 12th largest emitter of CO_2 globally, with fossil fuel sources being the largest source of CO_2 emissions. The major players in her primary energy mix by fuel consumption are oil (46%) and hydropower (28.3%), followed by natural gas (11.2%), renewables (7.5%), and coal (5.6%) (BRITISH PETROLEUM, 2018). Fossil fuels account for approximately 60% of the Brazilian energy matrix, and domestic oil and gas consumption is expected to increase in the coming years. Based on the Brazilian Ministry of Mines and Energy (MME) estimation, new reservoirs have grown from 15 billion in 2004 to over 30 billion in 2009 as a result of the discovery of the Brazilian pre-salt fields (GAFFNEY CLINE, 2010), making Brazil among the world's top 10 liquid fuel producers (BRAZILIAN MINISTRY OF MINES AND ENERGY (MME), 2014)

According to the information released by Petrobas, oil production in Brazil is expected to more than double, from 2.2 bpd in 2011 to 5 million bpd in 2020 (MINISTÉRIO DE MINAS E ENERGIA, 2011). In May 2019, domestic oil production reached a record high of 2.73 million b / d, as growth in the Santos Basin (mostly pre-salt) offset the decline in the Campos Basin (mostly conventional post-salt) (Fig I.3) (EMPRESA DE PESQUISA ENERGETICA (EPE), 2019). The reservoirs are characterized by high pressure and low-temperature fluid, high GOR (gas-oil ratio), and considerable CO_2 content. This is a major technological obstacle

for suitable and sustainable production in Brazilian pre-salt oil reservoirs (SANTOS et al., 2017). The primary contaminant is CO_2, and its average estimated concentration (maximum 80%) in the Santos and Campos basins is shown in Fig. I.4 (EMPRESA DE PESQUISA ENERGETICA (EPE), 2019).

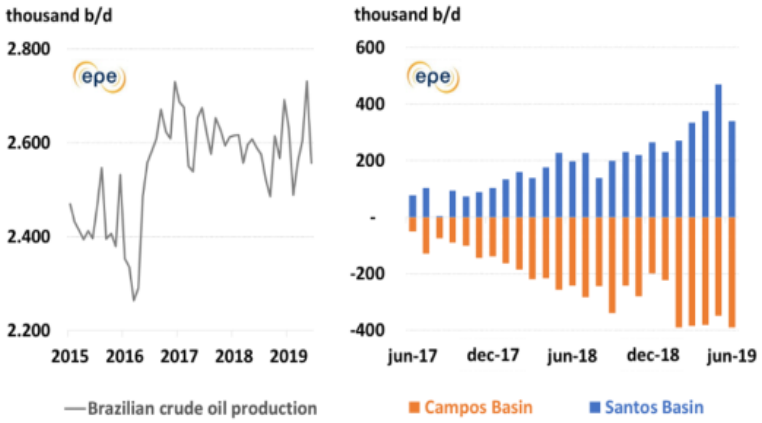

Figure I.3. National oil production and accumulated monthly change in Campos and Santos Basin oil production since May 2017 Data from ANP (2019)(NATIONAL AGENCY OF PETROLEUM, 2018)

Preliminary estimates suggest that CO_2 emissions would quadruple when mining these fields starts, as the pre-salt reservoir gases have 3 - 4 times more CO_2 than those of the post-salt fields(KETZER et al., 2014). Consequently, CO_2 emissions will rise from 51 million tonnes to approximately 200 million tonnes/year. However, there are measures further to reduce emissions(KETZER et al., 2014). CO_2-EOR is a proven procedure when a large amount of low-cost CO_2 is available. Based on the US Department of Energy (DOE) findings, if CO_2 is reinjected in the wells, it is possible to add up to 5% of the total oil in place to the oil reserves(US DEPARTMENT OF ENERGY, 2012). Other measures besides EOR to deal with CO_2 are reinjection into the reservoir in either deep saline aquifers or caves in the salt layer through carbon capture storage (CCS)(KETZER et al., 2014). According to Moreira et al. (2013) estimates (MOREIRA; PACCA; PARENTE, 2014), it is possible to prevent venting 0.90 billion tCO_2 time unit by assuming its total share as 15% of the total oil mass (MOREIRA; PACCA; PARENTE, 2014). Furthermore, they believe that the extraction and combustion of the 40 billion barrels of pre-salt oil will generate approximately 22.2 billion tCO_2 or even 26.9 billion tCO_2 if EOR is considered. However, total emissions due to the use of pre-salt oil could reach 21.3 billion tCO2 when 0.9 billion tCO_2 (Fig. 4) is avoided through CCS(MOREIRA;

PACCA; PARENTE, 2014). Thus, these options are not sufficient because of their net contribution to climate change mitigation (Fig.I 5).

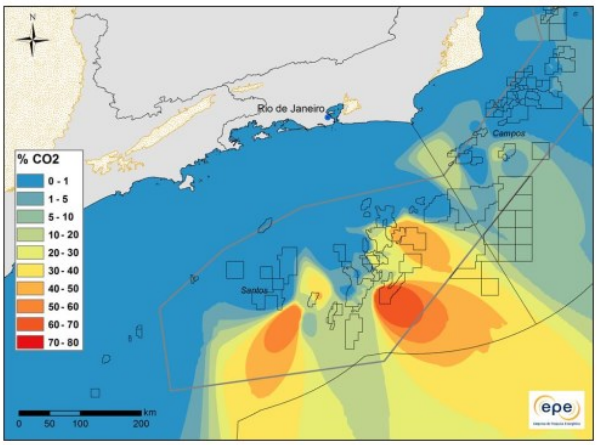

Figure I.4. CO_2 concentration in the eastern bank of Brazil's main exploration areas(EMPRESA DE PESQUISA ENERGETICA (EPE), 2019)

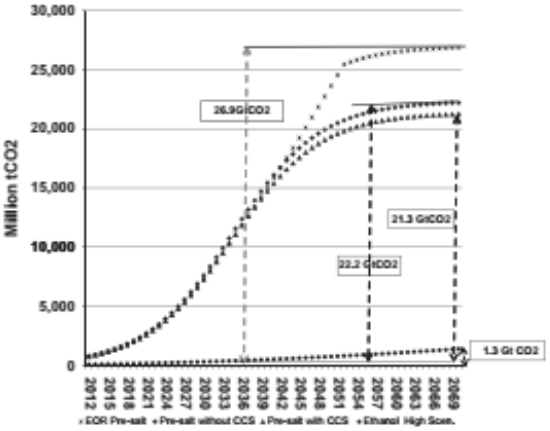

Figure I.5. Total emission of 4 liquid fuels scenario. (MOREIRA; PACCA; PARENTE, 2014)

Carbon dioxide conversion (CDU) can support the development of products and services with a lower CO_2 footprint and contribute to emission reductions. In particular, CO_2 reuse can support technology refinement, (in limited cases) early development of CO_2 transport infrastructure, and investment in CO_2 capture opportunities(INTERNATIONAL ENERGY AGENCY, 2019a). However, CDU cannot replace CO_2 storage by providing the significant emissions reductions needed to meet the pledge of reducing climate pacts(INTERNATIONAL ENERGY AGENCY, 2019a).

It is very difficult to assess the future market for CO_2-derived products and services. Global estimates range from less than 1 GtCO2 per year to 7 GtCO2 per year by 2030, depending on the assumptions applied(INTERNATIONAL ENERGY AGENCY, 2019a). IEA (INTERNATIONAL ENERGY AGENCY, 2019a) screening of the theoretical potential for CO_2 use and the potential climate benefits reveals that fuels have the most significant potential as a result of their vast market size, while building materials show the greatest climate change mitigation potential mainly because of the low energy requirements and the permanent retention of carbon in the product (Fig I.6) (INTERNATIONAL ENERGY AGENCY, 2019a).

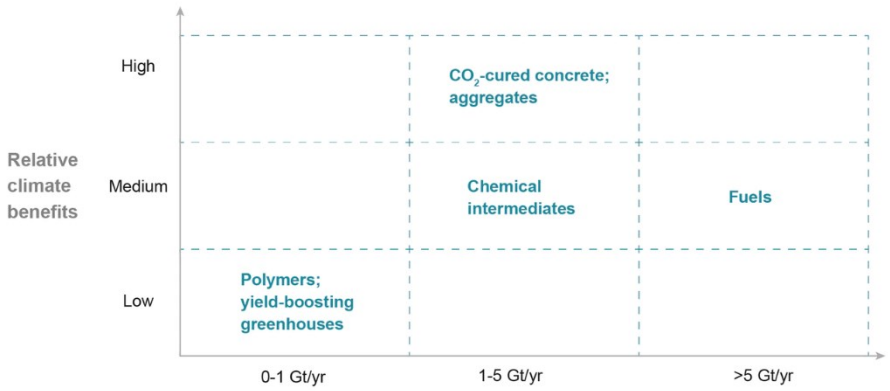

Figure I.6. Theoretical potential and climate benefits of CO_2-derived products and services. (INTERNATIONAL ENERGY AGENCY, 2019a)

Controlling CO_2 emissions involves setting objectives for emission mitigation(DONG; HUA; YU, 2018). However, it is becoming complicated(AMEYAW et al., 2019) because it is essential to consider the energy demand needed for economic development and the emission mitigation objectives. Therefore, frequent monitoring, evaluation, and adjustment of energy policies are required to achieve a set emission mitigation target (IEA, 2017). Furthermore, such surveillance, assessment, and changes require a rapid and sensible assessment of CO_2 emission mitigation processes. Thus, a need exists for a detailed analysis of the impact that different options/carbon conversion and utilization (CCU) processes have on the sector and under what conditions the products obtained may have a sustainable market (PÉREZ-FORTES et al., 2016).

In short, CO_2 reuse has great market potential for expansion with new applications in different sectors of the economy. Carbon dioxide utilization (CDU) technologies are presented as an alternative mitigation strategy for development, with great potential driven by carbon capture. According to the IEA (INTERNATIONAL ENERGY AGENCY, 2019a), CDU has the potential to complement the widespread deployment of CCS, which the body (IEA) has consistently identified as a critical part of the set of technologies needed to achieve climate goals (INTERNATIONAL ENERGY AGENCY, 2019a). Thus, CDU contribution should not be ignored as a mitigation strategy. Thus, this study aimed to evaluate a set of CO_2 conversion processes for integration with a large quantity source of CO_2 and the possible conditions to obtain a competitive result as opposed to conventional production.

Therefore, the reduction of CO_2 emissions plays an essential role in the Brazilian oil industry due to the strict environmental rules for pollutants and gas emissions and the need to

complement the two strategies discussed (CCS & EOR) of mitigating the volume of carbon dioxide by creating additional value.

I.2 Ionic Liquids for CO_2 Conversion.

Ionic liquids consist of ionic species, a bulky organic cation weakly coordinated to either an organic or an inorganic anion. This weak coordination and asymmetry of ions result in a reduction in ionic liquid's lattice energy and crystalline structure, lowering its melting point(ZAKRZEWSKA, 2021). These innovative fluids are even more unique because their structure can be easily tailored by changing cation/anion combinations and/or attaching functional groups. Consequently, physicochemical properties can be optimized according to the intended use requirements. Research into ILs has undergone exponential growth in the last two decades. As an environmentally more acceptable alternative to volatile organic solvents, ionic liquids have found their way into various industrial applications. Of course, to make any process large-scale, security of supply and cost must be assured. However, being a “designer solvents”, ionic liquids can be based on ions falling within an available (wide) price range (Zakrzewska, 2021). Additionally, recycling and reuse of the ionic liquids due to their negligible vapour pressure can be facilitated, further minimizing the relevance of the initial cost.

I.2.1 Room Temperature Ionic Liquids

The term "room-temperature ionic liquids"(RTIL) has been assigned to organic salts that are liquids close to ambient conditions. Ionic liquids are generally composed of relatively large organic cations and inorganic or organic anions (MARSH et al., 2002). They have been discovered as suitable solvents for the solubility of CO_2, and in the same vein, this property can make them a suitable promoter for CO_2 conversion (). RTILs has been used as solvent for a variety of organic reactions such as hydrogenation (MIILLER; DUPONT; SOUZA, 1998), hydroformylation(CHAUVIN; MUSSMANN; OLIVIER, 1995) and dimerization (SILVA et al., 1998). Reviews by Welton, 1999 (WELTON, 1999), Cull et al. 2000 (CULL et al., 2000) and Wasserscheid and Keim 2000 (WASSERSCHEID; KEIM, 2000) have summarized the use of ionic liquids as solvents for synthesis with and without the presence of homogeneous transition metal catalysts. Peng and Deng 2001 (PENG; DENG, 2001) reported the cycloaddition of CO_2 to propylene oxide catalyzed based on RTILs for cyclic carbonate synthesis in the absence of organic solvent. In this study, a number of RTILs based on 1-n-butyl-3-methylimidazolium and n-butylpyridinium salts and CL^-, BF4, and PF6 anions were

studied. It was reported that 1-n-butyl-3-methylimidazolium tetrafluoroborate showed the highest performance with nearly 100% conversion at optimal conditions (110° C, 6 h, 2.5 MPa of CO_2, 2.5 mmol of [BmIm][BF4] per 100 mmol of epoxide). Hu et al., 2018 (HU et al., 2018) studied and developed a novel dual IL system for synthesis of cyclic carbonate system with CO_2 and epoxides under 1 atm, and temperature range 30ºC-60ºC. In this work, a series of dual ILs were under investigation, among them, $[TMGH^+][^-O2MMIm^+][Br^-]$ showed the highest catalytic performance with 84% yield under optimal conditions (30◦ C, 12 h, 0.1 MPa of CO_2, 0.5 mmol of IL per 2 mmol of epichlorohydrin) in the absence of solvent and additives. They also reported the recyclability of the system up to six times without the loss of catalytic activity.

I.2.2 Anion-Functionalized Ionic Liquids

Traditional ILs can promote various CCU processes, but most of them have a limited ability to activate CO_2, necessitating high pressure (>1 MPa) or the use of additional metal catalysts(XIA et al., 2018). Anion-functionalized ILs have recently been developed for CO_2 absorption, with some of their CO_2 absorption capabilities exceeding 100 times that of conventional organic solvents(LEI; DAI.; CHEN, 2014; SONG; ZHOU; HE, 2017). They have also been reported to exhibit higher catalytic activities without metal catalysts (XIA et al., 2018). The presence of electron negative sites as N or O atoms can generally activate CO_2 because of their high alkalinity (WU et al., 2017; ZHAO et al., 2016b). Patil et al. (2009) discovered an alternate approach that uses [BMIm][OH] as a catalyst to efficiently generate quinazoline-2,4(1H,3H)-diones from CO_2 and 2-aminobenzonitriles(PATIL et al., 2009). Many inorganic bases, Et3N or conventional ILs ([BMIm][BF4] and [BMIm][HSO4]) show minimal or no action, with the exception of [BMIm][OH]. They proposed that [OH] activates the 2-aminobenzonitrile to initiate the reaction, while [BMIm] stabilizes the intermediate. Liu and coworkers recently used [BMIm][OAc] as a catalyst in the cyclization of 2-aminothiophenols using CO_2 and hydrosilane(GAO et al., 2015b). In the presence of [BMIm][OAc] and CO_2, a wide range of benzothiazoles can be produced in moderate to good yields. Furthermore, the same IL can provide good yields of benzimidazoles. Also, [BMIm][OAc] can simultaneously activate CO_2, substrates, and hydrosilane according to 1H NMR analysis. "CO_2-Phillic" ILs have been reported to be capable of absorbing various gases and catalyzing the conversion of CO_2 through the formation of intermediates and of carbonates or carbamates in mild conditions. Wu et al., 2017 (WU et al., 2017) explored a series of tetrabutylphosphonium ([Bu4P]+)-based ILs and different anions such as 2,4-dihydroxypyrimidine-5-carboxylic acid (2,4-OPym-5-Ac), 2,4-

dihydroxybenzoic acid (2,4-OB-Ac), 2,6-dihydroxypyridine-4-carboxylic acid (2,6-OPy-4-Ac), 4,6-dihydroxypyrimidine(4,6-OPym), 2-hydroxypyrimidine-5-carboxylic acid (2-OPym-5-Ac), 2-hydroxypyridine (2-OP), phenol (PhO), and imidazole (Im). These anions provide multiple sites for CO_2 activation and capture. $[Bu4P]_3$[2,4-OPym-5-Ac] shows the highest performance for the production of a series of α-alkylidene cyclic carbonates in moderate yields. Also, Deng et al, investigated the performance of different ILs in the formation of urea. The reaction involves reaction of CO_2 and 1,6- hexamethylenediamine to form polyuria(WANG et al., 2016). [P4446][ATriz] exhibits the best activity among the ILs used in this work.

I.2.3 Bifunctionalized Ionic Liquids

Due to their basicity, anion-functionalized ILs can increase CO_2 consumption. In many circumstances, however, cations in ILs can also help lower energy barriers by creating hydrogen bonds, and these ILs are referred to as bifunctional ILs(XIA et al., 2018). Yue et al, 2019 investigated five bifunctional imidazolium ionic liquids ([HEMim][Glu], [HEMim][Asp], [HEBim][Asp], [HEBim][Ala], [HEBim][His]) as catalyst in the synthesis of cyclic carbonate from CO_2 and epoxide(YUE; WANG; HAO, 2019). It was reported that the five bifunctional ionic liquids exhibited a good catalytic activity for the synthesis under mild conditions (IL: 0.8 mol%, CO_2: 0.25 MPa, 90 °C, 12 h) with high yields in the absence of co-catalyst or solvents. The minimum reusability of the catalyst was also reported to be four times with no significant drop in catalytic activity. In 2015, Luo et al. developed multiple amine-based ILs as dual roles in the capture and simultaneous fixation of CO_2 in fuel gas(LUO et al., 2016). Their findings show that cyclic carbonate formation from low CO_2 concentration (10%) is achievable with high conversion and better selectivity at high temperature (100^{o}C). ILs with multiple roles enable it as an efficient absorbent for simultaneous capture and catalyst for CO_2 utilization. Liu et al., 2014, reported a "CO_2-reactive" protic ionic liquid (PIL), [$HDBU^+$][TFE^{--}] as a bifunctional catalyst capable of simultaneously activating both CO_2 and 2-aminobenzonitriles to produce quinazoline-2,4(1*H*,3*H*)-diones with better catalytic performance resulting into high yields (ZHAO et al., 2014a).The hydrogen bond (HDBU and substrate) was found to be crucial for the synthesis of quinazoline-2,4(1*H*,3*H*)-diones. The bond is activated by the anion part of the bifunctional catalyst (TFE)

I.2.4 Poly Ionic liquids

Poly Ionic Liquids (polymeric Ionic liquids) are made up of covalently linked IL species(MECERREYES, 2011) with macromolecular properties. These properties allow them to combine some of the unique properties and functions of ILs with those of polymers (e.g., easy processability and shape durability). PILs have a poor capacity(absorption) for CO_2 (< 10% wt%) and a high cost to commercial CO_2 absorbent(ZHOU; WEBER; YUAN, 2019). However, their affinity for CO_2 can be customized through careful selection of IL groups and polymer backbones and structures(BATES et al., 2002; RAMDIN; DE LOOS; VLUGT, 2012). They can transform CO_2 into chemical products because of their catalytic capabilities(XU; GUO; YAN, 2018). Some of the discoveries in new PILs are polytriazoliums, deep eutectic monomer (DEM)–based PILs, and polyurethane PILs, represented in figure I.7.

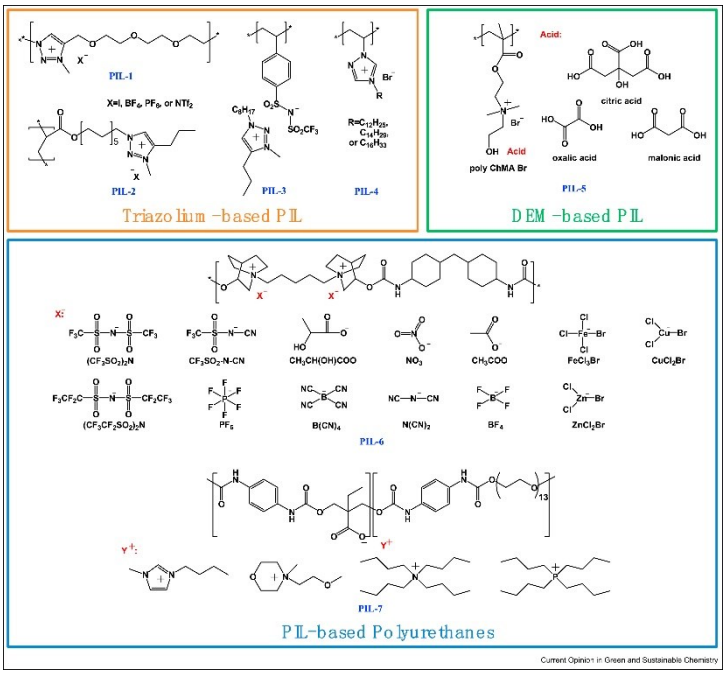

Figure I.7. Chemical structures of PILs newly developed during the past 3 years. PILs, poly(ionic liquid)s; DEM, deep eutectic monomer(ZHOU; WEBER; YUAN, 2019).

Marisol et al., 2014 synthesized new urethane-based PILs by adding diisocyanate to a difunctional polyol and diol mixture as catalyst for the CO_2 conversion to cyclic carbonate. Their findings show that the composition of PILs impacts their physical, thermal properties, and catalytic activity. PUEA BMIM (ethylenediamine) shows higher CO_2 conversion at mild conditions of 25 bar, 110° C, and 6 h. It was also reported the catalyst could be recycled without

any loss of catalytic activity. Ding and Jiang (2018) incorporated imidazolium-based PILs into an Metal–organic frameworks (MOF) material via in situ polymerization of encapsulated monomers, and such material showed significantly enhanced catalytic activity under mild conditions (CO_2 pressure of 1 bar or lower, ≤70 °C) (DING; JIANG, 2018).

Various studies have been conducted on the use of ILs as promoter and/or catalysts in hydrogenation of CO_2 to formic acid and methanol. However, few have considered ILs solely without a noble metal component as a potential catalytic system. Despite vast published literatures, the great rarity of noble metal-containing catalysts in the Earth's crust leads to a high cost of noble metal, which is not favourable for large-scale commercial applications as catalysts in CO_2 conversion. Hence, noble metal and metal-free catalytic systems are gaining a lot of interest due to their low cost, great recyclability, and comparable improved efficiency and selectivity(DUAN et al., 2017). Wu et al. 2019 reported a protocol of CO_2 conversion to formic acid over Pd/C in ionic liquid (1-butyl-3- methylimidazolium acetate, [Bmim][OAc]) under a mild condition in the absence of a base. Their findings show an effective catalytic system of Pd/C-[Bmim][OAc] at 40 °C, with a production rate of 233.5 $mmol \cdot g^{-1}.h^{-1}$ and turnover number (TON) of 594 (WU et al., 2019). Han et al. used Ru-immobilized silica as the heterogeneous catalyst to build a reaction/separation system for the synthesis of formic acid from CO_2 (4-18 MPa) and H_2 (1-9 MPa) at 60 ºC promoted by amino-based ILs(ZHANG et al., 2008). Filtration and evaporation may readily be used to recover the product and regenerate the catalyst. DuPont et al. 2018 used RuFe nanoparticles as catalysts in traditional IL [BMIM][Ac] under mild reaction conditions (1 MPa CO_2 and 2 MPa H_2). Other co-solvents such as H_2O and DMSO were also used. They reported a formic acid production occurred in IL containing basic anions, and other higher hydrocarbons (QADIR et al., 2018)) were formed in the presence of non-basic anion. Formic acid was generated with high TON and TOF values (400 and 23.52 h^{-1}, respectively). The pathway of CO_2 hydrogenation is related to the basicity and hydrophobicity of IL, mainly determined by the anion. The equilibrium of CO_2 hydrogenation to formic acid in the presence of IL 1,3-dipropyl-2-methylimidazolium formate was studied by Yoshiro et al. (YASAKA et al., 2010). Their findings revealed that formic acid production is enhanced due to the strong solvation of formic acid in 1,3-dipropyl-2-methylimidazolium formate by the strong coulombic solute-solvent interactions. From the equilibrium results, pressure for hydrogenation of CO_2 to formic acid could be reduced ~100 by using the IL instead of water.

I.3 Significance of Study

Although the conversion of CO_2 to various chemical products is energy intensive owing to its thermodynamic stability, the potential for providing a secure supply of chemicals and fuels, along with the escalating fossil-fuel prices, could become a powerful driver for the CCU (STYRING et al., 2011; YU et al., 2008). Nevertheless, CO_2 emissions from oil and gas production plants can be captured and converted to fuels and chemicals in a carbon conversion process. Thus, CO_2 conversion presents opportunities for the oil industry to participate in activities that will significantly reduce emissions and add value to oil and gas operations in oil-producing regions. In addition, gas flaring can be practically eliminated in oil field processes by converting the associated gas to fuels and chemicals.

I.4 Objectives

The thermodynamic limitations involved in CO_2 conversion to formic acid can be overcome by perturbing the reaction system with a secondary reaction using amine, ILs, and other types of solvents. The most recent works are the ones related to ionic liquids. However, there are a lot of ILs in literature and those that have not been explored. Most of the experimental results of recently studied ILs have been documented. However, these are just a fraction of the possible combinations of the cations and anions available. Moreover, the experimental approach is costly, time-consuming, and infeasible at times. Molecular approaches such as molecular dynamics and quantum chemistry provide insight into the thermodynamic properties of the ILs system. However, they are computationally costly. Activity coefficient models such as NRTL, UNIQUAC, and equations of state such as PC-SAFT have been successfully used; however, they require specific experimentally fitted parameters and have minimal predictive ability for novel systems without experimental data. Thus, reliable and efficient theoretical approaches to ILs testing are highly desirable in this respect. Recent studies have shown that the theoretical approach of the conductor-like screening model for real solvents (COSMO-RS) is a promising alternative for predicting thermodynamic properties of ILs without the use of group parameters or any system-specific adjustment. Since these ILs would be employed at an industrial scale, selecting a suitable solvent on a continuous process is good practice.

Thus, CHAPTER II's objective is to propose a method for selecting suitable ILs as solvation reaction and extraction media, combining CosmothermX and Aspen Plus to get insight into thermodynamic properties and process performance. The partial objectives are;

- Aggregate the potential list of ILs available in the software's database.

- Predict the thermodynamic and physical properties of all the ionic liquids using COSMO-RS model.
- Evaluate the effect of the potential candidate on the acquatic environment using the octanol water-coefficient as criteria.
- Evaluate the ILs performance on a continuous basis using a process simulator.

This work was published in the journal of Industrial & Engineering Chemistry Research, 60, 47, p. 17195–17206, 2021. https://doi.org/10.1021/acs.iecr.1c02910.

CHAPTER III presents insight into the possible ILs candidates for CO_2 conversion and product separation. However, there is a need to adequately assess the operating conditions for the favourable production of formic acid and methanol. Even though ILs are regarded as suitable solvents, the operating conditions on a continuous basis might not present favourable or improved production based on previously conducted work. Hence, this work employed ASPEN plus software to retrieve these technical parameters such as conversion, selectivity, and yield at the steady-state condition, as highlighted in **CHAPTER III**.

The main objective of CHAPTER III is to evaluate the feasibility of using the ionic liquid as a promoter for the hydrogenation reaction. The partial objectives are;

- Simulate a simplified process for the hydrogenation of CO_2 promoted by ionic liquid
- Determine the optimum operating condition for the favourable production of the hydrogenation product.
- Evaluate the conversion, selectivity and yield of the participating reactants and products.

The result of this work was presented at the 15th International Conference of Carbon Dioxide utilization, South Korea, and was published in the Chemical Engineering Science, v. 242, p. 116731, 2021. https://doi.org/10.1016/j.ces.2021.116731

CHAPTER IV. With the results of the studies in **CHAPTER III**, the specific role of the ILs need to be studied, thereby giving insight into thermodynamic, possible pathways, structural and energetic details and possibly supporting the results obtained from **CHAPTER III**. Hence, quantum chemical calculations were carried out using the capability of the ORCA software to evaluate the work in **CHAPTER IV**.

The objective here is to get insights into the mechanism of the reaction promoted by the ionic liquid. The partial objectives are;

- Retrieve the thermodynamic and kinetic data from the quantum calculation.
- Obtain information on the possible pathways of the reaction.
- Get insight about the role of the ionic liquid (to a certain extent) in the reaction.

The result from this work is being prepared for submission to a reputable journal.

CHAPTER V. With the possible process development, the economic implication of the process needs to be taken into account. For example, the project might seem promising but economically not viable. Hence, a techno-economic analysis on the deployment of this process was evaluated. ASPEN plus was employed to obtain technical information (e.g. mass and energy balance), Environmental parameters in terms of the CO_2 and water balance around the system, and the economic parameters related to the capital expenditure and operating expenditure. The discounted rate of return was evaluated to find out the minimum selling cost of the main product (formic acid). Also, the cost of raw materials was analyzed to obtain its correlation with the project's net present value. All this was addressed in **CHAPTER V**.

The objective is to model a standard industrial process plant for the production of formic acid and methanol. The partial objectives are;

- Retrieve techno-ecnomic parameters to evaluate the process feasibility
- Evaluate the impact of the process on the environment from its carbon footprint
- Determine the viable investment opportunities by comparing the NPVof the project.

This work was presented at the International Conference of Process System Engineering (PSE), Tokyo, Japan, 2021+ and published in the conference proceeding and as book chapter in Computer Aided Chemical Engineering, Jan 2022 https://doi.org/10.1016/B978-0-323-85159-6.50027-0

CHAPTER VI. Initial process design are always accompanied with various design defects, the design evolves and undergoes changes until an optimal design is achieved. This is always aimed at achieving process compactness, effective use of raw materials, product yield, saftey and, energy efficiency. Hence, the objective here is to identify bottleneck associated with the design and proposes new configuration for future development.

I.5 Thesis Structure

This document span from CHAPTERS II through VI, corresponding to conference papers and research articles in reputable international scientific journals. Their formats have been adjusted to provide a consistent framework, which means that all figures, tables, and equations have

been renumbered to correspond to each chapter. CHAPTERS II through VI also has their nomenclature, abbreviations, references, introduction, techniques, and conclusions.

CHAPTER I introduces the subject of this work, bringing the context of the research, its motivation, objectives, and the structure of the document.

CHAPTER II investigates screening of suitable ionic liquids for hydrogenation of CO_2 to formic acid and methanol. A theoretical approach that combines liquid-liquid equilibrium, gas solubility, physical properties, toxicity, and steady-state simulation model. These methods optimize the ILs for both solubility and recovery of products.

CHAPTER III presents the thermodynamic analysis in which CO_2 is converted simultaneously to formic acid and methanol. This explains the process conditions at an equilibrium condition. In addition, it evaluates the influence of the feed mixture, temperature, pressure, and Gibbs energy of the synthesis.

CHAPTER IV extends the previous investigations in chapter three by studying the role of the ionic liquid in the hydrogenation process. The result of the study correlates with the result from CHAPTER III. In addition, it employed computational chemistry calculation to understand better the mechanism of reaction and pathways involved.

CHAPTER V investigates the economic implications of deploying a commercial process plant for the production of formic acid and methanol using [Edmim][NO_2] as the reaction media. The technical and process parameters were carried out with the Aspen Plus V10 process simulation software.

CHAPTER VI introduces the general overview of process intensification, its underlying principles and methods. It shows the area of possible intensification in the process system, and a qualitatitaive evaluation for future development.

CHAPTER VII brings the concluding remarks, making an overview of the Thesis. Finally, Appendix A consists of published Supplementary Materials corresponding to the products' conversion, selectivity, and yield at different process conditions in CHAPTER III. Appendix B details published Supplementary Materials involving optimized geometries and thermodynamic and kinetic data of the mechanistic pathway of the synthesis in CHAPTER IV. Appendix C consists of published Supplementary Materials corresponding to the technical results from the Aspen simulation carried out in CHAPTER V. Finally, Apendix D consists of

published Supplementary Materials corresponding to the global thermodynamic and physical properties of the whole ILs studied in CHAPTER II.

I.6 References

AMEYAW, B. *et al.* Investigating , forecasting and proposing emission mitigation pathways for CO 2 emissions from fossil fuel combustion only : A case study of selected countries. **Energy Policy**, v. 130, n. 2006, p. 7–21, 2019.

BATES, E. D. *et al.* CO2 Capture by a Task-Specific Ionic Liquid. **Journal of the American Chemical Society**, p. 926–927, 2002.

BRAZILIAN MINISTRY OF MINES AND ENERGY (MME). **Brazilian energy outlook (in Portuguese)**. Disponível em: <http://www.mme.gov.br/documents/ 1138787/1732840/Resenhaþ Energetica þ-þ Brasilþ2015.pdf/4e6b9a34- 6b2e-48fa-9ef8-dc7008470bf2>. Acesso em: 17 maio. 2020.

BRITISH PETROLEUM, B. **BP Statistical Review of World Energy**. Disponível em: <https://www.bp.com/content/dam/bp/business-sites/en/global/corporate/pdfs/energy-economics/statistical-review/bp-stats-review-2018-full-report.pdf>. Acesso em: 17 maio. 2020.

CHAUVIN, Y.; MUSSMANN, L.; OLIVIER, H. A novel class of versatile solvents for two-phase catalysis: Hydrogenation, isomerization, and hydroformylation of alkenes catalyzed by rhodium complexes in liquid 1,3-dialkylimidazolium salts. **Angewandte Chemie (International Edition in English)**, v. 107, p. 2915–2917, 1995.

CULL, S. G. *et al.* Room-temperature ionic liquids as replacements for organic solvents in multiphase bioprocess operations. **Biotechnology and Bioengineering**, v. 69, n. 2, p. 227–233, 2000.

DING, M.; JIANG, H. L. Incorporation of Imidazolium-Based Poly(ionic liquid)s into a Metal-Organic Framework for CO2 Capture and Conversion. **ACS Catalysis**, v. 8, n. 4, p. 3194–3201, 2018.

DONG, F.; HUA, Y.; YU, B. Peak carbon emissions in China: Status, key factors and countermeasures-A literature review. **Sustainability (Switzerland)**, v. 10, n. 8, 2018.

DUAN, X. *et al.* Metal-Free Carbon Materials for CO2 Electrochemical Reduction. **Advanced Materials**, v. 29, n. 1701784, p. 1–20, 2017.

EMPRESA DE PESQUISA ENERGETICA (EPE). **BRAZILIAN OIL & GAS REPORT: TRENDS AND RECENT DEVELOPMENTS**. Disponível em:

<http://www.epe.gov.br/en>. Acesso em: 19 maio. 2020.

GAFFNEY CLINE, A. **Review and evaluation of ten selected discoveries and prospects in the pre-salt play of the deepwater Santos basin, Brazil**. [s.l: s.n.]. Disponível em: <www.anp.gov.br/?dw=39132>.

GAO, X. *et al.* Ionic Liquid-Catalyzed C-S Bond Construction using CO2 as a C1 Building Block under Mild Conditions: A Metal-Free Route to Synthesis of Benzothiazoles. **ACS Catalysis**, v. 5, n. 11, p. 6648–6652, 2015.

HU, J. *et al.* Dual-ionic liquid system: An efficient catalyst for chemical fixation of CO2 to cyclic carbonates under mild conditions. **Green Chemistry**, v. 20, n. 13, p. 2990–2994, 2018.

IEA. **CO2 Emissions from fosil combustion**. Disponível em: <www.iea.org>. Acesso em: 1 ago. 2018.

INTERGOVERNMENTAL PANEL ON CLIMATE CHANGE(IPCC). **IPCC, 2014: Climate Change 2014: Mitigation of Climate Change**. Contributi ed. Cambridge, United Kingdom and New York, NY, USA: Cambridge University Press, 2014.

INTERNATIONAL ENERGY AGENCY. **Putting CO2 to Use: Creating value from emissions**. Disponível em: <www.iea.org>. Acesso em: 17 maio. 2020.

KETZER, J. M. M. *et al.* **Brazilian Atlas of CO2 Capture and Geological Storage**. [s.l: s.n.].

LEI, Z.; DAI., C.; CHEN, B. Gas solubility in ionic liquids. **Chemical Reviews**, v. 114, p. 1289–1326, 2014.

LUO, X. *et al.* The capture and simultaneous fixation of CO2 in the simulation of fuel gas by bifunctionalized ionic liquids. **International Journal of Hydrogen Energy**, v. 41, n. 21, p. 9175–9182, 2016.

MARSH, K. N. *et al.* Room Temperature Ionic Liquids as Replacements for Conventional Solvents - A Review. **Korean Journal of Chemical Engineering**, v. 19, n. 3, p. 357–362, 2002.

MECERREYES, D. Polymeric ionic liquids: Broadening the properties and applications of polyelectrolytes. **Progress in Polymer Science (Oxford)**, v. 36, n. 12, p. 1629–1648, 2011.

MIILLER, L. A.; DUPONT, J.; SOUZA, R. F. DE. Two-phase catalytic NBR hydrogenation by RuHCl(CO)(PCy& immobilized in 1-butyl-3-methylimidazolium tetrafluoroborate molten

salt. **Macromol Rapid Communication**, n. 8, p. 409–411, 1998.

MINISTÉRIO DE MINAS E ENERGIA, E. M. **Plano Decenal de Energia 2020**. Disponível em: <https://www.epe.gov.br/pt/publicacoes-dados-abertos/publicacoes>. Acesso em: 17 maio. 2020.

MOREIRA, J. R.; PACCA, S. A.; PARENTE, V. The future of oil and bioethanol in Brazil. **Energy Policy**, v. 65, p. 7–15, 2014.

NATIONAL AGENCY OF PETROLEUM, N. G. AND B. A. **The Oil and Gas Industry in Brazil**. Disponível em: <https://www.gov.br/anp/pt-br>. Acesso em: 19 set. 2018.

OLAH, G. A.; GOEPPERT, A.; PRAKASH, G. K. S. Chemical Recycling of Carbon Dioxide to Methanol and Dimethyl Ether : From Greenhouse Gas to Renewable , Environmentally Carbon Neutral Fuels and Synthetic Hydrocarbons Chemical Recycling of Carbon Dioxide to Methanol and Dimethyl Ether : From Greenhouse. **Journal of Organic Chemistry**, v. 74, n. 2, 2009, p. 487–498, 2009.

PATIL, Y. P. *et al.* Synthesis of quinazoline-2,4(1H,3H)-diones from carbon dioxide and 2-aminobenzonitriles using [Bmim]OH as a homogeneous recyclable catalyst. **Catalysis Today**, v. 148, p. 355–360, 2009.

PENG, J.; DENG, Y. Cycloaddition of carbon dioxide to propylene oxide catalyzed by ionic liquids. **New Journal of Chemistry**, v. 25, n. 4, p. 639–641, 2001.

PÉREZ-FORTES, M. *et al.* Formic acid synthesis using CO2 as raw material: Techno-economic and environmental evaluation and market potential. **International Journal of Hydrogen Energy**, v. 41, n. 37, p. 16444–16462, 2016.

QADIR, M. I. *et al.* Selective Carbon Dioxide Hydrogenation Driven by Ferromagnetic RuFe Nanoparticles in Ionic Liquids. **ACS Catalysis**, v. 8, n. 2, p. 1621–1627, 2018.

RAMDIN, M.; LOOS, T. W. DE; VLUGT, T. J. H. State-of-the-art of CO2 capture with ionic liquids. **Industrial and Engineering Chemistry Research**, v. 51, n. 24, p. 8149–8177, 2012.

SANTOS, M. G. R. S. *et al.* Natural gas dehydration by molecular sieve in offshore plants: Impact of increasing carbon dioxide content. **Energy Conversion and Management**, v. 149, p. 760–773, 2017.

SILVA, S. M. *et al.* Selective linear dimerization of 1,3-butadiene by palladium compounds

immobilized into 1-n-butyl-3-methyl imidazolium ionic liquids. **Polymer Bulletin**, v. 40, n. 4–5, p. 401–405, 1998.

SONG, Q. W.; ZHOU, Z. H.; HE, L. N. Efficient, selective and sustainable catalysis of carbon dioxide. **Green Chemistry**, v. 19, n. 16, 2017.

STYRING, P. *et al.* **Carbon Capture and Utilisation in the green economy**. [s.l.] Centre for Low Carbon Futures New York, 2011.

US DEPARTMENT OF ENERGY, (DOE). **Fact sheet: CO2 enhanced oil recovery. DOE Office of Petroleum Reserves —Strategic Unconventional Fuels.** Disponível em: <http://fossil.energy.gov/programs/reserves/%0Anpr/CO2_EOR_Fact_Sheet.pdf>. Acesso em: 18 maio. 2020.

WANG, P. *et al.* Green synthesis of polyureas from CO2 and diamines with a functional ionic liquid as the catalyst. **RSC Advances**, v. 6, n. 59, p. 54013–54019, 2016.

WASSERSCHEID, P.; KEIM, W. Ionic LiquidsÐNew ªSolutionsº for Transition Metal Catalysis. **Angew. Chem. Int. Ed**, v. 39, p. 3772–3789, 2000.

WELTON, T. Room-Temperature Ionic Liquids. Solvents for Synthesis and Catalysis. **Chemical Reviews**, v. 99, p. 2071–2083, 1999.

WU, Y. *et al.* Tetrabutylphosphonium-Based Ionic Liquid Catalyzed CO<inf>2</inf> Transformation at Ambient Conditions: A Case of Synthesis of α-Alkylidene Cyclic Carbonates. **ACS Catalysis**, v. 7, n. 9, p. 6251–6255, 2017.

WU, Y. *et al.* Ionic Liquid Promoted CO2 Hydrogenation to Free Formic Acid over Pd/C. **Industrial and Engineering Chemistry Research**, v. 58, n. 16, p. 6333–6339, 2019.

XIA, S. M. *et al.* Ionic liquids catalysis for carbon dioxide conversion with nucleophiles. **Frontiers in Chemistry**, v. 6, n. SEP, p. 1–7, 2018.

XU, D.; GUO, J.; YAN, F. Porous ionic polymers: Design, synthesis, and applications. **Progress in Polymer Science**, v. 79, p. 121–143, 2018.

YASAKA, Y. *et al.* Controlling the equilibrium of formic acid with hydrogen and carbon dioxide using ionic liquid. **Journal of Physical Chemistry A**, v. 114, n. 10, p. 3510–3515, 2010.

YU, K. M. K. *et al.* Recent advances in CO2 capture and utilization. **ChemSusChem**, v. 1, n.

11, p. 893–899, 2008.

YUE, S.; WANG, P.; HAO, X. Synthesis of cyclic carbonate from CO2 and epoxide using bifunctional imidazolium ionic liquid under mild conditions. **Fuel**, v. 251, p. 233–241, 2019.

ZAKRZEWSKA, M. E. Ionic Liquids for CO2 Capture and Reduction. **Journal of Carbon Research**, v. 7, n. 1, p. 6, 2021.

ZHANG, Z. *et al.* Hydrogenation of carbon dioxide is promoted by a task-specific ionic liquid. **Angewandte Chemie - International Edition**, v. 47, n. 6, p. 1127–1129, 2008.

ZHAO, Y. *et al.* A protic ionic liquid catalyzes CO2 conversion at atmospheric pressure and room temperature: Synthesis of quinazoline-2,4(1H,3H)-diones. **Angewandte Chemie - International Edition**, v. 53, n. 23, p. 5922–5925, 2014.

ZHAO, Y. *et al.* Azole-Anion-Based Aprotic Ionic Liquids: Functional Solvents for Atmospheric CO<inf>2</inf> Transformation into Various Heterocyclic Compounds. **Chemistry - An Asian Journal**, v. 11, n. 19, p. 2735–2740, 2016.

ZHOU, X.; WEBER, J.; YUAN, J. Poly(ionic liquid)s: Platform for CO2 capture and catalysis. **Current Opinion in Green and Sustainable Chemistry**, v. 16, p. 39–46, 2019.

CHAPTER II
SYSTEMATIC SCREENING OF IONIC LIQUIDS FOR THE HYDROGENATION OF CARBON DIOXIDE TO FORMIC ACID AND METHANOL

This paper was published in Industrial & Engineering Chemistry Research, 60, 47, p. 17195–17206, 2021. https://doi.org/10.1021/acs.iecr.1c02910

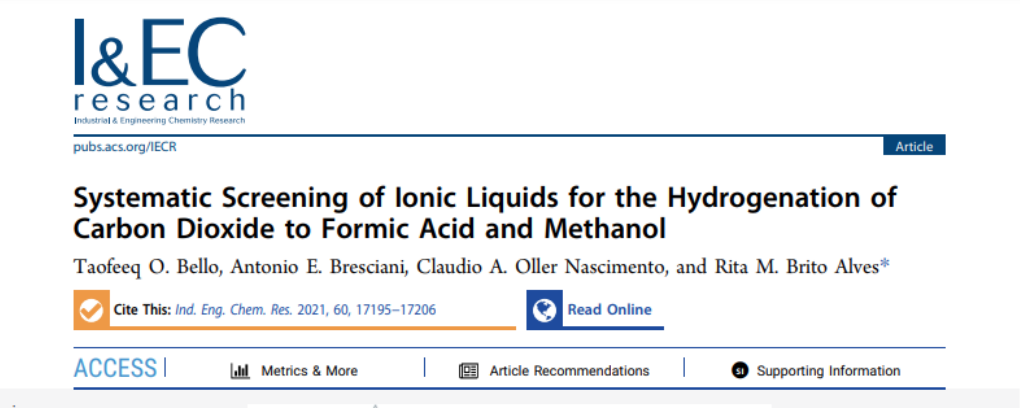
I&EC research
Industrial & Engineering Chemistry Research
pubs.acs.org/IECR
Article
Systematic Screening of Ionic Liquids for the Hydrogenation of Carbon Dioxide to Formic Acid and Methanol
Taofeeq O. Bello, Antonio E. Bresciani, Claudio A. Oller Nascimento, and Rita M. Brito Alves*
Cite This: Ind. Eng. Chem. Res. 2021, 60, 17195−17206
Read Online
ACCESS | Metrics & More | Article Recommendations | Supporting Information

Abstract

A systematic approach for the selection of suitable ionic liquids (ILs) for the hydrogenation of carbon dioxide (CO_2) to formic acid and methanol as reaction media and extraction solvent is presented. This approach combines phase equilibrium, gas solubility/capacity, physical property estimation, and toxicity, along with a simple regeneration process. First, independent predictions of the liquid-liquid equilibrium (LLE) of the component mixture (methanol and formic acid + ILs) and gas solubility of CO_2 in different ILs, and physical properties are estimated with the conductor-like screening model for real solvents (COSMO-RS). Then, a qualitative selection of the ILs that satisfied gas solubility and LLE-based routes were selected. In addition, the toxicity of ILs in the environment was also taken into account. Finally, the separation performance of the top ILs candidates with their products mixture in a continuous process was evaluated to identify process-based optimal solvents.

Highlights

1. 240 ionic liquids were screened as reaction media (solvent) for the hydrogenation of carbon dioxide to formic acid and methanol.
2. The COSMO-RS method was used to predict physical properties and liquid-liquid equilibrium.
3. The group contribution method was used to determine the effect of the ionic liquids on aqueous media.

4. The separation performance of the ionic liquids was evaluated on a continuous separation process.
5. 1-ethyl-2,3-dimethyl-imidazolium nitrite was selected as the optimal solvent for the hydrogenation process.

Keywords: COSMO-RS, Ionic liquids, Liquid-liquid equilibrium, Process simulation, Carbon dioxide solubility, Carbon dioxide hydrogenation

II.1 Introduction

Carbon dioxide (CO_2) is a significant greenhouse gas that contributes to global warming. Conversely, it is also a substantial source of carbon for synthesizing different chemicals. Therefore, the capture of CO_2 for emission control and its use is an increasingly important research concern. CO_2 capture techniques consist mainly of adsorption by aqueous amines, which contribute to the gas flow of a certain amount of water and solvent loss(ZHANG et al., 2006a). The conversion of CO_2 to formic acid in a one-step process using H_2 from renewable sources presents a more efficient alternative to the current synthesis, low resource-intensive, abundant use of CO_2, and less intermediate product formation (GRASEMANN; LAURENCZY, 2012; HULL et al., 2012). Unfortunately, the conversion is endergonic (ΔG = +32kJ/mol) and hence, unfavorable thermodynamically (LEITNER, 1995; SCHAUB; PACIELLO, 2011; WANG; HIMEDA, 2012). The use of suitable solvents (ÁLVAREZ et al., 2017a) or bases (INOUE et al., 1976) is one strategy often used to overcome thermodynamic limitations, making the reaction slightly exergonic(WANG; HIMEDA, 2012). Alternative solvents have been proposed over recent years; among them, ionic liquids (ILs), a new class of novel solvents (LAZZÚS, 2009), appear as a promising option. Significant advances over the years in applying ILs as alternative solvents are due to their unique features, such as low vapor pressure, wide range of liquid temperatures, better thermal and chemical stability, tunable physicochemical characteristics and selective dissolution of certain organic and inorganic materials(GORDON, 2001; WELTON, 1999). Additionally, ILs may be applied as catalyst, if they change the rate of reaction and without being altered at the end of the reaction. They have been successfully applied in Diels–Alder cycloadditions and their derivatives(DZYUBA; BARTSCH, 2002; SCHREINER, 2003) and other reactions(RADAI; KEGLEVICH; ZSUZSA KISS, 2018).

The use of these novel solvents has been thoroughly investigated in organic synthesis (WERNER; HAUMANN; WASSERSCHEID, 2010), catalysis (OLIVIER-BOURBIGOU; MAGNA; MORVAN, 2010), electrochemistry (LOMBARDO et al., 2013), biocatalysis

(MACFARLANE; KAR; PRINGLE, 2017), material science (MACFARLANE et al., 2016), and separation (HAN; ROW, 2010). One of the main benefits of these attractive solvents is that their cation (C) and anion (A) are selected from a wide range to achieve a suitable IL for a particular purpose (HU et al., 2019). Thus, ILs are commonly regarded as "designer solvents." However, many ILs remain restricted by the limited available experimental data for practical applications in industrial processes (FERRO et al., 2012a). ILs act as solvents and catalysts in chemical reactions, demonstrating optimal performances. ILs have gone beyond the limit as alternative reaction media. They have shown their significant role in controlling the reaction as catalysts(WELTON, 2004). ILs may behave as acidic, basic, or organocatalyst depending on the functional group of the cation and anion. In the hydrogenation reactions system, ILs fine-tune the solvent's property by altering the structure, immobilizing catalyst, activating CO_2, and consequently reducing the Gibbs energy. ILs that can activate CO_2 have high alkalinity due to electron-negative sites as N or O atoms (WU et al., 2017),(LUO et al., 2014). "CO_2-phillic" ILs, including azolate and pyrimidine-based ILs, have been reported to be capable of catalyzing the transformation of CO_2 by the formation of intermediates of carbonate or carbamates under mild conditions (WU et al., 2017), (ZHAO et al., 2016b). For example, 1-butyl-3-methyl-imidazolium hydroxide ([BMIM][OH]), a basic IL, was successfully used as a catalyst for the synthesis of substituted urea from carbon dioxide and amines(JIANG et al., 2008). To simplify this study, a detailed kinetic into the hydrogenation reaction has been carried out in a subsequent work. Hence, only the equilibrium study is considered in this work.

The primary objective of applying ILs as a specific extraction and reaction medium is to choose an appropriate solvent because different ILs have very distinct properties and separation efficiency. Research works on ILs still concentrate on basic laboratory experiments (DOMAŃSKA; KRÓLIKOWSKA, 2010; DOMAŃSKA; WLAZŁO, 2014; GAO et al., 2015a; HANSMEIER; MEINDERSMA; DE HAAN, 2011; ZHAO et al., 2016a). Experimental determination of thermo-physical properties of ILs and their mixtures has been performed extensively, and the results are collected in databases such as the IUPAC Ionic Liquid Databases (ILTHERMO, [s.d.]) and Dortmund databank (DORTMUND DATABANK, [s.d.]). However, even for the most thoroughly studied systems, only a small portion of a large number of possible cation-anion combinations has been covered experimentally. To maximize the potential of ILs-based extractions and reaction media, the search for a suitable solvent is of great importance (SONG et al., 2017). Since an experimental approach is costly (QIN et al.,

2016), time-consuming or even infeasible (FERRO et al., 2012a), reliable and efficient theoretical approaches to ILs testing are highly desirable (SONG et al., 2016)

In recent years, there has been increasing interest in theoretical applications to predict IL properties (FERRO et al., 2012a). The conductor-like screening model for real solvents (COSMO-RS) (KLAMT; ECKERT, 2000) has been shown to be an alternative to predict the thermodynamic properties of liquid mixtures and pure components, including ILs systems(KLAMT; ECKERT; ARLT, 2010). COSMO-RS can predict the activity coefficient of solutes that can be treated with the approximation of incompressible liquids (ECKERT; KLAMT, 2017) in the ILs and the phase equilibrium of the different ILs systems as a fully predictive thermodynamic model (ANANTHARAJ; BANERJEE, 2013; DIEDENHOFEN; ECKERT; KLAMT, 2003; FERREIRA et al., 2011, 2012). In this sense, COSMO-RS may be regarded as a fast ILs screening tool for various separation problems. However, COSMO-RS is an equilibrium theory; hence non-equilibrium properties cannot be predicted directly. Systems that cannot be treated with the theory of approximation of incompressible liquids need further information(ECKERT; KLAMT, 2017). Physical properties such as solubility/capacity play a significant role in determining the suitability of ILs as aqueous media (reaction media). For example, in a chemical reaction involving IL, the reacting chemical species availability in the IL reaction phase is necessary. Organic reactions require high thermodynamic solubility of the substrate in the IL and fast mass transfer of the chemical species into the ionic reaction layer (WASSERSCHEID; ANNEGRET, 2010). In addition, due to their low volatility, ILs are not atmospheric pollutants, but they have a high tendency to dissolve in water (ROPEL et al., 2005); consequently, their potential impacts on the aquatic and terrestrial environments are of significant concern.

Several contributions have been reported on screening ILs as extraction solvents(ANANTHARAJ; BANERJEE, 2010; FARAHIPOUR; MEHRKESH; KARUNANITHI, 2015; HU et al., 2019; LEI; ARLT; WASSERSCHEID, 2006; MARTINS et al., 2016; SONG et al., 2017), and solvents for CO_2 capture(FARAHIPOUR; AMIRHOSSEIN; KARUNANITHI, 2016; LEE; LIN, 2015; MORTAZAVI-MANESH; SATYRO; MARRIOTT, 2013; ZHANG; LIU; WANG, 2008; ZHAO et al., 2017) based on COSMO-RS. In these works, several thermodynamic properties such as the activity coefficient, Henry's constant, distribution coefficient, and selectivity at the infinite dilution condition are widely employed as the screening criteria; however, the majority of these screenings were performed independently to achieve a single application of the ILs under study. Moreover, the combination of these thermodynamic properties was seldom used to achieve a dual objective

in the previous IL screening studies. Therefore, the focus of this work is to accomplish a bi-objective application of a single IL as a reaction/solvation media for the hydrogenation of CO_2 and extraction solvent for product separation. This extends previous screening techniques by incorporating the gas capacity and toxicity of different ILs. To the best of the authors' knowledge, no previous studies have investigated bi-objectives/purposes of screening ILs for simultaneous hydrogenation of CO_2 to formic acid and methanol as the reaction solvent and extraction media. The overall approach herein presented combines mass-based LLE extraction calculation, gas capacity (mass), physical property estimation, toxicity to environmental animals and plants, and separation process evaluation. A case study is presented to demonstrate the proposed approach's effectiveness, and the optimal ILs with higher process separation performance are identified.

II.2 Methods

The entire IL screening procedure comprises five steps, as shown in Figure II.1. The first step consists of two independent mass-based parallel screenings (LLE and gas capacity) of the ILs, reactants (H_2 & CO_2), and products (formic acid & methanol). At any composition of interest, the COSMO-RS LLE and gas capacity (solubility) calculations were carried out considering the reactants and different ILs. ILs with greater distribution coefficient (β) and selectivity (S) and lower solvent loss (SL) than the benchmark solvent (a conventional organic solvent) were selected for the next screening stage. The second step involves estimating the melting point(PREISS; BULUT; KROSSING, 2010),(KOI et al., 2019) and the viscosity(EIDEN et al., 2011) by COSMO-RS of the selected potential candidates. Then the ILs that outperform the benchmark solvent were selected. The third step is the qualitative selection of the IL candidates that satisfy the LLE and gas capacity route. The following step is the estimation of the water/octanol partition coefficient of the selected ILs. Finally, the last step is the simulation and evaluation of the top IL candidates' continuous flash separation process. The optimums ILs with the highest process performance were selected. Due to the limitations of the CosmothermX software with an educational license, limited ILs can be selected from its database. Generally, ILs are defined as liquids composed entirely of cations and anions. Therefore, in the selection, all types of cations and anions were considered. The cations and anions were paired randomly by the software.

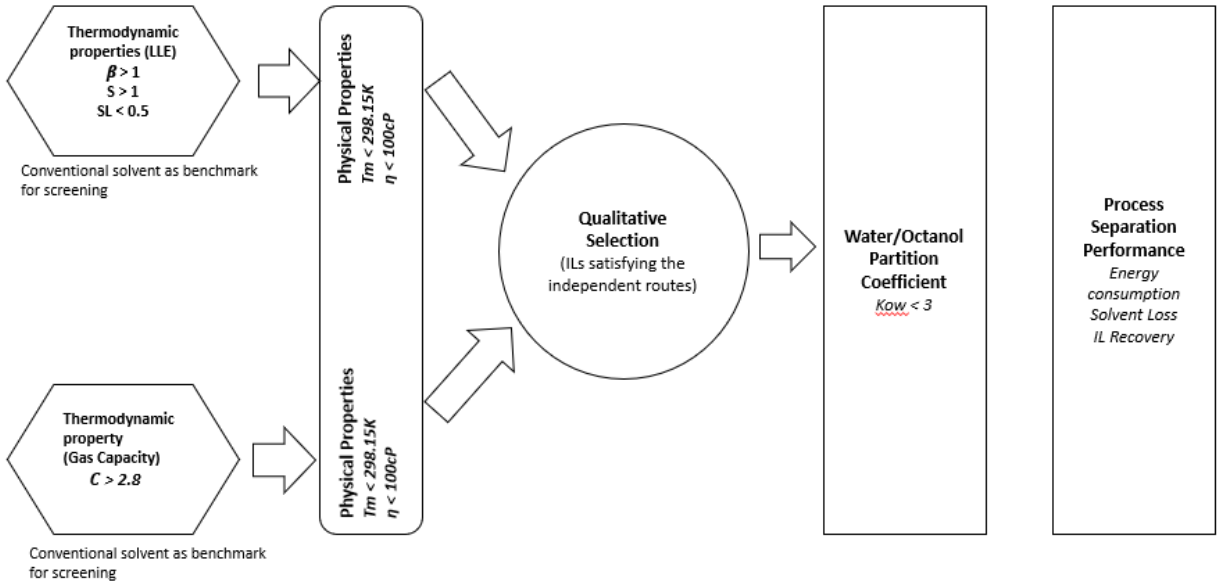

Figure II.8. Schematic diagram of the method employed for the screening of the ILs as reaction media and extraction solvents.

II.2.1 COSMO-RS Based Prediction

There are numerous contributions to the screening of ILs as solvents for extraction based on COSMO-RS (ANANTHARAJ; BANERJEE, 2010, 2013; FARAHIPOUR; MEHRKESH; KARUNANITHI, 2015; HU et al., 2019; SONG et al., 2017). These works typically include the extraction distribution coefficient (β), capacity (C), and selectivity at infinite dilution (S) as screening criteria:

$$\beta^{\infty} = {}^{1}/_{\gamma_{i,}^{\infty}} \tag{II.1}$$

$$S^{\infty} = {}^{\gamma_j^{\infty}}/_{\gamma_{i,}^{\infty}} \tag{II.2}$$

$$C^{\infty} = {}^{1}/_{\gamma_{i,IL}^{\infty}} \tag{II.3}$$

where, γ_i^{∞} and γ_j^{∞} refers to the infinite dilution activity coefficients of solute i and solute j in the IL phase, respectively.

COSMO-RS estimate these three parameters ($S^{\infty}, \beta^{\infty}, C^{\infty}$) on a molar basis, which provides a quick and straightforward evaluation of the separation performance of ILs. However, because the real extraction concentration is ignored, they may not be the best solvent for practical purposes (MARCINIAK, 2010). Therefore, the mass-based solvent use may also be evaluated to check the applicability of the different ILs (LEI; ARLT; WASSERSCHEID, 2006). The standard COSMO-RS calculation involves two steps: first, to obtain the distribution of screening charge density (σ-profile) of interested compounds through quantum chemical

calculations; follows the statistical thermodynamic treatment of molecular interactions on the σ–profile to obtain the component's chemical potential. The knowledge of the chemical potential allows assessing thermodynamic properties, such as selectivity, solubility, partition coefficient, relative volatility, etc. (SONG et al., 2017). The best prediction using COSMO-RS is made at room temperature, deviations increases for low or high temperatures(ECKERT; KLAMT, 2017).

The ability of COSMO-RS to calculate an arbitrary solution chemical potential in any pure or mixed solvent allows predicting the LLE of binary, ternary or multicomponent mixtures at any mixture composition. The LLE is calculated as the condition whereby the chemical potential of any compound is equal in both phases (KLAMT; ECKERT, 2000), (ECKERT; KLAMT, 2017). All the compounds in the system are distributed between the two phases according to their partition equilibrium constants (K_i) at the reference state;

$$K_i^x = \exp\left(\left(\mu_i^I - \mu_i^{II}\right)/RT\right) \quad \text{(II.4)}$$

where μ_i^I and μ_i^{II} designate the chemical potential of compound i in phase I and phase II, respectively. Phases I and II are assumed to be immiscible and to separate in thermodynamic equilibrium.

The chemical potentials and partition equilibrium constants are calculated with a given set of compositions. Thus, an initial set of compositions is first estimated in the LLE calculations. The procedure above is repeated until there is no change in the component compositions in the phase (KLAMT; ECKERT, 2000), (ECKERT; KLAMT, 2017). Recent studies proved that COSMO-RS provides excellent qualitative and acceptable quantitative capacity to calculate the LLE of ILs systems (ANANTHARAJ; BANERJEE, 2013; FERREIRA et al., 2011, 2012).

II.2.1.1 LLE Mass-Based Thermodynamic Properties

The software package CosmothermX (Version 19.0.1)(ECKERT; KLAMT, 2018) based on COSMO-RS was used to implement the LLE mass-based thermodynamic properties evaluation. This work performed LLE calculations using the Becke-Perdew Triple Zeta Valence Polarization (BP_TZVP)(ECKERT; KLAMT, 2017) parametrization of the cosmothermX software package. All the σ-profiles of the involved ILs ions (cations and anions) and the conventional compounds are directly taken from the BP_TZVP database. After obtaining the LLE results, the mass-based β, S, and SL are determined by equations 5 – 7. Then, parameters, as defined by equations (5) – (7), are applied as thermodynamic criteria to evaluate the extraction ability of the ILs for a specific extraction task.

$$\beta = {m_{solute}^{E}}/{m_{solute}^{R}} \quad \text{(II.5)}$$

$$S = \frac{{m_{solute}^{E}}/{m_{solute}^{R}}}{{m_{carrier}^{E}}/{m_{carrier}^{R}}} \quad \text{(II.6)}$$

$$SL = m_{solvent}^{R} \quad \text{(II.7)}$$

Where β, S, and SL represent the distribution coefficient, selectivity, and solvent loss, respectively. The solvent is the IL and superscripts, E and R represent the extract and the raffinate phase, respectively. (SONG et al., 2017)

II.2.2 Benchmark Solvent Estimation

Dimethylsulfoxide (DMSO) (MORET; DYSON; LAURENCZY, 2014a), tetrahydrofuran (THF), dimethylformamide (DMF) are common solvents used to promote CO_2 hydrogenation to formic acid (ARTZ et al., 2018; JESSOP; IKARIYA; NOYORI, 1995; SORDAKIS et al., 2018a). These organic solvents, together with three other solvents (Table II.1) capable of dissolving CO_2 according to Kunerth (1922) (KUNERTH, 1922) and Sordakis et al. (2018) (SORDAKIS et al., 2018b), were selected from Aspen Plus. The Soave-Redlich-Kwong (SRK) Equation of state (EoS) with Boston-Mathias (BM) alpha function was employed as thermodynamic model. The model was developed to represent well high-pressure species at temperatures far from the critical (e.g. H_2). A Huron-Vidal mixing rule was selected to represent the binary system, and the UNFAC (Dortmund) activity coefficient model was applied to estimate the non-ideality of the liquid phase.The solvent with optimal performance was chosen as the benchmark for the screening.

II.2.3. Gas Capacity

The capacity of the ILs at infinite dilution (C^{∞}) may be considered on a mass basis for evaluating the ability of the ILs to dissolve the maximum amount of any solute. The mass-based evaluation is more straightforward for assessing the practical applicability of different ILs (LEI; ARLT; WASSERSCHEID, 2006). The gas capacity is used to evaluate the ability to dissolve the maximum amount of a gas solute at infinite dilution. Hence, the ILs act as CO_2 solvation media. The calculated solvent capacity corresponds to the non-iterative solute of the solution in the ILs (solvent in this case) (ECKERT; KLAMT, 2015), (ECKERT; KLAMT, 2017). Therefore, the gas capacity is used as an initial solubility estimate for the screening. However, only the capacity for CO_2 is considered in this work. H_2 solubility is much lower in ILs (BERGER et al., 2001; DYSON et al., 2003; LINKE; SEIDELL, 1958; YOUNG, 1981);

consequently, it was not considered for the screening process. Mass transfer plays a significant role in hydrogenation reactions associated with low gas solubility. Sun and coworkers (1996) (SUN et al., 1996) noted that the vital kinetic parameter in asymmetric catalytic hydrogenation (enantioselectivity) is the concentration of molecular H_2 in the liquid phase. However, low solubility can be compensated by carrying out the reaction at relatively high pressures, which increases H_2 solubility in the reaction mixture (BERGER et al., 2001). Therefore, H_2 can be introduced in the reaction system rather than in the solvation media. Gas capacity is strongly dependent on the solvent-solute interaction effects (LETCHER et al., 2008). The mass-based capacity (solubility) is determined by equations 8 - 9:

$$C^{\infty} = {}^{1}/_{\gamma_{i,IL}^{\infty}} \tag{II.8}$$

$$G_I = C_I * {}^{M_{solute}}/_{M_{IL}} \tag{II.9}$$

where G_I, M_{solute}, C_I , $\gamma_{i,IL}^{\infty}$and M_{IL} are the mass-based gas capacity, the mass of the solute (CO_2), the mole capacity, the activity coefficient at infinite dilution of solute i in the IL phase, and the mass of ILs (solvent), respectively.

II.2.4 Physical Property Estimation

Physical properties play a significant role in assessing the suitability of ILs as solvating and extraction solvents. ILs need to be liquid at the working conditions (FARAHIPOUR; MEHRKESH; KARUNANITHI, 2015), and thus the melting point needs to be below the operating temperature (HU et al., 2019). In addition, the viscosity should be low to enhance mass transfer between the solute and ILs and reduce pumping cost and (LAZZÚS, 2012), (LAZZÚS; PULGAR-VILLARROEL, 2015). Finally, it is always a good practice to select a suitable solvent based on a continuous process (SONG et al., 2017).

COSMO-RS enables the calculation of a variety of ILs property(DIEDENHOFEN; KLAMT, 2010) using the (inbuilt) quantitative structure-activity relationship (QSAR/QSPR) descriptor model available in cosmothermX. The descriptor model has been widely reported in literature(LÓPEZ-MARTIN et al., 2007)(ZHANG et al., 2006b)(FAYET; ROTUREAU, 2012). For example, Lopez-Martin et al. (2007) developed and applied the QSPR approach on imidazolium-based ionic liquid. The result shows a good coefficient of determination (R^2 = 0.8690). In the same vein, Zhang et al. (2006) also reported R^2 value of 0.9207 on Imidazolium-based ionic liquid using the same approach. The QSARs have been implemented for single charged ions and the BP-TZVP level of theory in the software package (CosmothermX), and

some depend on specific parameterization (ECKERT; KLAMT, 2017). Equation 10 describes how the software calculates the melting point.

$$T_{fus} = (C\, r_m^3 + \, dH_{vdw}^0 + eH_{ring})/(a \ln \sigma + b_T + 1) \quad \text{(II.10)}$$

where, T_{fus} = Melting point (K), r_m is the mean IL radius (sum of mean radii of the ions), H_{ring} ,H_{vdw}^0 are the sum of COSMO-RS enthalpies of the ions in a 50:50 mixture at 25°C, σ= (σ+ σ-) is the symmetry number, and T = T+ T- is the torsional degree of freedom (DANNENFELSER; YALKOWSKY, 1996; PREISS; BULUT; KROSSING, 2010).

The pure compound liquid viscosity is another property calculated from quantitative structure-property relationships (QSPR) (ECKERT; KLAMT, 2017). Koi et al. (2019) developed and implemented a QSPR model on imidazolium-based ionic liquids. The model produced a low average absolute relative deviation (AARD) of 4.66%, root mean square error (RMSE) of 0.26, and coefficient of determination (R^2) of 0.965(KOI et al., 2019). Eiden et al. (2011) also reported a R^2 of COSMO model value of 0.91 and RMSE of 0.22 (EIDEN et al., 2011). The QSPR model as implemented by COSMO does not include a temperature dependency term so that the model is valid at a specific temperature only. All parameterizations include the viscosity QSPR parameters at room temperature. The liquid viscosity is calculated in the software using equations 11-12.

$$\ln\left({}^{x}/_{x_0}\right) = a \ln(r_m) + bE_{diel} + c\, \sigma^i + d \quad \text{(II.11)}$$

where $E_{diel} = E_{diel}(cation) + E_{diel}(anion)$is the sum of the dielectric energies (Ɛ=∞) of the ions.

$$\ln\left({}^{x(T)}/_{x_0}\right) = d + e * \ln(r_m) + f * \ln(\sigma) + h * E_{diel}/E_{diel0} \quad \text{(II.12)}$$

$$+g * E_{diel}/(R * T) + i * (E_{diel} * T_0)/(R * T^2) + d$$

where, X (T) = Temperature dependent viscosity (cP/mPa S) $E_{diel} = E_{diel}(cation) + E_{diel}(anion)$is the sum of the dielectric energies (Ɛ=∞) of the ions and E_{diel0} = 1 kJ·mol-1 and T_0 = 1K (ECKERT; KLAMT, 2017)

II.2.5 Qualitative selection of ILs Satisfying Gas Solubility and LLE

One of the main goals of this study is to screen ILs that may be used as a reaction media for CO_2 hydrogenation and enable the reaction product to be easily separated by a simple separation process. As such, this step screens the resulting IL candidates from physical property

screening. Therefore, the ILs selected at this step should satisfy both the capacity (solubility) and LLE screening routes.

II.2.6 Estimation of Water/Octanol Partition Coefficient by Group Contribution

Due to their distinctive characteristics, particularly their negligible vapor pressure, ILs are labeled as "green solvents" (COULING et al., 2006). Although ILs are environmentally friendly, if transferred to water bodies, they have a significant aquatic (environmental) effect (HU et al., 2019). Therefore, safety properties such as toxicity, reactivity, and flash point can be used to evaluate the environmental impact of ILs. Herein, we assumed the ILs have low vapor pressure, low reactivity, and high flash point, and hence, these properties do not affect the environment. Thus, only toxicity is used for evaluation.

The n-octanol / water partition coefficient (Kow) is therefore used to evaluate the toxicity of the ILs (ZHAO et al., 2014b). The group contribution method by Marrero and Gani (2002) (MARRERO; GANI, 2002) and continuum solvation model (MARENICH; CRAMER; TRUHLAR, 2009) (using density functional theory) was employed to estimate K_{ow}. The group contribution values were calculated by linear regression analysis using a data set of 9560 of K_{ow}. The data set included compounds ranging from C3 to C70, including large and heterocyclic compounds. The prediction is performed with the first-level estimation for simple and monofunctional compounds (MARRERO; GANI, 2002). Equation II.13 calculates the water/octanol partition coefficient. The octanol/water partion coefficient was computed from DFT from the continuum solvation model (SMD) free energies obtained in the two solvents (octanol and water) at 298.15 K as depicted in equations II.14-II.17.

$$log\ K_{ow} = \sum_i N_i \log K_{ow}(I)_i + K \tag{II.13}$$

$$K_{o/w} = \frac{[Solute]_{octanol}}{[Solute]_{water}} \tag{II.14}$$

$$\Delta G^o_{o/w_.} = \Delta G^o_{o_.} - \Delta G^o_{w_.} \tag{II.15}$$

$$Log\ K_{o/w} = \frac{-\Delta G^o_{o/w_.}}{2.303RT} \tag{II.16}$$

$$\Delta G^o_{solv_.} = \Delta G_{ENP_.} + \Delta G_{CDS_.} \tag{II.17}$$

Where log K_{ow} (I)i is the contribution to log K_{ow} of the first order group of type i occurring Ni times in the molecule, and K = 0.543 (± 0.012)(MARRERO; GANI, 2002).

$\Delta G^o_{o/w_.}$, $\Delta G^o_{o_.}$,, ΔG^o_w, $\Delta G^o_{solv_.}$ denotes the difference between the free energy of the solute molecule in 1- octanol and in water, solvation free energies of the solute molecule in water and

1- octanol and solvation energy in any solvent respectively. ΔG_{ENP} and ΔG_{CDS} are electrostatic (ΔGENP) and cavity-dispersion, R is Gas constant and T is the temperature.

II.2.7 Process Simulation

The theoretical models previously developed for separation processes using ILs (ARCE; RODRÍGUEZ; SOTO, 2007; MEINDERSMA, 2005; MEINDERSMA et al., 2006; MEINDERSMA; DE HAAN, 2008; SHIFLETT; YOKOZEKI, 2006) conclude that ILs can be regenerated from their mixtures with conventional organic solvents by low-pressure evaporation or organic solvent stripping. Thus, this study considers that the product mixtures, methanol, formic acid, and water can be easily recovered from the ILs by simple flash evaporation. Taylor et al. (2010) (TAYLOR et al., 2010), claim the feasibility of ILs vacuum distillation. Vacuum distillation was used with ILs in several other applications. For example, it was found during the reduction of ketones in 1-Butyl-3-methylimidazolium hexafluorophosphate ([BMIM][PF6]) that some of the alcohols produced could be removed under high vacuum, enabling to reuse of the ionic liquid for further reactions (HOWARTH; JAMES; DAI, 2001). Also, isolation of biaryl products obtained in a Suzuki cross-coupling reaction with 1-Butyl-3-methylimidazolium tetrafluoroborate ([BMIM][BF_4]) can be easily accomplished by heating under vacuum to 80ºC, allowing repeated catalytic runs (MATHEWS; SMITH; WELTON, 2000). 1-ethyl-3-methyl imidazolium 4-ethylbenzenesulfonate ([EMIM][e$PhSO_3$]) and 1-ethyl-3-methyl imidazolium methanesulfonate ([EMIM][$MeSO_3$]) were separated from methanol at 5kPa and 175ºC, in an application developed for BASF to alter the equilibrium of several azeotropic systems (JORK et al., 2004).

To evaluate the potential ILs candidates selected from the previous steps, a flash separation process based on VLE was rigorously simulated and optimized. The physical and chemical properties of the ILs need to be incorporated in the Aspen plus database to simulate the ILs-based separation process.

II.2.7.1 Component definition in Aspen Plus

ILs are pseudo-components in Aspen plus by specifying their normal boiling temperature, density, and molecular weight. The normal boiling point of ILs were estimated by the extended Group contribution (GC) method of Valderrama and Rojas (VALDERRAMA; FORERO; ROJAS, 2012); the densities were estimated by COSMO-RS calculation,(PALOMAR et al., 2007), while the molecular weights were known.

The other pseudo-component characteristics needed for the process simulation were estimated by the implicit techniques and models in Aspen Plus. Other compounds (formic acid, methanol,

CO_2, hydrogen, and water), except ILs, were defined as conventional components in the Aspen databank. The component definition method is reliable for the simulation of ILs-based aromatic/aliphatic hydrocarbon separation process (DE RIVA et al., 2016). The COSMO-SAC property model in Aspen Plus was chosen to predict the activity coefficients of all the components in the mixtures. Aspen Plus pure component parameters for the ILs, component molecular volumes (CSACVL), and sigma profiles were user-specified, while other components were retrieved from the Aspen database (FERRO et al., 2012a). A simple flash separation flowsheet depicting the presented case study is shown in figure II.9.

II.2.7.2 Computational Details

The computational procedure for optimization and energy calculation of the ILs molecular structure developed by Ferro et al. (2012) (FERRO et al., 2012a) was implemented in this study. The structures of the ILs were optimized using the Gaussian03 quantum chemical package at the computational level of B3LYP/6-31++G(d, p) basis set (FRISCH et al., 2004). The water/octanol partition was implemented with the continuum solvation model based on desity (SMD).

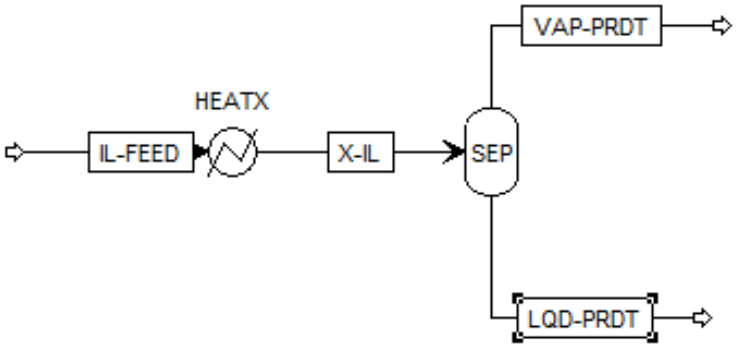

Figure II.9. Flowsheet of the process separation

II.3 Results and Discussions

This section presents findings for the selection of ILs using the approach proposed. It comprises conventional benchmark solvent, liquid-liquid equilibrium, Gas capacity, physical properties, partition coefficient, and continuous process separation.

II.3.1 Benchmark Screening

The results of the thermodynamic criteria on LLE and the capacity of six different organic solvents are presented in Table II.1 The organic solvents were screened by the gas capacity and LLE thermodynamic property criteria. Dimethylformamide (DMF) was selected as the organic solvent with better CO_2 capacity. However, the LLE mass-based results indicate no-phase splitting (β =1 and S =1). The solvent loss for the selected solvent (DMF) was higher than all

the ILs in this work. Therefore, values in the range of 0.001 to 1 can be used as the benchmark for the screening. However, in this work, a solvent loss given as IL/solute mass ratio equal to 0.5 was selected to allow a substantial number of ILs candidates for the next screening step. In the work by Song et al. (2017) (SONG et al., 2017), the solvent loss calculated for sulfolane, a conventional benchmark solvent, was 9.09 × 10−3 (unit). This value was used as a reference for this choice herein.

Table II.1. Capacity of organic solvents for CO_2 and H_2 extraction. Capacities calculated at 298.15 K and 1 bar with CosmothermX

Solvents	CO_2 Capacity (mol_{CO2}/mol $_{solvent}$)	H_2 Capacity (mol_{H2}/mol $_{solvent}$)
Dimethylsulfoxide	0.021	0.00017
Tetrahydrofuran	0.021	0.0037
Dimethylformamide	0.023	0.00029
Isopropylacetate	0.017	0.0006
n-butylacetate	0.020	0.00061
Isopentanol	0.022	0.00034

II.3.2 Pre-Screening by Thermodynamic Criteria

In COSMO-RS, 16 cations and 15 anions were chosen from the CosmothermX database, leading to 240 IL candidates. Details of the cations and anions are given in Table II.2. The global mass compositions of the mixture of the solvents (ILs) and other components (formic acid, methanol, and water) were assumed to be in equal proportion (1:1:1:1). These components are a mixture of the products of the reaction. The studied process considered the simultaneous production of methanol and formic acid at different reaction conditions(BELLO et al., 2021a). To compare the mass-based extraction of different ILs, the mass ratio of ILs to the solutes was set at an equal proportion in the LLE calculation. For example, 100g of water (phase 1), 100g of formic acid (phase 2), and 100g of the ionic liquid (phase 3) were set. The extended option in CosmothermX allows adding additional mole of any solute.

Table II.2. Cations and Anions of the ILs

Cations	Anions
1-heptyl-3-methyl-imidazolium	Sulphate (SO_4^-)

1-octyl-3-methyl-imidazolium	Chlorine (Cl^-)
Pyrrolidine+	Flouride (F^-)
Ammonium (NH_4^+)	2-chlorophenol
Hydronium (H_3O^+)	3-chlorophenol
Sodium (Na^+)	4-chlorophenol
1-butyl-2,3-dimethyl-imidazolium	Benzoate
1-butyl-3-methyl-imidazolium	Tetrafluoroborate (BF_4^-)
1-ethyl-2,3-dimethyl-imidazolium	Bis((trifluoromethyl)sulfonyl)imide
1-ethyl-3-methyl-imidazolium	Butylsulfate
1-hexyl-3-methyl-imidazolium	Ethylsulfate
1-pentyl-3-methyl-imidazolium	Nitrite (NO_2^-)
4-methyl-n-butylpyridinium	Octylsulfate
$Aniline^+$	Hexafluorophosphate (PF_6^-)
N-butyl-isoquinolinium	Toluene-4-sulfonate
$Pyridine^+$	

For the screening of ILs as extraction solvents, all the thermodynamic calculations were carried out at 298.15K, and atmospheric pressure (1bar) and the thermodynamic parameters (β, S, and SL) were correspondingly obtained from equations 5-7. Table S1 in the Supporting Information shows the results from COSMO-RS prediction of the LLE of all IL candidates. According to the thermodynamic screening, all the ILs satisfied the distribution coefficient criterion (β>1), while 211 ILs satisfied the selectivity criterion (S>1) and 98 ILs were selected after the solvent loss criterion was applied, as shown in Tables S2, S3 and S4, respectively, in the Supporting Information.

II.3.3 Gas Solubility/Capacity

The thermodynamic criteria consider the prediction of the capacity at infinite dilution. H_2 as a component in the solvating mixture was omitted, as previously stated. The predicted results based on the solubility of CO_2 are presented in the Supporting Information, in Table S5. The corresponding pre-screened ILs, after the criterion of molar basis capacity >0.023 was applied, are shown in Table S6 in the Supporting Information. It also reveals that mole-based screening

differs from mass-based screening. For instance, 1-butyl-2,3-dimethyl-imidazolium nitrite with gas capacity of 4.07 mol_{CO2}/mol_{IL} and corresponding capacity of 0.9 g_{CO2}/g_{IL} differs from 1-ethyl-3-methyl-imidazolium nitrite with 4.0 mol mol_{CO2}/mol_{IL} to 1.13 g_{CO2}/g_{IL} capacity.

II.3.4 Screening By Physical Property Constraints

The selected ILs from LLE (89) and capacity criteria (240) were screened out by the melting point and viscosity criteria to determine further prospective ILs with desired properties for the solvation and extraction processes. The ILs are requested to be liquid under operational conditions; therefore, the melting temperature of ILs should be below 298.15K (HU et al., 2019). Tables S7 and S8 in the Supporting Information showed that 157 and 40 ILs from the gas capacity and LLE criteria, respectively, satisfied the melting point constraint. Furthermore, these ILs were screened through the viscosity constraint < 100 cP (at 298.15 K) to ensure that the selected ILs have relatively low viscosity (Tables S9 and S10 in the Supporting Information). Viscosities above this threshold become an obstacle beyond which the number of needed transfer units would rapidly increase, and the ability to manage separation becomes increasingly difficult (SEILER et al., 2004).

Consequently, 11 and 10 ILs from capacity and LLE criteria, respectively, satisfied the viscosity constraint. These ILs are listed in Table II.3. Selected ILs after the first and second screenings (LLE-mass based route) and together with their LLE results (β, S, and SL), as well as their melting point (T_m) and viscosity (η). However, T_m and η of some ILs that satisfy the thermodynamic criteria could not be predicted by the software because the melting point model at Triple Zeta Valence Polarization (TZVP) level of theory parametrization in cosmothermX cannot be applied to the combination of cations and anions of the ILs in question. Therefore, although the ILs may meet the physical property constraints, they were discarded in this step.

Table II.3. Selected ILs after the first and second screenings (LLE-mass based route)

Combination Number	Cation	Anion	Melting Point (K)	Viscosity (cP)
42	Pyrrolidine	NO_2^-	133.3	58.1
117	1-butyl-3-methyl-imidazolium	NO_2^-	165.5	60.9
132	1-ethyl-2,3-dimethyl-imidazolium	NO_2^-	169.7	36.3
140	1-ethyl-3-methyl-imidazolium	3-chlorophenol	204.8	79.7
141	1-ethyl-3-methyl-imidazolium	4-chlorophenol	230.1	83.9

147	1-ethyl-3-methyl-imidazolium	NO_2^-	155.6	34.6
177	1-pentyl-3-methyl-imidazolium	NO_2^-	170.2	79.9
230	Pyridine	3-chlorophenol	185.3	94.2
231	Pyridine	4-chlorophenol	212.5	99.1
237	Pyridine	NO_2^-	130.5	35.1

Table II.4. Selected ILs after the first and second screenings (Gas capacity route)

Combination Number	Cation	Anion	Gas Capacity mol_{CO2}/mol_{IL}	Melting Point (K)	Viscosity (cP)
102	1-butyl-2,3-dimethyl-imidazolium	NO_2^-	4.1	178.8	60.4
117	1-butyl-3-methyl-imidazolium	NO_2^-	2.9	165.5	60.9
125	1-ethyl-2,3-dimethyl-imidazolium	3-chlorophenol	3.3	218.8	79.6
126	1-ethyl-2,3-dimethyl-imidazolium	4-chlorophenol	3.4	245.8	83.9
132	1-ethyl-2,3-dimethyl-imidazolium	NO_2^-	5.5	169.7	36.3
147	1-ethyl-3-methyl-imidazolium	NO_2^-	4.0	155.6	34.6
177	1-pentyl-3-methyl-imidazolium	NO_2^-	2.8	170.2	79.4
192	4-methyl-n-butylpyridinium	NO_2^-	3.4	172.1	59.4
222	n-butyl-isoquinolinium	NO_2^-	3.3	173.3	75.5
230	Pyridine	3-chlorophenol	1.22	185.26	94.2
231	Pyridine	4-chlorophenol	1.24	212.53	99.1

II.3.5 Qualitative Selection

From the screened ILs after physical property constraints through capacity and LLE thermodynamic criteria, it is evident that some ILs satisfy both cases. These ILs are subjected to the following screening step, and the remaining ones are discarded. Six ILs from both routes satisfy this constraint. The qualitative selection results are shown in table II.5.

Table II.5. Selected ILs satisfying gas capacity and LLE mass-based routes

Combination Number	Cation	Anion
117	1-butyl-3-methyl-imidazolium	NO_2^-
132	1-ethyl-2,3-dimethyl-imidazolium	NO_2^-
147	1-ethyl-3-methyl-imidazolium	NO_2^-
177	1-pentyl-3-methyl-imidazolium	NO_2^-
230	Pyridine	3-chlorophenol
231	Pyridine	4-chlorophenol

II.3.6 Octanol/Water Coefficient

To select a solvent with inherent safety, the potential solvent must comply with safety requirements. The octanol/water partition coefficient (K_{ow}) is defined as the concentration ratio of the concentrations of the organic substance in the n-octanol phase and the water phase at specified temperature after reaching distribution equilibrium (HU et al., 2019). K_{ow} is indirectly associated with the toxicity by lethal concentration (LC50), while LC50 is linearly related to log K_{ow} (HU et al., 2019). The value of LC50 is less than 2mg/L corresponding to log $K_{ow} < 3$ (MEDINA-HERRERA et al., 2014). The toxic effect of ILs on environmental organisms is based on many variables such as plant resistance, environmental concentration, or composition (anion, cation, and length of alkyl chain) (THUY PHAM; CHO; YUN, 2010). After the screening, all the pre-screened ILs from the previous steps that satisfy this constraint are selected for the final screening. The toxicity results are presented in table II.6.

Table II.6. IL candidates satisfying the toxicity constraint

Combination Number	Cation	Anion	Log K_{ow}	
			GC	DFT
117	1-butyl-3-methyl-imidazolium	NO_2^-	2.29	0.019
132	1-ethyl-2,3-dimethyl-imidazolium	NO_2^-	2.74	-0.007
147	1-ethyl-3-methyl-imidazolium	NO_2^-	1.39	-0.009
177	1-pentyl-3-methyl-imidazolium	NO_2^-	1.65	-0.007

II. 3.7 Process Separation Performance

The ability to favorably separate/extract the product of the CO_2 hydrogenation (methanol, water, and formic acid) from the ILs is one of the objectives of this work. Based on Table II.6, 1-butyl-3-methyl-imidazolium nitrite ([BMIM][NO_2]),1-ethyl-2,3-dimethyl-imidazolium nitrite ([EDMIM][NO_2]),1-ethyl-3-methyl-imidazolium nitrite ([EMIM][NO_2]), and 1-pentyl-3-methyl-imidazolium nitrite ([PMIM][NO_2]) were selected for the continuous separation process.

II. 3.7.1 Vapor-Liquid Equilibrium (VLE) of Mixture

The VLE diagrams of the mixture (ILs + methanol + formic acid + water) were calculated using the COSMO-SAC model (Aspen Plus, V9.0). COSMO-RS estimated VLE data with the ILs. A comparison with other published models was attempted, but the lack of sufficient details and unavailability of required parameters of the ionic liquid made it difficult. Since ionic liquids behave differently because of their composition, it becomes difficult to compare with a different system. Further to this work, we performed a computational calculation on the selected ILs, and the results were submitted for publication. Also, experimental works to ascertain the result of these theoretical calculations will be carried out further. Figures II.3a and b depict experimental results of the VLE of 1-methyl-3-ethyl-imidazolium bis(trifluoromethyl-sulfonyl)imide and Nonan-2-one conducted by Verevkin (2004) (VEREVKIN et al., 2004) and the ionic liquids selected in this work. At the time of this work, experimental data for the selected ILs for the final screening were not found in the literature. Moreover, for the validation of the predictive method used, this experimental data was chosen as a reference. According to the experimental result, there is a similar behavior to the selected

ILs at low pressure. The ILs are mainly in the liquid phase. The comparison presented here shows that this study's predictive method can be applied for other ILs.

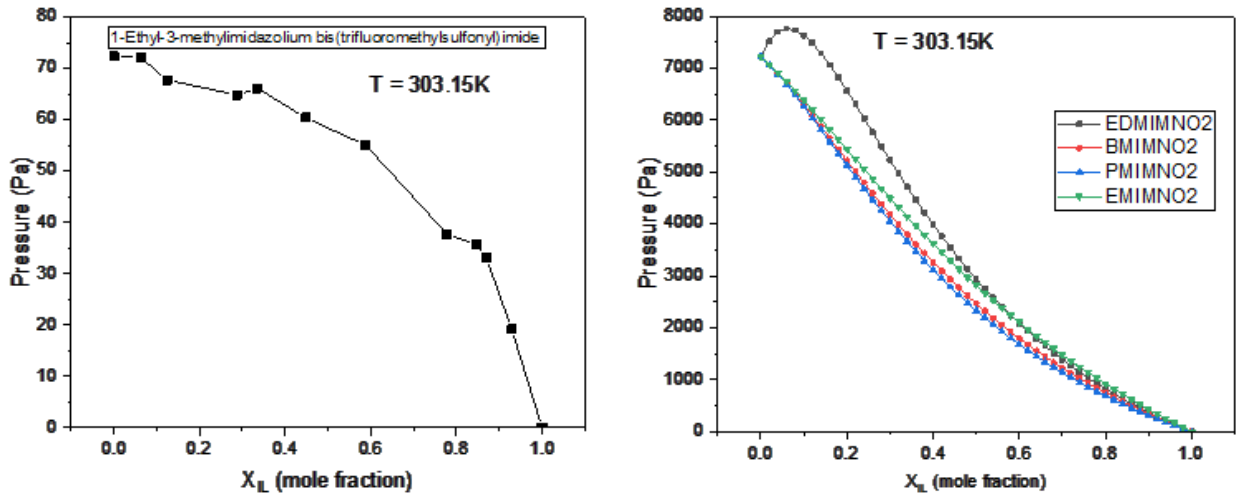

(a) **(b)**

Figure II.10: Phase diagrams: (a) C2mimNTf2 + Nonan-2-one as a reference, (b) selected ILs + organic solute (Formic acid or methanol)

II.3.7.2 Operating Conditions for the VL Separator/Regeneration of ILs

The results of the regeneration of the ILs from methanol, formic acid, and water in the product mixture are shown in Table S11 in the Supporting Information. The operating pressures depend on the nature of both the organic solute and the ILs. The separators were operated at pressures below atmospheric pressure (0.11 - 0.33bar) and a temperature of 150 ºC. This aligns with the recommendation by researchers on vacuum distillation to maintain the integrity of the ILs (to avoid thermal decomposition). The pressure should be decreased between 0.05 - 0.3bar to maintain the working temperature of the VL separator below 150ºC (FERRO et al., 2012b). According to Ferro et al. (2012) (FERRO et al., 2012a), low-pressure evaporation as a way of regenerating the ILs from their mixtures with organic solutes is a peculiar state of the VLE due to the high volatility difference of the components in the mixture. Herein, approximately 99.99% of the ILs were regenerated at T=150 ºC and 0.11 < P < 0.33bar as seen in table II.7

II.3.7.3 Separation Performance

The separation system was optimized to recover more than 99 % of the ILs (Table II.7). The mole fractions of the organic solute in the vapor product, formic acid, methanol, and water are approximately 0.28, 0.19, and 0.50, respectively. The separation performance of the ILs from their mixtures (ILs + products) is summarized in Table II.7

Table II.7. Mole fraction of recovered ILs at different operating pressures

Components	Pressure (bar)	Temperature (ºC)	IL Recovered (mole frac)
BMIMNO2	0.33	150	0.99
PMIMNO2	0.11	150	0.99
EMIMNO2	0.11	150	0.99
EDMIMNO2	0.11	150	0.99

II.3.7.4 Energy Consumption

For the systems under consideration (ILs + products), the organic solvent vaporization's net duties (separator) from its feed mixture of ILs are in the range of 1241 - 1296 kJ/kgIL regeneration. Additionally, the pre-heater net duties of the feed mixture are in the range of 49.5 – 52.3 kJ/kgIL. These results agree with the benchmark regeneration (DMF) duty (1983kJ/ kJ/kgDMF) as they are in the same order of magnitude. However, a significant fraction of DMF was lost at the operating condition of 150ºC and 0.11bar). The energy consumption results are presented in figure II.11.

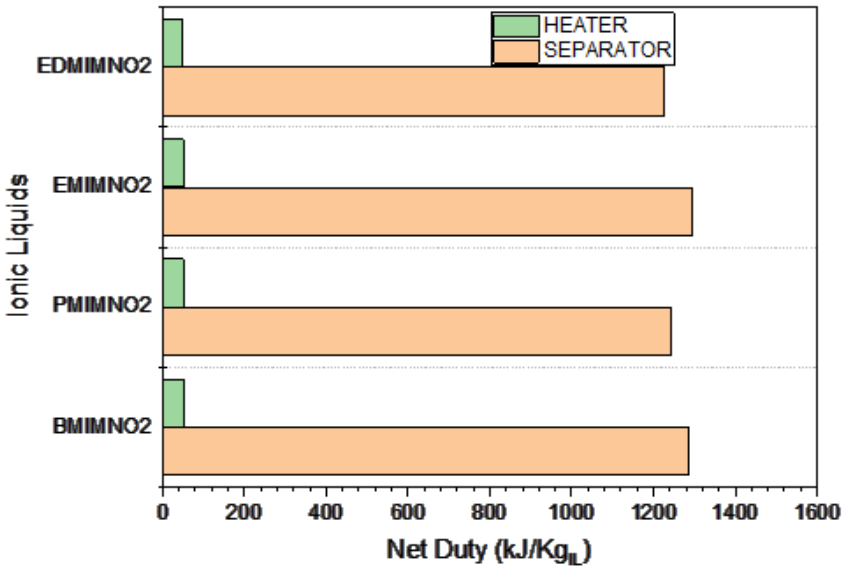

Figure II.11. Energy consumption of the feed mixture of ILs and solutes in the pre-heater and Separator

The calculated heat of vaporization (Qvap) of the ILs in the mixture is in the range of 297 - 601 kJ/kg IL regenerated; for the formic acid, 499 -508 kJ/kg IL regenerated; for the methanol,

663-757.6 kJ/kg IL regenerated and for the water, 1938 - 2145 kJ/kg IL regenerated as seen in figure II.1. In reference to Ferro et al. (2012) (FERRO et al., 2012a), Qvap can be considered a measure of the strength of the interactions between the ILs and the organic solutes in the liquid phase. Additionally, Qvap increases with the length of the alkyl chain in mixtures of ILs (imidazolium cations and NO_2 anion) and the products (Methanol + formic acid + water). The exception to this behavior is edmimNO_2, with the highest heat of vaporization of 601.7kJ/kg IL regenerated. This might be due to the multiple alkyl branches in the IL. A similar result from Ferro et al. (2012) (FERRO et al., 2012a) confirmed the increment in the heat of vaporization with an increase in the alkyl chain of 1-alkyl-3-methyl imidazolium NTf2 ILs with the studied organic solvents.

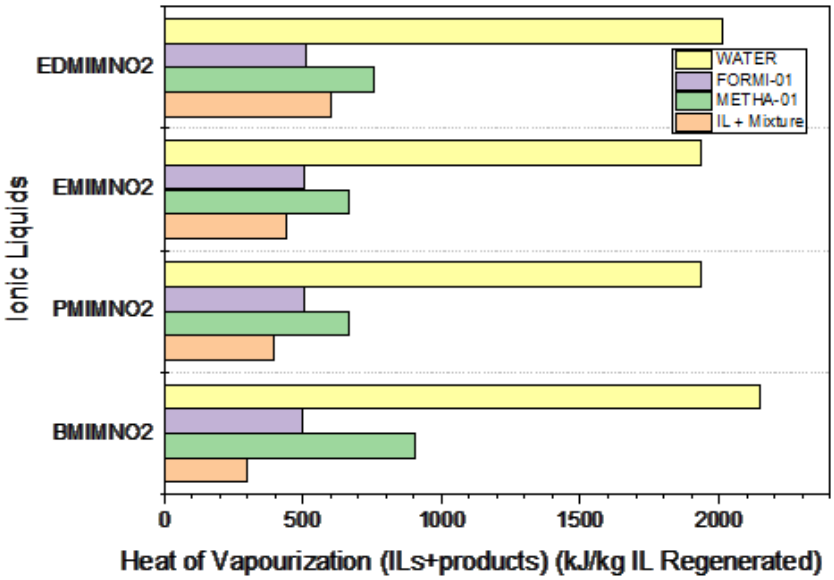

Figure II.12. The heat of vaporization of ILs + organic solutes at 150 oC and 0.11bar

II.4. Conclusion

This study has shown that the procedure developed can select suitable solvents for formic acid and methanol synthesis. Furthermore, the thermodynamic limitations of the hydrogenation process can be overcome with solvents with better physical and thermodynamic properties.

The solvent loss of individual ILs shows good agreement with the predicted LLE extraction. Recovery of more than 99% of the ILs from organic solvent mixtures is feasible by evaporating the volatile component under vacuum between 0.22 -0.66 bar and heat duty for the ILs regeneration of 4967 - 5185 kJ/hr. The separation duty increases with increasing alkyl chain content. ILs with more branch alkyl groups proved to be more efficient for this application than others with just one branch group because of their separation performance. The screening

method can be easily extended to select attractive ILs solvents for other multi-objective applications. Furthermore, for the estimation of physical and chemical properties of unknown ILs necessary for their selection, the calculation procedure was developed with comparable results with other work.

The availability of the selected ILs plays a significant factor in its industrial application; however, due to the unavailability of data in the literature on the final optimal ILs selected, their synthesis can follow a similar conventional synthesis method for room temperature halide-free IL most especially the imidazolium salts.

Acknowledgments

The authors gratefully acknowledge the support of the RCGI – Research Centre for Gas Innovation, hosted by the University of São Paulo (USP) and sponsored by FAPESP – São Paulo Research Foundation (2014/50279-4) and Shell Brasil. This study was financed in part by the Personnel Coordination of Improvement of Higher Level - Brazil (CAPES) - Finance Code 001

Supporting Information.

Information about the evaluated cations and anions and complete Tables of COSMO-RS estimated results by thermodynamic criteria (Gas capacity, Distribution coefficient, selectivity, and Solvent loss), Melting point, and Viscosity of Ionic Liquids. The Supporting Information is available free of charge on the ACS Publications website at http://pubs.acs.org/.

Author Contributions

The manuscript was written through the contributions of all authors. All authors have given approval to the final version of the manuscript. Taofeeq O. Bello, Antonio E. Bresciani, Claudio.A.O. Nascimento, and Rita M. B. Alves

Abbreviations

$BmimNO_2$	1-butyl-3-methyl-imidazolium nitrite
BmimOH	1-butyl-3-methyl-imidazolium hydroxide
BP_TZVP	Becke-Perdew Triple Zeta Valence Polarization
C	Molar Gas Capacity/Solubility

CO_2	Carbon dioxide
COSMO-RS	Conductor-like Screening Model for Real Solvents
COSMO-SAC	Conductor-like Screening Model for Solvents Activity coefficient
CSACVL	Component Molecular Volumes
DMF	Dimethylformamide
DMF	Dimethylformamide
DMSO	Dimethylsulfoxide
E_{diel}	Dielectric Energy
$EdmimNO_2$	1-ethyl-2,3-dimethyl-imidazolium nitrite
$EmimePhSO_3$	1-ethyl-3-methyl-imidazolium 4-ethylbenzenesulfonate
EmimMeSO3	1-ethyl-3-methyl-imidazolium methane sulfonate
EmimNO2	1-ethyl-3-methyl-imidazolium nitrite
ΔG	Change in Gibbs energy of reaction
GC	Group Contribution
G_i	Mass gas capacity
H_{ring}, H_{0vdw}	Sum of COSMO-RS enthalpies of the ions
ILs	Ionic Liquids
K_i	Partition equilibrium constant
$K_{ow}(I)$	Contribution to log K_{ow}
K_{ow}	Octanol/Water Partition coefficient
LC50	Lethal Concentration
LLE	Liquid-Liquid Equilibrium
$m^E_{carrier}$	Mass of carrier in the Extract

$m^{E}_{carrier}$	Mass of carrier in the Raffinate
m^{E}_{solute}	Mass of solute in the Extract
M_{IL}	Mass of the Ionic Liquid
m^{R}_{solute}	Mass of solute in the Raffinate
$m^{R}_{solvent}$	Mass of solvent in the Raffinate
M_{solute}	Mass of the solute
$PmimNO_2$	1-pentyl-3-methyl-imidazolium nitrite
QSAR	Quantitative Structure-Activity Relationship
QSPR	Quantitative Structure-Property Relationships
Qvap	Heat of Vaporization
R^2	Coefficient of Determination
rm	Mean ionic liquid radius
RMSE	Root Mean Square Error
S	Selectivity
SL	Solvent Loss
T^-	Torsional degree of freedom anion
T^+	Torsional degree of freedom cation
THF	Tetrahydrofuran
T_m	Melting Point (K)
TZVP	Triple Zeta Valence Polarization
VLE	Vapor-Liquid Equilibrium
B	Distribution Coefficient
$\gamma^{\infty}_{i,IL}$	Activity coefficient at infinite dilution of solute *i* in IL phase

ε	Sum of Dielectric energies
η	Viscosity (cP)
μ^{I}	Chemical potential of compound i in phase I
μ^{II}	Chemical potential of compound i in phase II
σ^{-}	Symmetry number of anion
σ^{+}	Symmetry number of cation
∞	Infinite dilution

II.5 References

ÁLVAREZ, A. et al. **Challenges in the Greener Production of Formates/Formic Acid, Methanol, and DME by Heterogeneously Catalyzed CO2Hydrogenation ProcessesChemical Reviews**, 2017.

ANANTHARAJ, R.; BANERJEE, T. COSMO-RS-based screening of ionic liquids as green solvents in denitrification studies. **Industrial and Engineering Chemistry Research**, v. 49, n. 18, p. 8705–8725, 2010.

ANANTHARAJ, R.; BANERJEE, T. Aromatic sulfur-nitrogen extraction using ionic liquids: Experiments and predictions using an a priori model. **AIChE Journal**, v. 59, n. 12, p. 4806–4815, 2013.

ARCE, A.; RODRÍGUEZ, H.; SOTO, A. Use of a green and cheap ionic liquid to purify gasoline octane boosters. **Green Chemistry**, v. 9, n. 3, p. 247–253, 2007.

ARTZ, J. et al. Sustainable Conversion of Carbon Dioxide: An Integrated Review of Catalysis and Life Cycle Assessment. **Chemical Reviews**, v. 118, n. Sustainable Chemistry, p. 434−504, 2018.

BELLO, T. O. et al. Thermodynamic analysis of carbon dioxide hydrogenation to formic acid and methanol. **Chemical Engineering Science**, v. 242, p. 116731, 2021.

BERGER, A. et al. Ionic liquid-phase asymmetric catalytic hydrogenation: Hydrogen concentration effects on enantioselectivity. **Tetrahedron Asymmetry**, v. 12, n. 13, p. 1825–

1828, 2001.

COULING, D. J. et al. Assessing the factors responsible for ionic liquid toxicity to aquatic organisms via quantitative structure-property relationship modeling. **Green Chemistry**, v. 8, n. 1, p. 82–90, 2006.

DANNENFELSER, R.-M.; YALKOWSKY, S. H. Estimation of Entropy of Melting from Molecular Structure: A Non-Group Contribution Method. **Industrial and Engineering Chemistry Research**, v. 35, n. 4, p. 1483–1486, 1996.

DE RIVA, J. et al. Aspen Plus supported conceptual design of the aromatic-aliphatic separation from low aromatic content naphtha using 4-methyl-N-butylpyridinium tetrafluoroborate ionic liquid. **Fuel Processing Technology**, v. 146, p. 29–38, 2016.

DIEDENHOFEN, M.; ECKERT, F.; KLAMT, A. Prediction of infinite dilution activity coefficients of organic compounds in ionic liquids using COSMO-RS. **Journal of Chemical and Engineering Data**, v. 48, n. 3, p. 475–479, 2003.

DIEDENHOFEN, M.; KLAMT, A. COSMO-RS as a tool for property prediction of IL mixtures-A review. **Fluid Phase Equilibria**, v. 294, n. 1–2, p. 31–38, 2010.

DOMAŃSKA, U.; KRÓLIKOWSKA, M. Measurements of activity coefficients at infinite dilution in solvent mixtures with thiocyanate-based ionic liquids using glc technique. **Journal of Physical Chemistry B**, v. 114, n. 25, p. 8460–8466, 2010.

DOMAŃSKA, U.; WLAZŁO, M. Effect of the cation and anion of the ionic liquid on desulfurization of model fuels. **Fuel**, v. 134, p. 114–125, 2014.

DORTMUND DATABANK. **Dortmund databank**. Disponível em: <http://www.ddbst.com>. Acesso em: 21 ago. 2019.

DYSON, P. et al. Determination of hydrogen concentration in ionic liquids and the effect (or lack of) on rates of hydrogenation. **Chemical Communications**, p. 2418–2419, 2003.

DZYUBA, S. V.; BARTSCH, R. A. Expanding the polarity range of ionic liquids. **Tetrahedron Letters**, v. 43, n. 26, p. 4657–4659, 2002.

ECKERT, F.; KLAMT, A. **COSMOtherm Version C3.0 Release 16.01**. Disponível em: <www.cosmologic.de>. Acesso em: 12 jun. 2019.

ECKERT, F.; KLAMT, A. **COSMOthermX User Guide**. Disponível em: <www.cosmologic.de>. Acesso em: 21 jul. 2019.

ECKERT, F.; KLAMT, A. **COSMOtherm**LeverkusenCOSMOlogic GmbH & Co, , 2018.

EIDEN, P. et al. In silico predictions of the temperature-dependent viscosities and electrical conductivities of functionalized and nonfunctionalized ionic liquids. **Journal of Physical Chemistry B**, v. 115, n. 2, p. 300–309, 2011.

FARAHIPOUR, R.; AMIRHOSSEIN, M.; KARUNANITHI, A. T. A systematic screening methodology towards exploration of ionic liquids for CO2 capture processes | Elsevier Enhanced Reader. **Chemical Engineering Science**, v. 145, p. 126–132, 2016.

FARAHIPOUR, R.; MEHRKESH, A.; KARUNANITHI, A. T. A systematic screening methodology towards exploration of ionic liquids for CO<inf>2</inf> capture processes. **Chemical Engineering Science**, v. 145, p. 126–132, 2015.

FAYET, G.; ROTUREAU, P. How to use QSPR-type approaches to predict properties in the context of Green Chemistry. **Biofuels, Bioproducts and Biorefining**, v. 6, n. 3, p. 246–256, 2012.

FERREIRA, A. R. et al. An overview of the liquid-liquid equilibria of (ionic liquid + hydrocarbon) binary systems and their modeling by the conductor-like screening model for real solvents. **Industrial and Engineering Chemistry Research**, v. 50, n. 9, p. 5279–5294, 2011.

FERREIRA, A. R. et al. Overview of the liquid-liquid equilibria of ternary systems composed of ionic liquid and aromatic and aliphatic hydrocarbons, and their modeling by COSMO-RS. **Industrial and Engineering Chemistry Research**, v. 51, n. 8, p. 3483–3507, 2012.

FERRO, V. R. et al. Introducing process simulation in ionic liquids design/selection for separation processes based on operational and economic criteria through the example of their regeneration. **Separation and Purification Technology**, v. 97, p. 195–204, 2012a.

FERRO, V. R. et al. Introducing process simulation in ionic liquids design/selection for separation processes based on operational and economic criteria through the example of their regeneration. **Separation and Purification Technology**, v. 97, p. 195–204, 2012b.

FRISCH, M. . et al. **Gaussian03**Wallingford CT, 2004.

GAO, H. et al. Extractive desulfurization of fuel using N-butylpyridinium-based ionic liquids. **RSC Advances**, v. 5, n. 38, p. 30234–30238, 2015.

GORDON, C. M. New developments in catalysis using ionic liquids. **Applied Catalysis A: General**, v. 222, n. 1–2, p. 101–117, 2001.

GRASEMANN, M.; LAURENCZY, G. Formic acid as a hydrogen source - Recent developments and future trends. **Energy and Environmental Science**, v. 5, n. 8, p. 8171–

8181, 2012.

HAN, D.; ROW, K. H. Recent applications of ionic liquids in separation technology. **Molecules**, v. 15, n. 4, p. 2405–2426, 2010.

HANSMEIER, A. R.; MEINDERSMA, G. W.; DE HAAN, A. B. Desulfurization and denitrogenation of gasoline and diesel fuels by means of ionic liquids. **Green Chemistry**, v. 13, n. 7, p. 1907–1913, 2011.

HOWARTH, J.; JAMES, P.; DAI, J. Immobilized baker's yeast reduction of ketones in an ionic liquid, [bmim]PF<inf>6</inf> and water mix. **Tetrahedron Letters**, v. 42, n. 42, p. 7517–7519, 2001.

HU, Y. et al. Systematic approach for screening organic and ionic liquid solvents in homogeneous extractive distillation exemplified by the tert-butanol dehydration. **Separation and Purification Technology**, v. 211, n. June 2018, p. 723–737, 2019.

HULL, J. F. et al. Reversible hydrogen storage using CO2 and a proton-switchable iridium catalyst in aqueous media under mild temperatures and pressures. **Nature Chemistry**, v. 4, n. 5, p. 383–388, 2012.

ILTHERMO. **ILThermo**. Disponível em: <http://ilthermo.boulder.nist.gov>. Acesso em: 21 ago. 2019.

INOUE, Y. ; et al. Catalytic Fixation of Carbon dioxide to Formic Acid by Transition-Metal Complexes under Mild Conditions. **Chemistry Letters**, p. 863–864, 1976.

JESSOP, P. G.; IKARIYA, T.; NOYORI, R. Homogeneous Hydrogenation of Carbon Dioxide. **Chemical Reviews**, v. 95, n. 2, p. 259–272, 1995.

JIANG, T. et al. Solvent-free synthesis of substituted ureas from CO2 and amines with a functional ionic liquid as the catalyst. **Green Chemistry**, v. 10, n. 4, p. 465–46, 2008.

JORK, C. et al. Influence of ionic liquids on the phase behavior of aqueous azeotropic systems. **Journal of Chemical and Engineering Data**, v. 49, n. 4, p. 852–857, 2004.

KLAMT, A.; ECKERT, F. COSMO-RS: a novel and efficient method for the a priori prediction of thermophysical data of liquids. **Fluid Phase Equilibria**, v. 172, n. 1, p. 43–72, 2000.

KLAMT, A.; ECKERT, F.; ARLT, W. COSMO-RS: An Alternative to Simulation for Calculating Thermodynamic Properties of Liquid Mixtures. **Annual Review of Chemical and Biomolecular Engineering**, v. 1, n. 1, p. 101–122, 2010.

KOI, Z. K. et al. Prediction of the viscosity of imidazolium-based ionic liquids at different

temperatures using the quantitative structure property relationship approach. **New Journal of Chemistry**, v. 43, n. 41, p. 16207–16217, 2019.

KUNERTH, W. Solubility of CO2 and N2O in certain solvents. **Physical Review**, v. 19, n. 5, p. 512–524, 1922.

LAZZÚS, J. A. Estimation of density as a function of temperature and pressure for imidazolium-based lonic liquids using a multilayer net with particle swarm optimization. **International Journal of Thermophysics**, v. 30, n. 3, p. 883–909, 2009.

LAZZÚS, J. A. A group contribution method to predict the melting point of ionic liquids. **Fluid Phase Equilibria**, v. 313, p. 1–6, 2012.

LAZZÚS, J. A.; PULGAR-VILLARROEL, G. A group contribution method to estimate the viscosity of ionic liquids at different temperatures. **Journal of Molecular Liquids**, v. 209, p. 161–168, 2015.

LEE, B. S.; LIN, S. T. Screening of ionic liquids for CO2 capture using the COSMO-SAC model. **Chemical Engineering Science**, v. 121, p. 157–168, 2015.

LEI, Z.; ARLT, W.; WASSERSCHEID, P. Separation of 1-hexene and n-hexane with ionic liquids. **Fluid Phase Equilibria**, v. 241, n. 1–2, p. 290–299, 2006.

LEITNER, W. Carbon Dioxide as a Raw Material: The Synthesis of Formic Acid and Its Derivatives from CO<inf>2</inf>. **Angewandte Chemie International Edition in English**, v. 34, n. 20, p. 2207–2221, 1995.

LETCHER, T. M. et al. Activity coefficients at infinite dilution measurements for organic solutes in the ionic liquid trihexyltetradecylphosphonium-bis-(2,4,4-trimethylpentyl)-phosphinate using g.l.c. at T = (303.15, 308.15, 313.15, and 318.15) K. **Journal of Chemical Thermodynamics**, v. 40, n. 8, p. 1243–1247, 2008.

LINKE, W. F.; SEIDELL, A. Solubilities of Inorganic and Metal-Organic Compounds. **ACS**, v. 1, p. 1075, 1958.

LOMBARDO, L. et al. Mixtures of ionic liquid-Alkylcarbonates as electrolytes for safe lithium-ion batteries. **Journal of Power Sources**, v. 227, p. 8–14, 2013.

LÓPEZ-MARTIN, I. et al. Anion and cation effects on imidazolium salt melting points: A descriptor modelling study. **ChemPhysChem**, v. 8, n. 5, p. 690–695, 2007.

LUO, X. et al. Significant improvements in CO<inf>2</inf> capture by pyridine-containing anion-functionalized ionic liquids through multiple-site cooperative interactions. **Angewandte**

Chemie - International Edition, v. 53, n. 27, p. 7053–7057, 2014.

MACFARLANE, D. R. et al. Ionic liquids and their solid-state analogues as materials for energy generation and storage. **Nature Reviews Materials**, v. 1, n. 2, 2016.

MACFARLANE, P. D. R.; KAR, D. M.; PRINGLE, D. J. M. **Fundamentals of Ionic Liquids Ionic Liquids in Biotransformations and Electrodeposition from Ionic Handbook of Green Chemistry – Green Solvents Electrochemical Aspects of Ionic Liquids , 2nd edition Nanocatalysis in Ionic Liquids**. [s.l: s.n.].

MARCINIAK, A. Influence of cation and anion structure of the ionic liquid on extraction processes based on activity coefficients at infinite dilution. A review. **Fluid Phase Equilibria**, v. 294, n. 1–2, p. 213–233, 2010.

MARENICH, A. V.; CRAMER, C. J.; TRUHLAR, D. G. Universal solvation model based on solute electron density and on a continuum model of the solvent defined by the bulk dielectric constant and atomic surface tensions. Journal of Physical Chemistry B, v. 113, n. 18, p. 6378–6396, 2009.

MARRERO, J.; GANI, R. Group-contribution-based estimation of octanol/water partition coefficient and aqueous solubility. **Industrial and Engineering Chemistry Research**, v. 41, n. 25, p. 6623–6633, 2002.

MARTINS, M. A. R. et al. Selection of Ionic Liquids to be Used as Separation Agents for Terpenes and Terpenoids. **ACS Sustainable Chemistry and Engineering**, v. 4, n. 2, p. 548–556, 2016.

MATHEWS, C. J.; SMITH, P. J.; WELTON, T. Palladium catalysed suzuki cross-coupling reactions in ambient temperatare ionic liquids. **Chemical Communications**, n. 14, p. 1249–1250, 2000.

MEDINA-HERRERA, N. et al. An approach for solvent selection in extractive distillation systems including safety considerations. **Industrial and Engineering Chemistry Research**, v. 53, n. 30, p. 12023–12031, 2014.

MEINDERSMA, G. W. **Extraction of Aromatics from Naphtha with Ionic Liquids; From Solvent Development to Pilot RDC Evaluation**. [s.l.] University of Twente, 2005.

MEINDERSMA, G. W. et al. Separation of aromatic and aliphatic hydrocarbons with ionic liquids. **Chemical Engineering Communications**, v. 193, n. 11, p. 1384–1396, 2006.

MEINDERSMA, G. W.; DE HAAN, A. B. Conceptual process design for aromatic/aliphatic

separation with ionic liquids. **Chemical Engineering Research and Design**, v. 86, n. 7, p. 745–752, 2008.

MORET, S.; DYSON, P. J.; LAURENCZY, G. Direct synthesis of formic acid from carbon dioxide by hydrogenation in acidic media. **Nature Communications**, v. 5, p. 1–7, 2014.

MORTAZAVI-MANESH, S.; SATYRO, M. A.; MARRIOTT, R. A. Screening Ionic Liquids as Candidates for Separation of Acid Gases: Solubility of Hydrogen Sulfide, Methane, and Ethane in Wiley Online Library. **American Institute of Chemical Engineers AIChE J**, v. 59, p. 2993–3005, 2013.

OLIVIER-BOURBIGOU, H.; MAGNA, L.; MORVAN, D. Ionic liquids and catalysis: Recent progress from knowledge to applications. **Applied Catalysis A: General**, v. 373, n. 1–2, p. 1–56, 2010.

PALOMAR, J. et al. Density and molar volume predictions using COSMO-RS for ionic liquids. An approach to solvent design. **Industrial and Engineering Chemistry Research**, v. 46, n. 18, p. 6041–6048, 2007.

PREISS, U.; BULUT, S.; KROSSING, I. In silico prediction of the melting points of ionic liquids from thermodynamic considerations: A case study on 67 salts with a melting point range of 337 °c. **Journal of Physical Chemistry B**, v. 114, n. 34, p. 11133–11140, 2010.

QIN, L. et al. Selection of Imidazolium-Based Ionic Liquids for Vitamin e Extraction from Deodorizer Distillate. **ACS Sustainable Chemistry and Engineering**, v. 4, n. 2, p. 583–590, 2016.

RADAI, Z.; KEGLEVICH, G.; ZSUZSA KISS, N. An Overview of the Applications of Ionic Liquids as Catalysts and Additives in Organic Chemical Reactions. **Current Organic Chemistry**, v. 22, n. 5883, p. 533–556, 2018.

ROPEL, L. et al. Octanol-water partition coefficients of imidazolium-based ionic liquids. **Green Chemistry**, v. 7, n. 2, p. 83–90, 2005.

SCHAUB, T.; PACIELLO, R. A. A process for the synthesis of formic acid by CO2 hydrogenation: Thermodynamic aspects and the role of CO. **Angewandte Chemie - International Edition**, v. 50, n. 32, p. 7278–7282, 2011.

SCHREINER, P. R. Metal-free organocatalysis through explicit hydrogen bonding interactions. **Chemical Society Reviews**, v. 32, n. 5, p. 289–296, 2003.

SEILER, M. et al. Separation of azeotropic mixtures using hyperbranched polymers or ionic

liquids. **AIChE Journal**, v. 50, n. 10, p. 2439–2454, 2004.

SHIFLETT, M. B.; YOKOZEKI, A. Separation of difluoromethane and pentafluoroethane by extractive distillation using ionic liquid. **Chimica Oggi**, v. 24, n. 2, p. 28–30, 2006.

SONG, Z. et al. Effect of cation alkyl chain length on liquid-liquid equilibria of {ionic liquids + thiophene + heptane}: COSMO-RS prediction and experimental verification. **Fluid Phase Equilibria**, v. 425, p. 244–251, 2016.

SONG, Z. et al. Systematic Method for Screening Ionic Liquids as Extraction Solvents Exemplified by an Extractive Desulfurization Process. **ACS Sustainable Chemistry and Engineering**, v. 5, n. 4, p. 3382–3389, 2017.

SORDAKIS, K. et al. Homogeneous Catalysis for Sustainable Hydrogen Storage in Formic Acid and Alcohols. **Chemical Reviews**, v. 118, n. 2, p. 372–433, 2018a.

SORDAKIS, K. et al. Homogeneous Catalysis for Sustainable Hydrogen Storage in Formic Acid and Alcohols. **Chemical Reviews**, v. 118, n. 2, p. 372–433, 2018b.

SUN, Y. et al. A re-examination of pressure effects on enantioselectivity in asymmetric catalytic hydrogenation. **Journal of the American Chemical Society**, v. 118, n. 6, p. 1348–1353, 1996.

TAYLOR, A. W. et al. High vacuum distillation of ionic liquids and separation of ionic liquid mixtures. **Physical Chemistry Chemical Physics**, v. 12, n. 8, p. 1772–1783, 2010.

THUY PHAM, T. P.; CHO, C.-W.; YUN, Y.-S. Environmental fate and toxicity of ionic liquids: A review. **Water Research**, v. 44, n. 2, p. 352–372, 2010.

VALDERRAMA, J. O.; FORERO, L. A.; ROJAS, R. E. Critical properties and normal boiling temperature of ionic liquids. Update and a new consistency test. **Industrial and Engineering Chemistry Research**, v. 51, n. 22, p. 7838–7844, 2012.

VEREVKIN, S. P. et al. Thermodynamic properties of mixtures containing ionic liquids: Activity coefficients of aldehydes and ketones in 1-methyl-3-ethyl-imidazolium bis(trifluoromethyl-sulfonyl) imide using the transpiration method. **Fluid Phase Equilibria**, v. 218, n. 2, p. 165–175, 2004.

WANG, W. .; HIMEDA, Y. Recent Advances in Transition Metal-Catalysed Homogeneous Hydrogenation of Carbon Dioxide in Aqueous Media. **School of Enviromental Sciences**, p. 250–264, 2012.

WASSERSCHEID, P.; ANNEGRET, S. **Green Solvents : Ionic Liquids**. Weinheim: Wiley-

VCH, 2010. v. 6

WELTON, T. Room-Temperature Ionic Liquids. Solvents for Synthesis and Catalysis. **Chemical Reviews**, v. 99, p. 2071–2083, 1999.

WELTON, T. Ionic liquids in catalysis. **Coordination Chemistry Reviews**, v. 248, n. 21–24, p. 2459–2477, 2004.

WERNER, S.; HAUMANN, M.; WASSERSCHEID, P. Ionic Liquids in Chemical Engineering. **Annual Review of Chemical and Biomolecular Engineering**, v. 1, n. 1, p. 203–230, 2010.

WU, Y. et al. Tetrabutylphosphonium-Based Ionic Liquid Catalyzed CO<inf>2</inf> Transformation at Ambient Conditions: A Case of Synthesis of α-Alkylidene Cyclic Carbonates. **ACS Catalysis**, v. 7, n. 9, p. 6251–6255, 2017.

YOUNG, C. L. **IUPAC Solubility Data Series**OxfordPergamon Press, , 1981.

ZHANG, S. et al. Fixation and conversion of CO2 using ionic liquids. **Catalysis Today**, v. 115, n. 1–4, p. 61–69, 2006a.

ZHANG, S. et al. Physical properties of ionic liquids: Database and evaluation. **Journal of Physical and Chemical Reference Data**, v. 35, n. 4, p. 1475–1517, 2006b.

ZHANG, X.; LIU, Z.; WANG, W. Screening of ionic liquids to capture CO2 by COSMO-RS and experiments. **AIChE Journal**, v. 54, n. 10, p. 2717–2728, out. 2008.

ZHAO, H. et al. Tuning task-specific ionic liquids for the extractive desulfurization of liquid fuel. **ACS Sustainable Chemistry and Engineering**, v. 4, n. 9, p. 4771–4780, 2016a.

ZHAO, Y. et al. Toxicity of ionic liquids: Database and prediction via quantitative structure-activity relationship method. **Journal of Hazardous Materials**, v. 278, p. 320–329, 2014.

ZHAO, Y. et al. Azole-Anion-Based Aprotic Ionic Liquids: Functional Solvents for Atmospheric CO<inf>2</inf> Transformation into Various Heterocyclic Compounds. **Chemistry - An Asian Journal**, v. 11, n. 19, p. 2735–2740, 2016b.

ZHAO, Y. et al. Ionic Liquids for Absorption and Separation of Gases: An Extensive Database and a Systematic Screening Method. **American Institute of Chemical Engineers AIChE J**, v. 63, p. 1353–1367, 2017.

CHAPTER III
THERMODYNAMIC ANALYSIS OF CARBON DIOXIDE HYDROGENATION TO FORMIC ACID AND METHANOL

This paper was published in Chemical Engineering Science, v. 242, p. 116731, 2021. https://doi.org/10.1016/j.ces.2021.116731

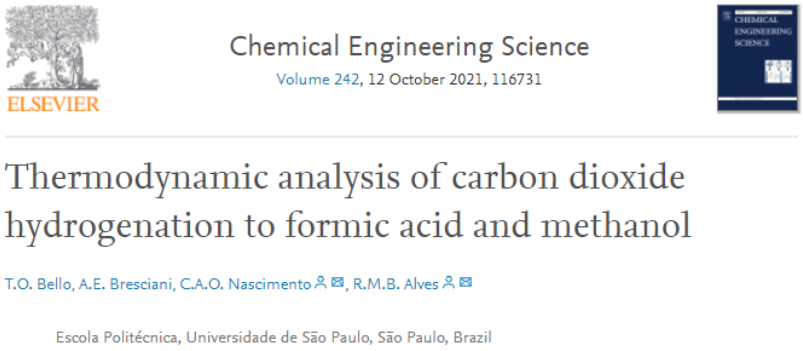

Abstract

Direct hydrogenation of carbon dioxide (CO_2) to formic acid is unfavorable thermodynamically, which makes its production limited. In this study, a thermodynamic analysis of CO_2 hydrogenation to binary product systems of methanol and formic acid promoted by ionic liquid (IL) (1-ethyl-2,3-dimethylimidazolium nitrite, ([Edmim][NO_2]) is presented. The analysis is conducted in Aspen Plus using the Gibbs energy minimization approach combined with a vapor-liquid equilibrium (VLE) for the solvation of CO_2 in IL. It is demonstrated that solvating CO_2 in ILs is an attractive alternative to overcome the thermodynamic difficulty associated with the product yield, especially formic acid. The [Edmim][NO_2] promoted system is very effective for the simultaneous production of formic acid and methanol at 25°C and 17bar with a yield of 35% formic acid and 30% methanol at a CO_2/H_2/IL ratio of 1/2/2. The results show a marked improvement in the yield of formic acid to other previously conducted studies on formic acid production.

Highlights

ILs favour the production of acid formic and methanol from CO_2 hydrogenation

Using ILs improves product yields to ~65% for formic acid and ~68% for methanol

CO_2 hydrogenation occurs at ambient temperature and low pressure conditions

Methanol is produced with less stoichiometric hydrogen requirement

Keywords

Carbon dioxide hydrogenation, Thermodynamics analysis, Gibbs energy, Ionic Liquid,

Formic acid, Methanol

III.1 Introduction

The greenhouse effect of carbon dioxide (CO_2) over the years has been recognized as the world's biggest problem in terms of global warming and climate change. Several countermeasures on general reductions methods in carbon dioxide emissions have been proposed until now (XU et al., 2011). In fact, the majority of measures and new process technologies, based on "CO_2 Recycling", among the viable strategy for the reduction of CO_2 emissions, are of scientific significance and technological importance (OLAH; GOEPPERT; PRAKASH, 2006). Nonetheless, the approach of using CO_2 as a "reagent" for the production of several chemicals and fuels in organic chemistry appears to be attractive due to possible replacements for conventional oil-based fuels (ARENA et al., 2007). Several products can be directly accessed through direct catalytic hydrogenation of CO_2, such as formic acid (LEITNER, 1995), methanol (ÁLVAREZ et al., 2017b), and hydrocarbons (GAO et al., 2017). Among these products, formic acid and methanol have a widespread application (ÁLVAREZ et al., 2017b; MELLMANN et al., 2016; OLAH; GOEPPERT; PRAKASH, 2006).

Since the pioneering work of Inoue et al. in 1976, direct hydrogenation of CO_2 to formic acid is considered an atomic-economic reaction; hence the research into its synthesis is of far-reaching significance and has been thoroughly investigated (INOUE et al., 1976; XU et al., 2011). Also, the transformation of CO_2 to methanol and its derivatives dimethylether (DME) has a great potential to process a large amount of CO_2 over a short time due to its reported high reaction rates (ÁLVAREZ et al., 2017b; OLAH; GOEPPERT; PRAKASH, 2006). Furthermore, formic acid and formaldehyde can be further converted into methanol, and a high overall yield of methanol can be obtained (OLAH, 2005). Therefore, research into the formic acid and methanol synthesis system from the hydrogenation of CO_2 is of high relevance and an additional attraction because the production of formic acid from CO_2 makes a significant contribution to the proposed "hydrogen economy" (CRABTREE; DRESSELHAUS; BUCHANAN, 2004).

Today, formic acid is most commonly synthesized by MeOH carbonylation, resulting in the formation of an ester, followed by hydrolysis with excess water (REUTEMANN; KIECZKA, 2000). Transformation of CO_2 into formic acid utilizing H_2 from renewable sources in a one-step process offers a more effective alternative to present synthesis, low resource-intensive, high CO_2 usage, and intermediate generation prevention (GRASEMANN;

LAURENCZY, 2012; HULL et al., 2012). Unfortunately, the hydrogenation of CO_2 into formic acid is endergonic in the gas phase (ΔG^O_{298} = +33 kJ/mol), and the reaction involves a phase change from gaseous reactant to liquid products. Hence, It's unfavorable thermodynamically (LEITNER, 1995; SCHAUB; PACIELLO, 2011; WANG; HIMEDA, 2012). Appropriate solvents (ÁLVAREZ et al., 2017b) or bases (INOUE et al., 1976) are one strategy that is often used to overcome thermodynamic limitations, making the reaction slightly exergonic (WANG; HIMEDA, 2012). The reaction is exergonic and possible when it is performed in the aqueous phase (ΔG^O_{298} = -4 kJ/mol) or with the addition of a base such as ammonia (Equation. 1.2, ΔG^O_{298} = -9.5 kJ/mol in the gas phase and is more favorable, ΔG^O_{298} = -35 kJ/mol, in the aqueous phase). In the presence of a base, the reaction is more favourable (Equation. 1.2, (ΔG^O_{298} = -35 kJ/mol in the aqueous phase) (JESSOP; IKARIYA; NOYORI, 1995); hence, solvent effects of water and deprotonation of formic acid with base are important for CO_2 hydrogenation. The other product of interest from the hydrogenation of CO_2 is methanol, which often finds its application as a liquid fuel, as well as in methanol fuel cell. Water, a by-product of hydrogenation of CO_2 to methanol, makes the reaction thermodynamically favorable (Equation. 1.5, (ΔG^O_{298} = -9.5 kJ/mol) in the gas phase (CRABTREE; DRESSELHAUS; BUCHANAN, 2004). Furthermore, it is more favorable thermodynamically in an aqueous solution (Equation. 1.5, (ΔG^O_{298} = -79 kJ/mol) (JESSOP; IKARIYA; NOYORI, 1995).

$$CO_2 + H_2 \leftrightarrow HCO_2H \quad \text{(III.1)}$$

$$CO_2 + H_2 + NH_3 \leftrightarrow HCO_2^- + NH_4^+ \quad \text{(III.2)}$$

$$CO_2 + H_2O \overset{pK1=6.35}{\longleftrightarrow} HCO_3^- + H^+ \overset{pK2=10.33}{\longleftrightarrow} CO_3^{2-} + 2H^+ \quad \text{(III.3)}$$

$$HCO_3^- + H_2 \leftrightarrow HCO_2^- + H_2O \quad \text{(III.4)}$$

$$CO_2 + 3H_2 \leftrightarrow CH_3OH + H_2O \quad \text{(III.5)}$$

Several catalyst systems with a highly active metal (Ir, Ru, and Pd) (MASUDA et al., 2018; MCNAMARA; HICKS, 2014; MORI; TAGA; YAMASHITA, 2017) have been described and reported. These catalysts system combined with inorganic (ELEK et al., 2003; HIMEDA et al., 2004) and organic bases (FILONENKO et al., 2014; PRETI; SQUARCIALUPI; FACHINETTI, 2010) drives the reaction forward to generate stable formates or formic acid adducts. However, there is a growing concern on the post-treatments

to get the final pure form of formic acid and recycling of the catalyst system (LEITNER, 1995; SU; LU; LIN, 2015).

Ionic liquids (ILs) may be viewed as a new and remarkable alternative class of solvents to conventional organic solvents. They are comprised entirely of cations and anions (organic and inorganic) with unique properties such as better solvating properties and low vapor pressure (ZENG et al., 2017). A significant benefit of ILs as a solvent in hydrogenation reactions is the ability to fine-tune the properties of the solvent by altering the structure, catalyst immobilization (GHAVRE; MORRISSEY; GATHERGOO, 2011; KOKORIN, 2012; MACFARLANE; KAR; PRINGLE, 2017) and CO_2 activation (WANG et al., 2015; YUE et al., 2014), consequently leading to a reduction in the Gibbs energy of formation. They act as solvents and catalysts in chemical reactions demonstrating optimal performances. ILs that can generally activate CO_2 must have high alkalinity due to the presence of electron-negative sites as N or O atoms (LUO et al., 2014; WU et al., 2017). "CO_2-Phillic" ILs, including azolate and pyrimidine-based ILs were reported to be capable of catalyzing the transformation of CO_2 through the formation of intermediates of carbonate or carbamates in mild conditions (WU et al., 2017; ZHAO et al., 2016b).

In this study, a thermodynamic analysis for hydrogenation of CO_2 to formic acid and methanol in a single-step reaction promoted by IL; 1-ethyl-2,3-dimethylimidazolium nitrite ([Edmim][NO_2]) is carried out. To the best of the author's knowledge, so far, there is no literature or comprehensive study regarding the thermodynamic study on CO_2 hydrogenation to methanol and formic acid promoted with this IL ([Edmim][NO_2]).

III.2 Method

Kinetics and thermodynamic plays a vital role in determining the composition of a reaction mixture, however, in this work, only the thermodynamics properties at equilibrium are considered. The reaction kinetics and catalyst effect on the reaction system could be studied in a sequential work for process development.

The method attempts to perform thermodynamic modeling and simulation following a two-step process. The solvation of CO_2 in [Edmim][NO_2] is represented using flash separation and the reaction is simulated using the Gibbs reactor model. All these steps were performed using a commercial software, Aspen plus version 9. The Gibbs reactor model implements the Gibbs energy minimization approach to accurately define the equilibrium composition of the reaction system.

III.2.1 Chemical Reaction Stoichiometry

Chemical reaction stoichiometry (CRS) implements the law of the conservation of mass (LCM) in a closed chemical system undergoing chemical change. It may be expressed as a set of linear equations involving the conservation of mass of chemical elements, or another appropriate quantity (GLASSER; SMITH, 2019). CRS express this information in terms of a set of stoichiometric equations, which are equivalent representations of the LCM and have the appearance of, but are distinct from, actual chemical reaction mechanisms. Glasser and Smith (GLASSER; SMITH, 2019) developed a Microsoft excel program to implement the matrix method calculation. The reaction evaluated from the matrix implementation is shown in table 2.1. However, the molar extents of reaction from equations 2.1 to 2.3 were zero. They were neither contributing nor competing in the reaction, hence they were not considered in the reactor.

Table III.8. Independent Reactions from the CRS implementation.

Number of Reactions = 5

$CO_2 + H_2 \leftrightarrow CO + H_2O$	(III.6)
$CO_2 + 2H_2 \leftrightarrow C(s) + 2H_2O$	(III.7)
$CO_2 + 4H_2 \leftrightarrow CH_4 + 2H_2O$	(III.8)
$CO_2 + H_2 \leftrightarrow CHOOH$	(III.9)
$CO_2 + 3H_2 \leftrightarrow CH_3OH + H_2O$	(III.10)

III.2.2 Thermodynamic model

Generally, ILs has been reported to be a non-volatile compound, hence in a gas-IL binary system, the IL is assumed as non-volatile and it is not present in the gaseous phase. Vapor-Liquid equilibrium is achieved when the fugacities of the gas component are equal in both phases at a constant temperature and pressure ($f_{gas}^{l} = f_{gas}^{v}$). Hence, the relationship of fugacity with temperature and pressure can be expressed by an equation of state (YAZDIZADEH; RAHMANI; FORGHANI, 2011).

Several researchers (MOTA MARTINEZ; KROON; PETERS, 2015; SHARIATI; PETERS, 2003, 2004) have implemented cubic state equation for various binary systems with different ILs as one component and other components (RAMDIN et al., 2014; SHOJAEIAN,

2017) as a different type of gas. It has also been proposed that the equation of state should be as simple as possible with fewer parameters, which have greater importance for each parameter, rather than be a very complicated thermodynamic model with many complex parameters to describe the overall state of the system (ALTHULUTH, 2014). The Peng Robinson equation of state (PR-EoS) (PENG; ROBINSON, 1976) has been reported to be widely used because of its simplicity and flexibility (VALDERRAMA, 2003). Shariati and Peters (SHARIATI; PETERS, 2003) applied PR-EoS to design an IL binary system consisting of fluoroform as the solute. Wei Ren et al. (REN; SENSENICH; SCURTO, 2010) and Freitas et al. (FREITAS et al., 2013) employed PR-EoS with van der Waals 2-parameter mixing rule to model and correlate experimental data of CO_2 and IL binary mixture. Several other sources (ALTHULUTH, 2014; BAGCHI; SATI; SHILAPURAM, 2017; MOTA MARTINEZ; KROON; PETERS, 2015) also have documented the application of PR-EoS to the VLE of ILs and CO_2 systems.

Thus, the PR-EoS with van der Waals fluid mixing rules was used to predict the system's thermodynamic and volumetric properties. The PR-EoS can be expressed as:

$$P = \frac{RT}{V_m - b} - \frac{a}{V_m\,(V_m + b) + b(V_m - b)} \tag{III.11}$$

$$a = \sum\sum x_i x_j a_{ij} \tag{III.12}$$

$$b = \sum\sum x_i x_j b_{ij} \tag{III.13}$$

$$a_{ij} = \sqrt{a_i a_j}\,(1 - k_{ij}) \qquad k_{ii} = k_{jj} = 0 \qquad k_{ij} = k_{ji} \tag{III.14}$$

$$b_{ij} = \frac{b_i + b_j}{2}\,(1 - l_{ij}) \qquad l_{ii} = l_{jj} = 0 \qquad l_{ij} \neq l_{ji} \tag{III.15}$$

Where P is pressure, T is temperature, V_m is the molar volume, a and b are constants contributing to molecular interaction and co-volume, respectively, R is the universal gas constant, k_{ij} and l_{ij} are binary interaction parameters.

III.2.3 Components Definition

From the authors, previous studies on the screening of ionic liquids for CO_2 hydrogenation to formic acid and methanol (BELLO et al., 2021b) (submitted for publication), 1-ethyl-2,3-dimethyl-imidazolium nitrite, [Edmim][NO_2], was selected as one of the ILs with optimal separation performance and optimal solvation property. [Edmim][NO_2] was defined as

pseudo-components by specifying the normal boiling temperature, density, and molecular weight in Aspen Plus V9. The normal boiling point of [Edmim][NO_2] was estimated by the extended Group contribution(GC) method of Valderrama and Rojas (VALDERRAMA; FORERO; ROJAS, 2012). The density of [Edmim][NO_2] was estimated by conductor-like screening method for real solvents (COSMO-RS) calculation (PALOMAR et al., 2007), while the molecular weight is known. Other pseudo-component properties such as standard enthalpy and Gibbs energy of formation and vapor pressure needed for process simulation were estimated by implicit techniques (Joback group contribution method) in Aspen Plus. Formic acid, methanol, CO_2, H_2, and water were defined as conventional components in the simulator databank. The component definition method was reported as reliable for the simulation of the IL-based aromatic/aliphatic hydrocarbon separation process (DE RIVA et al., 2016; FERRO et al., 2012a).

III.2.4 CO_2 Solvation in [Edmim][NO_2]

CO_2 dissolves in [Edmim][NO_2] to form a CO_2-[Edmim][NO_2] adduct (WU et al., 2019).The method prescribed by Bagchi et al. (BAGCHI; SATI; SHILAPURAM, 2017) for CO_2 solvation in ILs was employed in this section. Flash separation in Aspen Plus for vigorous VLE with two outlet streams was employed to carry out this process. Due to unavailability of experimental data in literature for CO_2-[Edmim][NO_2] and H_2-[Edmim][NO_2] mixture, the VLE equilibrium data of CO_2, [Edmim][NO_2], and H_2 were predicted by COSMO-RS at 1bar and 25^{o}C (BELLO et al., 2021b). Subsequently, the binary interaction parameters (CO_2-[Edmim][NO_2] and H_2-[Edmim][NO_2]) needed in the model were regressed from the predicted VLE data through the procedure prescribed by Sandler (SANDLER, 2015). One drawback, however, is that it was not possible to get experimental data of the binary mixture of [EDmim][NO_2]-CO_2 to validate the regressed binary interaction parameters, hence the parameters can be adjusted in further studies using experimental data for better result. The root-mean-square deviation (RMSD) between the COSMO-RS predicted and Peng-Robinson correlated compositions was obtained from Aspen plus regression method. The binary interaction parameters were regressed to fit the equations 2.11 and 2.12.

$$k_{ij} = k_{ij}^{(1)} + k_{ij}^{(2)} T + k_{ij}^{(3)} / T, \qquad k_{ij} = k_{ji} \tag{III.16}$$

$$l_{ij} = l_{ij}^{(1)} + l_{ij}^{(2)} T + l_{ij}^{(3)} / T \ , \ l_{ij} \neq l_{ji} \tag{III.17}$$

The estimated RMSD of [Edmim][NO_2] and CO_2 systems are 0.001041, and 0.001059, respectively, which indicate a suitable model regression quality. The coefficients of the regressed binary interaction parameters are shown in Table III.2.

Table III.9. Coefficients of the regressed binary interaction parameter for CO_2-Edmim][NO_2] according to equations III.16 and III.17 obtained from Aspen Plus

Binary interaction parameters coefficients								
$k_{ij}^{(1)}$	$k_{ij}^{(2)}x10^3$	$k_{ij}^{(3)}$	$l_{ij}^{(1)}$	$l_{ij}^{(2)}x10^2$	$l_{ij}^{(3)}$	$l_{ji}^{(1)}$	$l_{ji}^{(2)}x10^2$	$l_{ji}^{(3)}$
1.3166	-4.6160	32.4517	-18.2509	5.9572	-32.4517	10,1900	3.3736	-32.4517

III.2.5 H_2 Solvation in [Edmim][NO_2]

Hydrogen (H_2) is sparingly soluble in ionic liquids (BERGER et al., 2001; DYSON et al., 2003; LINKE; SEIDELL, 1958; YOUNG, 1983). However, low solubility issues can be compensated by carrying out the reaction at relatively high pressures, which increase H_2 solubility (BERGER et al., 2001). Therefore, H_2 was introduced directly into the Gibbs reactor in this study. As stated in the section 2.4, the predicted VLE data of H_2-[Edmim][NO_2]) from COSMO-RS were regressed to obtain the binary interaction parameter.

III.2.6 Gibbs Energy Minimization

The Gibbs energy minimization approach can accurately define the equilibrium composition of a reaction system (PERRY; GREEN; MALONEY, 1997). The stoichiometric knowledge of the reactant or possible reactions that might take place in the system is not required for this method (SMITH; VAN NESS; ABBOTT, 2005). At equilibrium condition, the system's total Gibbs energy is minimized. The thermodynamic analysis of the system was implemented through Aspen plus RGibbs reactor block. The total Gibbs energy of the system can be expressed at a specific temperature and pressure for a compound composition as:

$$G_T \sum_{i=1}^{m} n_i \ \mu_i = \sum_{i=1}^{m} n_i \ \mu_i^0 + RT \ \sum n_i \ \ln {f_i}/{f_i^0} \qquad \text{(III.18)}$$

Where n_i is the moles of species i, μ_i and f_i are the chemical potential and fugacity of component i in the gas mixture, respectively, μ_i^o and f_i^0 are the chemical potential and fugacity of component i in the standard state, respectively, R is the molar gas constant, T is the system temperature.

The composition of the product at the reactor outlet was determined by calculating the CO_2 and H_2 conversion, selectivity, and yield defined as follows:

$$Conversion,\ CO_2 = \frac{NCO_{2,in} - NCO_{2,out}}{NCO_{2,in}} * 100 \quad \text{(III.19)}$$

$$Conversion,\ H_2 = \frac{NH_{2,in} - NH_{2,out}}{NH_{2,in}} * 100 \quad \text{(III.20)}$$

$$Yield,\quad Y_i = \frac{j_i N_{out,in} - j_i N_{i,in}}{NCO_{2,in}} * 100 \quad \text{(III.21)}$$

$$Selectivity,\ S_i = \frac{j_i N_{i,out} - j_i N_{i,in}}{NCO_{2,in} - NCO_{2,out}} * 100 \quad \text{(III.22)}$$

Where $N_{i,in}$ and $N_{i,out}$ are the molar flow rate of species *i* at the inlet and outlet of the reactor, respectively, and j_i is the number of carbon atoms in species *i*.

III.2.7 Verification of the Model

As previously stated, there are no experimental data for the mixture ([Edmim][NO_2]-CO_2-H_2) in literature, however for the sake of simplicity, an IL mixture with available data in the literature was chosen for verification of the model. The experimental data of CO_2 and H_2S solubility in 1-butyl-3-methylimidazolium acetate, ([Bmim][OAc]) obtained by Haghtalab and Kheiri (HAGHTALAB; KHEIRI, 2015) were considered for the verification. The procedure above was verified by running a case study of the (mixture of CO_2-[Bmim][OAc]) in the simulation environment of Aspen Plus as seen in the process flow in Figure III.1

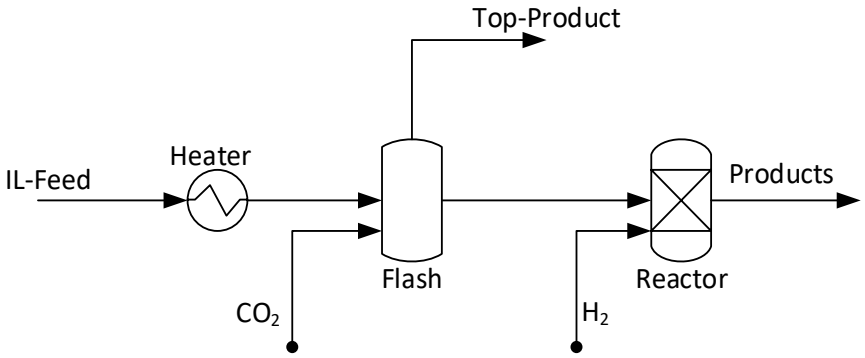

Figure III.13. Flowsheet for the Simulation of the Hydrogenation Reaction

The VLE data of CO_2 and H_2S solubility in [Bmim][OAc] at 70 ºC were regressed to obtain the binary interaction parameter of CO_2-H_2S-[Bmim][OAc]. However, [Bmim][OAc]-H_2 VLE data could not be obtained from the literature. Moreover, H_2 is known to be sparingly soluble in ILs; hence, the binary interaction parameter of [Edmim][NO_2]-H_2 estimated from COSMO-RS (BELLO et al., 2021b) was used instead.

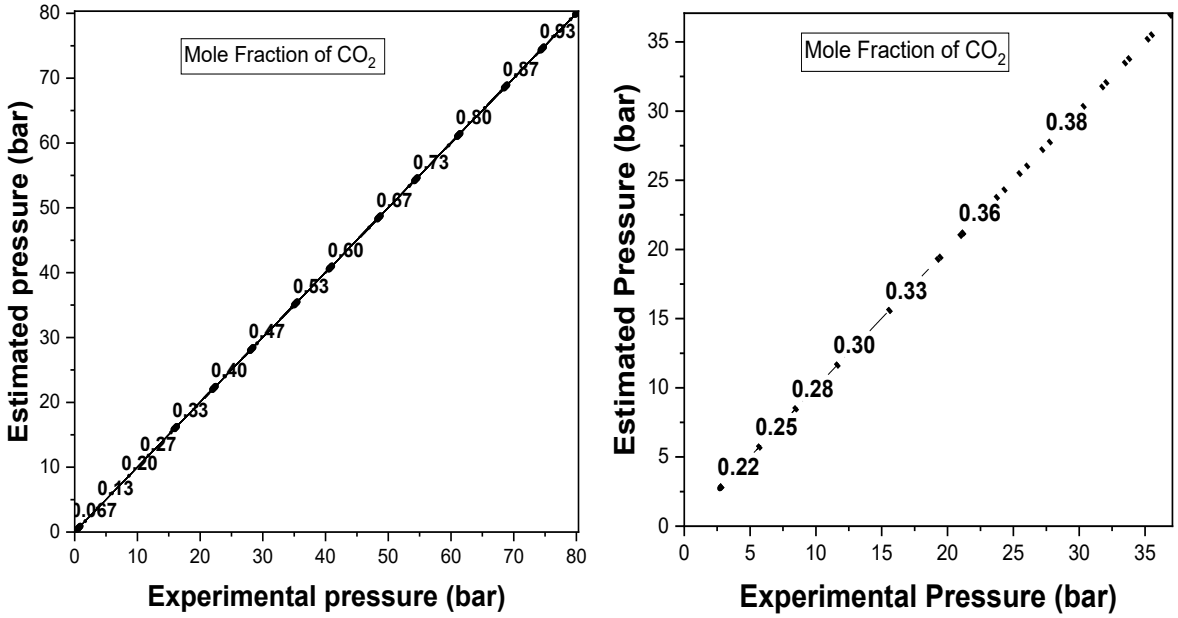

Figure III.14. CO_2 Solubility (a) experimental result for CO_2 + BmimOAc (Haghtalab and Kheiri, 2015) (b) this study for CO_2 + $EdmimNO_2$

The temperature and pressure of the flash block were determined by sensitivity analysis for complete solvation of CO_2 in [Bmim][OAc] (vapor fraction = 0, T = 63.5 ºC, and P = 28.98 bar). The value obtained in the simulation was close to the experimental value T = 70 ºC and P = 30.7 bar. Figures III.2a and III.2b present the parity plot of the calculated values in this work and the experimental values from the work of Haghtalab and Kheiri (HAGHTALAB; KHEIRI, 2015) reproduced in Aspen Plus , respectively. It can be verified that there is a good correlation between experimental and calculated data. Hence this methodology can be extended to other combinations of feed mole fractions and temperatures.

The graphs III.3a and III.3b shows the variation of pressure and temperature with respect to the mole fraction of CO_2 in [Edmim][NO_2] at fixed pressure of 1 bar (figure 3a) and fixed temperature of 25 ºC (figure III.3b). The model validates the CO_2 solubility in [Edmim][NO_2]. It is possible to see that the solubility of CO_2, increases when the pressure increases and the solubility decreases with increasing temperature of the system. This behavior was also observed in the literature (SHARIATI; PETERS, 2003, 2004)(FREITAS et al., 2013).

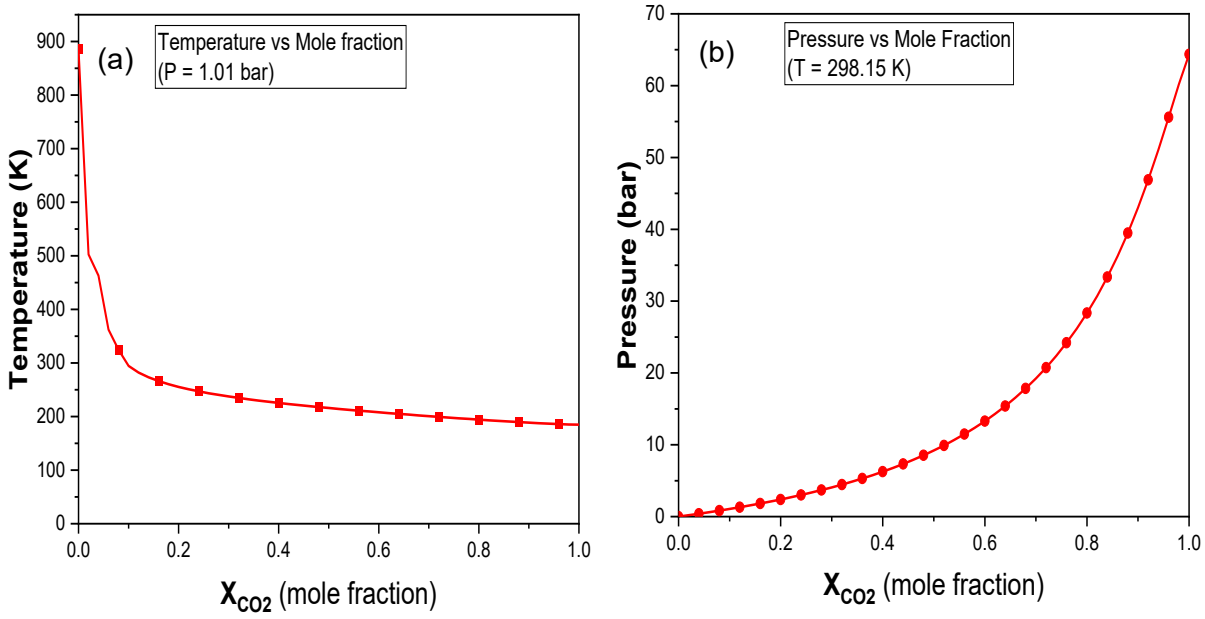

Figure III.15: Phase diagram of CO_2 (a) at fixed pressure (1.012 bar) (b) at fixed temperature (298.15 K)

III.3 Results and Discussion

This section outlines the results of the thermodynamic modeling and simulation and presents the effect of temperature, pressure, and feed ratio on the equilibrium conversion of carbon dioxide and hydrogen, selectivity, and yield of formic acid and methanol.

III.3.1 Influence of Temperature and Pressure at a Fixed Feed Ratio

Figures III.4a-c shows the equilibrium conversion of CO_2, formic acid and methanol yields at different reaction temperatures and pressures for a CO_2/H_2/[Edmim][NO_2] feed at a stoichiometric molar ratio of 1/1/1. The conversion of CO_2 was observed to decrease with increasing temperature at each observed pressure. The highest CO_2 conversion (~95%) at 25 bar was achieved at ambient temperature (0-30^{o}C), after which it decreases steadily with increasing temperature (at T >25 ^{o}C). In the same sense, H_2 conversion behaved similarly to CO_2 conversion (more details can be found in the Supplementary Material). The steady decrease may be due to the two regimes that of the process. The process regimes are: the solubilization of CO_2 in IL to form CO_2-IL adduct and the equilibrium of the two chemical reactions. The first regime (solubilization) is favorably governed by higher pressures and lower temperatures. With increasing pressure, more CO_2 is absorbed by the ionic liquid favouring the adduct formation. As the temperature increases, its effect becomes less dominant, overcoming the effect of pressure, and the CO_2 solubility in the ionic liquid decreases. When CO_2 adduct effect diminishes, then CO_2 becomes less activated and consequently the equilibrium conversion decreases. The second regime (reactions to formation of formic acid and methanol) is majorly controlled by temperature. However, an abrupt change (spike) in the trend of the graph was observed at T > 30 ^{o}C. This might be due to the preference to a specific product (methanol or formic acid) favorably produced at the operating condition. At a CO_2/H_2/IL ratio = 1/1/1, methanol formation was observed to decrease relatively constant beyond 30 ^{o}C. The highest yield of methanol at 20% was achievable at this operating range (Figure III.4c). However, formic acid showed a higher yield (~95%) at 25 bar and temperature (0 – 25 ^{o}C) range, as shown in figure III.4b. This explains the effect of [Edmim][NO_2], which activates the CO_2 by forming an [Edmim][NO_2]-CO_2 adduct, which enhances the formation at ambient temperature and low pressure unlike reaction without an IL as a promoter. Increasing temperature shows an exponential decrease in the formation of formic acid beyond 30^{o}C. However, methanol possesses higher selectivity under all reaction conditions, which indicates that the reaction is favorable towards methanol at all the operating conditions. (more details can be found in the Supplementary Material).

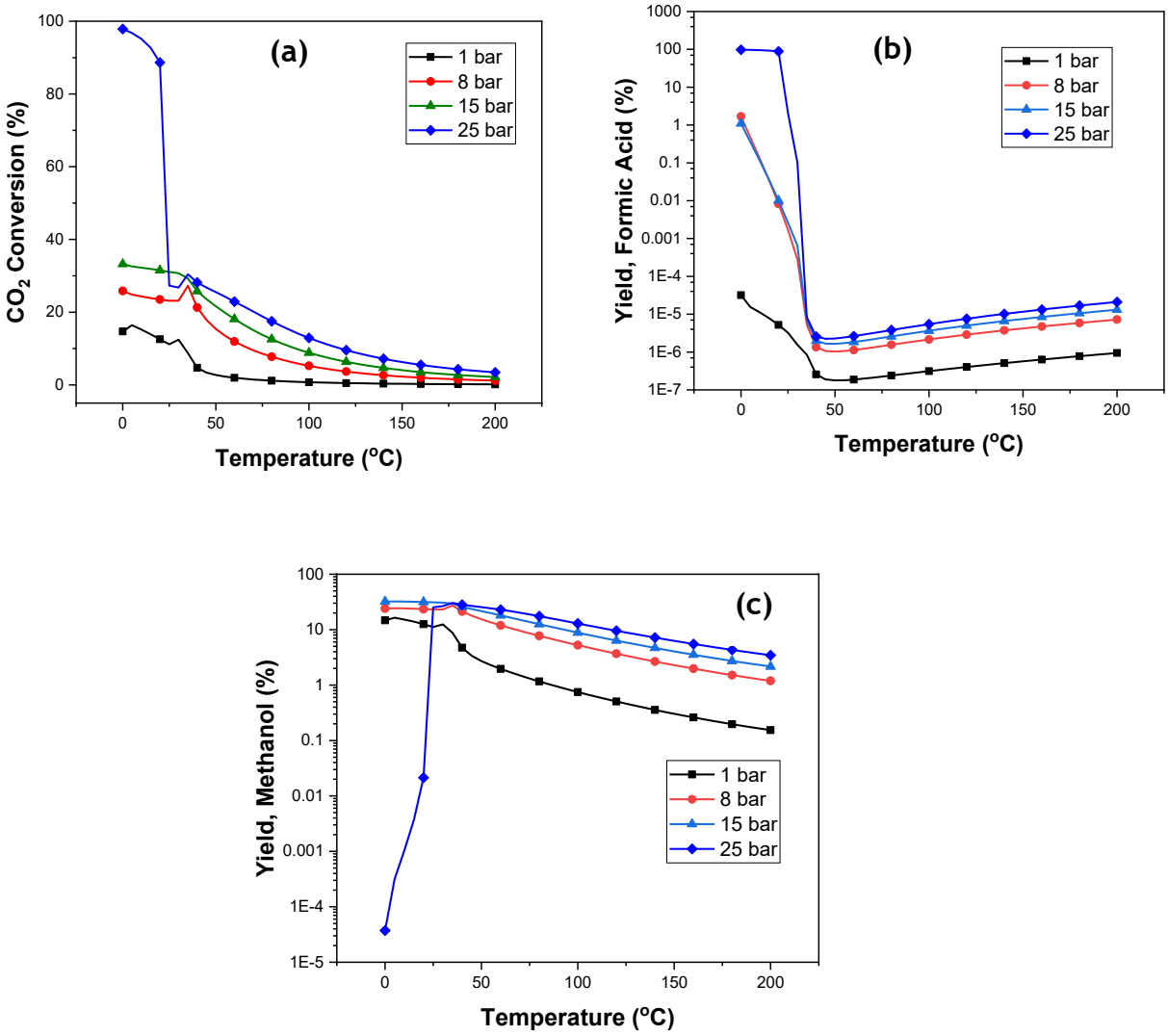

Figure III.16. Influence of Temperature and Pressure at ratio 1/1/1 (a) CO_2 conversion (b) Formic acid Yield (c) Methanol Yield

III. 3.2 Influence of H_2 ratio

The effect of the initial CO_2 /[Edmim][NO_2]/ H_2 ratio on the equilibrium was examined in the range of 1/1/1 to 1/1/5, at temperatures from 0 to 200 °C and pressure of 1 bar. The CO_2 conversion graph is presented in Figures III.5a. At 1 bar, increasing the H_2 ratio enhances the equilibrium conversion of CO_2. As the temperature is increased above 30 °C, the effect of the increased H_2 ratio diminishes, and consequently, the CO_2 conversion curves decrease exponentially. The reactions have become more exothermic with increase of the temperature. Figures III.5b and III.5c present the formation of methanol and formic acid at atmospheric

pressure (1 bar), varying the feed ratio of CO_2/[Edmim][NO_2]/H_2 from 1/1/1 to 1/1/5. The formation of methanol was favorable at atmospheric pressure at ratio 1/1/1, with a yield of ~15%. This explains the dominant effect towards methanol production with the minimum selectivity as high as 99.9% at 1 bar, consequently increasing its production as shown in figure III.5c (more details can be found in the Supplementary Material). This is unlike the hydrogenation reaction of CO_2 to methanol without IL, which is quite practically infeasible to be produced at atmospheric pressure (STANGELAND; LI; YU, 2018). The theoretical stoichiometric ratio for the hydrogenation of CO_2 to methanol is 1/1/3, but it was observed that at 1/1/2, methanol production was approximately 12%. This is beneficial in terms of process economics as less H_2 would be needed for the production of methanol. However, formic acid production is very low (less than 0.01%) in a wide range of temperature 0 – 200 °C and feed ratio (1/1/5). Nevertheless, its yield rapidly diminishes beyond 30 °C. This confirms the same scenario at a stoichiometric ratio of 1/1/1 that formic acid production promoted by [Edmim][NO_2] is unfavorable at temperatures beyond the temperature range 0 – 25 °C.

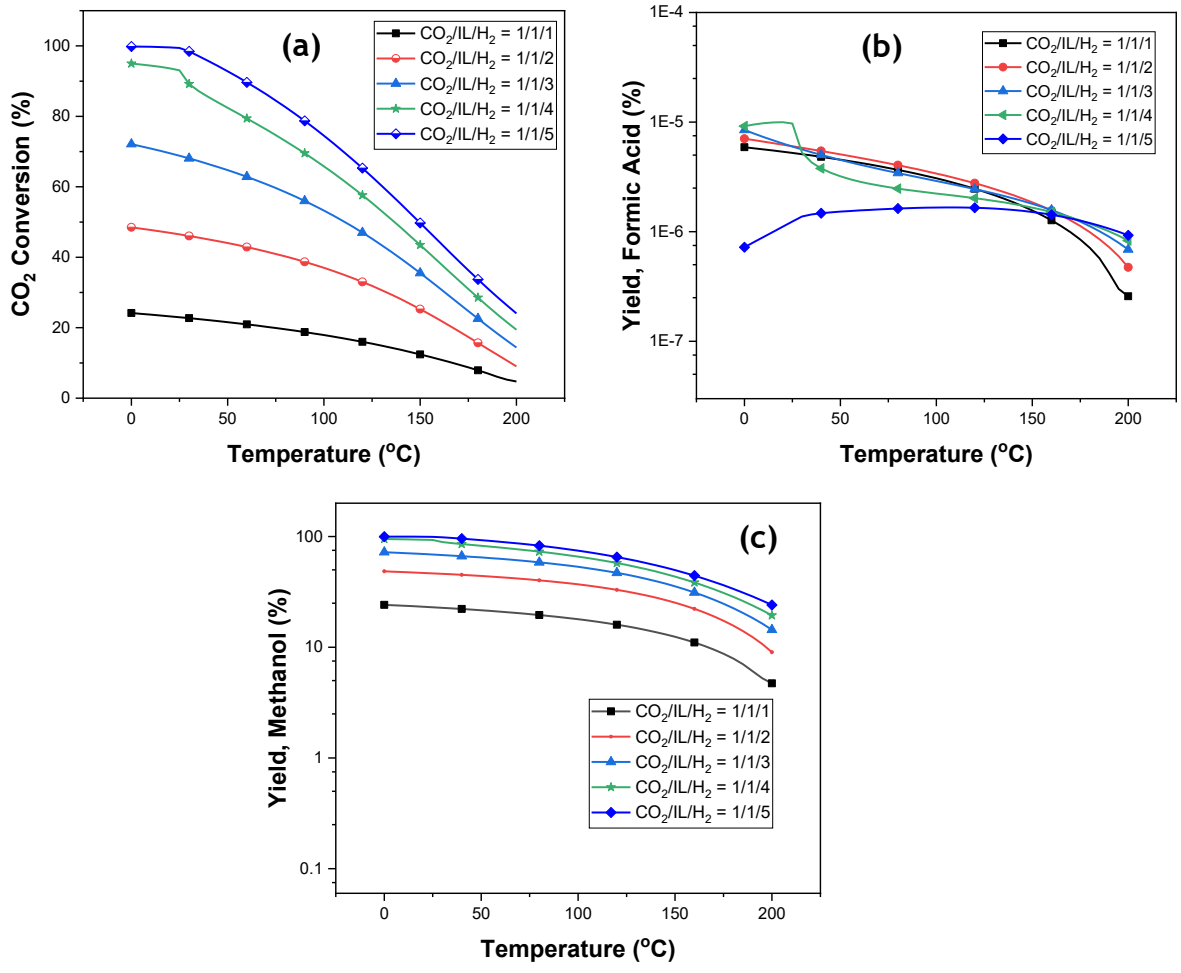

Figure III.17. Influence of H_2 ratio at 1 bar (a) CO_2 conversion (b) Formic acid Yield (c) Methanol Yield

III.3.3 Influence of [Edmim][NO_2] Ratio

The conversion of CO_2 and H_2 varying the IL feed ratio present the lowest equilibrium conversion at 1 bar, as shown in figures III.6a-c. This explains why the hydrogen gas in CO_2-[Edmim][NO_2] adduct phase is low. This can be attributed to the insufficient H_2 solubility in the adduct (CO_2-[Edmim][NO_2]) at 1 bar. Consequently, the reaction cannot proceed favorably towards product formation. The lowest equilibrium conversions (CO_2 =12%; H_2 = 20%) were observed at ratio above 2 of [Edmim][NO_2] feed ratio as compared to H_2 feed ratio at the same pressure of 1 bar (see figure III.6a). At atmospheric pressure, the selectivity of methanol is greater than 99% at all ratio explains the relative yield of methanol at ~15% compared to 0.001% of formic acid. However, methanol yield decreases with an increasing ratio of [Edmim][NO_2] up to 1/1/5. As the temperature is increased beyond 30 ºC, the methanol synthesis falls drastically. This is due to the effect of that the reaction is temperature controlled at this region and makes it more exothermic.

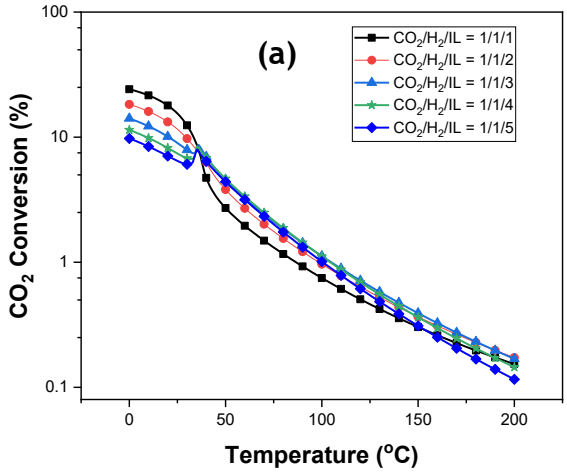

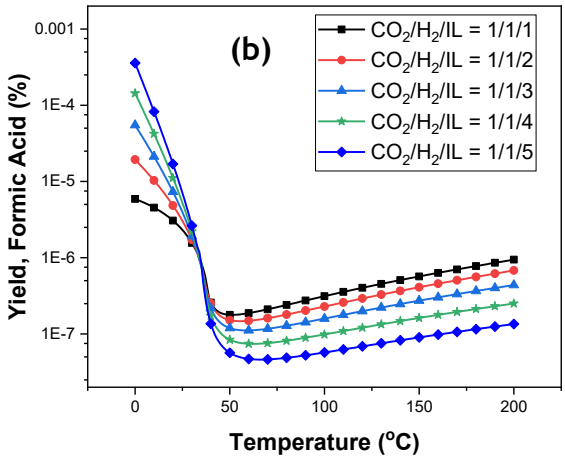

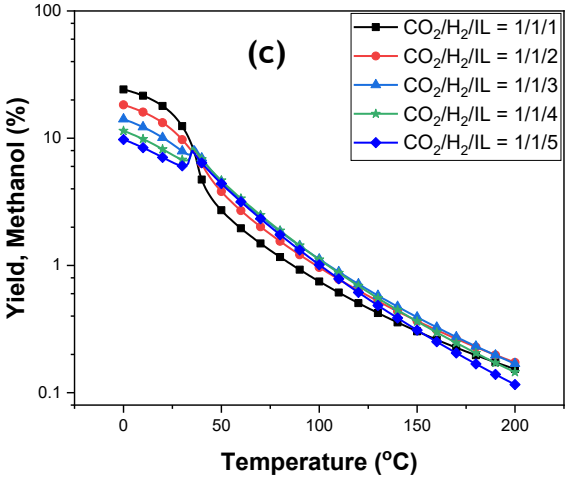

Figure III.18. Influence of [Edmim][NO_2] ratio at 1 bar (a) CO_2 conversion (b) Formic acid Yield (c) Methanol Yield

III.3.4 Influence of H_2 Ratio at Optimal Pressure for Simultaneous Formic Acid and Methanol Formation

As pressure is one of the dominant conditions for the formation of both methanol and formic acid, a sensitivity analysis was carried out to select the operating pressure that promotes the simultaneous production of both compounds at a reasonable CO_2 and H_2 conversion (< 80%). Figures III.7a-c depicts the effect of CO_2/[Edmim][NO_2]/H_2 ratio from 1/1/1 to 1/1/5 at 17 bar. As expected, the equilibrium conversion of CO_2, approximately 100%, was achieved at the ratio 1/1/5. A sharp decline in CO_2 conversion beyond 30 °C was observed in figure III.19a. This can be attributed to the fact that CO_2-IL adduct effect has diminished beyond 30 °C causing the reaction to be temperature controlled. The solubility of CO_2 in the ionic liquid decreased significantly with increasing temperature causing reduction in the amount of CO_2 activated and consequently decrease in equilibrium conversion of CO_2. At 17bar and H_2 ratio above 1/1/2, the reaction was favorable to the formation of methanol, while it was beneficial to formic acid at a lower ratio (2). This might be attributed to the increased partial pressure of H_2, which supports the reaction towards product formation according to the Le Chatelier principle. Even though the yield of methanol and formic acid decreases exponentially with increasing temperature, however, methanol formation was dominant, with selectivity of ~100% (More details can be found in the Supplementary Material). In the same sense, the reaction was also favorable to the formation of formic acid with a yield up to ~59% at the ratio 1/1/2 at the temperature range of 0 -25 °C. However, beyond 25 °C, a spike shows that there is a change of preference for methanol production as shown in figures III.7a-c.

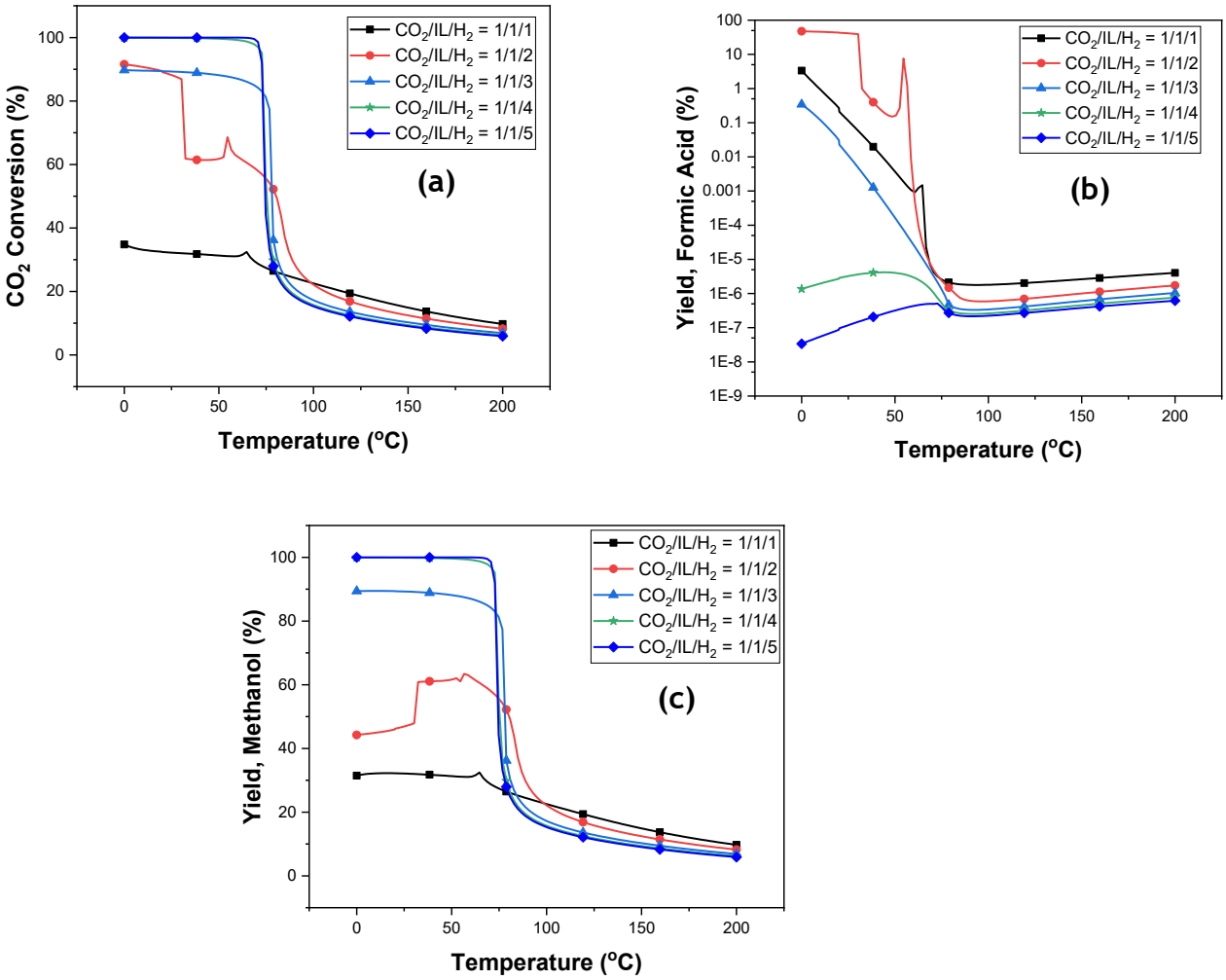

Figure III.19. Influence of H_2 ratio at for simultaneous formic acid and methanol formation at 17bar (a) CO_2 conversion (b) Formic acid Yield (c) Methanol Yield

III.3.5 Effect of [Edmim][NO_2] Ratio at Optimal Pressure for Simultaneous Formic Acid and Methanol Formation

The influence of [Edmim][NO_2] feed ratio to other components (H_2 and CO_2) is presented in figures III.8a-c. An increase in the feed ratio higher than 1/1/1 increases the equilibrium conversion of CO_2 by three times higher than ratio 1/1/1. The increased equilibrium conversion can be attributed to the increased effect of CO_2-EDMIMNO_2 adduct. CO_2 is able to occupy more "free spaces" in the IL and are readily activated for conversion. This explains why H_2 is consumed at all feed ratio of [Edmim][NO_2] at 0-30 °C (more can be found in the Supplementary Material). From figure III.8a, CO_2 is consumed up to ~97% at feed ratio greater 1/1/1. As a result, it is expected that the reaction is favored towards product formation. At a feed ratio greater than 1, formic acid was favorably produced at the expense of methanol attaining a yield ~99%. This can be seen from Figure III.8b and III.8c with the highest yield of methanol achieved at ~31%. However, at temperatures beyond 25°C, there is onset of the

decline of formic acid production (Figure III.8b). Simultaneously, the preference was towards methanol production at a reduced yield as illustrated in Figure III.8c. This might be related to the system deficient in H_2 for increased methanol formation or the temperature of the system has become dominant such that the CO_2-EDMIMNO$_2$ adduct effect has decreased considerably. Despite the limited formation of methanol at 0 -25 ^oC range, it was dominant from temperature beyond 25 ^oC.

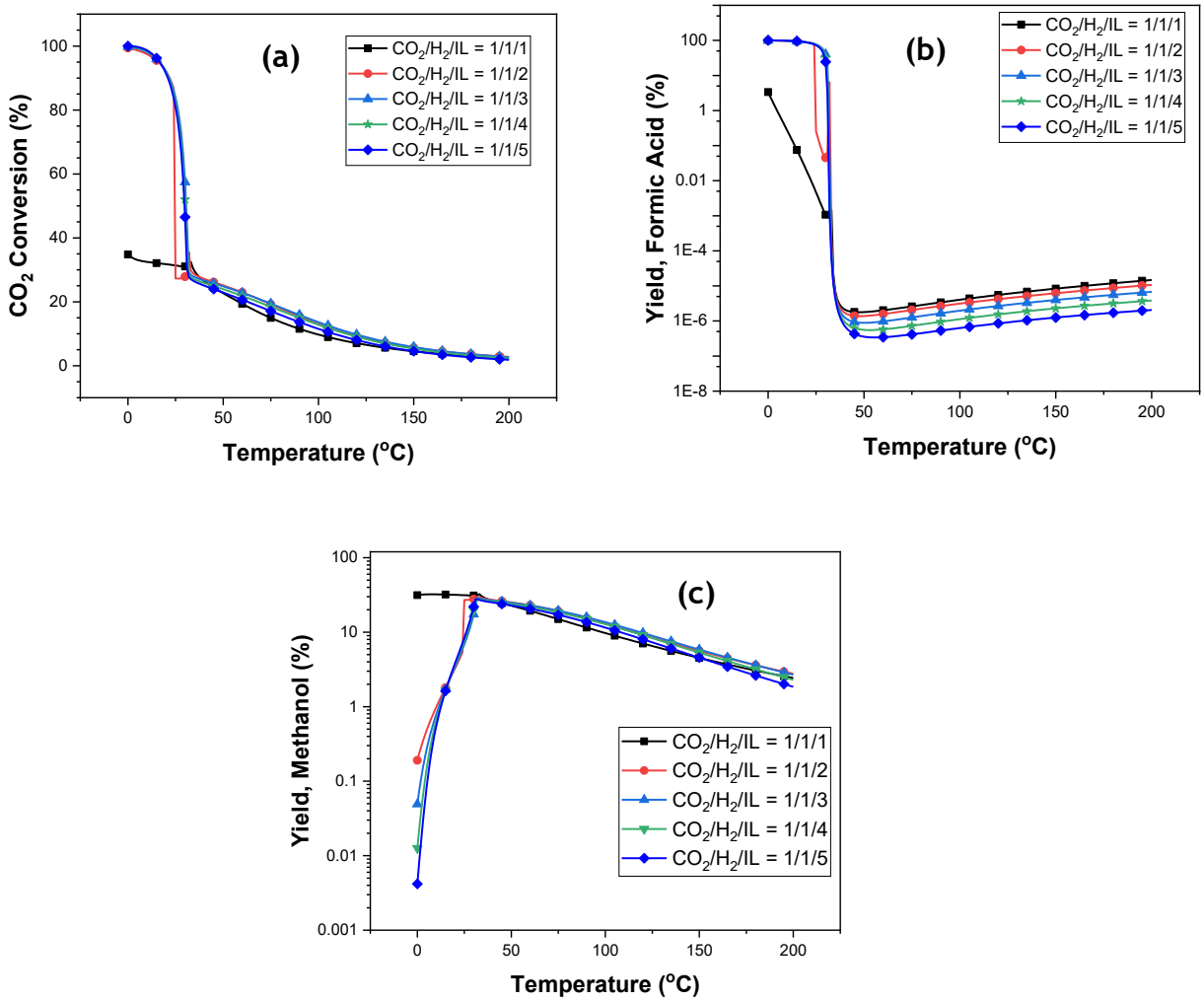

Figure III.20. Effect of [Edmim][NO$_2$] ratio for simultaneous formic acid and methanol formation at 17 bar (a) CO_2 conversion (b) Formic acid Yield (c) Methanol Yield

III.3.6 Optimal Operating Conditions for Simultaneous Formic Acid and Methanol Production

One of the objectives of this study is to obtain an operating condition needed for the formation of an appreciable amount of formic acid and methanol. The result of the analysis is presented in figures III.9a-b. At 17 bar and feed ratio $CO_2/H_2/[Edmim][NO_2]$ = 1/2/2, the equilibrium conversion of CO_2 decreases with increasing temperature, while H_2 conversion increases exponentially at 25 ºC and, finally, decrease rapidly at the same temperature. The decrease in equilibrium CO_2 conversion can be attributed to the effect of CO_2-$EDMIMNO_2$ adduct decreasing with increasing temperature. Despite the increase in H_2 conversion within the temperature range it immediately declining exponentially after attaining the peak. The effect of temperature on the reaction is more dominant in this instance because the reaction becomes more exothermic with increase temperature thereby reducing the H_2 conversion. This situation shows the preference towards methanol production at this temperature range (25–30 ºC) and why more H_2 was consumed at this temperature range.

Figure III.9b illustrates the yield of both formic acid and methanol. It was shown that the maximum yield of formic acid (~65%) was obtained in the range 0 -10 ºC and decreases steadily at 25 ºC, while methanol increases exponentially at 25 ºC-30 ºC. This scenario exemplifies the low temperature condition for the favourable formation of formic acid in the presence of an IL. For this system to produce an appreciable amount of formic acid and methanol simultaneously (CHOOH = ~35% and CH_3OH = ~30%), the optimum operating parameter was selected to be between 24 -25 ºC, 17 bar, and feed ratio $CO_2/H_2/[Edmim][NO_2]$ of 1/2/2. However, the equilibrium conversion of CO_2 and H_2 at this point is relatively lower (CO_2 =~64% H_2 = ~61%) as compared to producing a single product (either formic acid or methanol) at a point in time. (CHOOH: CO_2 =~80%, H_2 = ~58%; CH_3OH: CO_2 =~60%, H_2 = ~92%)

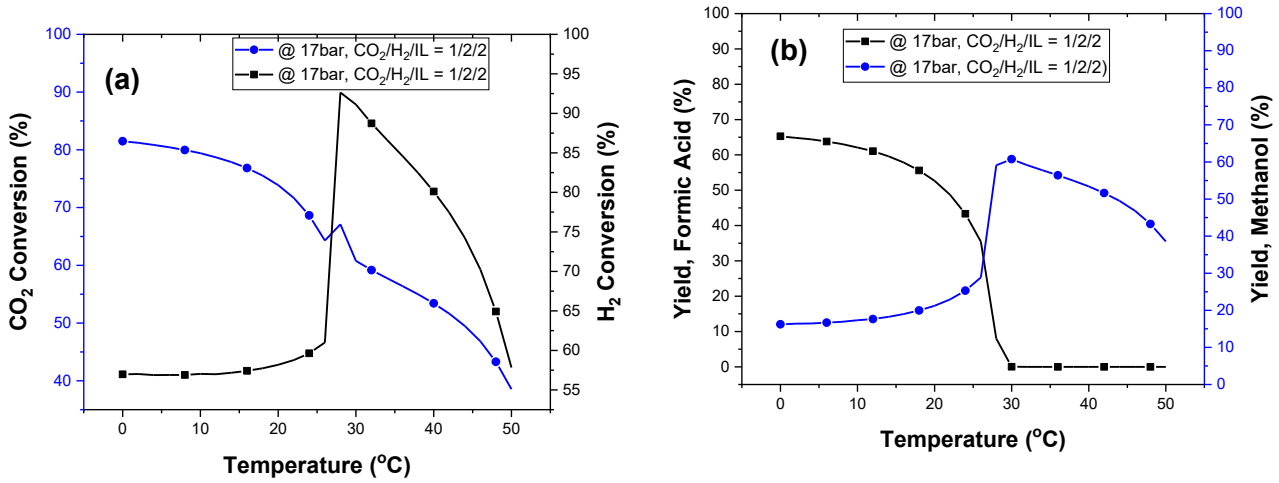

Figure III.21. Simultaneous formic acid and methanol production at 17 bar and 1/2/2 ratio (a) CO_2 and H_2 conversion (b) Formic acid and Methanol

III.3.7 Influence of Temperature and Pressure on Gibbs Energy of Reaction

Figures III.10a and III.10b illustrate the variation of temperature and pressure with the Gibbs energy (ΔG). Increasing the temperature at a fixed pressure of 17 bar makes the product formation increasingly difficult as Gibbs's energy becomes more positive. Therefore, a lower operating temperature is optimum for this reaction. In this same sense, increasing the pressure of the system at a fixed temperature 25°C, ΔG becomes more positive, consequently affecting ease of product formation. These two situations agree with the chosen operating conditions for this work (25°C and 17 bar).

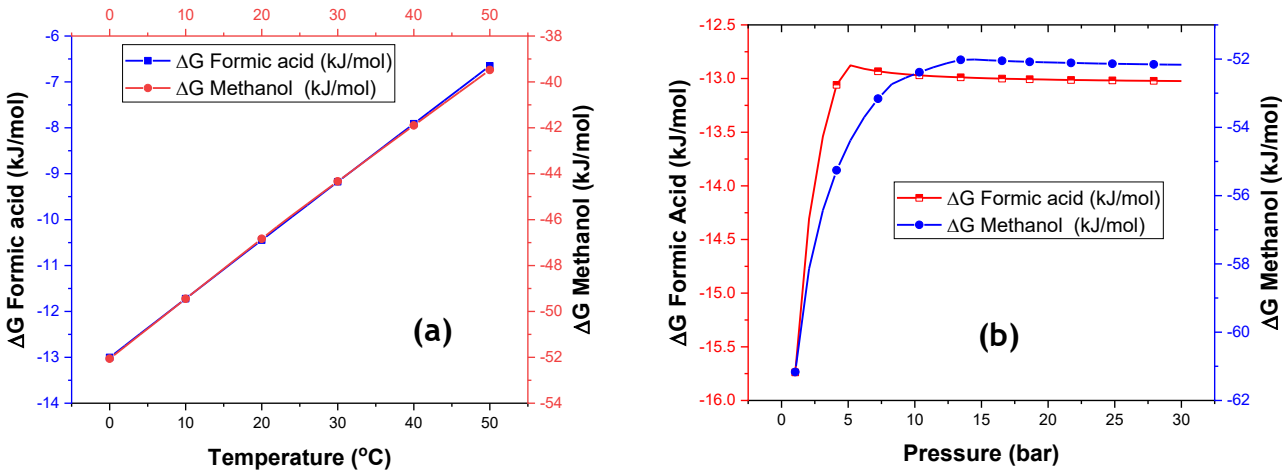

Figure III.22. Influence of operating conditions on Gibbs Energy of reaction (a). Variation of Temperature (b). Variation of Pressure

III.4 Conclusion

The thermodynamic analysis of CO_2 conversion to formic acid and methanol was performed in the presence of [Edmim][NO_2] by using the Aspen Plus process simulator. The formation of CO_2-[Edmim][NO_2] adduct during the solvation of CO_2 in [Edmim][NO_2]) greatly enhanced the formation of formic acid at ambient temperature. The effect of pressure, temperature, and feed ratio on CO_2 and H_2 conversion, yield, and selectivity of methanol and formic acid were studied. Moderate pressure, ambient temperature, and CO_2/H_2/[Edmim][NO_2] ratio = 1/2/2 were found to support the simultaneous synthesis of methanol and formic acid. At low temperature (0 -10 ^oC) and 17 bar, the yield of formic acid was ~65%, and CO_2 conversion was ~80%, while at 25 -32^OC the yield of methanol was ~67% and same CO_2 conversion. An approximately equal amount of formic acid and methanol (formic acid = 32% and methanol = 31%) was obtained at 24 – 25 ^OC.

AUTHOR INFORMATION

Corresponding Author: Rita Maria de Brito Alves

*Tel.: E-mail: rmbalves@usp.br

ORCID: **0000-0002-1914-5133**

Notes

The authors declare no competing financial interest.

Acknowledgments

The authors gratefully acknowledge the support of the RCGI – Research Centre for Gas Innovation, hosted by the University of São Paulo (USP) and sponsored by FAPESP – The São Paulo Research Foundation (2014/50279-4) and Shell Brasil. This study was financed in part by the Personnel Coordination of Improvement of Higher Level - Brazil (CAPES) - Finance Code 001.

Nomenclature

CO_2: Carbon dioxide

ILs: Ionic Liquids

H_2: Hydrogen gas

H_2S: Hydrogen Sulphide

VLE: Vapor-Liquid Equilibrium

COSMO-RS: Conductor-like Screening Model for Real Solvents

ΔG: Change in Gibbs energy of reaction

MeOH: Methanol

DME: Dimethyl ether

[Edmim][NO2]: 1-Ethyl-2,3-dimethylimidazolium nitrite

[Bmim][OAc]: 1-Butyl-3-methylimidazolium acetate

pK: Equilibrium dissociation constant

CRS: Chemical reaction stoichiometry

LCM: Law of the conservation of mass

PR-EOS: Peng Robinson Equation of state

P: Pressure

T: Temperature

Vm: Molar volume

a: constant contributing to molecular interaction

b: constant contributing to co-volume

R: Universal gas constant

kij: Binary interaction parameter

lij: Binary interaction parameter

III.5 References

ALTHULUTH, M. A. . **Natural Gas Sweetening Using Ionic Liquids**. [s.l.] Technische Universiteit Eindhoven, 2014.

ÁLVAREZ, A. et al. Challenges in the Greener Production of Formates/Formic Acid, Methanol, and DME by Heterogeneously Catalyzed CO 2 Hydrogenation Processes. **Chemical Reviews**, v. 117, n. 14, p. 9804–9838, 2017.

ARENA, F. et al. Synthesis, characterization and activity pattern of Cu-ZnO/ZrO2 catalysts in the hydrogenation of carbon dioxide to methanol. **Journal of Catalysis**, v. 249, n. 2, p. 185–194, 2007.

BAGCHI, B.; SATI, S.; SHILAPURAM, V. Modeling solubility of CO2/hydrocarbon gas in ionic liquid ([emim][FAP]) using Aspen Plus simulations. **Environmental Science and Pollution Research**, v. 24, n. 22, p. 18106–18122, 2017.

BELLO, T. O. et al. Systematic Screening of Ionic Liquids for Hydrogenation of Carbon dioxide to Formic Acid and Methanol. **Industrial & Engineering Chemistry Research**, 2021.

BERGER, A. et al. Ionic liquid-phase asymmetric catalytic hydrogenation: Hydrogen concentration effects on enantioselectivity. **Tetrahedron Asymmetry**, v. 12, n. 13, p. 1825–1828, 2001.

CRABTREE, G. W.; DRESSELHAUS, M. S.; BUCHANAN, M. V. The hydrogen economy. **Physics Today**, v. 57, n. 12, p. 39–44, 2004.

DE RIVA, J. et al. Aspen Plus supported conceptual design of the aromatic-aliphatic separation from low aromatic content naphtha using 4-methyl-N-butylpyridinium tetrafluoroborate ionic liquid. **Fuel Processing Technology**, v. 146, p. 29–38, 2016.

DYSON, P. et al. Determination of hydrogen concentration in ionic liquids and the effect (or lack of) on rates of hydrogenation. **Chemical Communications**, p. 2418–2419, 2003.

ELEK, J. ÁNOS et al. Homogeneous hydrogenation of carbon dioxide and bicarbonate in aqueous solution catalyzed by water-soluble ruthenium(II) phosphine complexes. **Applied Catalysis A: General**, v. 255, n. 1, p. 59–67, 2003.

FERRO, V. R. et al. Introducing process simulation in ionic liquids design/selection for separation processes based on operational and economic criteria through the example of their regeneration. **Separation and Purification Technology**, v. 97, p. 195–204, 2012.

FILONENKO, G. A. et al. Highly efficient reversible hydrogenation of carbon dioxide to formates using a ruthenium PNP-pincer catalyst. **ChemCatChem**, v. 6, n. 6, p. 1526–1530, 2014.

FREITAS, A. C. D. et al. Modeling vapor liquid equilibrium of ionic liquids + gas binary systems at high pressure with cubic equations of state. **Brazilian Journal of Chemical Engineering**, v. 30, n. 1, p. 63–73, 2013.

GAO, P. et al. Direct conversion of CO<inf>2</inf> into liquid fuels with high selectivity over a bifunctional catalyst. **Nature Chemistry**, v. 9, n. 10, p. 1019–1024, 2017.

GHAVRE, M.; MORRISSEY, S.; GATHERGOO, N. Hydrogenation in Ionic Liquids. **Ionic Liquids: Applications and Perspectives**, 2011.

GLASSER, L.; SMITH, W. Chemical Reaction Stoichiometry : A Key Link between Thermodynamics and Kinetics , and an Excel Implementation Chemical Reaction Stoichiometry : A Key Link between Thermodynamics and Kinetics , and an Excel Implementation. **chemrxiv**, n. 2, p. 1–20, 2019.

GRASEMANN, M.; LAURENCZY, G. Formic acid as a hydrogen source - Recent developments and future trends. **Energy and Environmental Science**, v. 5, n. 8, p. 8171–8181, 2012.

HAGHTALAB, A.; KHEIRI, A. High pressure measurement and CPA equation of state for solubility of carbon dioxide and hydrogen sulfide in 1-butyl-3-methylimidazolium acetate. **Journal of Chemical Thermodynamics**, v. 89, p. 41–50, 2015.

HIMEDA, Y. et al. Half-sandwich complexes with 4,7-dihydroxy-1,10-phenanthroline: Water-soluble, highly efficient catalysts for hydrogenation of bicarbonate attributable to the generation of an oxyanion on the catalyst ligand. **Organometallics**, v. 23, n. 7, p. 1480–1483, 2004.

HULL, J. F. et al. Reversible hydrogen storage using CO2 and a proton-switchable iridium catalyst in aqueous media under mild temperatures and pressures. **Nature Chemistry**, v. 4, n. 5, p. 383–388, 2012.

INOUE, Y. ; et al. Catalytic Fixation of Carbon dioxide to Formic Acid by Transition-Metal Complexes under Mild Conditions. **Chemistry Letters**, p. 863–864, 1976.

JESSOP, P. G.; IKARIYA, T.; NOYORI, R. Homogeneous Hydrogenation of Carbon Dioxide. **Chemical Reviews**, v. 95, n. 2, p. 259–272, 1995.

KOKORIN, A. **Ionic Liquids: Applications and Perspectives**. [s.l: s.n.].

LEITNER, W. Carbon Dioxide as a Raw Material: The Synthesis of Formic Acid and Its Derivatives from CO<inf>2</inf>. **Angewandte Chemie International Edition in English**, v. 34, n. 20, p. 2207–2221, 1995.

LINKE, W. F.; SEIDELL, A. Solubilities of Inorganic and Metal-Organic Compounds. **ACS**, v. 1, p. 1075, 1958.

LUO, X. et al. Significant improvements in CO<inf>2</inf> capture by pyridine-containing anion-functionalized ionic liquids through multiple-site cooperative interactions. **Angewandte Chemie - International Edition**, v. 53, n. 27, p. 7053–7057, 2014.

MACFARLANE, P. D. R.; KAR, D. M.; PRINGLE, D. J. M. **Fundamentals of Ionic Liquids Ionic Liquids in Biotransformations and Electrodeposition from Ionic Handbook of Green Chemistry – Green Solvents Electrochemical Aspects of Ionic Liquids , 2nd edition Nanocatalysis in Ionic Liquids**. [s.l: s.n.].

MASUDA, S. et al. PdAg Nanoparticles Supported on Functionalized Mesoporous Carbon: Promotional Effect of Surface Amine Groups in Reversible Hydrogen Delivery/Storage Mediated by Formic Acid/CO<inf>2</inf>. **ACS Catalysis**, v. 8, n. 3, p. 2277–2285, 2018.

MCNAMARA, N. D.; HICKS, J. C. CO<inf>2</inf> capture and conversion with a multifunctional polyethyleneimine-tethered iminophosphine iridium catalyst/adsorbent. **ChemSusChem**, v. 7, n. 4, p. 1114–1124, 2014.

MELLMANN, D. et al. Formic acid as a hydrogen storage material-development of homogeneous catalysts for selective hydrogen release. **Chemical Society Reviews**, v. 45, n. 14, p. 3954–3988, 2016.

MORI, K.; TAGA, T.; YAMASHITA, H. Isolated Single-Atomic Ru Catalyst Bound on a Layered Double Hydroxide for Hydrogenation of CO2 to Formic Acid. **ACS Catalysis**, v. 7, n. 5, p. 3147–3151, 2017.

MOTA MARTINEZ, M. T.; KROON, M. C.; PETERS, C. J. Modeling CO2 solubility in an ionic liquid: A comparison between a cubic and a group contribution EoS. **Journal of Supercritical Fluids**, v. 101, p. 54–62, 2015.

OLAH, G. A. Beyond Oil and Gas: The Methanol Economy. **Angewandte Chemie International Edition**, v. 44, n. 18, p. 1–10, 2005.

OLAH, G. A.; GOEPPERT, A.; PRAKASH, G. K. S. **Beyond Oil and Gas: The Methanol Economy**. Weinheim: Wiley-YCH, 2006.

PALOMAR, J. et al. Density and molar volume predictions using COSMO-RS for ionic liquids. An approach to solvent design. **Industrial and Engineering Chemistry Research**, v. 46, n. 18, p. 6041–6048, 2007.

PENG, D.-Y.; ROBINSON, D. B. A New Two-Constant Equation of State. **Industrial and Engineering Chemistry Fundamentals**, v. 15, n. 1, p. 59–64, 1976.

PERRY, R. H.; GREEN, D. W.; MALONEY, J. O. **Perry's Chemical Engineers' Handbook**. New York: McGraw-Hills, 1997.

PRETI, D.; SQUARCIALUPI, S.; FACHINETTI, G. Production of hcooh/net3 adducts by

co2/h2 incorporation into neat NEt3. **Angewandte Chemie - International Edition**, v. 49, n. 14, p. 2581–2584, 2010.

RAMDIN, M. et al. Solubility of CO<inf>2</inf> and CH<inf>4</inf> in ionic liquids: Ideal CO<inf>2</inf>/CH<inf>4</inf> selectivity. **Industrial and Engineering Chemistry Research**, v. 53, n. 40, p. 15427–15435, 2014.

REN, W.; SENSENICH, B.; SCURTO, A. M. High-pressure phase equilibria of {carbon dioxide (CO2) + n-alkyl-imidazolium bis(trifluoromethylsulfonyl)amide} ionic liquids. **Journal of Chemical Thermodynamics**, v. 42, n. 3, p. 305–311, 2010.

REUTEMANN, W.; KIECZKA, H. Formic acid. **Ullmann's Encyclopedia of Industrial Chemistry**, 2000.

SANDLER, S. I. **Using Aspen Plus in thermodynamics instruction: A step-by-step guide**. New Jersey: John Wiley & Sons, 2015.

SCHAUB, T.; PACIELLO, R. A. A process for the synthesis of formic acid by CO2 hydrogenation: Thermodynamic aspects and the role of CO. **Angewandte Chemie - International Edition**, v. 50, n. 32, p. 7278–7282, 2011.

SHARIATI, A.; PETERS, C. J. High-pressure phase behavior of systems with ionic liquids: Measurements and modeling of the binary system fluoroform + 1-ethyl-3-methylimidazolium hexafluorophosphate. **Journal of Supercritical Fluids**, v. 25, n. 2, p. 109–117, 2003.

SHARIATI, A.; PETERS, C. J. High-pressure phase behavior of systems with ionic liquids: Part III. The binary system carbon dioxide + 1-hexyl-3-methylimidazolium hexafluorophosphate. **Journal of Supercritical Fluids**, v. 30, n. 2, p. 139–144, 2004.

SHOJAEIAN, A. Thermodynamic modeling of solubility of hydrogen sulfide in ionic liquids using Peng Robinson-Two State equation of state. **Journal of Molecular Liquids**, v. 229, p. 591–598, 2017.

SMITH, J. M.; VAN NESS, H. C.; ABBOTT, M. **Introduction to chemical engineering thermodynamics**. New York: McGraw-Hill Education, 2005.

STANGELAND, K.; LI, H.; YU, Z. Thermodynamic Analysis of Chemical and Phase Equilibria in CO2 Hydrogenation to Methanol, Dimethyl Ether, and Higher Alcohols. **Industrial and Engineering Chemistry Research**, v. 57, n. 11, p. 4081–4094, 2018.

SU, J.; LU, M.; LIN, H. High yield production of formate by hydrogenating CO<inf>2</inf> derived ammonium carbamate/carbonate at room temperature. **Green Chemistry**, v. 17, n. 5, p. 2769–2773, 2015.

VALDERRAMA, J. O. The state of the cubic equations of state. **Industrial and Engineering Chemistry Research**, v. 42, n. 8, p. 1603–1618, 2003.

VALDERRAMA, J. O.; FORERO, L. A.; ROJAS, R. E. Critical properties and normal boiling temperature of ionic liquids. Update and a new consistency test. **Industrial and Engineering Chemistry Research**, v. 51, n. 22, p. 7838–7844, 2012.

WANG, W. .; HIMEDA, Y. Recent Advances in Transition Metal-Catalysed Homogeneous Hydrogenation of Carbon Dioxide in Aqueous Media. **School of Enviromental Sciences**, p. 250–264, 2012.

WANG, Y. et al. Activation of CO2 by ionic liquid EMIM-BF4 in the electrochemical system: a theoretical study. **Physical Chemistry Chemical Physics**, v. 17, n. 36, p. 23521–23531, 2015.

WU, Y. et al. Tetrabutylphosphonium-Based Ionic Liquid Catalyzed CO<inf>2</inf> Transformation at Ambient Conditions: A Case of Synthesis of α-Alkylidene Cyclic Carbonates. **ACS Catalysis**, v. 7, n. 9, p. 6251–6255, 2017.

WU, Y. et al. Ionic Liquid Promoted CO2 Hydrogenation to Free Formic Acid over Pd/C. **Industrial and Engineering Chemistry Research**, v. 58, n. 16, p. 6333–6339, 2019.

XU, W. et al. Thermodynamic analysis of formic acid synthesis from CO2hydrogenation. **ICMREE 2011 - Proceedings 2011 International Conference on Materials for Renewable Energy and Environment**, v. 2, p. 1473–1477, 2011.

YAZDIZADEH, M.; RAHMANI, F.; FORGHANI, A. A. Thermodynamic modeling of CO2 solubility in ionic liquid ([Cn-mim] [Tf2N]; n=2, 4, 6, 8) with using Wong-Sandler mixing rule, Peng-Rabinson equation of state (EOS) and differential evolution (DE) method. **Korean Journal of Chemical Engineering**, v. 28, n. 1, p. 246–251, 2011.

YOUNG, C. L. **INTERNATIONAL UNION OF PURE AND APPLIED CHEMISTRY Solubility data series**. [s.l.] Pergamon Press, 1983. v. 5/6

YUE, C. et al. Amino-functional imidazolium ionic liquids for CO2 activation and conversion to form cyclic carbonate. **Catalysis Letters**, v. 144, n. 7, p. 1313–1321, 2014.

ZENG, S. et al. Ionic-Liquid-Based CO<inf>2</inf> Capture Systems: Structure, Interaction and Process. **Chemical Reviews**, v. 117, n. 14, p. 9625–9673, 2017.

ZHAO, Y. et al. Azole-Anion-Based Aprotic Ionic Liquids: Functional Solvents for Atmospheric CO<inf>2</inf> Transformation into Various Heterocyclic Compounds. **Chemistry - An Asian Journal**, v. 11, n. 19, p. 2735–2740, 2016.

CHAPTER IV

A MECHANISTIC STUDY ON CONVERSION OF CARBON DIOXIDE INTO FORMIC ACID PROMOTED BY 1-ETHYL-2,3-DIMETHYL-IMIDAZOLIUM NITRITE

This paper is being prepared for submission in a reputable Journal

Abstract

The carbon dioxide (CO_2) conversion to formic acid (FA) promoted by the hydrogenation reaction with 1-ethyl-2,3-dimethyl imidazolium Nitrite (EDIN) ionic liquid was investigated by theoretical calculations. The purpose is to understand better the role of the catalytic sites in the EDIN. Therefore, two mechanistic reaction pathways were thermodynamically and kinetically computed by quantum chemical calculations at two levels of theory: Restricted Hartree Fock (RHF) and density functional theory (DFT). The calculations showed that the nitrite (NO_2^-) group is the more active site in the EDIN. The nucleophilic oxygen site activates the H_2 molecule in a favored pathway, whereas the nitrogen site may be activated in a second pathway with a minor barrier of 108.90 kJ/mol kinetically overcome. Moreover, the favorable Gibbs energy variation indicates the formation of more stable FA product through the EDIN. Therefore, our results showed that H_2 may be rather suffer activation with subsequent attacked/activation of CO_2 by the EDIN. These results have valuable implications for the development of more effective active sites and routes in ionic liquid catalysts for the hydrogenation of CO_2.

Highlights

- Hydrogenation of CO_2 to formic acid catalyzed by EDIN was investigated.
- Thermodynamic and kinetic properties obtained by quantum chemical calculations.
- Two possible mechanistic pathways were proposed and computed.
- The nitrite anion in the ionic liquid displays a critical role mainly in the H_2 activation process.

Keywords: Carbon dioxide; formic acid; ionic liquid; theoretical calculations; mechanistic pathways

IV.1 Introduction

In recent decades, earth's atmosphere has witnessed increased emission of greenhouse gas concentrations, particularly carbon dioxide (CO_2). This has exacerbated a range of environmental issues, such as ocean acidification and declining biodiversity. Consequently, it has become imperative to control excessive CO_2 emissions through carbon capture, utilization, and storage (CCUS) processes, having drawn significant attention worldwide (MELZER, 2012). CO_2 is an inexpensive source of carbon. From an economic and environmental point of view, CO_2 conversion into valuable products is led by beneficial processes (JESSOP, PHILLIP G. ; IKARIYA, TAKAO ; NOYORI, 1994)(LEITNER, 1995). A prospective solution to achieving an environmentally friendly and safe carbon cycle (BORETTI, 2013) is the catalytic CO_2 conversion by hydrogenation from renewable energy-powered water electrolysis to produce formic acid (HCOOH), methane (CH_4), and methanol (CH_3OH) (OU et al., 2019).

A very promising carbon conversion alternative is related to the synthesis of formic acid (FA) utilized in many industrial applications such as the leather industry as a tanning agent, preservative in livestock feeds, cleaning agent, and other essential platform chemicals. With global production currently at 800,000 tons annually, FA is an important chemical that will continue to be in high demand, especially in a hydrogen-driven economy (SCHLAPBACH; ZÜTTEL, 2001). According to Schlapbach and Zuttel (SCHLAPBACH; ZÜTTEL, 2001), FA production could greatly increase due to effective FA dehydrogenation catalysts that could find application in a hydrogen economy(SCHLAPBACH; ZÜTTEL, 2001). Nevertheless, effective FA production is imperative, which largely depends on the selection of suitable catalytic hydrogenation pathways (MORET; DYSON; LAURENCZY, 2014b).

Currently, industrial FA production mostly operates using methanol-CO reaction mechanism under basic conditions, with subsequent methyl-formate hydrolysis(SREDOJEVIĆ et al., 2018). This process has some drawbacks, such as multisteps that consumes a large amount of energy, sensitivity to moisture and CO_2, and intermediates that require several separations steps leading to high cost(BULUSHEV; ROSS, 2018). However, FA production from H_2 and CO_2 could be an efficient approach from an atom-economy view.

CO_2 hydrogenation in organic solvents, supercritical CO_2, and aqueous solutions with organic or inorganic base or task-specific ionic liquids (IL) as promoters have been investigated in the recent past (HIMEDA et al., 2005; JESSOP; JOÓ; TAI, 2004). The conversion of CO_2

into FA utilizing H_2 from renewable sources in a one-step process offers a more effective alternative to the present synthesis approaches because of low resource-intensive, high CO_2 usage, and reduction in an intermediates generation (GRASEMANN; LAURENCZY, 2012; HULL et al., 2012). However, the presence of the covalent double bond makes CO_2 thermodynamically stable and kinetically inert. Hence, converting CO_2 with high efficiency and selectivity usually requires the combination of a favorable solvent to stabilize the hydrogenation product and a good catalyst to reduce the energy barrier through possible intermediates(CHEN; MU, 2019). Therefore, the efficient CO_2 hydrogenation process has been a major challenge for researchers in recent times. Interestingly, transition-metal-based catalysts for CO_2 reduction have gained ground in recent years (BALARAMAN et al., 2011; BONTEMPS; VENDIER; SABO-ETIENNE, 2014). However, the cost of these catalysts and their imminent toxicity remains the main drawbacks for large-scale industrial application (GHARA; CHATTARAJ, 2019).

Numerous approaches involving CO_2 hydrogenation as an alternative route have been developed. For instance, Han et al. utilized amino-based ILs with Ru-immobilized silica as the heterogeneous catalyst to develop a reaction/separation system for the synthesis of FA from CO_2 hydrogenation at 60ºC (ZHANG et al., 2008). The recovery of products and catalyst regeneration were easily achieved by evaporation and filtration. Furthermore, Dupont's group utilized [BMIM][Ac] as the reaction solvent with two other co-solvent, H_2O and DMSO, in the presence of RuFe as catalysts to produce FA at a lower pressure (1 MPa CO_2 and 2 MPa H_2) (WEILHARD et al., 2018). Notwithstanding the stride of these studies, reactions promoted by ILs with nitrite anions were seldomly considered. Additionally, the cost of catalyst and separation of intermediates are the major stumbling blocks of these reactions for industrial application (CHEN; MU, 2019). Therefore, considering the economic value of FA, developing a cost-effective catalytic and environmentally viable system is imperative to off-shoot complex downstream processes involved in the recovery of the final product(PATIL et al., 2008)

Considering their numerous unique benefits of nonvolatility, nonflammability, recyclability, and the ability to dissolve a variety of materials, ILs have gained great attention in organic compounds synthesis. ILs have been subject of considerable interest as benign (mild) reaction media in organic synthesis(BHARGAVA; YASAKA; KLEIN, 2011). ILs have marched well beyond this frontier lately, demonstrating their important role in controlling the reaction as catalysts (RATTI, 2014; WASSERSCHEID; ANNEGRET, 2010; WELTON, 1999,

2004). Besides, ILs are known to play an important part in reaction kinetics and equilibrium by their unique solvation of reactants by the ions (BHARGAVA; YASAKA; KLEIN, 2011).

Additionally, theoretical investigations could be useful in understanding the mechanism of transformations, adsorption modes, activation energies, nature of transition states, and the role of catalyst (PENG et al., 2012)·(REN et al., 2011). Recently, Ghara and Chattaraj(GHARA; CHATTARAJ, 2019) used density functional theory (DFT) to investigate the mechanism of the CO_2 hydrogenation to FA promoted by a bridged Frustrated Lewis Pair (FLP) (GHARA; CHATTARAJ, 2019). Their findings suggested that both the Lewis basic and acidic centers can activate hydrogenation through two possible pathways. This implies that FLP might be a potential candidate as a catalyst for CO_2 hydrogenation. In two other theoretical studies, Esrafili and Dinparast (ESRAFILI; DINPARAST, 2017), Esrafili and Nejadebrahimi (ESRAFILI; NEJADEBRAHIMI, 2019) found that Ti-doped graphene nanoflake and single Colbat (Co) atom incorporated nitrogen-doped graphene are potential catalysts for the CO_2 hydrogenation into FA. Similarly, Sirijaraensre and Limtrakul (SIRIJARAENSRE; LIMTRAKUL, 2016) employed DFT calculations and found that Cu-doped graphene is also a promising catalyst for CO_2 hydrogenation into FA.

As no theoretical study has been performed on the CO_2 hydrogenation promoted by the 1-ethyl-2,3-dimethyl-imidazolium nitrite (EDIN) ionic liquid, herein, we provide insights into possible pathways, structural and energetic details for EDIN as a possible catalyst toward the FA production. For that, thermodynamic and kinetic theoretical calculations were performed. The method attempts to perform quantum chemical calculations to simulate the reaction pathways for the process of CO_2 hydrogenation promoted by the EDIN. In addition, geometry optimization, vibrational frequency analysis, and intrinsic reaction coordinate calculations were computed. The calculations were performed at two levels of theory: Restricted Hartree Fock (RHF) and density functional theory (DFT).

IV.2 Computational Details

All quantum chemical calculations were performed at the RHF and DFT levels using the ORCA computational software package version 4.2(NEESE et al., 2020). The calculations were implemented with a valence double-zeta polarization (Def2-SVP) basis set for both RHF and DFT levels. According to the recommendation from the software, a polarized double-zeta basis set, such as Def2-SVP, can converge considerably well geometry and energies for both HF and DFT calculations(NEESE et al., 2020). Additionally, hybrid functional B3LYP was

used for the DFT calculation. B3LYP functional is proposed to converge rapidly with increasing basis set and optimal in cost-to-benefit ratio on much larger molecules. It is also the most popular functional, and its results can lead to vibrational force fields, frequencies, and spectra, as well as thermochemical properties, of superior accuracy (STEPHENS et al., 1994).

It should be stressed that the focus of our work is to verify the possible reaction mechanisms of the hydrogenation of CO_2 into FA according to the possible catalytic sites of the EDIN promoter/IL toward the reaction. In the gas phase, experimental results show that ILs are free from free ions or higher aggregates (at low pressure and temperatures above 474 K) and can be composed by neutral ion pairs(LEAL et al., 2007). Some theoretical works show also that dispersion forces can display a role important to describe ILs(IZGORODINA et al., 2017; LEAL et al., 2007; VEREVKIN et al., 2010; ZAHN et al., 2014). Therefore, our optimization, kinetics, and thermodynamics calculations were carried out in the gas phase. For that, our calculations performed at the RHF and DFT levels in gas phase with B3LYP functional and dispersion forces tend to be enough to produce accurate description of the interactions simulated in our models.

IV.2.1 Kinetic Calculations

The Nudged Elastic Band Transition State (NEB-TS) approach, which is a combination of the Climbing Image-NEB (CI-NEB) and Eigenvector-Following (EF) methods in Orca, was used to find the minimum energy path (MEP) connecting the energy surface to the minimum reactant and product states. The ORCA implementation is defined in detail in references (ASGEIRSSON et al., 2020)(NEESE et al., 2020). This method uses the CI-NEB to first get a reasonable initial guess for the saddle point configuration from which an EF saddle point search is initiated. The main benefit of the NEB-TS method is that only gradients are needed (unlike transit-guided quasi-Newton, STQN), as in regular optimizations (no specific Hessian needed) or surface scans, but unlike surface scans, the procedure converges to the MEP and allows for convenient optimization of the saddle point in the same calculation. In the NEB-TS approach, an initial pathway is generated and represented by a discrete set of atom configurations, known as the system images. The number of images is determined by the user and must be sufficiently large to obtain adequate path resolution. The straight line between images is shown in Table 1. The spring type for image distribution (distance between adjacent images) is energy weighted with a constant between 0.0100 to 0.1000 Eh/Bohr^2.

Table IV.10. Straight line distance between images along the path

Image	Distance (Ang.)	Image	Distance (Ang.)
D (0- 1)	5.7767	D (5- 6)	0.8215
D (1- 2)	3.4543	D (6- 7)	0.9587
D (2- 3)	2.1304	D (7- 8)	2.3525
D (3- 4)	1.1777	D (8- 9)	3.4420
D (4- 5)	0.6687		

All molecules were set up and edited using the Avogadro software (Orca version) (AVOGADRO(ORCA), 2020)(HANWELL et al., 2012). Herein, the reactants (i.e., H_2 + CO_2 + EDIN) and products (i.e., FA + EDIN) are defined as a collection of molecules. Geometry optimization of all structures, including reactants, transition states (TS), intermediates, and products, were performed in the gas phase with RHF and DFT levels of theory. The calculation was performed in the gas phase due to computational resources. Further evaluation can be done in the aqueous phase to confirm variation in the energetic pathways. However, we believe that the reaction steps should be the same in solution but changes in variation in the energy barriers(REN et al., 2011). The optimized structures related to stationary points (local minimum for reactants, intermediates, and products, or first-order saddle point for transitional states) were checked through the vibrational frequency analysis. An intrinsic reaction coordinate (IRC) analysis was carried out to ensure that the TS links the two desired minima correctly(NEESE et al., 2020)

IV.2.2 Thermochemistry

From vibrational frequency calculations, the thermochemical analyses based on ideal gas statistical mechanics can be evaluated. Thermodynamic properties such as heat of formation, dissociation energies, Gibb's energy, and other similar properties can be obtained through these calculations. The internal energy is calculated as the contribution of the total energy from the terms of electronic energy (E_{el}), zero temperature vibrational energy from the frequency calculation (E_{ZPE}), vibrational energy (E_{vib}), rotational thermal energy (E_{rot}), and translational thermal energy (E_{trans}) according to equation IV.1:

$$U = E_{el} + E_{ZPE} + E_{vib} + E_{rot} + E_{trans} \quad \text{(IV. 1)}$$

Enthalpies (H) were evaluated as the addition of the internal energy with the Boltzman's constant at 298.15K corrected with thermal enthalpy value (Equation IV.2). The entropy (S) was calculated as the sum of the contribution of the terms of electronic entropy (S_{el}), vibrational (S_{vib}), rotational (S_{rot}), and translational (S_{trans}) (Equation IV.3). Finally, the Gibbs energy (G) was evaluated by equations V.4. The changes in the thermodynamic properties of enthalpy (Equation IV.5) and Gibbs (Equation IV.6) energies were calculated as the energy difference between the sum of products and reactants.

$$H = U + kB * T \quad \text{(IV. 2)}$$

$$T * S = T * S_{(el)} + S_{(vib)} + S_{(rot)} + S_{(trans)} \quad \text{(IV. 3)}$$

$$G = H - T * S \quad \text{(IV.4)}$$

$$\Delta H = \sum H_{products} - \sum H_{reactants} \quad \text{(IV. 5)}$$

$$\Delta G = \sum G_{products} - \sum G_{reactants} \quad \text{(IV. 6)}$$

IV.3 Result and Discussion

In order to verify the validity of the results and support the choice of the possible catalyst in our study, the reaction of CO_2 hydrogenation into FA in the absence of promoter/IL was carried out in the gas phase. The Gibbs energy variations are calculated in 29.99 and 31.00 kJ/mol for RHF and DFT, respectively. These results conform with literature values (32.00 kJ/mol)(HAO et al., 2011), considering the level of theory adopted.

Figure IV.1 depicts the results of the reaction pathway profile that connects the reactant, transition state, and the product of the unpromoted reaction at 298.15K and 1atm. Two transition structures were found in both levels of theory. Figures S1 and S2 in supplementary information show the minimized geometries of the transition states, intermediates, and products of the unpromoted reaction with HF and DFT, respectively. In Figure IV.23, the TS1 and TS2 transition states have imaginary vibrational frequencies of -2214.32 and -643.1i cm^{-1} for DFT, respectively, whereas RHF is -2709.46 and -457.51i cm^{-1}, respectively. For both levels of theory, the TS1 structure corresponds to the cleavage of the H-H bond and an atom/radical of hydrogen weakly attached to the oxygen center of the CO_2 to form an O-H bond, whereas a structural rotation of the C=O and C-H bond around the carbon center is related to the TS2 structure. Table IV.2 shows the energy variation of the reaction with the transition states connecting the reactants and the product from the unpromoted reaction at both levels of

theory. The high Gibbs energy barriers of 304.00 and 394.00 kJ/mol display the difficulty associated with the hydrogenation reaction to take place in the absence of a possible catalyst or promoter.

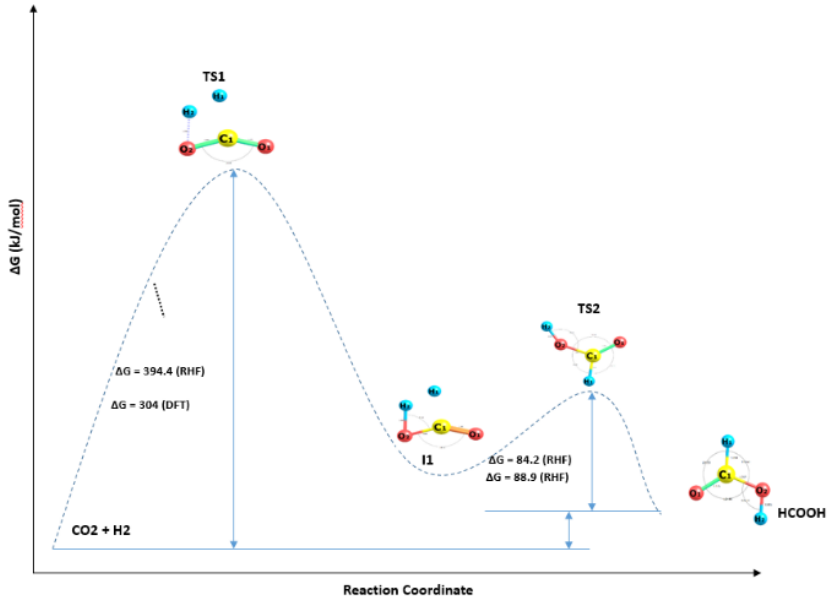

Figure IV.23 Energy profile of reactants, transition states, and products of the unpromoted reaction of CO_2 hydrogenation into formic acid (FA) with Restricted Hartree Fock (RHF) and density functional theory (DFT) levels.

Table IV.11. Gas Phase Gibbs Energy of unpromoted reaction with RHF and DFT at 298.15K and 1atm.

Theory	ΔG_R (kJ/mol)	TS1 (kJ/mol)	TS2 (kJ/mol)	I1 (kJ/mol)
RHF	30.0	394.4	88.9	30.0
DFT	31.41	304.1	84.2	50.42

Tables S1, S2, and S3 in Supplementary Information show the contributions of the internal energy, entropy, and enthalpy of the unpromoted reaction with RHF, respectively. Tables-S4, S5, and S6 show the contributions of the internal energy, entropy, and enthalpy of the unpromoted reaction with DFT, respectively.

To confirm that the NO_2^- group is the main active center in the EDIN ionic liquid, and the 'regiochemical preference'(REN et al., 2011) for the hydrogenation, we calculated the molecular orbital (FUKUI; FUJIMOTO, 1997)(HOFFMANN, 1988) (Figure IV.2). It can be

observed that the s and p_y-orbitals of the N23 site and the p_y-orbital of the O24 site have a major influence on the highest occupied molecular orbital (HOMO).

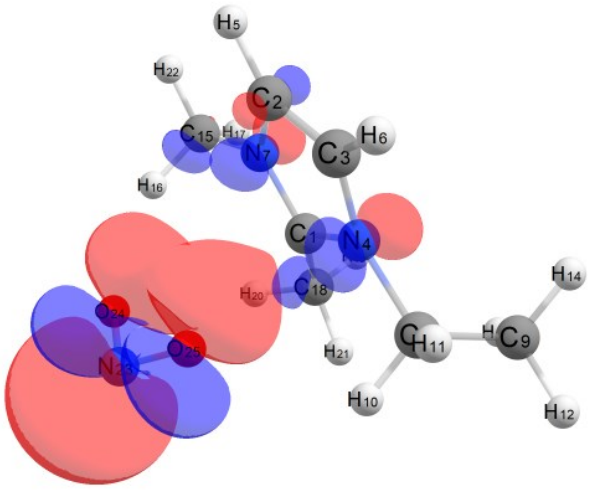

Figure IV.24. Highest Occupied Molecular Orbital (HOMO) calculated for the the 1-ethyl-2,3-dimethyl-imidazolium nitrite (EDIN) ionic liquid.

IV.3.1 Reaction Pathway A

The reaction pathway A is based on the theoretical calculation from the CO_2 hydrogenation into FA promoted by EDIN with the RHF computational level of theory. The calculated reaction pathway and the structures related to transition states, intermediates, and products are shown in Figures IV.3 and IV.4, respectively.

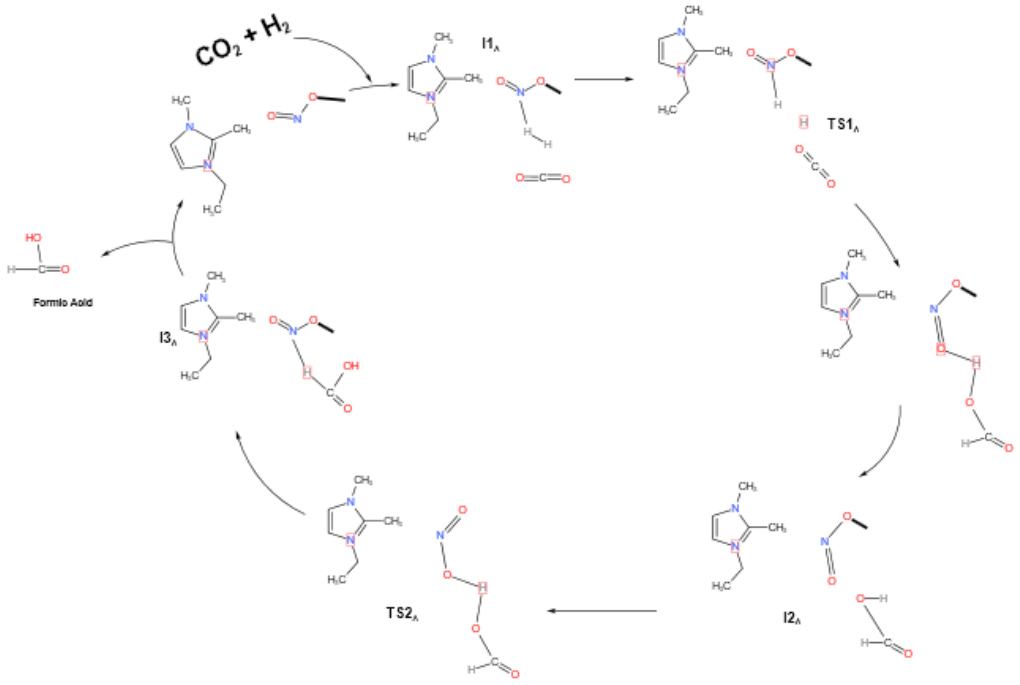

Figure IV.25. Proposed mechanism A for the CO_2 hydrogenation promoted by the 1-ethyl-2,3-dimethyl-imidazolium nitrite (EDIN) ionic liquid, in which nitrogen center activates H_2.

From Figure IV.4, the NO_2^- group of the IL activates the H_2 molecule by cleaving the bond into free hydrogen ions. The reaction mechanism is observed to begin with a "pre-reacting" complex I, where the hydrogen molecule is weakly interacting with the nitrogen center of the NO_2^- group with a bond length of 1.88Å. The CO_2 molecule is still relatively linear in the complex with a bond angle of 176.84º and well-positioned below the weakly bonded hydrogen molecule to the NO_2^- group. Afterward, the cleavage of the H-H sigma bond takes place. One hydrogen is attached weakly to the nitrogen center of the NO_2^- group, whereas the second hydrogen moved freely, characterizing the transition state 1 ($TS1_A$). Here, the CO_2 fragment bond angle has undergone transformation (bending) 150.21º, yet well positioned below the cleaved hydrogen molecule.

The hydrogenation of CO_2 was then initiated simultaneously by the hydrogen atom weakly interacting (1.30Å) with the nitrogen center and free hydrogen in the complex to reach an intermediate 2 ($I2_A$) through the $TS1_A$ transition state. Consequently, the $I2_A$ intermediate goes to the product complex/intermediate 3 ($I3_A$) through the $TS2_A$ transition state. The $I2_A$ intermediate is characterized by the strong interaction of the cleaved hydrogen atom (H1) from the $TS1_A$ transition state with the nitrogen center of the NO_2^- group and free hydrogen (H2). The transition state 2 ($TS2_A$) corresponds to the bending of the CO_2 group (127.37º) and the unstable FA product characterized by the tendency to delocalize the electron on the unsaturated carbon-to-oxygen (C=O) double bond. In the $I3_A$ intermediate, a weak interaction exists between the oxygen center of the NO_2^- group and the acidic hydrogen center of FA with a bond length of 1.80Å.

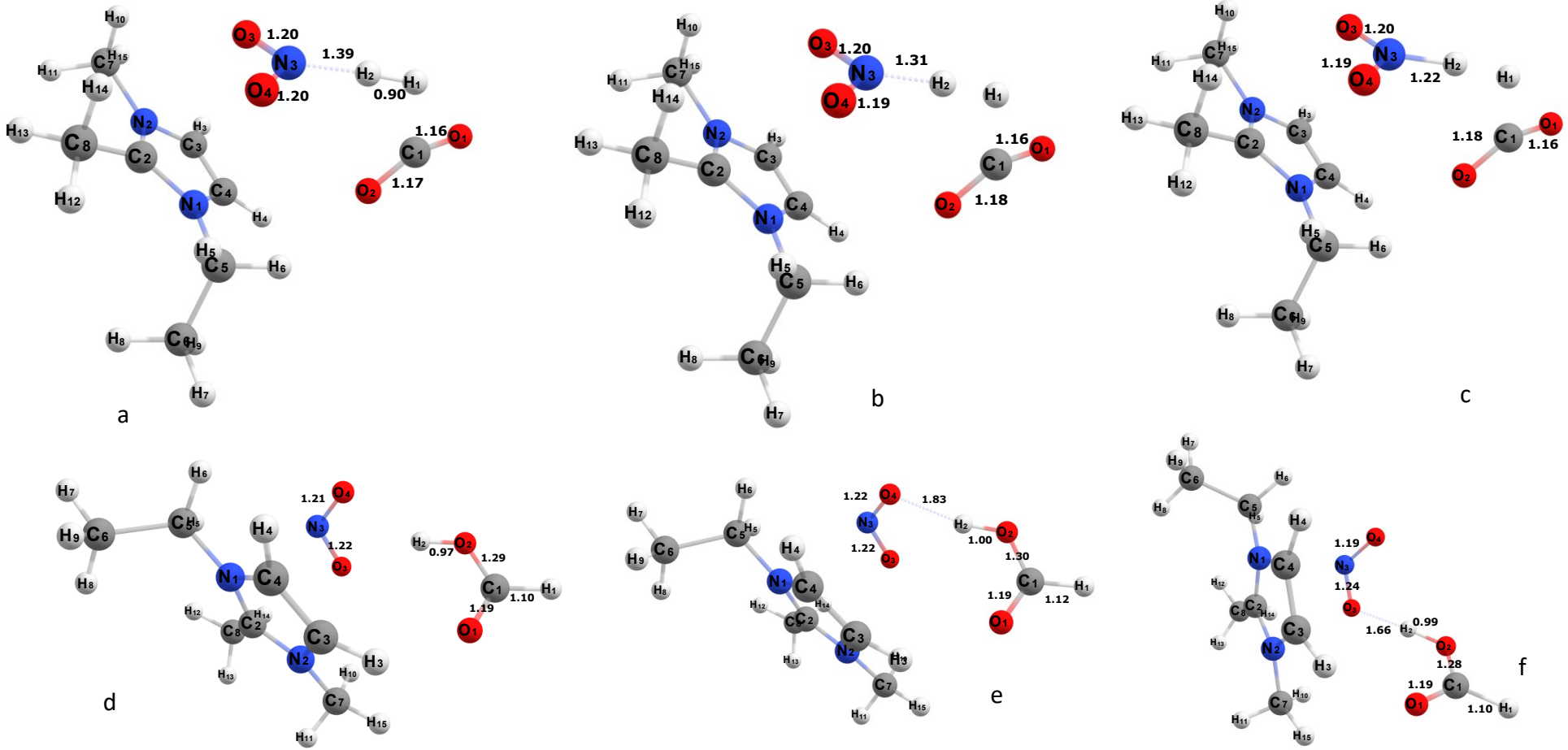

Figure IV.26. Structures of the CO2 hydrogenation to FA promoted by the 1-ethyl-2,3-dimethyl-imidazolium nitrite (EDIN) ionic liquid and optimized by Restricted Hatree Fock (RHF): (a) intermediate 1 (pre-reacting complex), (b) transition state 1, (c) intermediate 2, (d) transition state 2, (e) intermediate 3 (product complex), and (f) products.

IV.3.2 Energetics Pathway A

Figure IV.5 shows the energy profile of the reaction pathway A calculated by the Restricted Hartree Fock (RHF) theory level for the CO_2 hydrogenation into FA promoted by the 1-ethyl-2,3-dimethyl-imidazolium nitrite (EDIN) according to the optimized structures in Figure IV.4. This energy profile shows that the CO_2 hydrogenation promoted by the EDIN ionic liquid is a process with two transition states. First, the initial pre-reacting complex ($I1_A$ intermediate) is formed with 0.57kJ/mol lower in Gibbs energy from the reactants. The $I1_A$ intermediate goes to the $I2_A$ intermediate through the $TS1_A$ transition state with a higher energy barrier of 211.90 kJ/mol with respect to the reactant. Here, the formation of the $I2_A$ and $I3_A$ intermediates are exergonic, accompanied by energy release of 10.69 and 8.47 kJ/mol, respectively. The $TS1_A$ and $TS2_A$ transition states are characterized by one single imaginary frequency of –1562.3 and -192*i* cm^{-1}, respectively, corresponding to the cleavage of the H-H bond and the bending of CO_2 simultaneously. The H-H bond length increases to 0.99Å at the $TS1_A$ transition state from its equilibrium bond length of 0.75Å, and the bond angle in CO_2 (O-C-O) becomes 158° at the $TS1_A$ transition state. Tables S7, S8, and S9 in the supporting information show the contributions of the internal energy, entropy, and enthalpy of the promoted reaction with RHF, respectively.

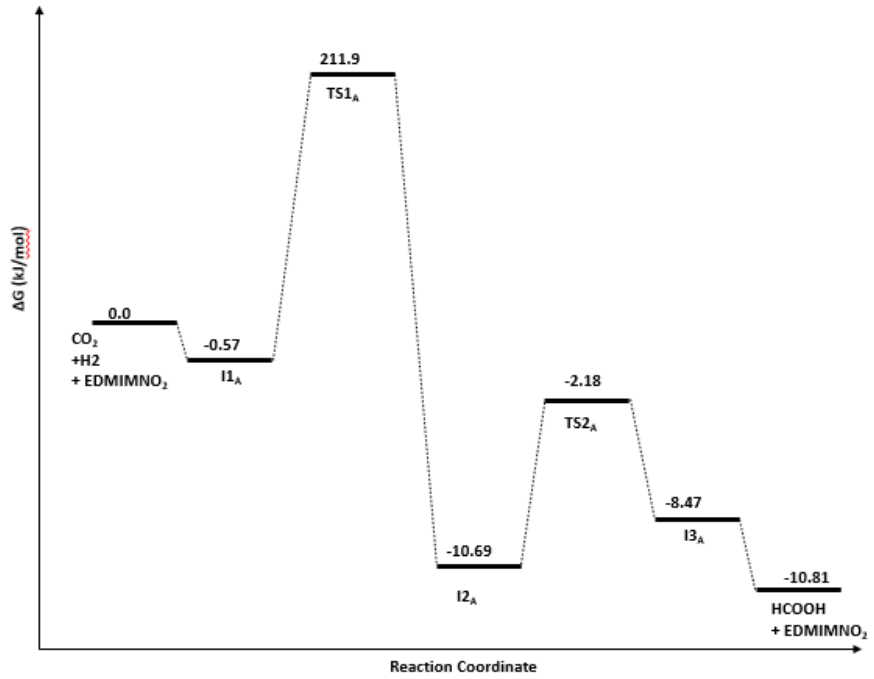

Figure IV.27. Energy profile of the reaction pathway A calculated by the Restricted Hartree Fock (RHF) theory level for CO2 hydrogenation into FA promoted by EDIN.

IV.3.3 Reaction Pathway B

The reaction pathway B is obtained through DFT calculations. The proposed mechanism B and the optimized structures of the reactants, transition states, intermediates, and products are shown in figures IV.5 and IV.6 respectively. The "pre-reacting" complex/intermediate 1 (I_B) is formed between the IL and the H_2 molecule. The H_2 molecule is weakly attached to the nucleophilic oxygen atom center of the NO_2^- group is 1.69Å. The oxygen center of the NO_2^- group activates the H_2 molecule. The length between the H_2 molecule and the oxygen center is reduced to 1.33Å at the $TS1_B$ transition state, which has the H-to-H sigma bond distance increased to 0.96Å from 0.78Å. This geometric result shows a tendency of cleavage of the H-to-H bond to reach an intermediate state 2 ($I2_B$) through the $TS1_B$ transition state. Therefore, in the $I2_B$ intermediate, the H-to-H bond in H_2 is completely broken; one hydrogen is attached to the oxygen center of the NO_2^- group and the other hydrogen a is freely available. In the next step, the $I2_B$ intermediate goes to the $I3_B$ intermediate through the addition of the free H to the carbon center of the CO_2 at the $TS2_B$ transition state. Then, the $I3_B$ intermediate goes to the $I4_B$ intermediate (product complex) through another transition state, $TS3_B$. This second transition state corresponds to the re-arrangement of the oxygen atoms bonded to the carbon center (O1 and O2) of carbon dioxide and the shifting of hydrogen in the

OH bond (O2-H2) closer to the carbon atom center from 1.56Å at the $I2_B$ intermediate to 1.50Å at the $TS3_B$ transition state. Subsequently, the $I4_B$ intermediate reaches another product complex, the $I5_B$ intermediate, through the $TS4_B$ transition state. Here, there is a structural shift of the OH of the COOH moiety from the nucleophilic oxygen center of the NO_2^- group to the stable oxygen center (from O4 to O3). The FA molecule is removed from the $I5_B$ product complex to complete the catalytic cycle.

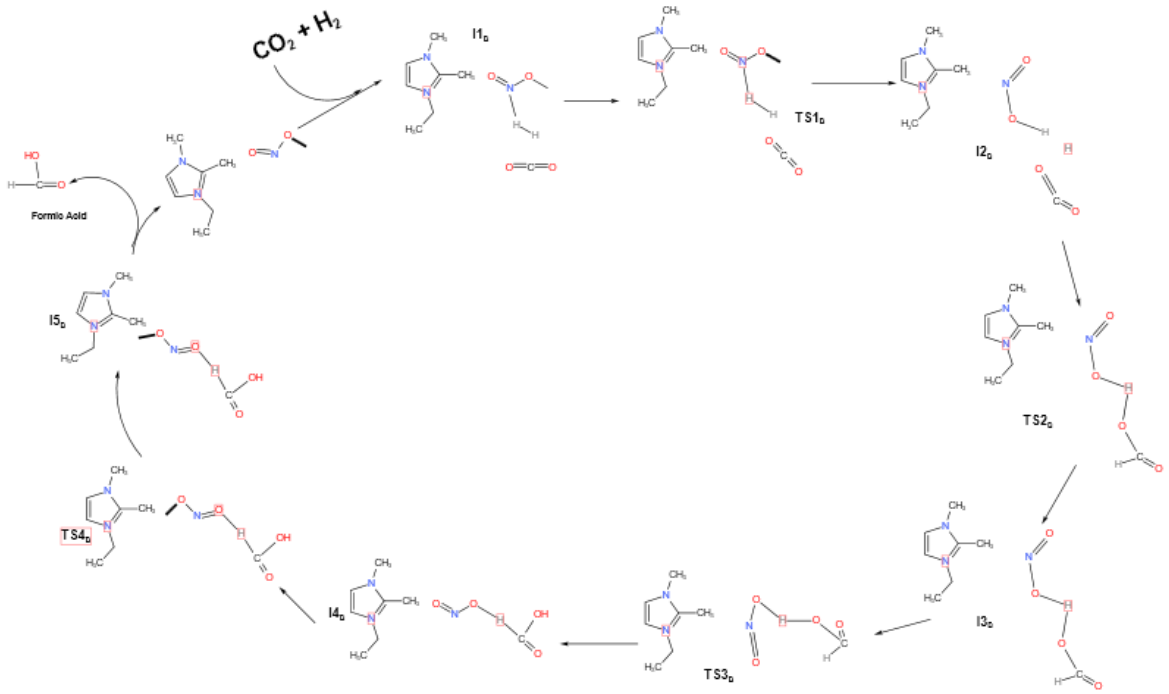

Figure IV.28. Proposed mechanism B for the CO_2 hydrogenation promoted by the 1-ethyl-2,3-dimethyl-imidazolium nitrite (EDIN) ionic liquid, in which the oxygen center activates H_2.

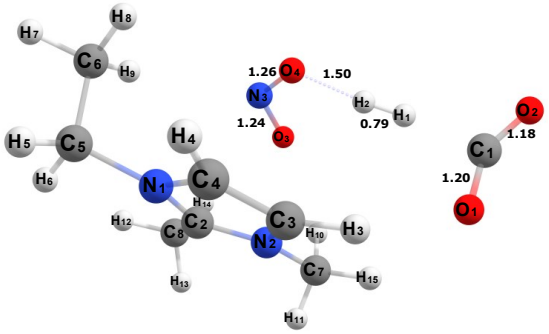

a

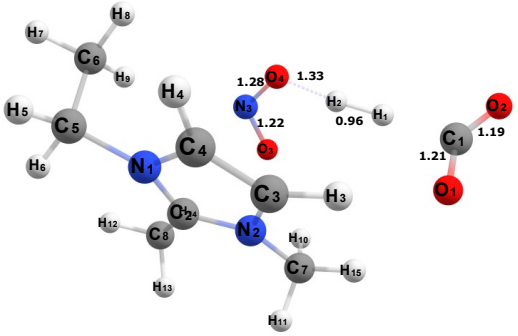

b

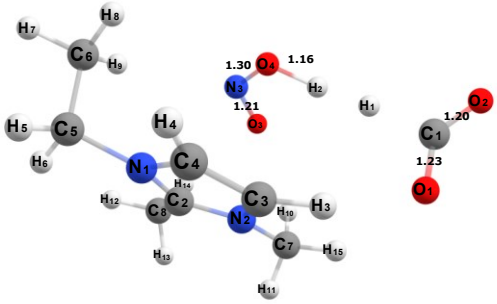

c

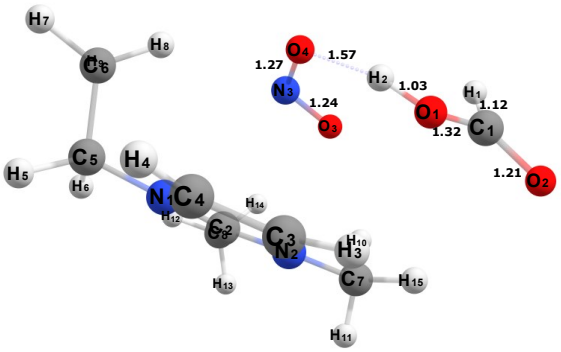

d

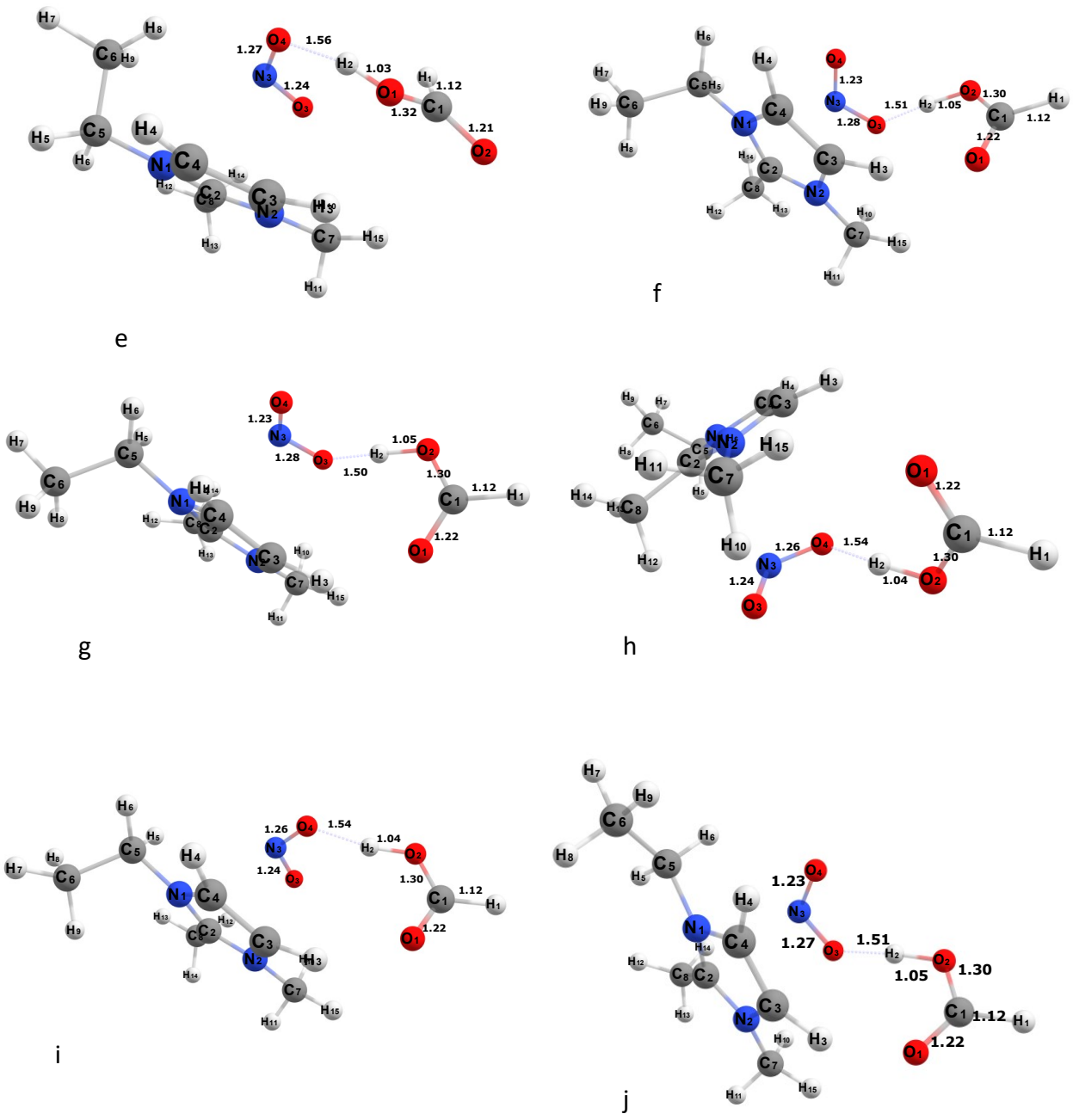

Figure IV.29. Structures of the CO2 hydrogenation to FA promoted by the 1-ethyl-2,3-dimethyl-imidazolium nitrite (EDIN) ionic liquid and optimized by the density functional theory (DFT) level: (a) intermediate 1 (pre-reacting complex), (b) transition state 1, (c) in intermediate 2, (d) transition state 2, (e) intermediate 3, (f) trasition state 3, (g) intermediate 4 (product complex), (h) transition state 4, (i) intermediate 5 (product complex), and (j) products.

IV.3.4 Energetics Pathway B

Figure IV.7 shows the energy profile of the reaction pathway B calculated by the density functional theory (DFT) level for the CO_2 hydrogenation into FA promoted by the 1-ethyl-2,3-dimethyl-imidazolium nitrite (EDIN) ionic liquid according to the optimized structures in Figure IV.6. The CO_2 hydrogenation promoted by the EDIN ionic liquid at the DFT level of theory is composed of four transition states. An initially activated complex of the $I1_B$ intermediate is formed with 22.60 kJ/mol lower in Gibbs energy from the reactants. Then the complex goes to the $I2_B$ intermediate through the $TS1_B$ transition state with an energy barrier of 108.90 kJ/mol with respect to the reactant. Herein, it was observed that the formation of the $I3_B$, $I4_B$, and $I5_B$ intermediates are exergonic and accompanied by energy release of 16.83, 27.60, and 28.5 kJ/mol, respectively. Additionally, the $TS1_B$, $TS2_B$, $TS3_B$, and $TS4_B$ transition states are characterized by one single imaginary frequency with respective values of –654.27, -183.78, -232.24, and -100*i* cm^{-1}, corresponding to the cleavage of the H-H bond and the bending of CO_2 progressively. At the $TS2_B$ transition state, the H-H bond length was increased to 0.96Å from its equilibrium bond distance of 0.75 Å, with CO_2 bond angle (O-C-O) of 146.60° and 123.30°. The CO_2 bond angle has 127.9° at both $TS3_B$ and $TS4_B$ transition states.

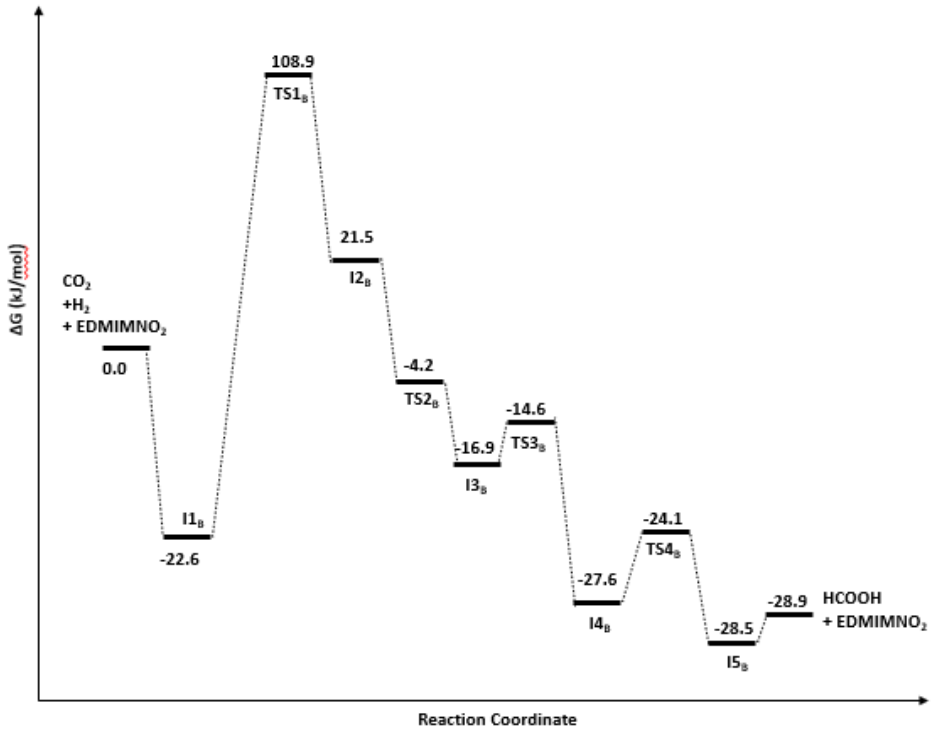

Figure IV.30. Energy profile of the reaction pathway B calculated by the density functional theory (DFT) level for the CO2 hydrogenation into FA promoted by EDIN according to the optimized structures in Figure IV.6.

Tables S10, S11, and S12, in the supporting information, show the contributions of the internal energy, entropy, and enthalpy of the promoted reaction with DFT, respectively.

Comparing the results from the RHF and DFT calculations, there is a significant difference in the values of the Gibbs energy. This might be related to the smaller basis set used with RHF for a complex system because both levels of theory (RHF and DFT) showed similar results when implemented with the reaction unpromoted by EDIN. This difference was also observable in the energetic pathway of both mechanisms. Overall, the pathway A shows a higher barrier to overcome (211.90 kJ/mol), making this pathway more difficult than pathway B, which has a barrier of 108.90 kJ/mol then being kinetically easier to overcome.

IV.4 Conclusion

At the RHF and DFT levels of theory, the entire catalytic cycle of the CO_2 hydrogenation to the FA formation promoted by the EDIN ionic liquid has been investigated. Our study indicates that the NO_2^- group is the main active center of EDIN, which plays a critical role in the catalytic cycle. In particular, the oxygen and the nitrogen center of the NO_2^- group activates the H_2 molecule, and then it facilitates the cleavage of the H-H bond in the reaction.

Kinetically, the calculated energy barrier of the reaction for the unpromoted reaction is about four times higher (394.00 kJ/mol) than the reaction promoted by the EDIN ionic liquid. The overall reaction Gibbs energy is calculated to be -10.98 and -29.00 kJ/mol for RHF and DFT, respectively. These values show an indication of overcoming the kinetic barrier of the high activation complex in an unpromoted hydrogenation reaction. Therefore, our theoretical results provide a clear profile for the detailed reaction mechanism and help understand the intrinsic properties of different reaction mechanisms. While a pathway has a lower barrier of 108.9kJ/mol, another one could prove to be an effective route energetic for the CO_2 hydrogenation into FA by the EDIN ionic liquid.

AUTHORS INFORMATION

Corresponding Author: Dr. Rita M B Alves

* E-mail: rmbalves@usp.br

ORCID: **0000-0002-1914-5133**

The authors declare no competing financial interest.

Acknowledgments

The authors gratefully acknowledge the support of the RCGI – Research Centre for Gas Innovation, hosted by the University of São Paulo (USP) and sponsored by FAPESP – São Paulo Research Foundation (2014/50279-4) and Shell Brazil. This study was financed in part by the Personnel Coordination of Improvement of Higher Level - Brazil (CAPES) - Finance Code 001

Nomenclature

[Bmim][OAc]	1-Butyl-3-methylimidazolium acetate
[Edmim][NO2]	1-Ethyl-2,3-dimethylimidazolium nitrite

ΔG	Change in Gibbs energy of reaction
B3LYP	Becke, 3-Parameter, Lee–Yang–Parr
CCUS	Carbon Capture, Utilization, and Storage
CH_3OH	Methanol
CH_4	Methane
CI-NEB	Climbing Image- Nudged Elastic Band
CO_2	Carbon dioxide
Def2-SVP	Valence Double-Zeta Polarization
DFT	Density Functional Theory
DMSO	Dimethyl sulfoxide
EDIN	1-Ethyl-2,3-dimethylimidazolium nitrite
E_{el}	Electronic Energy
EF	Eigenvector-Following
E_{rot}	Rotational Thermal Energy
E_{trans}	Translational Thermal Energy
E_{vib}	Finite Temperature Correction to Ezpe due to Population of Excited Vibrational States
E_{ZPE}	Zero Temperature Vibrational Energy
FA	Formic Acid
FLP	Frustrated Lewis Pair
H	Enthalpy
H_2	Hydrogen gas
HCOOH	Formic Acid
ILs	Ionic Liquids
MeOH	Methanol
MEP	Minimum Energy Path
NEB-TS	Nudged Elastic Band Transition State
NO_2^-	Nitrite anion
P	Pressure
PES	Potential Energy Surface
RHF	Restricted Hartree-Fock

S	Entropy
STQN	Transit-Guided Quasi-Newton
T	Temperature

IV.5 References

ASGEIRSSON, V. et al. Efficient Optimization Method for Finding Minimum Energy Paths of Magnetic Transitions. **(In prep)**, 2020.

AVOGADRO(ORCA). **Avogadro: an open-source molecular builder and visualization tool.**, 2020. Disponível em: <http://avogadro.cc/>

BALARAMAN, E. et al. Efficient hydrogenation of organic carbonates, carbamates and formates indicates alternative routes to methanol based on CO 2 and CO. **Nature Chemistry**, v. 3, n. 8, p. 609–614, 2011.

BHARGAVA, B. L.; YASAKA, Y.; KLEIN, M. L. Hydrogen evolution from formic acid in an ionic liquid solvent: A mechanistic study by ab initio molecular dynamics. **Journal of Physical Chemistry B**, v. 115, n. 48, p. 14136–14140, 2011.

BONTEMPS, S.; VENDIER, L.; SABO-ETIENNE, S. Ruthenium-catalyzed reduction of carbon dioxide to formaldehyde. **Journal of the American Chemical Society**, v. 136, n. 11, p. 4419–4425, 2014.

BORETTI, A. Renewable hydrogen to recycle CO2 to methanol. **International Journal of Hydrogen Energy**, v. 38, n. 4, p. 1806–1812, 2013.

BULUSHEV, D. A.; ROSS, J. R. H. Towards Sustainable Production of Formic Acid. **ChemSusChem**, v. 11, n. 5, p. 821–836, 2018.

CHEN, Y.; MU, T. Conversion of CO2 to value-added products mediated by ionic liquids. **Green Chemistry**, v. 21, n. 10, p. 2544–2574, 2019.

ESRAFILI, M. D.; DINPARAST, L. A DFT study on the catalytic hydrogenation of CO2 to formic acid over Ti-doped graphene nanoflake. **Chemical Physics Letters**, v. 682, p. 49–54, 2017.

ESRAFILI, M. D.; NEJADEBRAHIMI, B. Theoretical insights into hydrogenation of CO 2 to formic acid over a single Co atom incorporated nitrogen-doped graphene: A DFT study. **Applied Surface Science**, v. 475, n. January, p. 363–371, 2019.

FUKUI, K.; FUJIMOTO, H. **FRONTIER ORBITALS AND REACTION PATHS**. Singapore: World Scientific, 1997.

GHARA, M.; CHATTARAJ, P. K. A computational study on hydrogenation of CO2, catalyzed by a bridged B/N frustrated Lewis pair. **Structural Chemistry**, 2019.

GRASEMANN, M.; LAURENCZY, G. Formic acid as a hydrogen source - Recent developments and future trends. **Energy and Environmental Science**, v. 5, n. 8, p. 8171–8181, 2012.

HANWELL, M. D. et al. "Avogadro: An advanced semantic chemical editor, visualization, and analysis platform". **Journal of Cheminformatics**, 2012.

HAO, C. et al. Hydrogenation of CO2 to formic acid on supported ruthenium catalysts. **Catalysis Today**, v. 160, n. 1, p. 184–190, 2 fev. 2011.

HIMEDA, Y. et al. Recyclable catalyst for conversion of carbon dioxide into formate attributable to an oxyanion on the catalyst ligand. **Journal of the American Chemical Society**, v. 127, n. 38, p. 13118–13119, 2005.

HOFFMANN, R. A chemical and theoretical way to look at bonding on surfaces. **Reviews of Modern Physics**, v. 60, n. 3, p. 601–628, 1988.

HULL, J. F. et al. Reversible hydrogen storage using CO2 and a proton-switchable iridium catalyst in aqueous media under mild temperatures and pressures. **Nature Chemistry**, v. 4, n. 5, p. 383–388, 2012.

IZGORODINA, E. I. et al. Quantum Chemical Methods for the Prediction of Energetic , Physical , and Spectroscopic Properties of Ionic Liquids. 2017.

JESSOP, PHILLIP G.; IKARIYA, TAKAO; NOYORI, R. Homogeneous Catalytic Hydrogenation of supercritical carbon dioxide. **Nature**, v. 368, p. 231–233, 1994.

JESSOP, P. G.; JOÓ, F.; TAI, C. C. Recent advances in the homogeneous hydrogenation of carbon dioxide. **Coordination Chemistry Reviews**, v. 248, n. 21–24, p. 2425–2442, 2004.

LEAL, P. et al. The Nature of Ionic Liquids in the Gas Phase. p. 6176–6182, 2007.

LEITNER, W. Carbon Dioxide as a Raw Material: The Synthesis of Formic Acid and Its Derivatives from CO<inf>2</inf>. **Angewandte Chemie International Edition in English**, v. 34, n. 20, p. 2207–2221, 1995.

MELZER, L. **Carbon Dioxide Enhanced Oil Recovery (CO2 EOR): Factors Involved in Adding Carbon Capture , Utilization and Storage (CCUS) to Enhanced Oil Recovery**. Texas: [s.n.].

MORET, S.; DYSON, P. J.; LAURENCZY, G. Direct synthesis of formic acid from carbon dioxide by hydrogenation in acidic media. **Nature Communications**, v. 5, p. 1–7, 2014.

NEESE, F. \The ORCA program system. **Computational Molecular Science**, v. 2, n. 1, p. 73–78, 2012.

NEESE, F. et al. **Orca 4.2: An ab initio, DFT and semiempirical SCF-MO package**. 4.2.1 ed. Mulheim: Max-Planck-Institut fur Kohlenforschung, 2020.

OU, Z. et al. A comprehensive DFT study of CO2 catalytic conversion by H2 over Pt-doped Ni catalysts. **International Journal of Hydrogen Energy**, v. 44, n. 2, p. 819–834, 2019.

PATIL, Y. P. et al. Cesium carbonate catalyzed efficient synthesis of quinazoline-2,4(1H,3H)-diones using carbon dioxide and 2-aminobenzonitriles. **Green Chemistry Letters and Reviews**, v. 1, n. 2, p. 127–132, 2008.

PENG, G. et al. CO2 hydrogenation to formic acid on Ni(110). **Surface Science**, v. 606, n. 13–14, p. 1050–1055, 2012.

RATTI, R. Ionic Liquids: Synthesis and Applications in Catalysis. **Advances in Chemistry**, v. 2014, n. 3, p. 1–16, 2014.

REN, Y. et al. A computational study on the chemical fixation of carbon dioxide with 2-aminobenzonitrile catalyzed by 1-butyl-3-methyl imidazolium hydroxide ionic liquids. **Computational and Theoretical Chemistry**, v. 978, n. 1–3, p. 47–56, 2011.

SCHLAPBACH, L.; ZÜTTEL, A. Hydrogen-storage materials for mobile applications. **Nature**, v. 414, n. November, p. 353–358, 2001.

SIRIJARAENSRE, J.; LIMTRAKUL, J. Hydrogenation of CO 2 to formic acid over a Cu-embedded graphene: A DFT study. **Applied Surface Science**, v. 364, p. 241–248, 2016.

SREDOJEVIĆ, D. N. et al. **Formic Acid Synthesis by CO2 Hydrogenation over Single-Atom Catalysts Based on Ru and Cu Embedded in GrapheneChemistrySelect**, 2018.

STEPHENS, P. J. et al. Ab Initio calculation of vibrational absorption and circular dichroism spectra using density functional force fields. **Journal of Physical Chemistry®**, v. 98, n. 45, p. 11623–11627, 1994.

VEREVKIN, S. P. et al. Thermochemistry of imidazolium-based ionic liquids : experiment and first-principles calculations w. p. 14994–15000, 2010.

WASSERSCHEID, P.; ANNEGRET, S. **Green Solvents : Ionic Liquids**. Weinheim: Wiley-VCH, 2010. v. 6

WEILHARD, A. et al. Selective CO2 Hydrogenation to Formic Acid with Multifunctional Ionic Liquids. **ACS Catalysis**, v. 8, n. 3, p. 1628–1634, 2018.

WELTON, T. Room-Temperature Ionic Liquids. Solvents for Synthesis and Catalysis. **Chemical Reviews**, v. 99, p. 2071–2083, 1999.

WELTON, T. Ionic liquids in catalysis. **Coordination Chemistry Reviews**, v. 248, n. 21–24, p. 2459–2477, 2004.

ZAHN, S. et al. Understanding ionic liquids from theoretical methods. **Journal of Molecular Liquids**, v. 192, p. 71–76, 2014.

ZHANG, Z. et al. Hydrogenation of carbon dioxide is promoted by a task-specific ionic liquid. **Angewandte Chemie - International Edition**, v. 47, n. 6, p. 1127–1129, 2008.

CHAPTER V: PROCESS DESIGN OF FORMIC ACID AND METHANOL PRODUCTION PROMOTED BY IONIC LIQUID: TECHNO-ECONOMIC ANALYSIS

This paper is an extended copy of the published article in Proceedings of the 14th International Symposium on Process Systems Engineering – PSE 2022, June 19-23, 2021+, Kyoto, Japan 2022 Elsevier B.V The extended paper is being prepared for submission to a peer review journal

Abstract

Carbon dioxide conversion technologies have been extensively investigated as a viable pathway for lowering greenhouse gas emissions. However, numerous routes have been proposed due to thermodynamic and product separation limitations. This work presents a techno-economic study of formic acid and methanol production promoted by ionic liquid at a commercial scale. To that aim, Aspen Plus® V10 was employed to build a simulation that included the solubilization of CO_2 in 1-ethyl-2,3-dimethylimidazolium nitrite ([Edmim][NO_2]) ionic liquid (IL), synthesis of the CO_2-[Edmim][NO_2] adduct with hydrogen, product separation, and recycling of the IL. The CO_2 conversion (87 %) resulted in ~83 % and ~14 % yield of formic acid and methanol, respectively. This result is an improvement in previous conducted findings. Furthermore, it was discovered that a discount rate between 4-5 % (@ 0.78 USD/kg of formic acid) or 0.93-1 USD/kg (@ 10% discount rate) would make the project profitable.

V.1 Introduction

Carbon dioxide (CO_2) conversion in the production of fuels, chemicals, and materials are potentially promising CO_2 abatement alternatives by reducing fossil fuel usage, lowering CO_2 emissions (PÉREZ-FORTES; TZIMAS, 2016), and also providing a chemical storage alternative for intermittent renewable electricity (SCHLÖGL, 2013). It can significantly contribute to the decarbonization of the energy system (OLAH; GOEPPERT; PRAKASH, 2009b). Formic acid (FA) and methanol (MeOH) are typical chemicals and liquid energy carriers.

In the organic chemical industry, formic acid is a fundamental chemical feedstock. It is employed as a mordant in the dyeing industry, a neutralizer in tanning, and a disinfectant and preservative agent in sanitary stations in the perfume industry(HAO et al., 2011). It is used in the chemical industry to foster the production of formate esters, which are used to make a wide range of organic derivatives such as aldehydes, ketones, carboxylic acids, and amides(HAO et al., 2011). Furthermore, formic acid can be converted into methanol (OLAH, 2005) and has been proposed as a candidate for methanol-alternative fuels in methanol fuel cells as a direct fuel for power generation(HAO et al., 2011). Currently, most formic acid production is derived from a two-step process of hydrolysis of methyl formate in the presence of a solid base catalyst and direct synthesis from carbon monoxide and water (ARTZ et al., 2018) (MORET; DYSON; LAURENCZY, 2014b). These conventional methods require excessive water for its hydrolysis and consequently consume a lot of energy to remove the water from the product mixture(ARTZ et al., 2018)(HAO et al., 2011). Alternative production route to hydrolysis of formate is the direct hydrogenation of CO_2, with H_2. However, the hydrogenation of CO_2 to formic acid is endergonic in the gas phase (ΔG^{o}_{298} = +33 kJ/mol), hence, thermodynamically unfavorable (Wang & Himeda, 2012; (LEITNER, 1995). The thermodynamic limitation can be overcome by perturbing the reacting system with a secondary reaction or molecular interaction. One of the available strategies is the neutralization of the reaction with a weak base (tertiary amines or alkali/alkaline earth bicarbonates) to yield formamides (XU et al., 2011)(JESSOP; IKARIYA; NOYORI, 1999). However, there are concerns about the post-treatment of intermediates to get a pure formic acid. (LEITNER, 1995)(SU et al., 2015). Ionic liquids (ILs) play an essential role in solving these two problems due to their solvating and low volatility property (ZENG et al., 2017). In addition, ILs can fine-tune the properties of the solvent by altering the structure, catalyst immobilization

(GHAVRE; MORRISSEY; GATHERGOO, 2011; KOKORIN, 2012; MACFARLANE; KAR; PRINGLE, 2017), and CO_2 activation (WANG et al., 2015). Hence, in this work, the economic implications of deploying a process plant for the hydrogenation of CO_2 to formic acid and methanol using IL ([Edmim][NO_2]) as the reaction media was examined. The evaluation to retrieve technical and process significant parameters was carried out with the Aspen Plus V10 process simulation software.

V.2 Materials and Methods

A novel steady-state model for the synthesis for CO_2 conversion into formic acid and methanol was created in Aspen Plus V10. A liquid-phase process in an ionic liquid ([Edmim][NO_2]) was studied. The technical performance of the process was evaluated by the mass and energy balances generated from the process. The capital and operating costs of the process were estimated and used to calculate the net present value (NPV) over the project lifetime. Finally, the environmental impact was analyzed from the result of utilities and raw materials used in the process. The boundaries of the present work are summarized in Figure V.1.

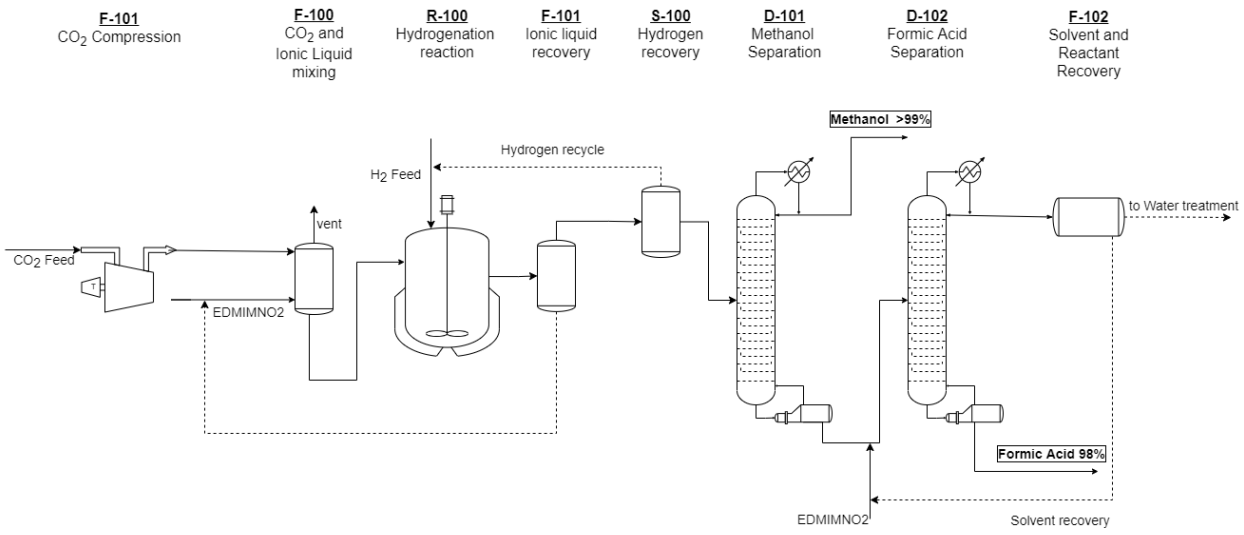

Figure V.31: Proposed process flowsheet of CO_2 hydrogenation with [Edmim][NO_2] as reaction media

V.2.1 Process Description

The thermodynamic model for the CO_2 solubilization and synthesis section is the conductor-like screening model for segment activity coefficient (COSMO-SAC) with Peng Robinson-Wong Sandler equation of state (ESPRWS). The reactor was modelled using RYield with two independent reactions (FA and MeOH formation) (Bello et al., 2021). The solubilization column was modelled using the rigorous vapour-liquid equilibrium with a two-outlet flash. These two models were selected because ILs are practically less volatile; hence COSMO-SAC cannot predict the behaviour in the gaseous phase. The distillation columns (D-100 and D-101) were modelled with a rigorous RADFRAC model in equilibrium mode. All the property methods were selected following the guidelines of Tower and Sinnott (Towler & Sinnott, 2013) and taking into account the reaction system's temperature, pressure, and volatility. Multistage compressors were selected and modelled as isentropic with a fixed discharge pressure from the last stage. Heat exchangers were modelled by the shortcut method.

V.2.2 Process Simulation

This section presents the process conditions and asumptions of the different process unit in the production of formic acid and methanol from feed to the products.

V.2.2.1 Carbon Dioxide Solubilization

This unit was modelled with a flash block employing the rigorous vapour-liquid equilibrium. Stream of compressed CO_2 at 80 bar and partially heated stream of [Edmim][NO_2] at 40ºC was sent to the flash column. CO_2 feed stream was assumed to be free from other impurities, together with stream [Edmim][NO_2] (at 25bar and 40ºC) was fed at to the column (F-100) operating at 80 bar and 20ºC to simulate the absorption of CO_2 in the ionic liquid. This operating condition allows the solubilization/absorption of CO_2 at high pressure and low temperature (BELLO et al., 2021b). A CO_2-[Edmim][NO_2] adduct is formed in this process. The adduct leaves the column to the reactor (R-100) for the synthesis section.

V.2.2.2 Synthesis Unit

A YIELD reactor (R-100) was employed to model this process unit. The operating conditions are 17 bar and 25^{O}C. The yield reactor was selected as there are no kinetic data for the reaction at the time of this report; however, the reaction's stoichiometry is available. Due to its low solubility in ILs, hydrogen was introduced into this reactor(BELLO et al., 2021a) together with the

[Edmim][NO_2]-CO_2 adduct. Herein, two simultaneous reactions for formic acid and methanol were considered, according to Bello et al. (BELLO et al., 2021a). The reactions are shown in equations V.1 and V.2 below. The fractional conversion of CO_2 to formic acid was set to 0.7. The outlet stream was sent to column F-101 for separation. The column separates the [Edmim][NO_2], and other products (Methanol, Formic acid, and other unreacted gases) were collected as vapour in the outlet streams. The outlet streams from F-100 were cooled, and the unreacted hydrogen was separated in the separator block (S-100). Other products of the reaction were sent to the separation unit.

$$CO_2 + H_2 \leftrightarrow CHOOH \quad (V.1)$$

$$CO_2 + 3H_2 \leftrightarrow CH_3OH + H_2O \quad (V.2)$$

V.2.3 Separation Unit

The main separation unit comprises two distillation columns modelled with the RADFRAC block. The separation unit employed the typical distillation for the separation of methanol and the extractive distillation to remove the azeotropic mixture of formic acid and water. Herein, the volatile component of the mixture (Methanol) was separated. The normal distillation column (D-100) was operated as an equilibrium distillation with 22 stages. The feed enters the column above the 11th stage. Methanol is collected as a top product with a purity of 99.9%, while water and formic acid leave the column as the bottom product. The bottom products were sent to the extractive distillation column operated with 22 stages. All other specifications of the distillation columns are highlighted in Table V.1. [Edmim][NO_2] was employed as the extractive solvent entering the column at the top stage. The rich stream in water was collected as the top product together, while the rich stream in formic acid was collected as bottom product with a purity of 97.7%w/w. Finally, the water-rich stream was sent to a separation column (F-102). The block F-102 operates as a simple flash separation column and separates water and [Edmim][NO_2]. The water was collected as the top product while the [Edmim][NO_2] was recycled back into the extractive distillation system.

Table V.12. Operating conditions for the main process equipment (Copyright 2022 Elsevier B.V)

Units		Operating Conditions
Compression	CMP-101	Pexit = 80 bar, Number of stages = 3
Solubilization Column	F-100	T = 20 ºC; P = 80 bar
Separator	F-101	T = 150 ºC; P = 0.1 bar
Reactor	R-100	T = 20 ºC; P = 17 bar
Distillation Column	D-100	P = 1 bar; Stages = 22; Feed stage = 11; Reflux ratio = 4; Condenser: Full.
Extractive Distillation Column	D-101	P = 1 bar; Stages = 23; Feed stage = 2; Reflux ratio = 0.01; Condenser: full; Distillate to feed ratio = 0.69

V.2.3 Environmental Analysis

The process's environmental impact was measured in terms of CO_2, energy, and water balance(NIEMINEN; LAARI; KOIRANEN, 2019). The amount of CO_2 supplied to the process was subtracted from the sum of direct and indirect CO_2 emissions associated with the process. CO_2 from outlet streams and generated due to the use of utilities (steam and electricity) were all included in these emissions. The processes' specific energy consumption was computed, and the CO_2 emissions were obtained from the simulation result. The fuel (natural gas) emissions and process waste streams were considered. The water balance took into account cooling water input and wastewater output.

V.2.4 Economic parameter Analysis

In any chemical project, estimating capital (CAPEX) and operational (OPEX) costs are critical components in determining the long-term viability of any chemical process. The fixed CAPEX comprises costs such as equipment, land, and installation. The capital cost (CAPEX) is the total cost of the plant, including direct and indirect costs such as total installed cost, contracts, contingencies, overheads, and other costs. The cost of equipment is evaluated by utilizing the Aspen Economic Analyzer. Aspen software's cost basis calculation is based on the first quarter of 2016. When compared to other cost correlations, this method can provide reasonably accurate cost estimates during the conceptual phase(TOWLER; SINNOTT, 2012). The installation costs of the sized equipment were then calculated. The operational cost (OPEX) consists of the total cost of raw material, utility, operating labor, and other manufacturing costs (such as operating charges,

plant overhead, and general and administrative expenses) were estimated by Aspen Economic Analyzer.

A cost of 50 $/t was assumed based on the International Energy Agency report (INTERNATIONAL ENERGY AGENCY, 2019b). The intended purpose of this study is an integrated CO_2 synthesis unit on an offshore platform; hence, the transportation cost was not considered. The overall cost of hydrogen production based on the natural gas production source was $1.5/kg of hydrogen (INTERNATIONAL ENERGY AGENCY, 2018). All process units were assumed to be powered by electricity from natural gas, available at an assumed market cost of 70 USD/MWh(INTERNATIONAL ENERGY AGENCY, 2021). The electricity consumption of the synthesis unit was calculated in the Aspen Plus process models. Table V.2 summarizes the factors, parameters, and assumptions used in the economic evaluation.

Table V.13. Economic parameters and assumptions (Copyright 2022 Elsevier B.V)

Parameter	Value
Project lifetime (y)	20
Construction period (y)	2
Plant availability (h/y)	8,000
Tax rate (%) [45]	29.72
Depreciation	straight-line
Depreciation period (y)	15
Salvage value (MM USD)	4
Cost of Land (MM USD)	2
Cost component	Value
Purchased Equipment Cost (PEC)	
ISBL (Inside Battery Limit)	1.37×PEC
OSBL (Outside Battery Limit)	12% ISBL
Indirect costs (IC)	0.89 (ISBL+ OSBL)
Fixed Capital Investment (FCI)	Contingencies+ISBL+ OSBL+IC
Working Capital (WC)	12% FCI
Total Capital Investment (TCI)	FCI+WC

There are no prices available for [Edmim][NO_2] as it is not readily available commercially at the time of this report. However, the price of a typical ionic liquid can be safely assumed at 50USD/kg (SHIFLETT et al., 2010). Due to the low volatility of [Edmim][NO_2], its purchase is estimated to be on a biannual basis because all the ILs were favourably recovered at the end of the synthesis and separation process. The price of methanol and formic acid are 0.50USD/kg and 0.78USD/kg, respectively, taken from the European manufactured good (PRODCOM) database(EUROSTAT, 2020). A discounted cash flow analysis was performed assuming a 15-year plant lifespan. The projected interest rate was 10%, the tax rate was 45%, and depreciation was calculated using the straight-line technique for project years. Finally, we evaluated the impact of the product price and discount rate on the project's Net Present Value (NPV). Cumulative net present value (NPV) was used because it has been determined to be the most acceptable economic criterion when optimizing process flow sheets (NANDIYANTO, 2018; PINTARIČ; KRAVANJA, 2006).

V.3 Results and Discussion

This section presents findings from the simulation employing the methods and procedure stated in the previous sections. This includes the technological, environmental and economic results.

V.3.1 Technological Metrics

Table V.3 summarizes the FA and MeOH plant technological key performance indicators. Detailed balances with the inlet and outlet streams can be found in Tables S1–S2 in the Supplementary Material. As stated in section V.2.4, [Edmim][NO_2] was assumed to be replenished twice a year. The CO_2 conversions around the reactor and overall plant are defined in equations V.3 and V.4. As depicted in Table V.3, 86 % conversion of CO_2 per pass was achieved in the presence of the [Edmim][NO_2] as reaction media. The CO_2 conversion results in 2.68 t/h and 0.46 t/h of formic acid and methanol. The unreacted CO_2-[Edmim][NO_2] adduct can be recycled back to the reacting system, which will allow a nearly 100 % CO_2 conversion. Simple flash distillation is adequate for recycling ~99% of the IL. All the other products of the reaction (FA + MeOH + Water+ unreacted components) escapes as vapour products. The products were cooled, and unreacted H_2 was separated and recycled back to the system. Other products (FA, MeOH, and Water) were separated in the distillation column. Formic acid separation tends to be more energetic because of the large amount of fluid processed. Approximately 99% purity of methanol was obtained as the top product. The azeotropic mixture of formic acid and water gives a separation of 97.7% w/w of

formic acid with the use of [Edmim][NO_2] as an extractive solvent. The mixture of water and the [Edmim][NO_2] leaves as bottom product and separated through a simple flash distillation. The [Edmim][NO_2] IL is recycled back to the system.

$$CO_2ConvR = \left(\frac{CO_2in \ - \ CO_2out}{CO_2in}\right) Reactor \qquad (V.3)$$

$$CO_2ConvP = \left(\frac{CO_2in \ - \ CO_2out}{CO_2in}\right) Process \qquad (V.4)$$

Table V.14. Technological Metrics of the simulated process.

Mass balance	**Values**	**Units**
Inlet CO_2	3.14	t/h
Inlet H_2	5	t/h
Make up H_2	0.2	t/h
Outlet FA	2.62	t/h
Outlet MeOH	0.46	t/h
Outlet H_2O	0.26	t/h
Outlet CO_2	0.45	t/h
Outlet H_2	4.8	t/h
Waste H_2O +FA	0.2	t/h
Overall CO_2 Conversion (%)	99.99%	%
Per Pass CO_2 Conversion	86	%
Conversion factor (FA)	1.17	tCO_2/t FA
Conversion factor (MeOH)	6.87	tCO_2/t MeOH
MeOH Produced	0.46	t/h
FA Produced	2.68	t/h
FA Purity	97.7	%
MeOH Purity	99.9	%

Table V.4 below shows that the most significant contribution to energy requirement is cooling. In terms of cooling, the reactor required a substantial percentage of cooling. This can be attributed to the exothermic nature of the reaction even though the reactor is operated at ambient temperature. The second largest contributor to cooling is the exchanger unit for the outlet streams from F101 unit, a large amount of cooling is required because of its high operating condition (high temperature). The second most significant contributor to energy requirement is the electricity consumed. This is a result of CO_2 and H_2 compression and solubilization requirements.

Table V.15. Energy balance of the simulated process.

Energy Parameters	Values	Units
Enthalpy in	-7.26	MW
Enthalpy out	-8.24	MW
Hot utility	4.24	MW
Cold utility	-11.39	MW
Electricity Consumption	6.16	MW

V.3.2 Environmental Metrics

The CO_2 and water balances of the process are presented in Table V.5. The net balance of CO_2 emission was positive. A positive CO_2 balance signifies that the amount of CO_2 consumed in formic acid and methanol synthesis was lower than the sum of the process's direct and indirect CO2 emissions (NIEMINEN; LAARI; KOIRANEN, 2019). The compression of H_2 and CO_2 (electricity) contributes to the largest source of indirect CO_2 emission. However, a negative emission can be achieved if the CO_2 source is at an elevated pressure before entering the process.

Table V.16. Calculated Environmental Parameters of the process

CO_2 balance,	Unit (t/h)
CO_2 emitted	3.5E-3
Inlet streams	-3.1
Outlet streams	0
Hot utility (natural gas)	1
Electricity	2.1

Cooling water input	981.9

V.3.3 Economic Metrics

Table V.6 summarizes the economic breakdown of plant investment and operation cost. The raw material and utility constitute the larger shares of the OPEX. The percentage of the IL in the raw material cost is relatively low because the price was compensated by its unique property (~99.9% of the ILs were recovered). On the other hand, the utility cost is majorly influenced by the compression of H_2 and CO_2, which is required to fulfill the solubilization and synthesis requirements of CO_2 and H_2, respectively.

Table V.17. Estimated CAPEX, OPEX and revenues of simulated process

CAPEX	**USD**
Purchased Equipment Cost	11,775,700
ISBL	15,308,410
OSBL	1,837,009
Indirect costs (IC)	15,259,423
Project Contingency	3,240,484
Process Contingency	1,620,242
Fixed Capital Investment (FCI)	37,265,569
Working Capital (WC)	4,471,868
Cost of Land	2,000,000
Total Capital Investment (TCI)	43,737,436
OPEX	**USD**
Raw Material Cost	4,089,956
Utilities	4,157,864
Operating Labour Cost	1,483,442
Other Manufacturing Cost	3,051,827
REVENUE	**USD/YR**
Formic Acid @ 0.78	16,715,161
Methanol @ 0.5	1,827,864

V.3.4 Sensitivity Analysis

The net present values at different discount rates and formic acid prices are presented in Figure V.2 and V.3, respectively. At a discount rate of 10%, the project is not economically viable. Hence, a sensitivity analysis of discount rate from 4% to 10% was carried out to determine the discounted cash-flow rate of return (DCFROR, when NPV =0). From the result, a discount rate between 4-5% makes the project profitable. At this discount rate, a free cost of CO_2 would improve the NPV as only H_2 is the major contributor to the raw material cost since the ionic liquid cost is estimated on a biannual basis (low volatility). In figure V.3, the price of formic acid was varied to observe the behavior of the NPV at a 10% discount rate. At NPV =0, the selling cost of formic acid is 0.935 USD/kg, which makes it the minimum selling point for the project to be viable at a 10 % discount rate. The project would be profitable if there were incentives to the amount of CO_2 consumed or generated. The project is profitable with a carbon credit tax of 66 USD/tCO_2 at the current 10% tax rate. Additionally, at present formic acid and methanol prices, a significant reduction in the hydrogen cost would be necessary to make these processes competitive.

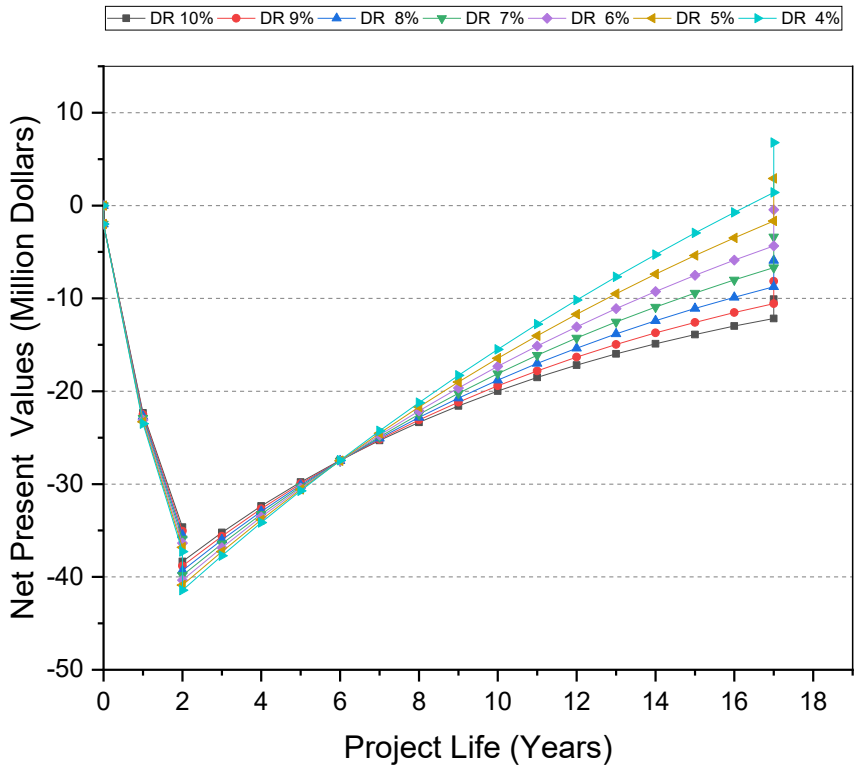

Figure V.32. Cash flow diagram at different discount rates

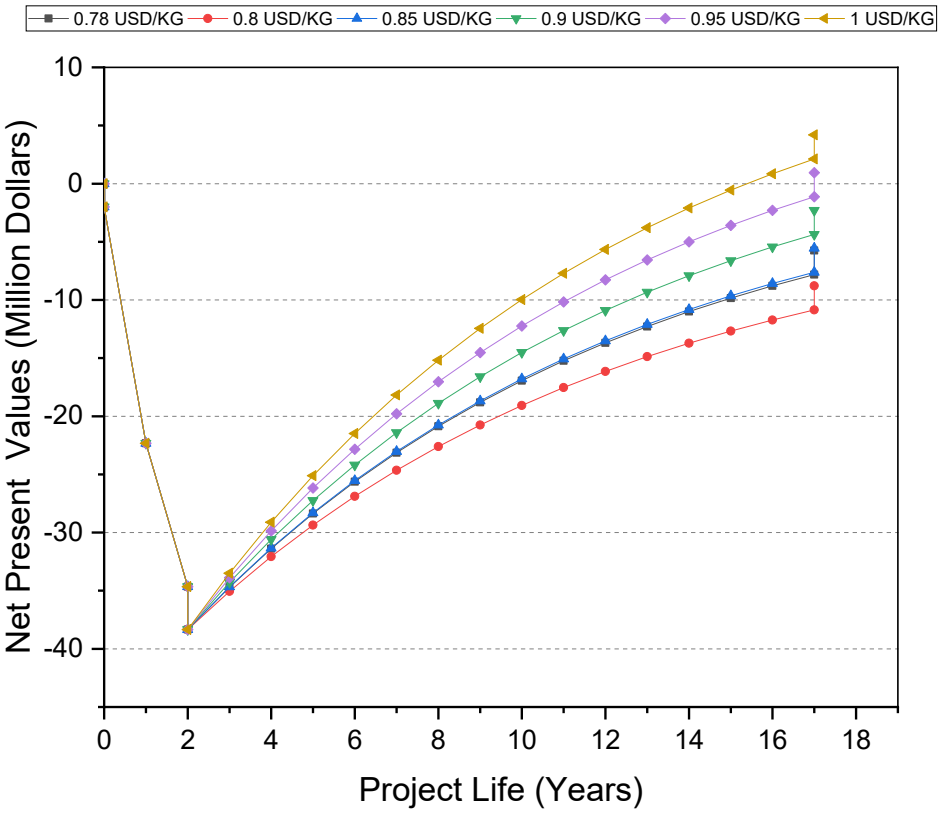

Figure V.33. Cash flow diagram at various selling prices of formic acid

V.4 Conclusion

A novel synthesis route for the simultaneous hydrogenation of CO_2 to formic acid and methanol using an IL as a promoter and a recovery solvent. The techno-economic study based on process simulation has proven the economic feasibility of the hydrogenation of CO_2 promoted by [Edmim][NO_2] at a commercial scale. The results showed that the CAPEX and OPEX required are 43.9 MUSD and 12.7 MUSD, respectively. To ensure economic profitability, the calculated minimum selling cost of formic acid was 0.935-1 USD/kg. In addition, at the current 10% discount rate, the project is profitable with a carbon credit tax of 66 USD/tCO_2. The project's minimum payback time was evaluated to be four years.

Acknowledgments

The authors gratefully acknowledge the support of the RCGI – Research Centre for Gas Innovation, hosted by the University of São Paulo (USP) and sponsored by FAPESP – São Paulo Research Foundation (2014/50279-4) and Shell Brazil. This study was financed in part by the Personnel Coordination of Improvement of Higher Level - Brazil (CAPES) - Finance Code 001

V.5 References

ARTZ, J. et al. Sustainable Conversion of Carbon Dioxide: An Integrated Review of Catalysis and Life Cycle Assessment. **Chemical Reviews**, v. 118, n. Sustainable Chemistry, p. 434−504, 2018.

BELLO, T. O. et al. Thermodynamic analysis of carbon dioxide hydrogenation to formic acid and methanol. **Chemical Engineering Science**, v. 242, p. 116731, 2021a.

BELLO, T. O. et al. Systematic Screening of Ionic Liquids for Hydrogenation of Carbon dioxide to Formic Acid and Methanol. **Industrial & Engineering Chemistry Research**, 2021b.

EUROSTAT. **Prodcom Annual Data 2020 (updated 15/07/2021)**. Disponível em: <https://ec.europa.eu/eurostat/web/prodcom/data/excel-files-nace-rev.2>. Acesso em: 25 out. 2021.

GHAVRE, M.; MORRISSEY, S.; GATHERGOO, N. Hydrogenation in Ionic Liquids. **Ionic Liquids: Applications and Perspectives**, 2011.

HAO, C. et al. Hydrogenation of CO2 to formic acid on supported ruthenium catalysts. **Catalysis Today**, v. 160, n. 1, p. 184–190, 2 fev. 2011.

INTERNATIONAL ENERGY AGENCY. **Hydrogen production costs by production source**. Disponível em: <https://www.iea.org/data-and-statistics/charts/hydrogen-production-costs-by-production-source-2018>. Acesso em: 29 out. 2021.

INTERNATIONAL ENERGY AGENCY. **Levelised cost of CO2 capture by sector and initial CO2 concentration, 2019**. Disponível em: <https://www.iea.org/data-and-statistics/charts/levelised-cost-of-co2-capture-by-sector-and-initial-co2-concentration-2019>. Acesso em: 29 out. 2021.

INTERNATIONAL ENERGY AGENCY. **World Energy Model**. Disponível em: <https://www.iea.org/reports/world-energy-model>. Acesso em: 29 out. 2021.

JESSOP, P. G.; IKARIYA, T.; NOYORI, R. Homogeneous catalysis in supercritical fluids. **Chemical Reviews**, v. 99, n. 2, p. 475–494, 1999.

KOKORIN, A. **Ionic Liquids: Applications and Perspectives**. [s.l: s.n.].

LEITNER, W. Carbon Dioxide as a Raw Material: The Synthesis of Formic Acid and Its Derivatives from CO<inf>2</inf>. **Angewandte Chemie International Edition in English**, v. 34, n. 20, p. 2207–2221, 1995.

MACFARLANE, P. D. R.; KAR, D. M.; PRINGLE, D. J. M. **Fundamentals of Ionic Liquids Ionic Liquids in Biotransformations and Electrodeposition from Ionic Handbook of Green Chemistry – Green Solvents Electrochemical Aspects of Ionic Liquids , 2nd edition Nanocatalysis in Ionic Liquids**. [s.l: s.n.].

MORET, S.; DYSON, P. J.; LAURENCZY, G. Direct synthesis of formic acid from carbon dioxide by hydrogenation in acidic media. **Nature Communications**, v. 5, p. 1–7, 2014.

NANDIYANTO, A. Cost analysis and economic evaluation for the fabrication of activated carbon and silica particles from rice straw waste. **Journal of Engineering Science & Technology**, v. 13, n. 6, p. 1523-1539, 2018.

NIEMINEN, H.; LAARI, A.; KOIRANEN, T. CO2 hydrogenation to methanol by a liquid-phase process with alcoholic solvents: A techno-economic analysis. **Processes**, v. 7, n. 7, p. 1–24, 2019.

OLAH, G. A. Beyond Oil and Gas: The Methanol Economy. **Angewandte Chemie International Edition**, v. 44, n. 18, p. 1–10, 2005.

OLAH, G. A.; GOEPPERT, A.; PRAKASH, G. K. S. Chemical Recycling of Carbon Dioxide to Methanol and Dimethyl Ether: From Greenhouse Gas to Renewable, Environmentally Carbon Neutral Fuels and Synthetic Hydrocarbons. **The Journal of Organic Chemistry**, v. 74, n. 2, p. 487–498, 16 jan. 2009.

PÉREZ-FORTES, M.; TZIMAS, E. **Techno-economic and environmental evaluation of CO2 utilisation for fuel production. Synthesis of methanol and formic acidScientific and Technical Research Series**. Luxembourg: [s.n.]. Disponível em: <https://ec.europa.eu/jrc/en>.

PINTARIČ, Z. N.; KRAVANJA, Z. Selection of the economic objective function for the optimization of process flow sheets. **Industrial & Engineering Chemistry Research**, v. 12, p. 4222-4232, 2006.

SCHLÖGL, R. **The Solar Refinery. In Chemical Energy Storage**. Boston, MA, USA: Walter de Gruyter GmbH: Berlin, Germany, 2013.

SHIFLETT, M. B. et al. Carbon dioxide capture using ionic liquid 1-butyl-3-methylimidazolium acetate. **Energy and Fuels**, v. 24, n. 10, p. 5781–5789, 2010.

SU, J. et al. Highly efficient hydrogen storage system based on ammonium bicarbonate/formate redox equilibrium over palladium nanocatalysts. **ChemSusChem**, v. 8, n. 5, p. 813–816, 2015.

TOWLER, G.; SINNOTT, R. **Chemical Engineering Design Principles, Practice and Economics of Plant and Process Design**. Second Edi ed. Oxford: Elsevier, 2013.

TOWLER, G.; SINNOTT, R. K. **Chemical engineering design: principles, practice and economics of plant and process design**. [s.l.] Elsevier, 2012.

WANG, W. .; HIMEDA, Y. Recent Advances in Transition Metal-Catalysed Homogeneous Hydrogenation of Carbon Dioxide in Aqueous Media. **School of Enviromental Sciences**, p. 250–264, 2012.

WANG, Y. et al. Activation of CO2 by ionic liquid EMIM-BF4 in the electrochemical system: a theoretical study. **Physical Chemistry Chemical Physics**, v. 17, n. 36, p. 23521–23531, 2015.

XU, W. et al. Thermodynamic analysis of formic acid synthesis from CO2hydrogenation. **ICMREE 2011 - Proceedings 2011 International Conference on Materials for Renewable Energy and Environment**, v. 2, p. 1473–1477, 2011.

ZENG, S. et al. Ionic-Liquid-Based CO<inf>2</inf> Capture Systems: Structure, Interaction and Process. **Chemical Reviews**, v. 117, n. 14, p. 9625–9673, 2017.

CHAPTER VI

INTENSIFICATION OF THE PROCESS SYSTEM: QUALITATIVE ANALYSIS

VI.1 Introduction

Process intensification (PI) is a promising pathway in the development of sustainable and cost-effective chemical process systems(FERNANDEZ RIVAS et al., 2020) (VAN GERVEN; STANKIEWICZ, 2009). Process intensification is defined as a set of often radically innovative principles applied in chemical reaction engineering and process design. The pioneering work of Stankiewicz and Moulijn proposed this definition of chemical processes(STANKIEWICZ; MOULIJN, 2000). This definition applicable to chemical process can bring significant benefits in terms of lower capital and operating expenses, quality, less wastes, improved, process and efficiency and higher quality products(DIMIAN; BILDEA; KISS, 2014).

Process Intensification has enabled the opening of "Novel Process Windows", allowing for improved process performance in terms of conversion, selectivity, and safety(ILLG; LÖB; HESSEL, 2010). It is possible to attain good performance for reactions attributed with strong limits (e.g., high exothermicity, low miscibility of the reactants) according to Illg et. al(ILLG; LÖB; HESSEL, 2010), this can be achieved by applying PI concepts, which allow for excellent mixing and thermal control when using milli and microreactors. For example, explosive conditions that cannot be achieved in a conventional apparatus (such as Kolbe-Schmitt synthesis or the bromination of 3-nitrotoluene (ILLG; LÖB; HESSEL, 2010)), as well as the development of one-pot processes synthesis, which reduce waste compared to traditional methods for the synthesis of chemical intermediates, were all made possible by this factor (e.g., synthesis of phenyl boronic acid(HESSEL et al., 2004). Since residence periods for fast reactions can be on the order of milliseconds, they can be investigated, and exact kinetic data can be obtained to improve the chemical process.

VI.2 Principles and Approaches in Process Intensification

A widely used framework is the classification of PI into four domains of action: spatial, thermodynamic, functional, and temporal. The concept was proposed by van Gerven and Stankiewicz (VAN GERVEN; STANKIEWICZ, 2009), and it has since been expanded and

demonstrated in a newly released textbook(STANKIEWICZ; VAN GERVEN; STEFANIDIS, 2019). The concept is complemented by four PI principles as shown in figure VI.1

- maximizing the effectiveness of intra- and intermolecular events;
- giving each molecule the same processing experience;
- optimizing the driving forces, and maximizing the specific areas to which these forces apply; and
- maximizing synergistic effects between partial processes

The classification is independent of any particular process or equipment, and one of its most useful aspect is its application at several dimensions, ranging from molecular processes, microfluidics, macroscale (reactors), and finally to megascale (plants, sites, and businesses) (MOULIJN et al., 2007).

VI.2.1 Maximize the Effectiveness of Intra- and Intermolecular Events

The first principle describes the aspect of PI which aims at changing kinetics. Kinetics play a key part in process synthesis and has been attributed the key "root" of low conversions and selectivities of unwanted side-products(VAN GERVEN; STANKIEWICZ, 2009). The simplest collision theory shows that the number/frequency of collisions, geometry of approach, mutual orientation of molecules at the time of collisions, and their energy all have a role in effectiveness of a reaction event(DIMIAN; BILDEA; KISS, 2014; VAN GERVEN; STANKIEWICZ, 2009).

VI.2.2 Give Each Molecule the Same Processing Experience

Processes that subject all molecules to the same history produce products that are ideally uniform and waste-free. Not only does macroscopic residence time distribution, dead zones, or bypassing play a part here, but so do meso- and micromixing, as well as temperature gradients(STANKIEWICZ; VAN GERVEN; STEFANIDIS, 2019; VAN GERVEN; STANKIEWICZ, 2009). For example, in comparison to a stirred-tank reactor with jacket heating, a plug-flow reactor with gradientless, volumetric heating will be obviously be closer to the ideal represented by the second principle (DIMIAN; BILDEA; KISS, 2014; VAN GERVEN; STANKIEWICZ, 2009)

VI.2.3 Optimize the Driving Forces at Every Scale and Maximize the Specific Surface Area to Which These Forces Apply

This principle is about the transport rates across interfaces. The interfacial area to which the driving force applies must be maximized in order to get the desired result of the driving forces (e.g, the concentration difference). Moving from mm to μm scales of channel diameters can result in increased transfer areas (or surface-to-volume ratios). For instance, a 400 μm circular micro-channel in a microreactor gives a specific area of 15,000 m^2/m^3. However, amazingly, this amount is lower than what is seen in natural systems: capillary veins, for example, are 10μm in diameter, with specific areas of around 400,000m^2/m^3 (DIMIAN; BILDEA; KISS, 2014; STANKIEWICZ; VAN GERVEN; STEFANIDIS, 2019; VAN GERVEN; STANKIEWICZ, 2009).

VI.2.4 Maximize the Synergistic Effects from Partial Processes

Synergistic effects should be necessary and used wherever possible and at all possible scales. At the macroscale, such uses takes the form of multi-functionality, as in reactive separation units, where the reaction equilibrium is changed by removing the products in-situ from the reaction environment.(DIMIAN; BILDEA; KISS, 2014; VAN GERVEN; STANKIEWICZ, 2009)

VI.3 Approaches and the Scales

A totally intensified process realizes all of the four principles by utilizing one or more fundamental ways to process intensification. In four domains, we differentiate four such approaches: spatial, thermodynamic, functional, and temporal. The approaches should be implemented over all relevant time and length scales. The scales can range from molecules (down to femtoseconds and metres) through processing units and even plants (up to days and hundreds of meters)(STANKIEWICZ; VAN GERVEN; STEFANIDIS, 2019; VAN GERVEN; STANKIEWICZ, 2009).

VI.3.1 PI Approach in the Spatial Domain (Structure)

In order to prevent spatial randomness, structure is often introduced. Any of the four PI principles can be implemented for process intensification by using spatial structure. Structural modifications can influence (improved) reaction event effectiveness on a molecular scale (STANKIEWICZ; VAN GERVEN; STEFANIDIS, 2019; VAN GERVEN; STANKIEWICZ, 2009)

VI.3.2 PI Approach in the Thermodynamic Domain (Energy)

In the thermodynamic domain, Energy is the focus of the PI approach. The fundamental query here is how energy can be transferred from source to recipient in the required form, in the required amount, on the required moment, and at the required position. (STANKIEWICZ; VAN GERVEN; STEFANIDIS, 2019; VAN GERVEN; STANKIEWICZ, 2009)

VI.3.3 PI Approach in the Functional Domain (Synergy)

This focus on bringing multiple functions together in one component (a molecule, a phase, or a reactor) often leads to significantly better performance than the separate functions executed sequentially(STANKIEWICZ; VAN GERVEN; STEFANIDIS, 2019; VAN GERVEN; STANKIEWICZ, 2009).

VI.3.4 PI Approach in the Temporal Domain (Time)

The methods for process intensification in the temporal domain are essentially twofold and entail either changing the time scales at which certain process steps proceed or introduction of dynamic states to an existing process, often in the form of periodicity(STANKIEWICZ; VAN GERVEN; STEFANIDIS, 2019; VAN GERVEN; STANKIEWICZ, 2009).

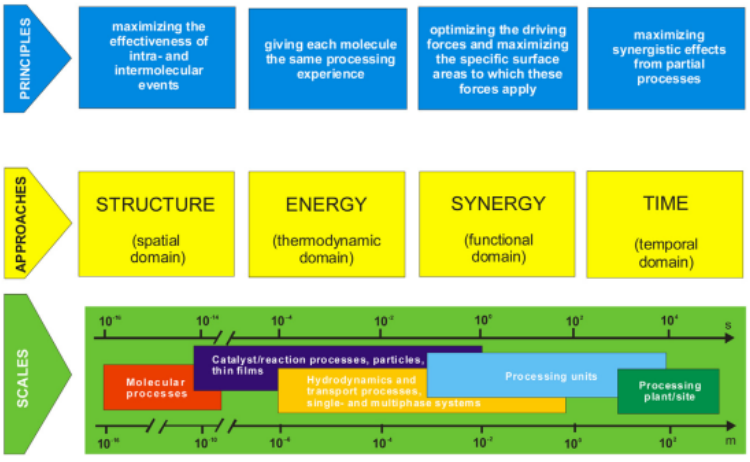

Figure VI.34 Fundamental view on process intensification divided by principles, approaches, and the scales to which it applies(VAN GERVEN; STANKIEWICZ, 2009).Copyright 2009 American Chemical Society

VI.4 Process Intensification Toolbox

A schematic of PI toolbox is shown in Figure VI.2. It includes process-intensifying equipment (PI hardware) and process-intensifying methods (PI software).

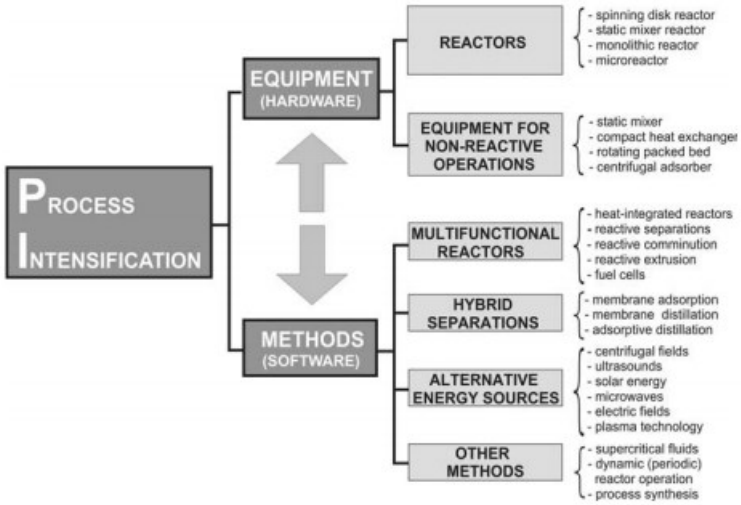

Figure VI.35. Schematic of process intensification toolbox(STANKIEWICZ; MOULIJN, 2004)

VI.4.1 Process-Intensifying Equipment

VI.4.1.1 Static Mixers

In industrial processes, mixing is crucial because how reagents are combined impact the reactions' selectivity and, in turn, the effectiveness of the process. They are often seen as one of the technological breakthrough in process engineering(STANKIEWICZ; MOULIJN, 2004). They offer more size and energy-efficient method for mixing or contacting fluids as shown with examples in figure VI.3. However, nowadays, their roles has transcend ordinary mixing, they can be applied be applied in processes in which simultaneous mixing and intensive heat removal or supply are necessary, such as in nitration or neutralization reactions(DIMIAN; BILDEA; KISS, 2014; HAASE; TOLVANEN, 2022; STANKIEWICZ; MOULIJN, 2000). Despite these advantages, they suffer from their sensitivity to clogging by solids, hence, their use for reactions involving slurry catalysts is limited.

Figure VI. 36. Different types of static mixers (STANKIEWICZ; MOULIJN, 2004)

VI.4.1.2 Monolithic catalysts

Monolithic packings consist of an array of parallel flow channels, and combine large specific surface areas of several 1000 m^2/m^3 with high porosities of 80% or more(TOMAŠIĆ, 2007). They are made of metallic or nonmetallic materials that offer a large number of straight, narrow channels with uniform cross sectional shapes.Examples are shown in figure VI.4. Monolith channels are majorly coated a thin layer of washcoat, which serves as support for the catalytically active species (DIMIAN; BILDEA; KISS, 2014; HAASE; TOLVANEN, 2022; STANKIEWICZ; MOULIJN, 2000). Monoliths are characterized by; low pressure drop in single and two-phase flow (1-2 order of magnitude) lower than the conventional packed system, good performance in processes where selectivity is hampered by mass-transfer resistances, high geometrical areas per reactor volume (1.5–4 times higher than in the reactors with particulate catalysts), high catalytic efficiency (100%), They suffer a major setback in (especially for gas-phase catalytic processes), because of the difficulty to remove heat due to absence of radial dispersion. The heat transport mechanism is the conductivity through the monolith material because their channel are separated from each other(STANKIEWICZ; MOULIJN, 2004).

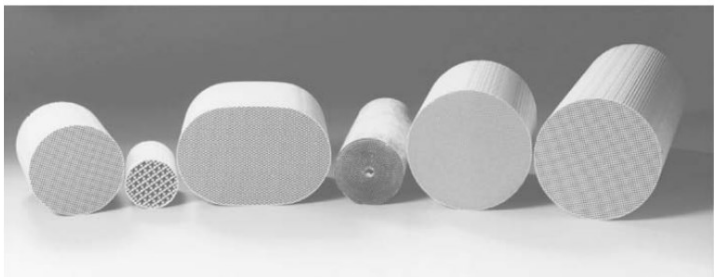

Figure VI.37.Various Sizes of Monolithic Catalyst (STANKIEWICZ; MOULIJN, 2004)

VI.4.1.3 Rotating devices

The spinning Disk reactor (SDR) is primarily intended for fast and extremely fast quick liquid/liquid reactions with a significant heat effect. Examples of such reactions are; nitrations, sulfonations, and polymerizations(BOODHOO; J.; RAMSHAW, 1997). It was develop by the Ramshaw group at the Newcastle University. In SDRs, a very thin layer of liquid that is generally 100 µm thick travels over the top of a spinning disc that may reach speeds of up to 1,000 rpm. Heat is effectively removed from the reacting liquid at heat-transfer rates surpassing 10,000 W/m^2K at very short residence time (usually 0.1 s) (DIMIAN; BILDEA; KISS, 2014; HAASE; TOLVANEN, 2022; STANKIEWICZ; MOULIJN, 2000). A schematic of SDR is shown in figure VI..5

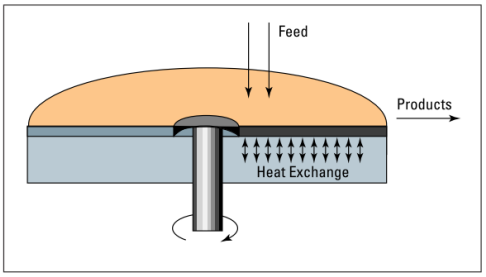

Figure VI.38.Schematic of the spinning-disk reactor (STANKIEWICZ; MOULIJN, 2004)

VI.4.1.4 Microreactors

Microreactors are known for their extremely small dimensions that usually have a sandwich-like structure consisting of a number of slices (layers) with micro-machined channels (10–100 µm in diameter). They have up to 20,000 W/m^2K heat transfer coefficient than heat exchanger reactors (HEX)(JÄCKEL, 1995). The slices (layers) carry out a variety of tasks, including mixing, heat exchange, separation, and catalytic reaction(DIMIAN; BILDEA; KISS, 2014). The most

significant benefits of microreactors is the integration of these different functions into a single device. Due to their high heat transfer rates, they can confidently be used in highly exothermic processes. This is crucial for doing kinetic investigations. Microreactors have extremely low reaction volume to surface area ratios(STANKIEWICZ; VAN GERVEN; STEFANIDIS, 2019).

VI.4.2 Process-intensifying methods

According to Garvin et al and as highlighted in figure VI.2, most process intensifying techniques may be grouped into three distinct categories; developing novel hybrid separations, integrating reaction and one or more unit operations into multifunction reactors, and use of alternative forms and sources of energy for processing.

VI.4.2.1 Multifunctional reactors

These are characterized as reactors that incorporate at least one extra function (often a unit operation) that would typically be carried out in a different piece of equipment in order to improve the chemical conversion and attain a greater degree of integration. The reverse-flow reactor is a well-known illustration of combining reaction and heat transfer in a multifunctional device (MATROS; BUNIMOVICH, 1996; STANKIEWICZ; VAN GERVEN; STEFANIDIS, 2019). When it comes to exothermic operations, frequent flow reversal in such units enables nearly perfect utilization of the heat of reaction by storing it inside the catalyst bed and utilizing it for preheating the cold reactant gases once the flow direction is reversed. Examples of industrial operations that have exploited reverse-flow reactors(MATROS; BUNIMOVICH, 1996; STANKIEWICZ; VAN GERVEN; STEFANIDIS, 2019) are; Total oxidation of hydrocarbon in off-gases and NOx reduction.

VI.4.2.2 Membrane Reactors

In these reactor systems, the membrane can perform a number of different tasks. For example, it can be used for selective in-situ separation of reaction products, resulting in a beneficial shift in equilibrium(STANKIEWICZ; MOULIJN, 2000; STANKIEWICZ; VAN GERVEN; STEFANIDIS, 2019). In order to increase the overall yield or selectivity of a process (such as in fixed-bed or fluidized-bed membrane reactors(ADRIS; GRACE, 1997; STANKIEWICZ; VAN GERVEN; STEFANIDIS, 2019; TSOTSIS et al., 1992), it can also be applied for a controlled distributed feed of some of the reacting species. Alternatively, it can be used to facilitate mass transfer(STANKIEWICZ; MOULIJN, 2000; STANKIEWICZ; VAN GERVEN; STEFANIDIS,

2019), direct bubble-free oxygen supply, or dissolution in the liquid phase via hollow-fiber membranes. The membrane can also facilitate the in-situ separation of catalyst particles from reaction products. (STANKIEWICZ; MOULIJN, 2000; STANKIEWICZ; VAN GERVEN; STEFANIDIS, 2019)

VI.4.2.3 Hybrid separations

The membrane acts as a permeable barrier between the liquid and gas phases in membrane absorption and stripping(STANKIEWICZ; MOULIJN, 2004). Large mass-transfer areas may be made by utilizing hollow-fiber membrane modules. This consequently translate to compact equipment. Additionally, absorption membranes operate independently of the gas and liquid flow rates, without entrainment, flooding, channeling, or foaming(STANKIEWICZ; VAN GERVEN; STEFANIDIS, 2019) (50,51). The most well-known hybrid method is likely membrane distillation (STANKIEWICZ; VAN GERVEN; STEFANIDIS, 2019)

VI.4.2.4 Alternative form of energy

In PI, a number of unconventional processing methods that depend on alternate energy sources and forms are crucial. The ability of various irradiation types to create strong localized heating, turbulence, and chemical effects makes them important and useful for process intensification(STANKIEWICZ, 2006; STANKIEWICZ; MOULIJN, 2004). Alternate forms energy include, Ultrasound, microwave heating, solar energy and plasma

VI.4.2.4.1 Ultrasound/Sonochemistry

Sonochemistry refers to the use of ultrasound in a process to facilitate mass transfer or the dissolution of solid reactants, or to increase the efficiency of a reaction. The effect of ultrasound originates from the formation of microbubbles' (cavities) in the liquid reaction medium. The bubbles are characterized by extremely high local temperatures and pressures release (temperature rises of up to 5,000 K and negative pressures of up to 10,000 atm were reported(MASON, 1991; STANKIEWICZ; MOULIJN, 2004). The collapse of these bubbles creates microimplosions with release of high local enegies. Their collapse creates microimplosions with very high local energy release (temperature rises of up to 5,000 K and negative pressures of up to 10,000 atm are reported(MASON, 1991; STANKIEWICZ; MOULIJN, 2004). The implosion have various effect on the reacting species, from free radicals formation, hemolytic bond breakage to fragmentation of polymer chains by the shockwave in the liquid surrounding the collapsing bubble.

VI.4.2.4.2 Solar energy

Solar energy can also play important role in chemical production. Studies has shown that a novel high-temperature reactor has in which solar energy is absorbed by a cloud of reacting particles to supply heat directly to the reaction site(GANZ et al., 1994; STANKIEWICZ; MOULIJN, 2004). In another study, thermal reduction of MnO_2 took place in a two small-scale solar chemical reactors(GANZ et al., 1994; STANKIEWICZ; MOULIJN, 2004).

VI.4.2.4.3 Microwave

Microwave heating has been successfully used and has shown to allow some organic syntheses proceed up to 1,240 times faster than the conventional techniques(GEDYE; SMITH; WESTAWAY, 1988). The main significant advantages of microwave irradiation is selective and targeted heating. Microwaves are characterized with frequencies between 0.1-300GHz range making it sit between the infrared and radio wave regions. In-situ desorption of hydrocarbons from zeolites used to remove volatile organic compounds can also be accomplished using microwave heating(CURTIS et al., 1997). Electric fields have been effectively employed to regulate nucleation rates in boiling heat transfer(STANKIEWICZ; MOULIJN, 2004; STANKIEWICZ; VAN GERVEN; STEFANIDIS, 2019).Processes involving liquid/liquid mixtures can benefit from the use of electric fields, particularly liquid/liquid extraction (STANKIEWICZ; MOULIJN, 2004)(67), which has been shown to increase rate by 200–300%(YAMAGUCHI, 1994).

VI.4.2.4.4 Plasma Energy

According to Haase et al(HAASE; TOLVANEN, 2022), Plasma energy is defined as the fourth state of matter. An ionized substance becoming highly electrically conductive characterizes this state of matter. Its behavior is dominated by the long range electric and magnetic fields. Plasma is finding its usage in a wide range of applications in laboratory and on industrial scale(STANKIEWICZ; MOULIJN, 2004). Some of its applications includes; destruction of volatile organic compounds in air, destruction of N_2O, reforming of heavy petroleum residues, CO_2 dissociation, activation of organic fibers, methane transformation to acetylene and hydrogen, natural gas conversion to synthesis gas, and SO_2 reduction to elemental sulfur(STANKIEWICZ; MOULIJN, 2004; STANKIEWICZ; VAN GERVEN; STEFANIDIS, 2019).

VI.5 Potential Areas of Application of PI in this work

With the aforementioned general overview on process intensification, the process system (this work) has shown to have some bottlenecks. These bottlenecks can be potentially resolved by intensifying the process methods and/or equipments. These configurations in figures VI.8 and VI.9 has shown that the process design can be improved in terms of footprint and energy efficiency, ultimately leading to huge savings in CAPEX and OPEX. These configurations are areas of process improvement which are aimed at future studies.

VI.5.1 Solubilization and Synthesis Unit

The solubilization and synthesis unit can be intensified as a multifunctional unit. The solubilization of CO_2 in the ionic liquid is favourable at a lower temperature. At the same time, the reaction proceed favourably at ambient temperature, hence, intensifying the units would be favourable for both synthesis and solubilization. Addittionaly, the solubility of hydrogen in the ionic liquid might be potentially taken care of by the increased pressure of the solubilization unit. Consequently, the hydrogen is favourably used in the reaction and less is recycled back to the reaction system. Due to the ambient condition of the reaction, multifunctional reactor (reverese plugflow or miroreactor) would be an ideal in this situation, as the exothermic heat from the reaction can be used effectively either to maintain the condition (temperature) of the ionic liquid or used for other heating requirement.The intensification would reduced the capital and operating cost as a result of reduced footprint and effective use of energy in a single unit of equipment.

VI.5.2 Adduct and Hydrogen recycle unit

The unreacted products, ionic liquids, and the main products can be intensified in a single unit. The use of a hybrid separation unit to favourably separate the unreacted hydrogen gas, the adduct mixture, and formic acid. Another alternative is to intensify this unit with the solubilization and synthesis unit. The introduction of a membrane reactor, capable of simultaneously allowing the synthesis and as well in-situ separation of the product of reaction (formic acid, methanol, and water). All other reactant are retained within the reactor.

VI.5.3 Formic acid and Methanol Separation unit

The use of advanced process intensification and integration techniques, such as thermally connected distillation columns or dividing-wall columns(DWC), to address the high energy needs of the traditional distillation is a solution that is gaining momentum. With over 120 chemical

industry applications, DWC is an excellent example of proven process intensification technology in distillation(KISS, ANTON, 2013). DWC, in fact, provides for much cheaper investment and operational expenses while also lowering equipment and carbon footprint(YILDIRIM; KISS; KENIG, 2011). DWC provides improved thermodynamic efficiency, compact configuration(2 columns in one shell), potential energy saving up to 25-30%, reduce capital investment by 20-30% due to the use of only 1 reboiler + 1 condenser, large range of application (P = 10mbar – 10 bar, up to 100 trays, purity levels ~1ppm). However, it has its limitations related to high pressure drop, one operating pressure, and high temperature difference(PARKINSON, 2007; STANKIEWICZ; VAN GERVEN; STEFANIDIS, 2019).

With the aforementioned features, advantages, and disadvantages, formic acid and methanol can be favourably separated with a DWC. The energy can be greatly reduced and the footprint of the two distillation column reduced to one.

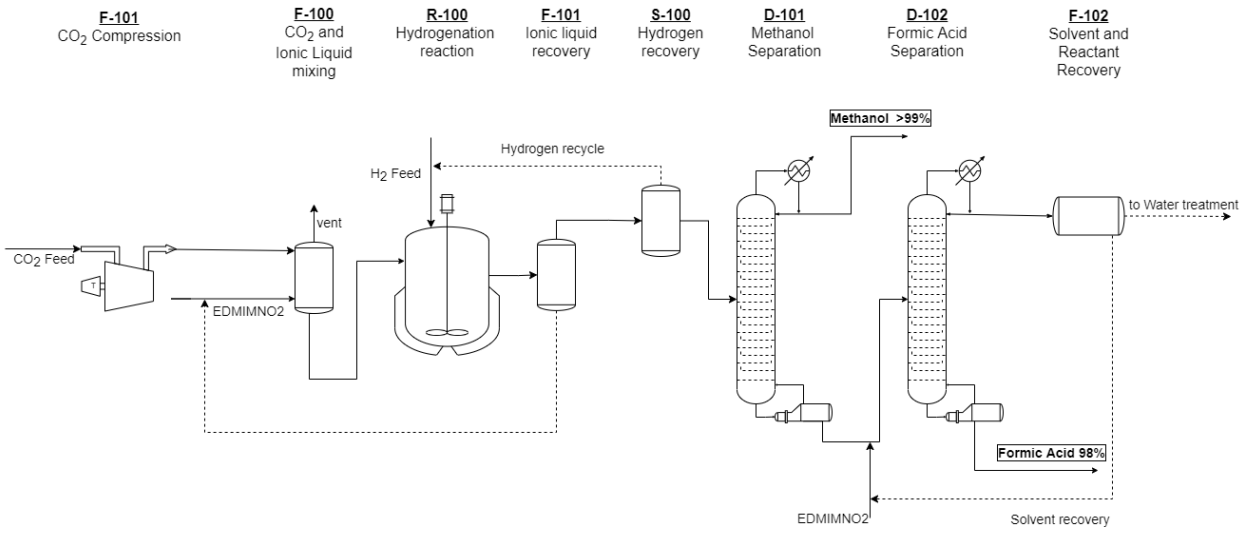

Figure VI.39. Schematic of the base case configuration of the process system

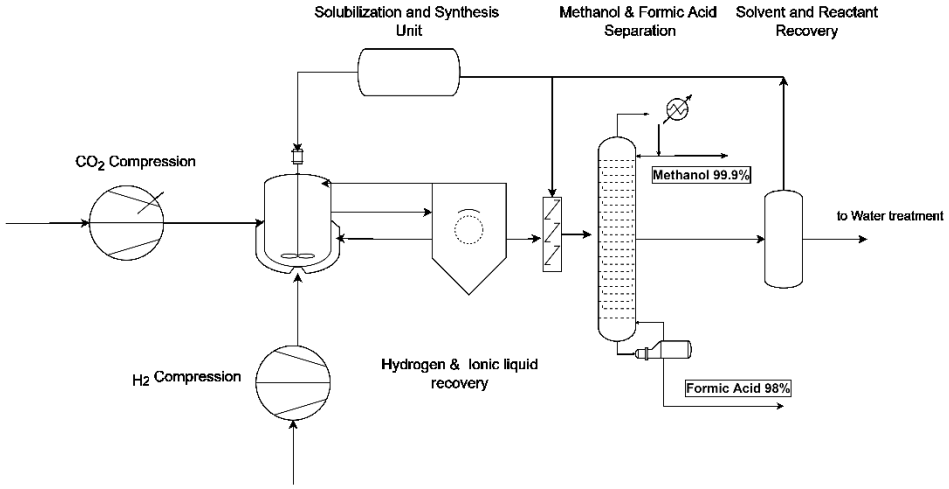

Figure VI.40.Schematic 1 of the intensified configuration of the process system

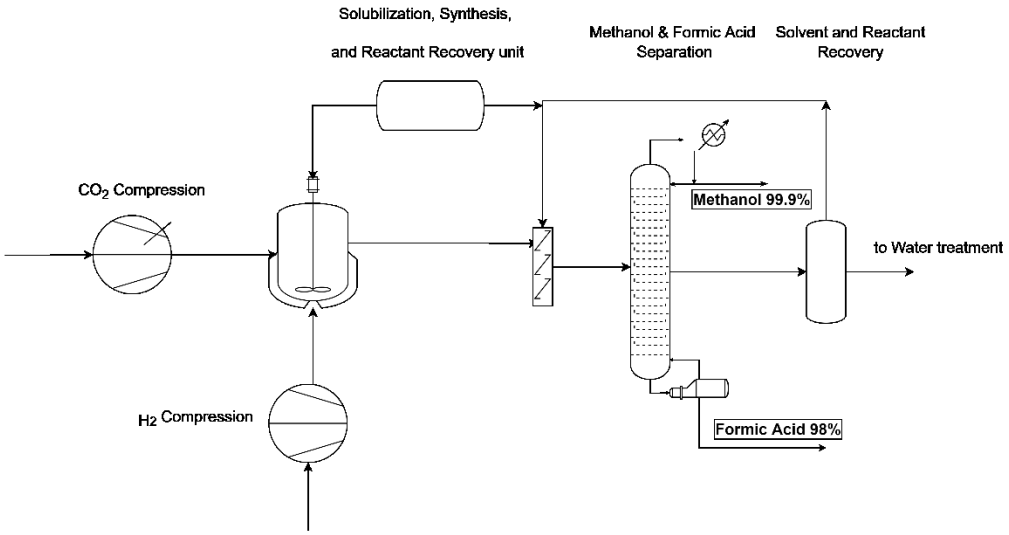

Figure VI.41.Schematic 2 of the intensified configuration of the process system

VI.6 Conclusion

Theoretically, from the qualitative analysis on the areas of intensification in this project, it can be safely concluded that this project indeed could be intensified and some major benefit can be accomplished.

The footprint of the process unit can be drastically reduced by intensifying the separation unit of distillation column in one unit. In the operation of this unit, energy usage can be reduced as one

condenser and a reboiler would be employed. Consequently, the CAPEX and OPEX could be potentially reduced largely.

The intensification of the solubilization unit and the synthesis unit with a multipurpose reactor would reduce the footprint and subsequently, a reduced CAPEX. The amount of unreacted H_2 would be reduced and less is recycled back to the reactor benefitting from a better mixing and mass transfer across the interface of the adduct layer for the hydrogenation reaction. Moreover, utilities are effectively used within in a single unit and consequently leading to reduced operating cost.

Finally, even though the carbon balance is relatively low because of the use of utilities, the intensification of the whole process plant could potentially drive down the carbon generation from the use of utilities by effective heat usage in the process system.

VI.7 References

ADRIS, A.-E. M.; GRACE, J. R. Characteristics of Fluidized-Bed Membrane Reactors: Scale-up and Practical Issues. **Industrial & Engineering Chemistry Research**, v. 36, n. 11, p. 4549–4556, 1997.

BOODHOO, K. V. K.; J., J.; RAMSHAW, C. **Spinning Disk Reactor for the Intensification of Styrene Polymerisation**. Proceedings, 2nd International Conference Process Intensification in Practice. **Anais**...London: BHR Group, 1997

CURTIS, W. et al. **Microwave Sorption Reactor Engineering**. AIChE Annual Meeting,. **Anais**...Los Angeles: 1997

DIMIAN, A. C.; BILDEA, C. S.; KISS, A. A. **Process Intensification**. [s.l: s.n.]. v. 35

FERNANDEZ RIVAS, D. et al. Process intensification education contributes to sustainable development goals. Part 2. **Education for Chemical Engineers**, v. 32, p. 15–24, 2020.

GANZ, J. et al. **A Novel Volumetric Solar Reac tor for Metal Oxides Reduction**. Proceedings, 7th Intlernational Symposium on Solar Thermal Concentrator Technology. **Anais**...Moscow: 1994

GEDYE, R. N.; SMITH, F. E.; WESTAWAY, K. C. The Rapid Synthesis of Organic Compounds in Microwave Ovens. **Canadian Journal of Chemistry**, v. 66, n. 1, p. 17–26, 1988.

HAASE, S.; TOLVANEN, P. 2022-Review-Process Intensification in Chemical Reaction Engineering.pdf. p. 1–23, 2022.

HESSEL, V. et al. Selectivity gains and energy savings for the industrial phenyl boronic acid process using micromixer/tubular reactors. **Organic Process Research and Development**, v. 8, n. 3, p. 511–523, 2004.

ILLG, T.; LÖB, P.; HESSEL, V. Flow chemistry using milli- and microstructured reactors-From conventional to novel process windows. **Bioorganic and Medicinal Chemistry**, v. 18, n. 11, p. 3707–3719, 2010.

JÄCKEL, K.-P. Microtechnology: Application Opportunities in the Chemical Industry. In: **Monograph Series 132**. Dechema, Frankfurt: [s.n.]. p. 29–50.

KISS, ANTON, A. **Advanced distillation technologies**. Chichester; United Kingdom: John Wiley

& Sons, 2013.

MASON, T. J. **Practical Sonochemistry "User's Guide to Applications in Chemistry and Chemical Engineering,"**. Ellis Horwood, New York: [s.n.].

MATROS, Y. S.; BUNIMOVICH, G. A. Reverse-Flow Operation in Fixed-Bed Catalytic Reactors. **Catalysis Reviews - Science and Engineering**, v. 38, n. 1, p. 1–68, 1996.

MOULIJN, J. et al. Process intensification and process systems engineering: A friendly symbiosis. **Computers & Chemical Engineering**, v. 32, p. 3–11, 2007.

PALO, D. R. et al. Industrial Applications of Microchannel Process Technology in the United States. v. 5, 2006.

PARKINSON, G. Dividing-wall columns find greater appeal. **Chemical Engineering Progress**, v. 103, n. 5, p. 8–11, 2007.

STANKIEWICZ, A. Energy matters: Alternative sources and forms of energy for intensification of chemical and biochemical processes. **Chemical Engineering Research and Design**, v. 84, p. 511–521, 2006.

STANKIEWICZ, A. I.; MOULIJN, J. A. Process Intensification: Transforming Chemical. **Chemical Engineering Progress**, n. January, p. 22–34, 2000.

STANKIEWICZ, A.; MOULIJN, J. **RE-ENGINEERING THE CHEMICAL PROCESSING Process Intensification**. Madison Avenue, New York: Marcel Dekker, Inc, 2004.

STANKIEWICZ, A.; VAN GERVEN, T.; STEFANIDIS, G. **The fundamentals of Process Intensification**. Weinheim, Germany: Wiley-VCH, 2019. v. 7

TOMAŠIĆ, V. Application of the monoliths in DeNOx catalysis. **Catalysis Today**, v. 119, n. 1–4, p. 106–113, 2007.

TSOTSIS, T. T. et al. Packed Bed Catalytic Membrane Reactors. **Chemical Engineering Science**, v. 47, n. 9–11, p. 2903–2908, 1992.

VAN GERVEN, T.; STANKIEWICZ, A. Structure, energy, synergy, time-the fundamentals of process intensification. **Industrial and Engineering Chemistry Research**, v. 48, n. 5, p. 2465–2474, 2009.

YAMAGUCHI, M. Liquid-Liquid Extraction Equipment. In: GODFREY, J. C.; SLATER, M. J. (Eds.). . **Electrically Aided Extraction and Phase Separation Equipment**. New York: [s.n.]. p. 585–624.

YILDIRIM, Ö.; KISS, A. A.; KENIG, E. Y. Dividing wall columns in chemical process industry: A review on current activities. **Separation and Purification Technology**, v. 80, n. 3, p. 403–417, 2011.

CHAPTER VII: CONCLUDING REMARKS

This work proposed and evaluated a novel method for CO_2 hydrogenation to formic acid and methanol promoted by IL. The evaluation was based on suitability and performance through the theoretical method of COSMO-RS and Aspen Process Simulator; Technical, economic, and environmental metrics by Aspen Simulator and assessment of the insight into the reaction by density functional theorem as a possible catalyst for CO_2 hydrogenation.

The method of evaluation using the theoretical approach has shown to be a valuable approach to significantly reduce the efforts in search of the appropriate ILs for a specific application especially, experimental measurement of CO_2 solubility in ILs.

The result have shown that the COSMO-RS model can be used to make a priori prediction of ILs and other organic compounds with no experimental data. Furthermore, the predictions have been proven with experimental results for volumetric properties such as density and molecular volume of other ILs. However, experimental studies need to be conducted to verify these predictions in this work scientifically.

It has been successfully demonstrated that low-pressure evaporation of ILs from their mixtures with the organic solute mixture is possible, such as formic acid-methanol-water-IL multicomponent mixtures. The energy consumption of the process is comparably lower to the benchmark considered in this study. Moreover, 35% of the benchmark solvent is lost in the vapour phase, requiring another process unit for its recovery.

In the search of suitable ILs for CO_2 solvation and product extraction, physical properties such as boiling point and viscosity play a critical role because the ILs need to be in a liquid state and low viscosity for easy mass transfer and lower pumping cost. The results from these studies have shown

that the selected ILs are capable of supporting/promoting the reaction of CO_2 and extraction of products from the reaction mixture.

The technical process metrics revealed that the hydrogenation of CO_2 to formic acid promoted by the ILs could be carried out at a low temperature and ambient pressure. At a range of process conditions such as temperature and pressure, formic acid and methanol can be preferentially produced to the other by altering the process conditions. The results show that the IL used has a high absorption capacity for CO_2 hence a high amount of CO_2 could be converted, which might significantly contribute to reaching a reduced emission in point source with significant CO_2 emission. The effective use of heat supplied and removed could be improved by an appropriate heat exchanger network. This would contribute further to reduction of operating cost and significantly reduce the carbon footprint from the utilities.

The mechanistic study through density functional theory into the insight of the reaction mechanism shows that the ionic liquid may activate H_2 for CO_2 hydrogenation as opposed to other studies in which CO_2 is always activated.

[Edmim][NO_2] ionic liquid could be a potential catalyst for the hydrogenation of CO_2 to formic acid in further experimental studies.

This thesis would contribute greatly to overcoming the bottleneck associated with CO_2 conversion. Furthermore, it offers possible solutions to the chemical industries and, more importantly, to the oil and gas industries in areas of waste valorization. Future developments could extend the same analysis, including ILs screening, process design, and sustainability assessment to discover other ILs with better thermodynamic and physical properties for CO_2 conversion. Moreover, the ionic

liquid ([Edmim][NO_2]) is not available commercially; hence, a detailed experimental study is necessary to understand better the insight into the behavior of the selected IL.

APPENDIXES

Appendix A. Supplementary data

Thermodynamic Analysis of Carbon Dioxide Hydrogenation to Formic Acid and Methanol

T.O. Bello, R.M.B. Alves, A.E. Bresciani, C.A.O. Nascimento

Escola Politécnica, Universidade de São Paulo, São Paulo, Brazil

The following figures presented herein show conversions of H2 and selectivity of methanol and formic acid under different operating conditions.

The conversion of H_2 decreases steadily after attaining the peak at T >25ºC with an increasing pressure. Increase in conversion in the first region was predominately controlled by high pressure and low temperature because more CO_2 is activated (CO_2-EDMIMNO_2 adduct) for hydrogenation. As the temperature increases, the reaction becomes more exothermic and less CO_2 available for activation and consequently leading to decrease in the H_2 conversion.

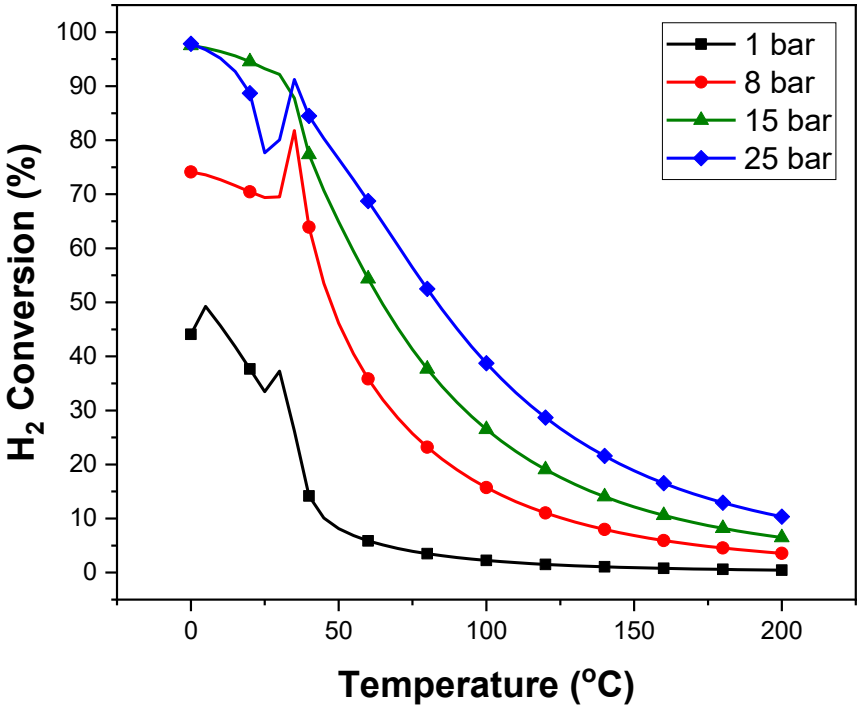

Figure S1. Influence of Temperature and Pressure at ratio 1/1/1: H_2 conversion

The preference for the production of formic acid was predominant at 8, 15 and 25 bar within the temperature range of 0-25°C 9Figure S2). This reveals that production of formic acid at low temperature and ratio 1:1:1 can only be possible at an increasing pressure. In the same vein, the reaction was selective towards methanol at all operating conditions (Figure S3). This can be attributed to the effect of CO_2-EDMIMNO_2 adduct and increasing pressure of the system. At ambient pressure, production of formic acid is not feasible.

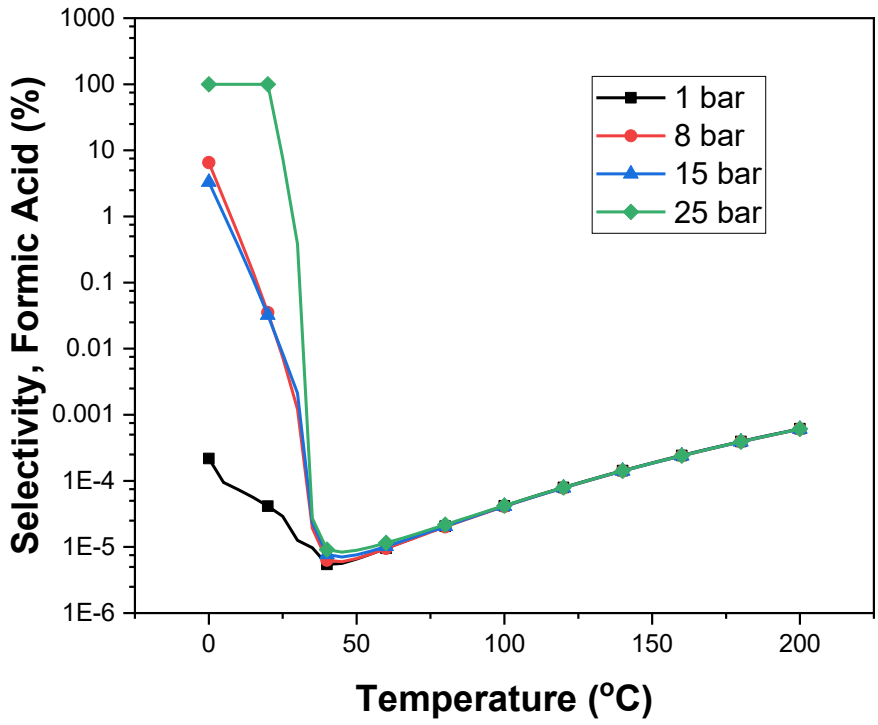

Figure S2. Influence of Temperature and Pressure at ratio 1/1/1: Formic Acid selectivity.

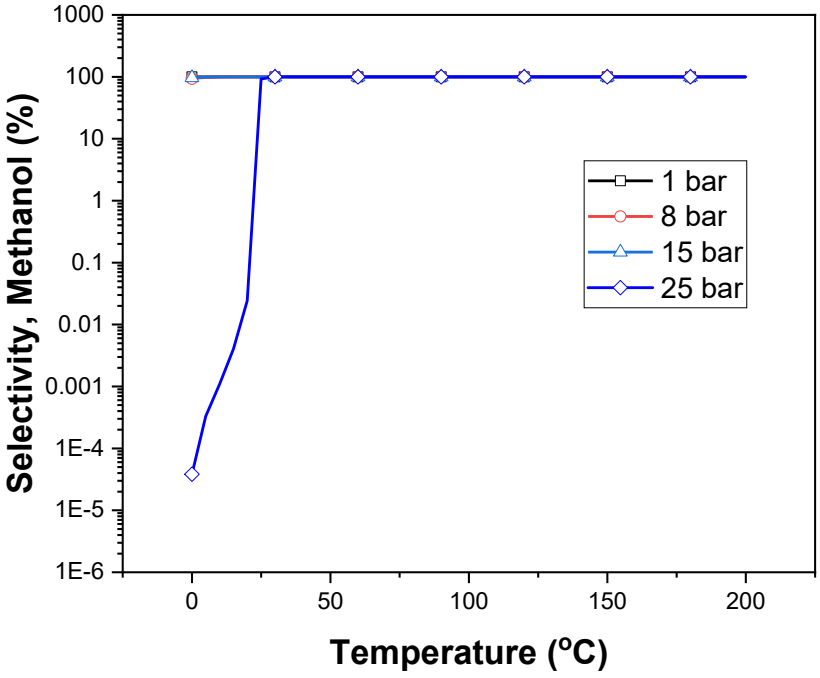

Figure S3. Influence of Temperature and Pressure at ratio 1/1/1: Methanol Selectivity

Increasing the H_2 ratio at 1 bar does not improve its equilibrium conversion. As it can be seen from the figure S4, the lowest conversion of H_2 was obtained at the highest ratio of 5. This is because, at 1 bar, the CO_2-EDMIMNO$_2$ adduct is low which makes less CO_2 molecule available for activation, consequently leading to decrease in H_2 conversion. Additionally, the influence of increased temperature enhances CO_2 desorption and reaction more exothermic leading to decrease in conversion.

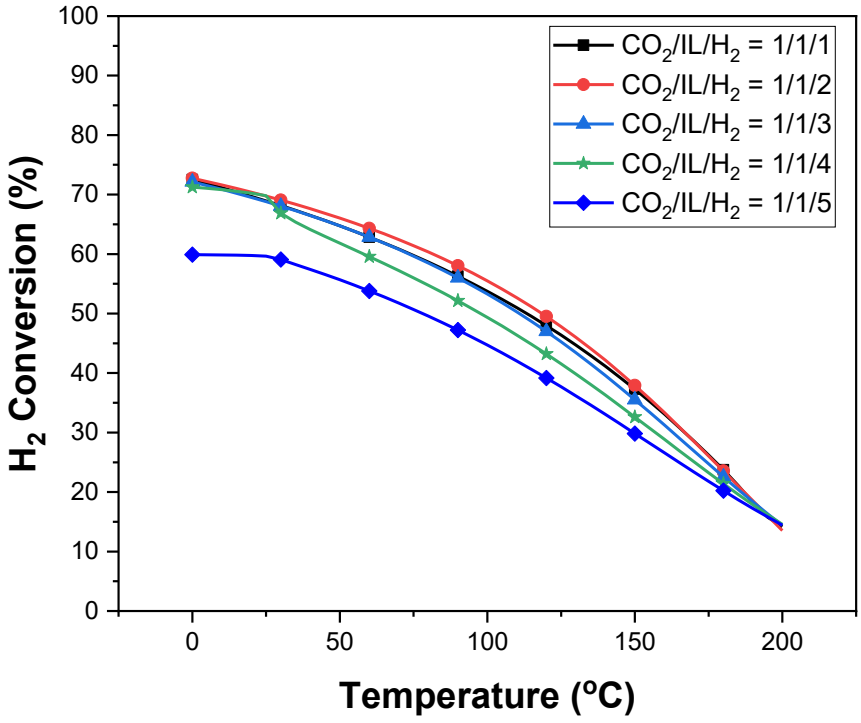

Figure S4. Influence of H_2 ratio at 1 bar: H_2 conversion.

From figure S5, the selectivity towards formic acid was insignificant at all operating conditions. Hence this affirms the earlier statement on figure S2 which emphasize that formic acid synthesis may not occur at ambient pressure even in the presence of CO_2-EDMIMNO$_2$ adduct. This can be explained that increasing pressure would favour the absorption of CO_2 in the ionic liquid and consequently more CO_2 available for activation. At all operating conditions, the reaction preference is towards methanol production as seen in figure S6.

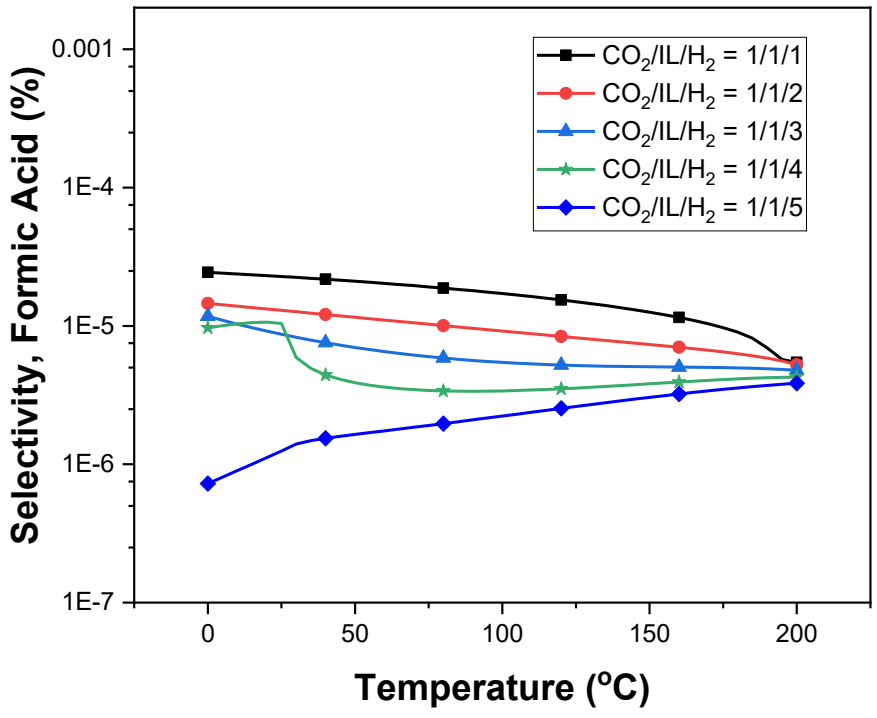

Figure S5. Influence of H_2 ratio at 1 bar: Formic acid selectivity

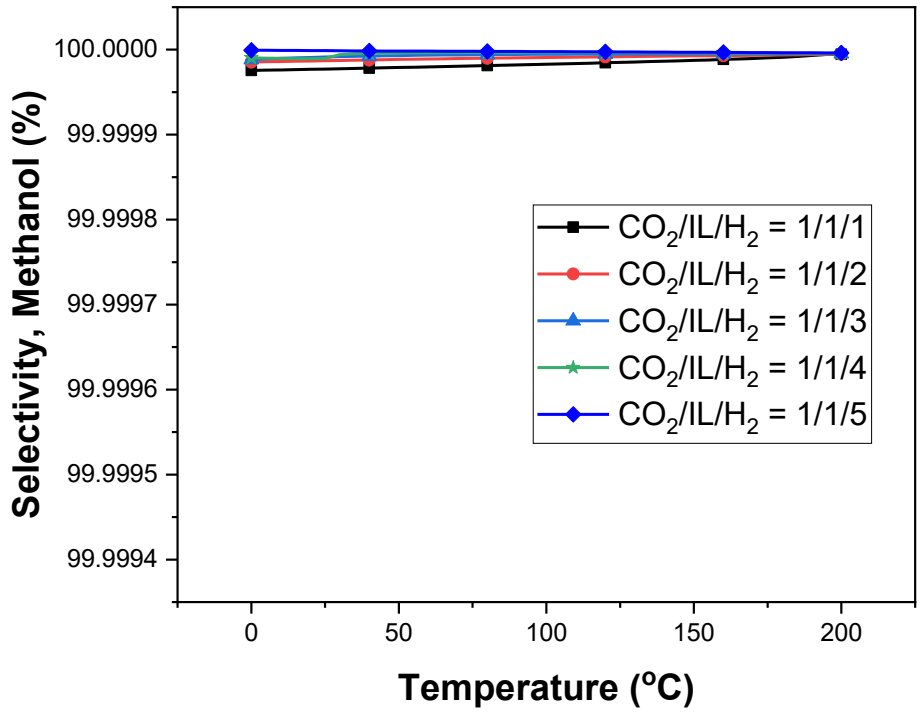

Figure S6. Influence of H_2 ratio at 1 bar: Methanol selectivity.

Similarly, increasing the $EDMIMNO_2$ ratio does not enhance the equilibrium conversion. From graph S7, the highest conversion was attained at the ratio 1. At 1 bar, CO_2-$EDMIMNO_2$ adduct is low which makes less CO_2 molecule available for activation, consequently resulting into decrease in H_2 conversion.

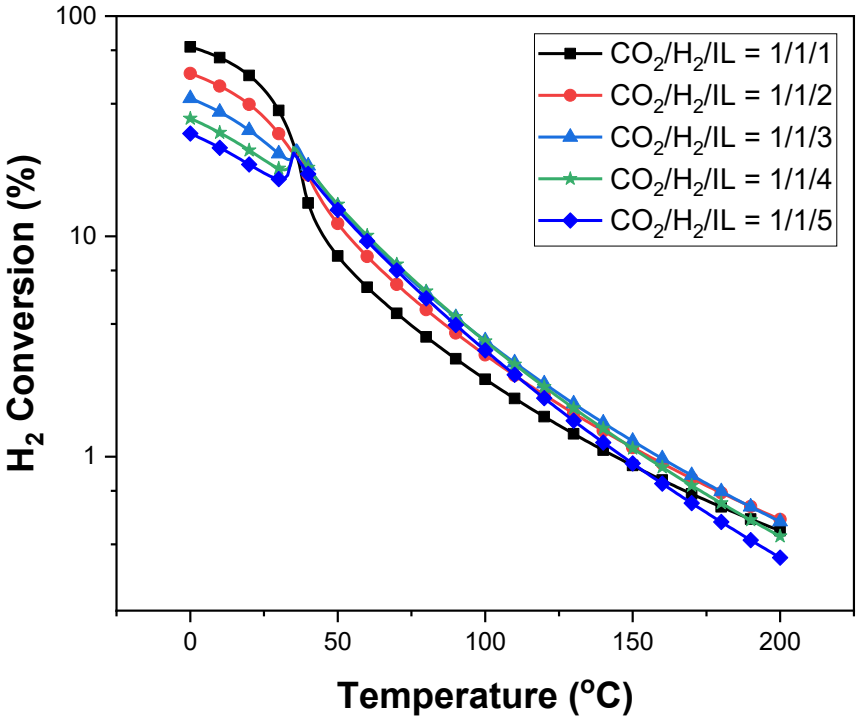

Figure S7. Influence of [Edmim][NO_2] ratio at 1 bar: H_2 conversion.

In a similar explanation to the trend in figure S5, the selectivity towards formic acid (figure S8) was insignificant at all operating conditions as oppose to the preference towards methanol (figure S9). This may be attributed to the same reason as figure S5.

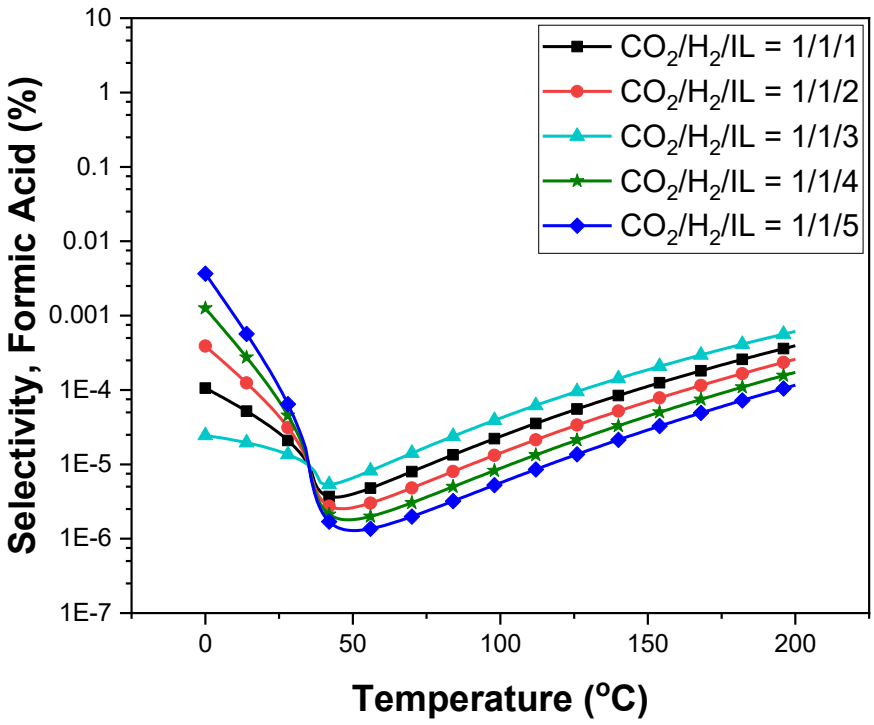

Figure S8. Influence of [Edmim][NO_2] ratio at 1 bar: Formic acid selectivity.

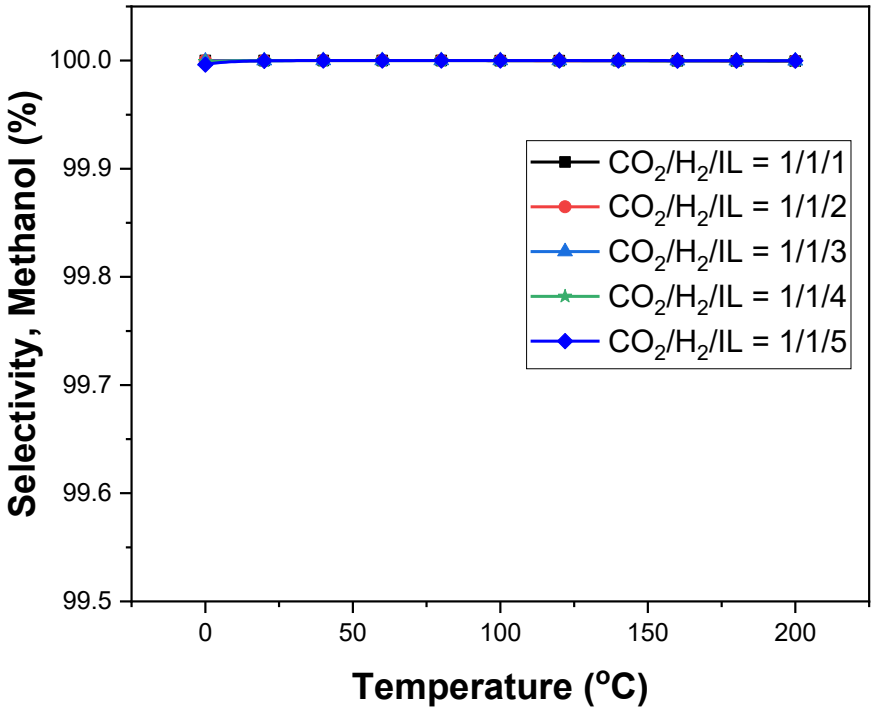

Figure S9. Influence of [Edmim][NO_2] ratio at 1 bar: Methanol selectivity.

From a close look at Figure S10, at H_2 ratio of 1, the highest conversion was achieved. The conversion decreases with increasing temperature at 17bar. H_2 conversion remain almost constant between 0-50°C, before it finally decreases exponentially. At this region, the effect of temperature is dominant, making the reaction more exothermic and consequently leading to low conversion.

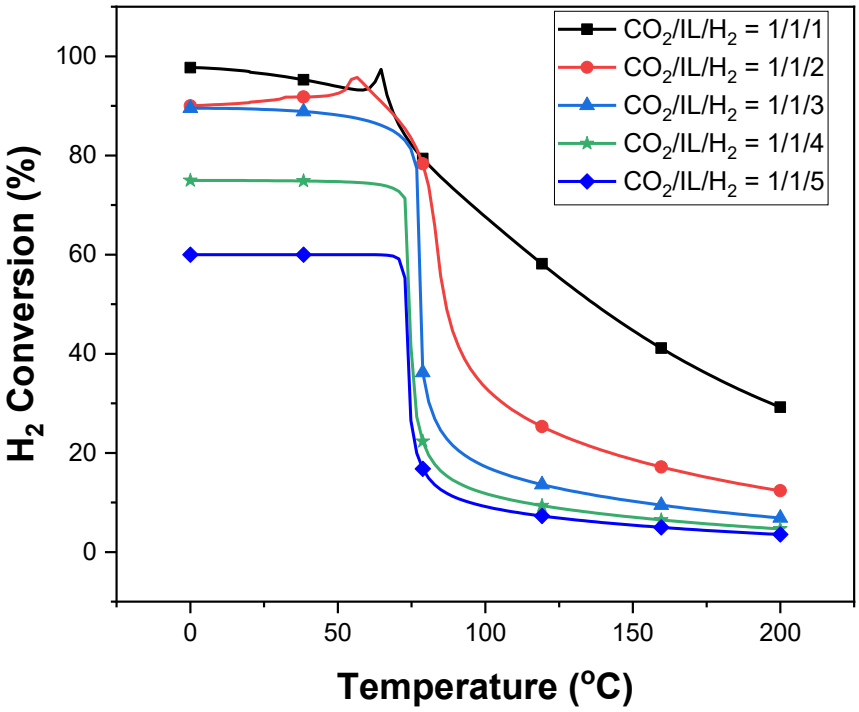

Figure S10. Influence of H_2 ratio at for simultaneous formic acid and methanol formation at 17bar: H_2 conversion

The preference towards formic acid was very low at ratio above 2 (Figure S11). The highest selectivity towards formic acid was achieved at ratio 2. At this ratio, increasing the H_2 ratio would not be beneficial towards formic acid synthesis. However, at all other ratio except 2, the preference

was towards methanol.

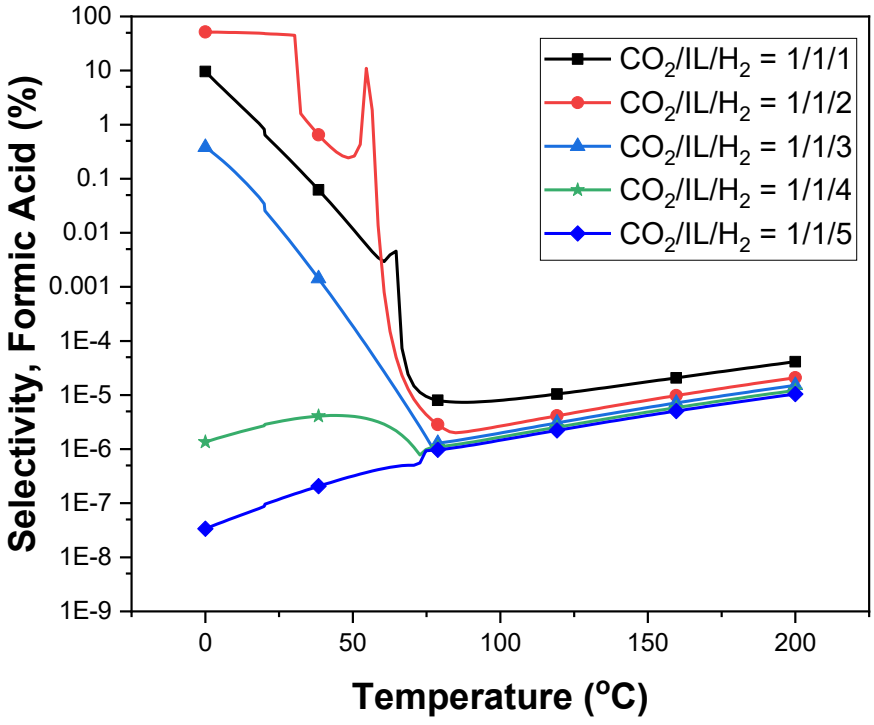

Figure S11.Influence of H_2 ratio at for simultaneous formic acid and methanol formation at 17bar: Formic acid selectivity

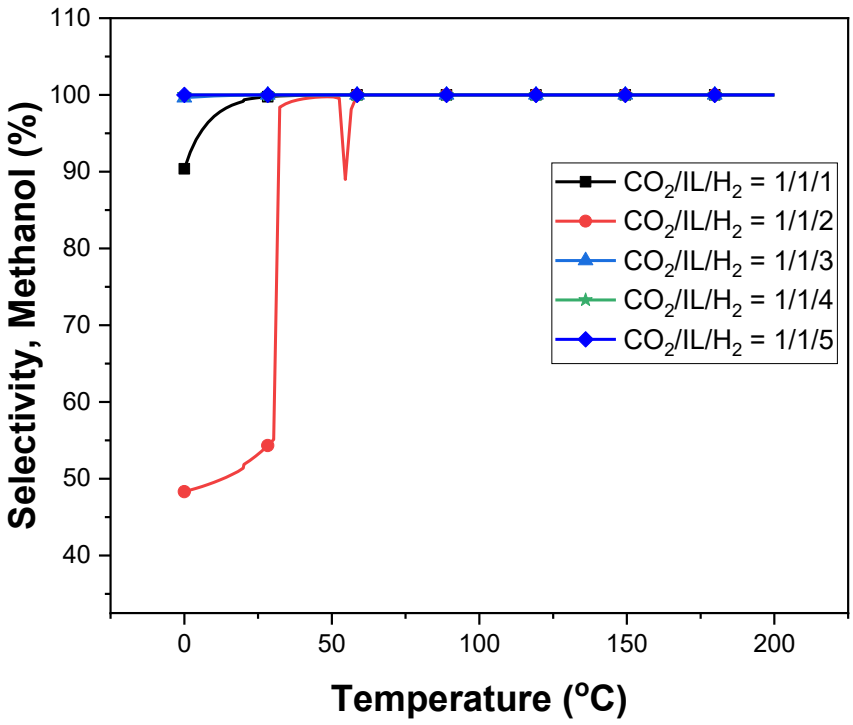

Figure S12. Influence of H_2 ratio at for simultaneous formic acid and methanol formation at 17bar: Methanol selectivity

From figure S13, the highest conversion occurred at ratio 5. A decline in the H_2 conversion was observed in figure S13. It might be attributed to less CO_2 is available for activation beyond 30°C. Consequently, the H_2 conversion also decrease.

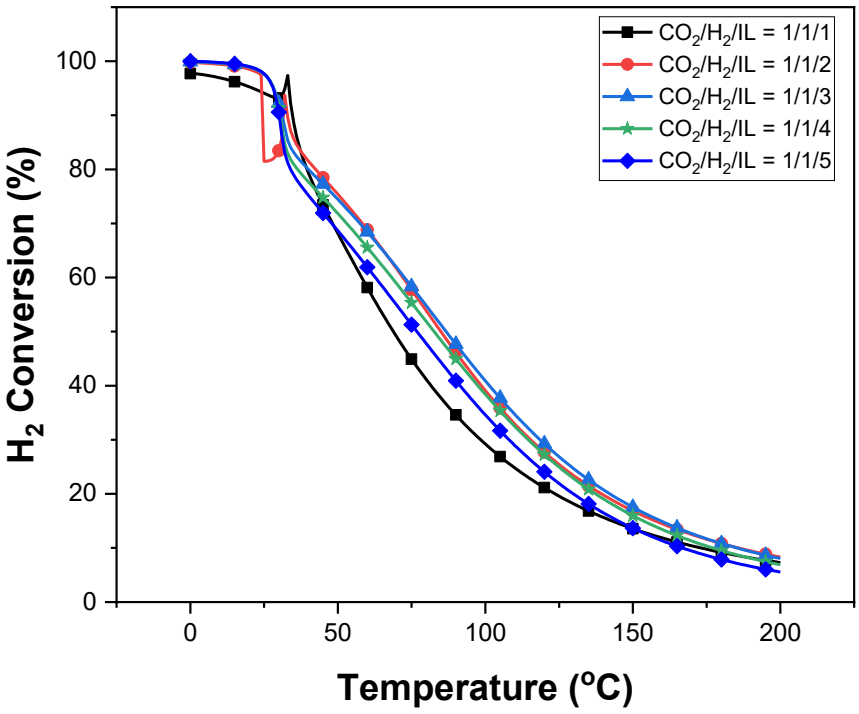

Figure S13. Effect of [Edmim][NO_2] ratio for simultaneous formic acid and methanol formation at 17 bar: H_2 conversion

At all $EDMIMNO_2$ ratio except 1, the selectivity was ~99%. As the temperature increase beyond 30°C, the selectivity decreases drastically. This may be attributed to the reaction being temperature-controlled at this region. However, beyond 30°C, the preference was towards methanol even though the productionwas low.

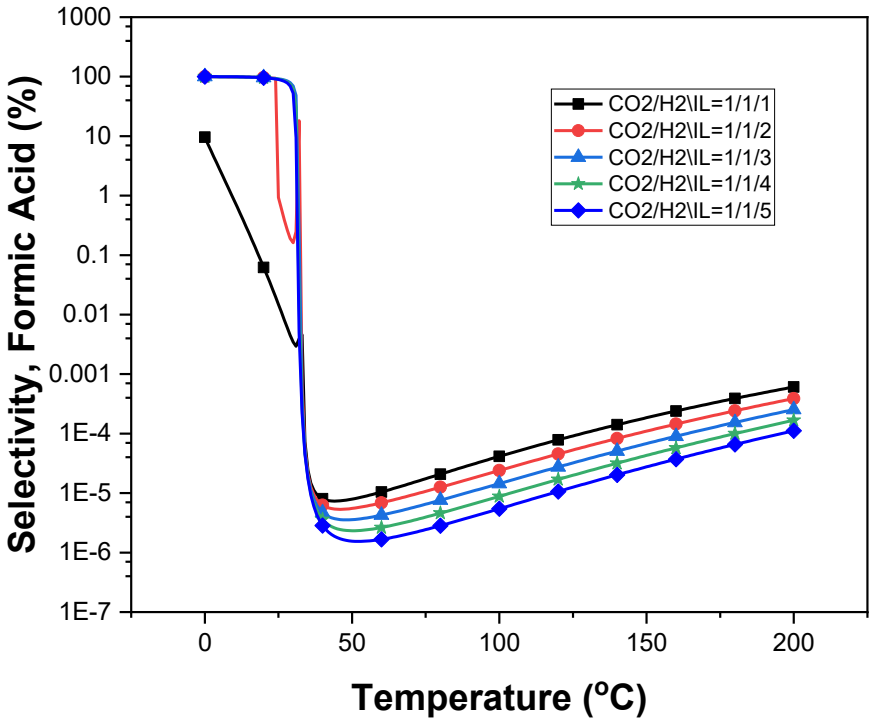

Figure S14. Effect of [Edmim][NO_2] ratio for simultaneous formic acid and methanol formation at 17 bar: Formic acid selectivity.

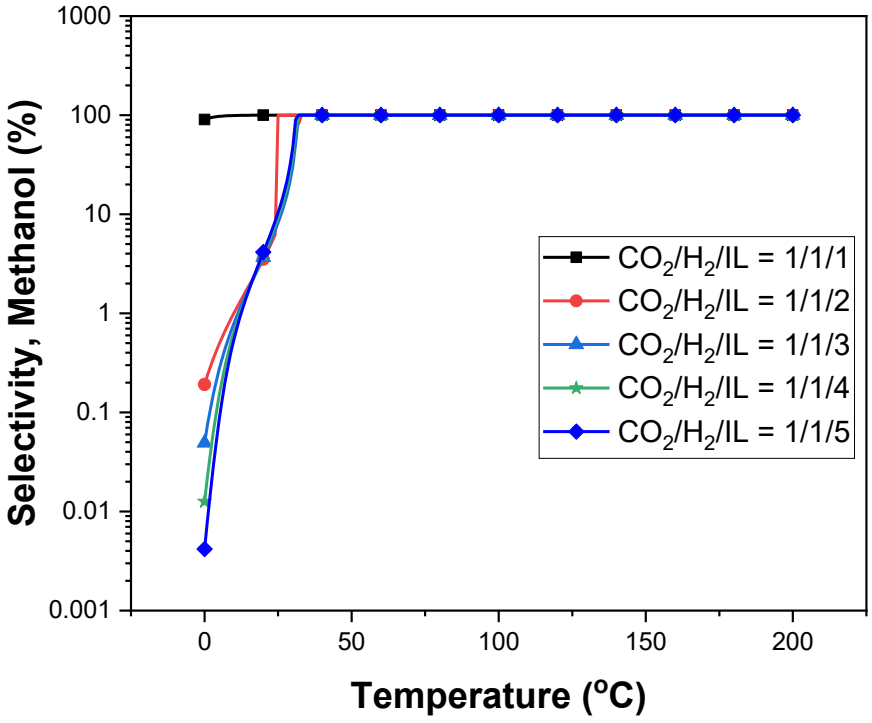

Figure S15. Effect of [Edmim][NO_2] ratio for simultaneous formic acid and methanol formation at 17 bar: Methanol selectivity.

At the optimal operating condition (P= 17 bar, CO2/H2/IL = 1/2/2), the selectivity towards formic acid was observed to commence at a very low temperature and then decreases as the temperature increase. However, methanol was dominant at temperature beyond 30^{O}C and remain steadily constant at the temperature range. This scenario explains the optimum operating condition for their simultaneous production

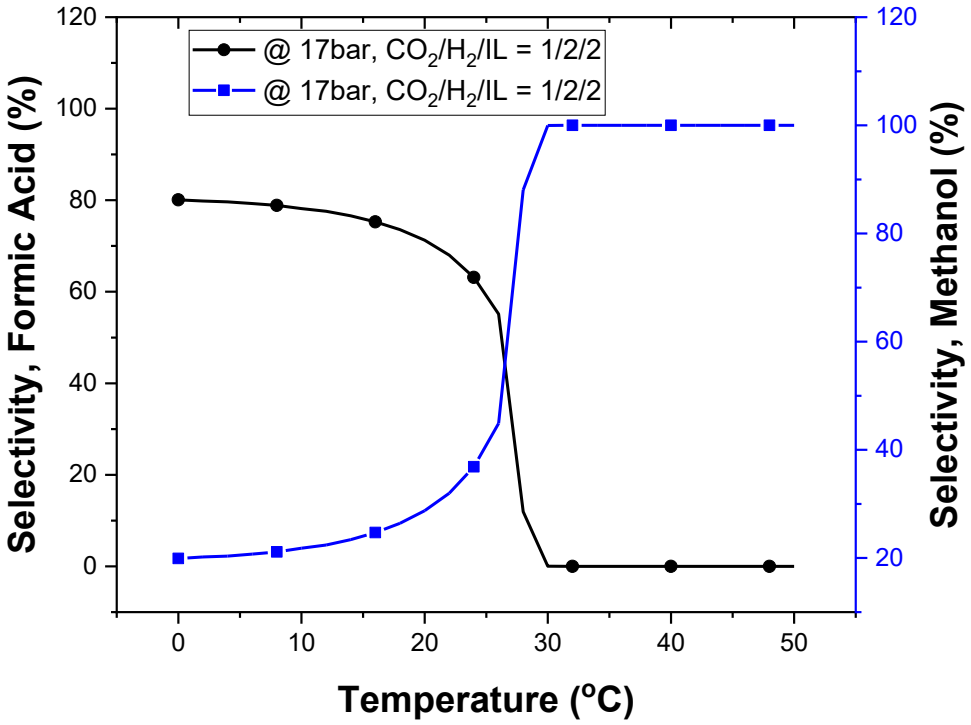

Figure S16. Simultaneous formic acid and methanol production at 17 bar and 1/2/2 ratio: Formic acid and methanol selectivity.

Appendix B. Supplementary data

A Mechanistic Study on Conversion of Carbon Dioxide to Formic Acid Promoted by 1-Ethyl-2,3-Dimethyl-Imidazolium Nitrite

T.O. Bello, R.M.B. ALVES, A.E. Bresciani, R.S. Alvim, C.A.O. Nascimento

Escola Politecnica, Universidade de São Paulo, São Paulo, Brazil.

All energies are in Hartrees

Figure S1. Optimized geometric structures with selected structural parameters (bond distances in Å and bond angle in deg) for the reactants and product.

Geometry and Vibrational frequency calculations by using RHF with basis set (Def2-SVP) of product (HCOOH + $EDMIMNO_2$), reactants (CO2 + H2), Transition structures and Intermediates at 298.15K and 1.00atm

Throughout the following assumptions are being made:

(1) The electronic state is orbitally nondegenerate

(2) There are no thermally accessible electronically excited states

(3) Hindered rotations indicated by low frequency modes are not treated as such but are treated as vibrations and this may cause some error

(4) All equations used are the standard statistical mechanics equations for an ideal gas

(5) All vibrations are strictly harmonic

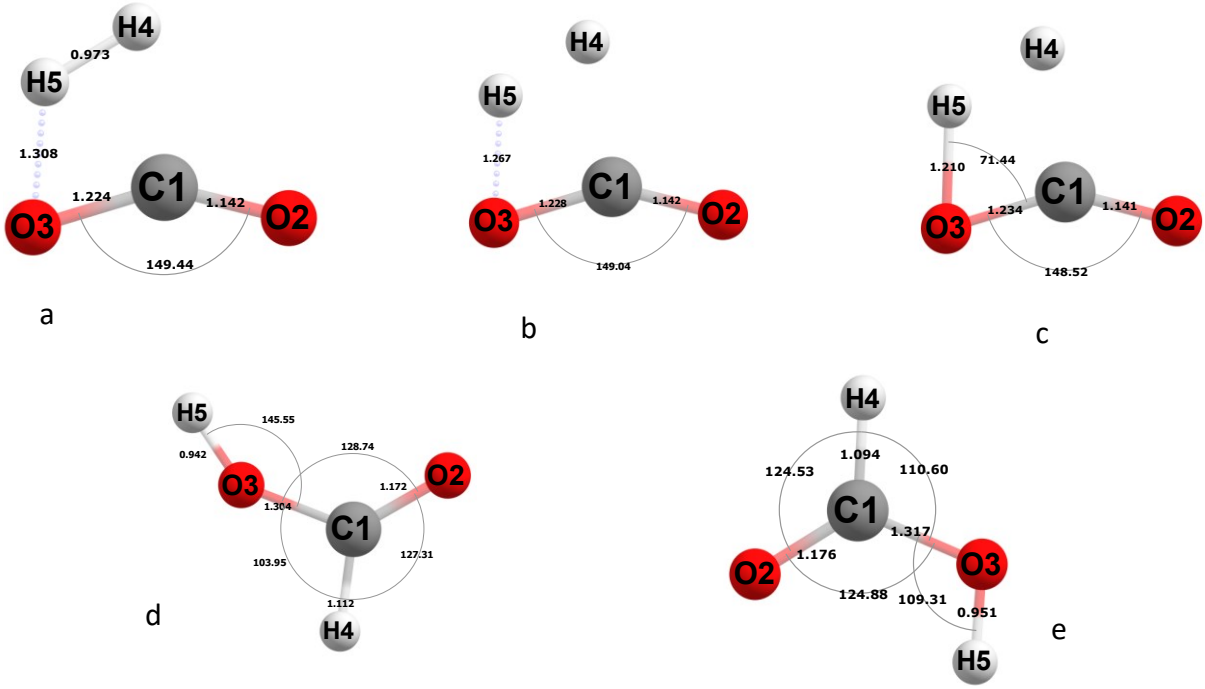

Figure 2: Unpromoted geometries of Intermediates, Transition states and product with RHF: (a) Pre-reacting Complex, (b) Transition state 1, (c) Intermediate 1, (d) Transition state 2,(e) Product

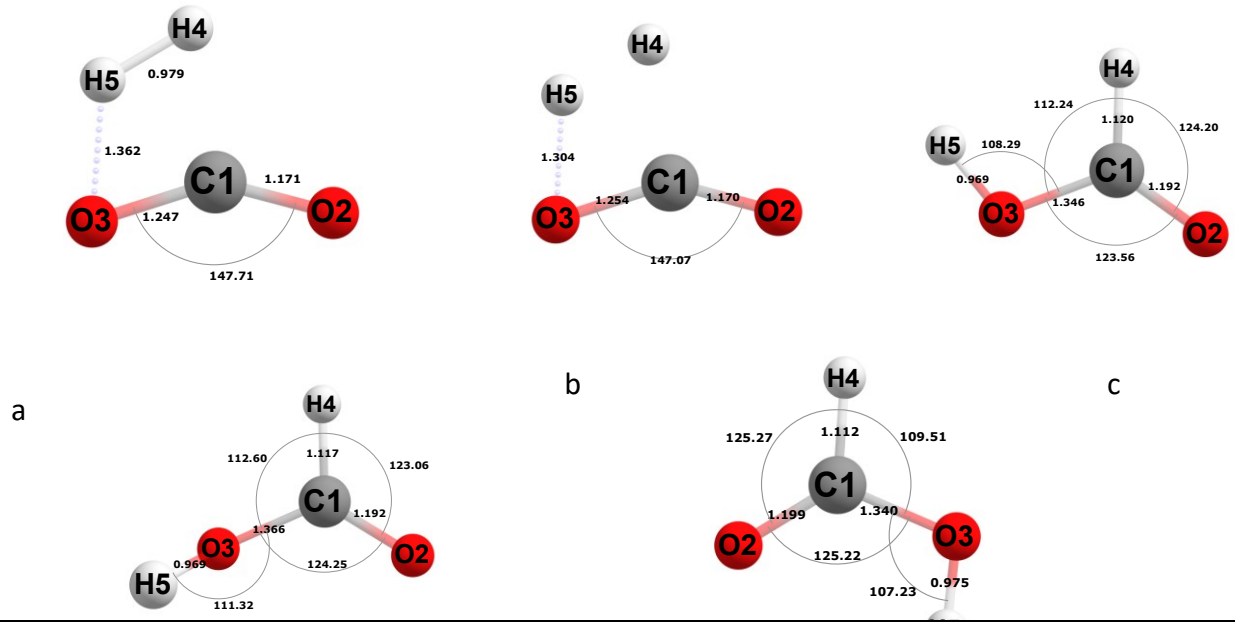

Figure 3: Unpromoted geometries of Intermediates, Transition states and product with DFT: (a) Pre-reacting Complex, (b) Transition state 1, (c) Intermediate 1, (d) Transition state 2,(e) Product

Table S1: Inner Energy (U) calculations using RHF with basis set Def2-SVP of product (HCOOH), reactants (CO_2 + H_2), Transition structures and Intermediates at 298.15K and 1.00atm for unpromoted reaction.

	E_{el}	E_{ZPE}	E_{vib}	E_{rot}	E_{trans}
Product	-188.62117192	0.03710856	0.00026034	0.00141627	0.00141627
Reactants	-188.61669435	0.02461396	0.00292714	0.00141627	0.00141627
TS1	-188.47174335	0.02640042	0.00029647	0.00141627	0.00141627
TS2	-188.59478973	0.03338783	0.00055039	0.00141627	0.00141627
I1	-188.62117192	0.03710870	0.00026035	0.00141627	0.00141627

Table S2: Entropy contributions (T*S) calculations using RHF with basis set Def2-SVP of product (HCOOH), reactants (CO_2 + H_2), Transition structures and Intermediates at 1.00atm for unpromoted reaction.

	$(T*S)_{el}$	S_{vib}	S_{rot}	S_{trans}
Product	0.00000000	0.00033043	0.00993972	0.01777224
Reactants	0.00000000	0.00569034	0.01065322	0.01777224
TS1	0.00000000	0.00037749	0.00985599	0.01777224
TS2	0.00000000	0.00085558	0.00991806	0.01777224
I1	0.00000000	0.00033045	0.00993970	0.01777224

Table S3: Enthalpy (H), Entropy(T*S), Gibbs Energy (G) calculations using RHF with basis set Def2-SVP of product (HCOOH), reactants (CO_2 + H_2), Transition structures and Intermediates at 298.15K and 1.00atm for unpromoted reaction

	H	**T*S**	**G**	**Vibrational Frequency(**cm^{-1}**)**
Product	-188.5800263	0.02804239	-188.6080687	
Reactants	-188.5853765	0.0341158	-188.6194923	
TS1	-188.4412697	0.02800572	-188.4692754	-2709.46i
TS2	-188.5570748	0.02854588	-188.5856206	-457.51i
I1	-188.5800261	0.02804239	-188.6080685	

Table S4: Inner Energy (U) calculations using DFT with basis set Def2-SVP of product (HCOOH), reactants (CO_2 + H_2), Transition structures and Intermediates at 298.15K and 1.00atm for unpromoted reaction.

	E_{el}	E_{ZPE}	E_{vib}	E_{rot}	E_{trans}
Product	-189.52976386	0.03391517	0.00032096	0.00141627	0.00141627
Reactants	-189.52795573	0.02316026	0.00283933	0.00141627	0.00141627
TS1	-189.41627327	0.02421316	0.00036326	0.00141627	0.00141627
TS2	-189.50752250	0.03175003	0.00022258	0.00141627	0.00141627

I1	-189.52211237	0.03350772	0.00040070	0.00141627	0.00141627

Table S5: Entropy contributions (T*S) calculations using DFT with basis set Def2-SVP of product (HCOOH), reactants (CO_2 + H_2), Transition structures and Intermediates at 1.00atm for unpromoted reaction.

	$(T*S)_{el}$	S_{vib}	S_{rot}	S_{trans}
Product	0.00000000	0.00041059	0.00998874	0.01777224
Reactants	0.00000000	0.00534084	0.01059482	0.01777224
TS1	0.00000000	0.00046917	0.00991993	0.01777224
TS2	0.00000000	0.00027882	0.01000026	0.01777224
I1	0.00000000	0.00052831	0.00995479	0.01777224

Table S6: Enthalpy (H), Entropy(T*S), Gibbs Energy (G) calculations using DFT with basis set Def2-SVP of product (HCOOH), reactants (CO_2 + H_2), Transition structures and Intermediates at 298.15K and 1.00atm for unpromoted reaction

	H	**T*S**	**G**	**Vibrational Frequency(**cm^{-1}**)**
Product	-189.491751	0.02817156	-189.5199225	
Reactants	-189.4981794	0.03370789	-189.5318873	
TS1	-189.3879201	0.02816134	-189.4160814	-2214.32i
TS2	-189.4717731	0.02805131	-189.4998245	-643.1

I1	-189.4844272	0.02825534	-189.5126825	

Table S7: Inner Energy (U) calculations using RHF with basis set Def2-SVP of products ($HCOOH + EDMIMNO_2$), reactants ($CO_2 + H_2$), Transition structures and Intermediates at 298.15K and 1.00atm for promoted reaction.

	E_{el}	E_{ZPE}	E_{vib}	E_{rot}	E_{trans}
Products	-773.79005988	0.26013473	0.01504559	0.00141627	0.00141627
Reactants	-773.77093861	0.24812298	0.01768437	0.00141627	0.00141627
$TS1_A$	-773.69562133	0.25065178	0.01491604	0.00141627	0.00141627
$TS2_A$	-773.78678391	0.25974578	0.01458206	0.00141627	0.00141627
$I1_A$	-773.77049701	0.24795292	0.01788073	0.00141627	0.00141627
$I2_A$	-773.78845849	0.26062692	0.01491546	0.00141627	0.00141627
$I3_A$	-773.78918372	0.26017523	0.01500672	0.00141627	0.00141627

Table S8: Entropy contributions (T*S) calculations using RHF with basis set Def2-SVP of products ($HCOOH + EDMIMNO_2$), reactants ($CO_2 + H_2$), Transition structures and Intermediates at 1.00atm for promoted reaction.

	$(T*S)_{el}$	S_{vib}	S_{rot}	S_{trans}
Products	0.00000000	0.02804926	0.01529544	0.01996993
Reactants	0.00000000	0.03360785	0.01536934	0.01996993

$TS1_A$	0.00000000	0.02793897	0.01538526	0.01996993
$TS2_A$	0.00000000	0.02718957	0.01529311	0.01996993
$I1_A$	0.00000000	0.03427163	0.01539242	0.01996993
$I2_A$	0.00000000	0.02768130	0.01532417	0.01996993
$I3_A$	0.00000000	0.02802741	0.01530631	0.01996993

Table S9: Enthalpy (H), Entropy(T*S), Gibbs Energy (G) calculations using RHF with basis set Def2-SVP of product (HCOOH + $EDMIMNO_2$), reactants (CO_2 + H_2), Transition structures and Intermediates at 298.15K and 1.00atm for promoted reaction.

	H	**T*S**	**G**	**Imaginary Frequency(**cm^{-1}**)**
Products	-773.51110280	0.06331463	-773.5744174	
Reactants	-773.50135450	0.06894712	-773.5703016	
$TS1_A$	-773.4262768	0.06329417	-773.4895709	-1562.30
$TS2_A$	-773.50867933	0.06245262	-773.5711319	-192.54
$I1_A$	-773.5008866	0.06963398	-773.5705206	
$I2_A$	-773.5091394	0.0629754	-773.5721148	
$I3_A$	-773.510225	0.06330365	-773.5735287	

Table S10: Inner Energy (U) calculations using DFT with basis set Def2-SVP of products (HCOOH + $EDMIMNO_2$), reactants (CO_2 + H_2), Transition structures and Intermediates at 298.15K and 1.00atm for promoted reaction.

	E_{el}	E_{ZPE}	E_{vib}	E_{rot}	E_{trans}
Products	-777.95523475	0.24111844	0.01536795	0.00141627	0.00141627
Reactants	-777.93188548	0.23133235	0.01778707	0.00141627	0.00141627
$TS1_B$	-777.89410870	0.23266394	0.01532466	0.00141627	0.00141627
$TS2_B$	-777.94639023	0.24094685	0.01470042	0.00141627	0.00141627
$TS3_B$	-777.95038804	0.24087113	0.01457527	0.00141627	0.00141627
$TS4_B$	-777.95382022	0.24072704	0.01464510	0.00141627	0.00141627
$I1_B$	-777.95196548	0.24028280	0.01526475	0.00141627	0.00141627
$I2_B$	-777.92470583	0.23234947	0.01741979	0.00141627	0.00141627
$I3_B$	-777.95090445	0.24118584	0.01530139	0.00141627	0.00141627
$I4_B$	-777.95534596	0.24131520	0.01510191	0.00141627	0.00141627
$I5_B$	-777.95429783	0.24083509	0.01548913	0.00141627	0.00141627

Table S11: Entropy contributions (T*S) calculations using DFT with basis set Def2-SVP of products (HCOOH + $EDMIMNO_2$), reactants (CO_2 + H_2), Transition structures and Intermediates at 1.00atm for promoted reaction.

	$(T*S)_{el}$	S_{vib}	S_{rot}	S_{trans}
Products	0.00000000	0.02836151	0.01529951	0.01996993
Reactants	0.00000000	0.03328477	0.01535036	0.01996993
$TS1_B$	0.00000000	0.02839090	0.01540799	0.01996993
$TS2_B$	0.00000000	0.02702873	0.01523357	0.01996993
$TS3_B$	0.00000000	0.02672612	0.01528915	0.01996993
$TS4_B$	0.00000000	0.02686224	0.01527764	0.01996993
$I1_B$	0.00000000	0.02825496	0.01534179	0.01996993
$I2_B$	0.00000000	0.03269793	0.01556103	0.01996993
$I3_B$	0.00000000	0.02815235	0.01524343	0.01996993
$I4_B$	0.00000000	0.02768228	0.01529483	0.01996993
$I5_B$	0.00000000	0.02902255	0.01527052	0.01996993

Table S12: Enthalpy (H), Entropy(T*S), Gibbs Energy (G) calculations using DFT with basis set Def2-SVP of product (HCOOH + $EDMIMNO_2$), reactants (CO_2 + H_2), Transition structures and Intermediates at 298.15K and 1.00atm for promoted reaction.

	H	**T*S**	**G**	**Imaginary Frequency(**cm^{-1}**)**
Products	-777.6949716	0.06363096	-777.7586026	
Reactants	-777.6789893	0.06860506	-777.7475944	
$TS1_B$	-777.6423434	0.06376882	-777.7061122	-654.27
$TS2_B$	-777.6869662	0.06223223	-777.7491984	-183.78
$TS3_B$	-777.6911649	0.06198521	-777.7531501	-232.24
$TS4_B$	-777.6946713	0.06210982	-777.7567812	-100.14
$I1_B$	-777.6926412	0.06356668	-777.7562079	
$I2_B$	-777.6711598	0.0682289	-777.7393887	
$I3_B$	-777.6906405	0.06336571	-777.7540062	
$I4_B$	-777.695152	0.06294705	-777.758099	
$I5_B$	-777.694197	0.064263	-777.75846	

Appendix C. Supplementary data

Process Design Of Formic Acid And Methanol Production Promoted By Ionic Liquid: Techno-Economic Analysis

T.O. Bello, R.M.B. ALVES, A.E. Bresciani, R.S. Alvim, C.A.O. Nascimento

Escola Politecnica, Universidade de São Paulo, São Paulo, Brazil.

Table S1: Stream condition of the inlet and outlets stream into the system

mn2	**FEEDS**					**PRODUCTS**			
	CO2	**MKUP-H2**	**IL-SOLV**	**IL-FEED**	**H2**	**FORMIC ACID**	**METHANOL**	**PURGE-H2**	**WASTEH2O**
Phase	Vapor Phase	Vapor Phase	Liquid Phase		Vapor Phase	Liquid Phase	Liquid Phase	Vapor Phase	Vapor Phase
Temperature (C)	40	50	90.8	25.6	50.0	36.0	64.2	50	90
Pressure (bar)	2	2	2	1	2	0.09	1	2	1
Mass Vapor Fraction	1	1	0	0.12	1	0	0	1	1
Mass Liquid Fraction	0	0	1	0.88	0	1	1	0	0
Mass Density (kg/cum)	3.41	0.15	845.02	14.47	0.15	1163.30	744.60	0.15	0.61
Average MW	44.01	2.02	170.27	125.75	2.02	44.50	32.05	2.02	18.28
Mass Flows (kg/hr)	3137	201.17	1000.99	3585.23	5000.00	2678.71	456.97	0.00	202.49
METHANOL	0	0	0	4.31E-03	0	0.27	456.51	0	0
FORMIC ACID	0	0	0.52	6.84E-02	0	2619.40	0.43	0	4.74
WATER	0	0	0.48	2.58E-04	0	59.04	0.03	0	197.75
H2	0	201.16	0	3.65E-03	4999.9	0	0	1.92E-06	0
CO2	3137	0	0	448.16	0	0	0	0	0
EDMIMNO2	0	0	999.99	3137.00	0	1.85E-06	0	0	3.57E-05
Mass Fractions									
METHANOL	0	0	0	1.20E-06	0	1.02E-04	0.99	0	0
FORMIC ACID	0	0	5.15E-04	1.91E-05	0	0.977	9.42E-04	0	0.02
WATER	0	0	4.75E-04	7.2E-08	0	2.20E-02	5.80E-05	0	0.98
H2	0	1	0	1.01E-06	1	0	0	1	0
CO2	1	0	0	0.13	0	0	0	0	0
EDMIMNO2	0	0	0.999	0.87	0	6.91E-10	0	0	1.76E-07

Table S2: Utility requirments and the corresponding CO_2 emitted in the system

Cooling Utility					
Block ID	**Block type**	**Duty** (cal/sec)	**Usage** (kg/hr)	**Cost** ($/hr)	**CO2 emission rate**
S-100	SEPARATOR	159261	57507.5	0.51	
S-101	SEPARATOR	9535.95	3443.33	0.03	
C-100	HEATER	490252	177025	1.57	
C-101	HEATER	33075	11943	0.11	
C-102	HEATER	9886.08	3569.76	0.03	
C-103	HEATER	1190.77	429.97	0.00	
C-104	HEATER	2542.25	917.979	0.01	
F-100	FLASH2	18205.1	6573.65	0.06	
D-100	RADFRAC	97557.1	35226.8	0.31	
D-101	RADFRAC	90148.1	32551.5	0.29	
R-100	RSTOIC	195672	70655	0.63	
COMP-101	COMPRESSOR	108230	39080.8	0.35	
COMP-102	COMPRESSOR	1.50E+06	543052	4.81	
Heating Utility					
F-102	FLASH2	33925.9	262.52	1.28	33.62
H-100	HEATER	3757.56	25.84	0.11	3.72
H-101	HEATER	11871.1	81.63	0.34	11.77
F-101	FLASH2	767195	5683.02	25.44	760.34
D-100	RADFRAC	106537	789.18	3.53	105.59
D-101	RADFRAC	88317.6	654.22	2.93	87.53
Electricity					
P-100	PUMP	74.90	0.31	0.02	0.11
P-101	PUMP	65.84	0.28	0.02	0.10
P-102	PUMP	26.57	0.11	0.01	0.04
P-106	PUMP	72.98	0.31	0.02	0.11
COMP-101	MCOMPR	84039.4	351.86	27.27	122.06
COMP-102	MCOMPR	1.39E+06	5810	450.28	2015.51

Table S1. COSMO-RS predicted liquid-liquid equilibria of all IL candidates {methanol + formic acid + water + IL} at the initial mass ratio of 1:1:1:1

Combination No	Cation	Anion	Distribution Coefficient (gsolute/g solute)	Selectivity (gsolute/g carrier)	Solvent Loss (g_{IL})	Melting Point (K)	Viscosity (cP)
1	1-heptyl-3-methyl-imidazolium	SO_4	317641	573.67	0.629	107.0	7.36E+11
2	1-heptyl-3-methyl-imidazolium	Cl	10606	19.16	0.632	N/A	407.9
3	1-heptyl-3-methyl-imidazolium	F	257522	465.09	0.629	N/A	390.1
4	1-heptyl-3-methyl-imidazolium	2-chlorophenol	979	1.77	0.813	218.2	314.6
5	1-heptyl-3-methyl-imidazolium	3-chlorophenol	1012	1.83	0.805	218.6	244.8
6	1-heptyl-3-methyl-imidazolium	4-chlorophenol	1203	2.17	0.768	238.3	258.1
7	1-heptyl-3-methyl-imidazolium	Benzoicacid	1926	3.48	0.703	233.2	1018.3
8	1-heptyl-3-methyl-imidazolium	BF_4	640	1.16	0.874	246.1	338.7
9	1-heptyl-3-methyl-imidazolium	Bis((trifluoromethyl)sulfonyl)imide	447	0.81	2.375	255.1	629.1
10	1-heptyl-3-methyl-imidazolium	Butylsulfate	550	0.99	1.211	221.7	568.2
11	1-heptyl-3-methyl-imidazolium	Ethylsulfate	650	1.17	0.973	215.1	435.3
12	1-heptyl-3-methyl-imidazolium	NO_2	2442	4.41	0.650	177.0	129.4
13	1-heptyl-3-methyl-imidazolium	Octylsulfate	471	0.85	1.764	230.5	674.4
14	1-heptyl-3-methyl-imidazolium	PF_6	544	0.98	1.191	301.4	489.3
15	1-heptyl-3-methyl-imidazolium	Toluene-4-sulfonate	648	1.17	1.102	238.3	589.4
16	1-octyl-3-methyl-imidazolium	SO_4	317626	573.64	0.716	105.1	9.08E+11
17	1-octyl-3-methyl-imidazolium	Cl	10591	19.13	0.719	N/A	435.9
18	1-octyl-3-methyl-imidazolium	F	257507	465.07	0.715	N/A	418.1
19	1-octyl-3-methyl-imidazolium	2-chlorophenol	964	1.74	0.899	220.2	381.9
20	1-octyl-3-methyl-imidazolium	3-chlorophenol	997	1.80	0.891	220.6	297.3
21	1-octyl-3-methyl-imidazolium	4-chlorophenol	1188	2.14	0.854	239.5	313.4
22	1-octyl-3-methyl-imidazolium	Benzoicacid	1910	3.45	0.789	234.6	1235.7
23	1-octyl-3-methyl-imidazolium	BF_4	625	1.13	0.960	246.0	418.4
24	1-octyl-3-methyl-imidazolium	Bis((trifluoromethyl)sulfonyl)imide	432	0.78	2.461	255.5	657.1
25	1-octyl-3-methyl-imidazolium	Butylsulfate	534	0.97	1.297	223.5	596.2
26	1-octyl-3-methyl-imidazolium	Ethylsulfate	635	1.15	1.059	217.1	543.2
27	1-octyl-3-methyl-imidazolium	NO_2	2427	4.38	0.737	180.2	161.7
28	1-octyl-3-methyl-imidazolium	Octylsulfate	455	0.82	1.850	232.3	702.4
29	1-octyl-3-methyl-imidazolium	PF_6	529	0.96	1.277	297.5	517.3
30	1-octyl-3-methyl-imidazolium	Toluene-4-sulfonate	633	1.14	1.188	239.8	617.4
31	Pyrrolidine	SO_4	322417	582.30	0.015	124.6	3.87E+11
32	Pyrrolidine	Cl	15383	536.08	0.018	N/A	206.6
33	Pyrrolidine	F	262298	978.47	0.014	N/A	188.8
34	Pyrrolidine	2-chlorophenol	5756	401.83	0.198	184.3	200.2
35	Pyrrolidine	3-chlorophenol	5788	1.81	0.190	185.0	155.9
36	Pyrrolidine	4-chlorophenol	5979	2.29	0.153	212.4	164.1
37	Pyrrolidine	Benzoicacid	6702	3.53	0.088	203.9	651.6
38	Pyrrolidine	BF_4	5417	1.41	0.259	229.7	174.7
39	Pyrrolidine	Bis((trifluoromethyl)sulfonyl)imide	5223	0.84	1.760	240.5	427.7
40	Pyrrolidine	Butylsulfate	5326	1.07	0.596	194.1	495.9
41	Pyrrolidine	Ethylsulfate	5427	1.20	0.358	185.6	266.2
42	Pyrrolidine	NO_2	7218	113.50	0.036	133.3	118.12
43	Pyrrolidine	Octylsulfate	5247	0.84	1.149	205.4	473.1
44	Pyrrolidine	PF_6	5321	4.94	0.576	346.0	288.0
45	Pyrrolidine	Toluene-4-sulfonate	5425	0.65	0.487	210.9	388.1
46	H_3O	SO_4	601898	1087.05	0.000	N/A	157.7
47	H_3O	Cl	294863	532.53	0.004	N/A	107.6
48	H_3O	F	541779	978.47	0.000	N/A	89.8
49	H_3O	2-chlorophenol	285236	515.15	0.184	N/A	234.8
50	H_3O	3-chlorophenol	285269	515.20	0.176	N/A	235.2
51	H_3O	4-chlorophenol	285460	515.55	0.139	N/A	234.4
52	H_3O	Benzoicacid	286183	516.85	0.074	N/A	237.8
53	H_3O	BF_4	284897	514.53	0.245	N/A	151.8
54	H_3O	Bis((trifluoromethyl)sulfonyl)imide	284704	514.18	1.746	N/A	328.7
55	H_3O	Butylsulfate	284806	514.37	0.582	N/A	267.9
56	H_3O	Ethylsulfate	284907	514.55	0.344	N/A	214.9
57	H_3O	NO_2	286699	517.79	0.021	N/A	119.6
58	H_3O	Octylsulfate	284728	514.23	1.135	N/A	374.1
59	H_3O	PF_6	284801	514.36	0.562	N/A	189.0
60	H_3O	Toluene-4-sulfonate	284905	514.55	0.473	N/A	289.1
61	NH_4	SO_4	603860	1090.59	0.000	N/A	163.4
62	NH_4	Cl	296826	536.08	0.003	N/A	113.3
63	NH_4	F	543741	982.01	0.000	N/A	95.5
64	NH_4	2-chlorophenol	287199	518.69	0.184	N/A	240.5
65	NH_4	3-chlorophenol	287231	518.75	0.176	N/A	240.9
66	NH_4	4-chlorophenol	287422	519.09	0.139	N/A	240.2
67	NH_4	Benzoicacid	288145	520.40	0.074	N/A	243.5
68	NH_4	BF_4	286860	518.08	0.245	N/A	157.6
69	NH_4	Bis((trifluoromethyl)sulfonyl)imide	286666	517.73	1.746	N/A	334.5
70	NH_4	Butylsulfate	286769	517.91	0.582	N/A	273.6
71	NH_4	Ethylsulfate	286870	518.10	0.344	N/A	220.6
72	NH_4	NO_2	288661	521.33	0.021	N/A	125.4
73	NH_4	Octylsulfate	286690	517.77	1.135	N/A	379.8
74	NH_4	PF_6	286763	517.90	0.562	N/A	194.7
75	NH_4	Toluene-4-sulfonate	286867	518.09	0.473	N/A	294.8
76	Na	SO_4	539154	973.73	0.000	N/A	151.1
77	Na	Cl	232120	419.22	0.004	N/A	100.9

78	Na	F	479036	865.15	0.000	N/A	83.1
79	Na	2-chlorophenol	222493	401.83	0.184	N/A	228.1
80	Na	3-chlorophenol	222525	401.89	0.176	N/A	228.5
81	Na	4-chlorophenol	222716	402.23	0.139	N/A	227.8
82	Na	Benzoicacid	223439	403.54	0.074	N/A	231.1
83	Na	BF_4	222154	401.22	0.245	N/A	145.2
84	Na	Bis((trifluoromethyl)sulfonyl)imide	221960	400.87	1.746	N/A	322.1
85	Na	Butylsulfate	222063	401.05	0.582	N/A	261.3
86	Na	Ethylsulfate	222164	401.24	0.344	N/A	208.3
87	Na	NO_2	223955	404.47	0.021	N/A	113.0
88	Na	Octylsulfate	221984	400.91	1.135	N/A	367.4
89	Na	PF_6	222058	401.04	0.562	N/A	182.4
90	Na	Toluene-4-sulfonate	222162	401.23	0.473	N/A	282.4
91	1-butyl-2,3-dimethyl-imidazolium	SO_4	317632	573.65	0.549	121.6	3.54E+11
92	1-butyl-2,3-dimethyl-imidazolium	Cl	10597	19.14	0.552	N/A	353.0
93	1-butyl-2,3-dimethyl-imidazolium	F	257513	465.08	0.549	N/A	335.2
94	1-butyl-2,3-dimethyl-imidazolium	2-chlorophenol	970	1.75	0.733	223.9	156.5
95	1-butyl-2,3-dimethyl-imidazolium	3-chlorophenol	1003	1.81	0.725	224.4	121.8
96	1-butyl-2,3-dimethyl-imidazolium	4-chlorophenol	1194	2.16	0.688	248.6	128.4
97	1-butyl-2,3-dimethyl-imidazolium	Benzoicacid	1916	3.46	0.623	242.5	507.2
98	1-butyl-2,3-dimethyl-imidazolium	BF_4	631	1.14	0.794	265.9	162.1
99	1-butyl-2,3-dimethyl-imidazolium	Bis((trifluoromethyl)sulfonyl)imide	438	0.79	2.295	267.5	574.2
100	1-butyl-2,3-dimethyl-imidazolium	Butylsulfate	540	0.98	1.131	226.5	513.3
101	1-butyl-2,3-dimethyl-imidazolium	Ethylsulfate	641	1.16	0.893	220.4	215.0
102	1-butyl-2,3-dimethyl-imidazolium	NO_2	2433	4.39	0.570	178.8	60.4
103	1-butyl-2,3-dimethyl-imidazolium	Octylsulfate	461	0.83	1.684	234.3	619.5
104	1-butyl-2,3-dimethyl-imidazolium	PF_6	535	0.97	1.111	341.5	434.4
105	1-butyl-2,3-dimethyl-imidazolium	Toluene-4-sulfonate	639	1.15	1.022	246.8	534.5
106	1-butyl-3-methyl-imidazolium	SO_4	317708	573.79	0.392	113.6	3.63E+11
107	1-butyl-3-methyl-imidazolium	Cl	10674	19.28	0.395	N/A	324.3
108	1-butyl-3-methyl-imidazolium	F	257589	465.21	0.392	N/A	306.5
109	1-butyl-3-methyl-imidazolium	2-chlorophenol	1047	1.89	0.576	210.8	164.1
110	1-butyl-3-methyl-imidazolium	3-chlorophenol	1079	1.95	0.567	211.3	127.8
111	1-butyl-3-methyl-imidazolium	4-chlorophenol	1270	2.29	0.531	234.0	134.7
112	1-butyl-3-methyl-imidazolium	Benzoicacid	1993	3.60	0.465	228.0	532.2
113	1-butyl-3-methyl-imidazolium	BF_4	708	1.28	0.637	247.1	166.0
114	1-butyl-3-methyl-imidazolium	Bis((trifluoromethyl)sulfonyl)imide	514	0.93	2.138	253.7	545.5
115	1-butyl-3-methyl-imidazolium	Butylsulfate	617	1.11	0.973	214.9	390.8
116	1-butyl-3-methyl-imidazolium	Ethylsulfate	718	1.30	0.735	208.1	224.4
117	1-butyl-3-methyl-imidazolium	NO_2	2509	4.53	0.413	165.5	60.9
118	1-butyl-3-methyl-imidazolium	Octylsulfate	538	0.97	1.527	223.9	590.8
119	1-butyl-3-methyl-imidazolium	PF_6	612	1.10	0.953	318.4	405.7
120	1-butyl-3-methyl-imidazolium	Toluene-4-sulfonate	716	1.29	0.865	233.1	959.7
121	1-ethyl-2,3-dimethyl-imidazolium	SO_4	317671	573.72	0.393	129.1	2.21E+11
122	1-ethyl-2,3-dimethyl-imidazolium	Cl	10637	19.21	0.396	N/A	296.3
123	1-ethyl-2,3-dimethyl-imidazolium	F	257553	465.15	0.393	N/A	278.5
124	1-ethyl-2,3-dimethyl-imidazolium	2-chlorophenol	1010	1.82	0.577	218.3	102.2
125	1-ethyl-2,3-dimethyl-imidazolium	3-chlorophenol	1042	1.88	0.568	218.8	79.6
126	1-ethyl-2,3-dimethyl-imidazolium	4-chlorophenol	1233	2.23	0.532	245.8	83.9
127	1-ethyl-2,3-dimethyl-imidazolium	Benzoicacid	1956	3.53	0.467	239.0	331.7
128	1-ethyl-2,3-dimethyl-imidazolium	BF_4	671	1.21	0.638	270.1	100.7
129	1-ethyl-2,3-dimethyl-imidazolium	Bis((trifluoromethyl)sulfonyl)imide	477	0.86	2.139	267.3	517.5
130	1-ethyl-2,3-dimethyl-imidazolium	Butylsulfate	580	1.05	0.974	221.1	245.1
131	1-ethyl-2,3-dimethyl-imidazolium	Ethylsulfate	681	1.23	0.736	215.0	139.1
132	1-ethyl-2,3-dimethyl-imidazolium	NO_2	2472	4.47	0.414	169.7	36.3
133	1-ethyl-2,3-dimethyl-imidazolium	Octylsulfate	501	0.91	1.528	229.0	562.8
134	1-ethyl-2,3-dimethyl-imidazolium	PF_6	575	1.04	0.955	365.9	377.8
135	1-ethyl-2,3-dimethyl-imidazolium	Toluene-4-sulfonate	679	1.23	0.866	242.9	604.4
136	1-ethyl-3-methyl-imidazolium	SO_4	317781	573.92	0.260	119.1	2.15E+11
137	1-ethyl-3-methyl-imidazolium	Cl	10746	19.41	0.263	N/A	269.0
138	1-ethyl-3-methyl-imidazolium	F	257662	465.35	0.260	N/A	251.2
139	1-ethyl-3-methyl-imidazolium	2-chlorophenol	1119	2.02	0.444	204.3	102.4
140	1-ethyl-3-methyl-imidazolium	3-chlorophenol	1152	2.08	0.435	204.8	109.72
141	1-ethyl-3-methyl-imidazolium	4-chlorophenol	1343	2.42	0.399	230.1	103.97
142	1-ethyl-3-methyl-imidazolium	Benzoicacid	2066	3.73	0.334	223.4	332.4
143	1-ethyl-3-methyl-imidazolium	BF_4	780	1.41	0.505	299.21	97.8
144	1-ethyl-3-methyl-imidazolium	Bis((trifluoromethyl)sulfonyl)imide	587	1.06	2.006	252.6	490.1
145	1-ethyl-3-methyl-imidazolium	Butylsulfate	689	1.25	0.841	208.8	247.5
146	1-ethyl-3-methyl-imidazolium	Ethylsulfate	790	1.43	0.603	202.0	138.5
147	1-ethyl-3-methyl-imidazolium	NO_2	2582	4.66	0.281	155.6	34.6
148	1-ethyl-3-methyl-imidazolium	Octylsulfate	611	1.10	1.395	218.0	535.5
149	1-ethyl-3-methyl-imidazolium	PF_6	684	1.24	0.822	339.2	350.4
150	1-ethyl-3-methyl-imidazolium	Toluene-4-sulfonate	788	1.42	0.733	228.3	613.0
151	1-hexyl-3-methyl-imidazolium	SO_4	317659	573.70	0.547	109.1	5.92E+11
152	1-hexyl-3-methyl-imidazolium	Cl	10624	19.19	0.550	N/A	380.1
153	1-hexyl-3-methyl-imidazolium	F	257540	465.13	0.546	N/A	362.3
154	1-hexyl-3-methyl-imidazolium	2-chlorophenol	997	1.80	0.730	216.2	257.3
155	1-hexyl-3-methyl-imidazolium	3-chlorophenol	1030	1.86	0.722	216.6	200.3
156	1-hexyl-3-methyl-imidazolium	4-chlorophenol	1221	2.20	0.686	237.2	211.1
157	1-hexyl-3-methyl-imidazolium	Benzoicacid	1944	3.51	0.620	231.9	833.2
158	1-hexyl-3-methyl-imidazolium	BF_4	658	1.19	0.792	246.6	271.9
159	1-hexyl-3-methyl-imidazolium	Bis((trifluoromethyl)sulfonyl)imide	465	0.84	2.292	254.8	601.3

160	1-hexyl-3-methyl-imidazolium	Butylsulfate	567	1.02	1.128	219.8	540.4
161	1-hexyl-3-methyl-imidazolium	Ethylsulfate	668	1.21	0.890	213.2	354.8
162	1-hexyl-3-methyl-imidazolium	NO_2	2460	4.44	0.568	173.8	102.7
163	1-hexyl-3-methyl-imidazolium	Octylsulfate	489	0.88	1.682	228.7	646.6
164	1-hexyl-3-methyl-imidazolium	PF_6	562	1.02	1.108	306.3	461.5
165	1-hexyl-3-methyl-imidazolium	Toluene-4-sulfonate	666	1.20	1.019	237.0	561.6
166	1-pentyl-3-methyl-imidazolium	SO_4	317682	573.74	0.466	111.3	4.68E+11
167	1-pentyl-3-methyl-imidazolium	Cl	10647	19.23	0.469	N/A	352.3
168	1-pentyl-3-methyl-imidazolium	F	257563	465.17	0.466	N/A	334.5
169	1-pentyl-3-methyl-imidazolium	2-chlorophenol	1020	1.84	0.650	214.0	207.3
170	1-pentyl-3-methyl-imidazolium	3-chlorophenol	1053	1.90	0.642	214.5	161.4
171	1-pentyl-3-methyl-imidazolium	4-chlorophenol	1243	2.25	0.605	236.1	170.1
172	1-pentyl-3-methyl-imidazolium	Benzoicacid	1966	3.55	0.540	230.5	671.9
173	1-pentyl-3-methyl-imidazolium	BF_4	681	1.23	0.711	247.3	214.6
174	1-pentyl-3-methyl-imidazolium	Bis((trifluoromethyl)sulfonyl)imide	487	0.88	2.212	254.6	573.4
175	1-pentyl-3-methyl-imidazolium	Butylsulfate	590	1.07	1.048	217.8	512.6
176	1-pentyl-3-methyl-imidazolium	Ethylsulfate	691	1.25	0.809	211.1	284.8
177	1-pentyl-3-methyl-imidazolium	NO_2	2483	4.48	0.487	170.2	79.9
178	1-pentyl-3-methyl-imidazolium	Octylsulfate	511	0.92	1.601	226.7	618.8
179	1-pentyl-3-methyl-imidazolium	PF_6	585	1.06	1.028	312.4	433.7
180	1-pentyl-3-methyl-imidazolium	Toluene-4-sulfonate	689	1.24	0.939	235.5	1200.3
181	4-methyl-n-butylpyridinium	SO_4	317655	573.70	0.496	119.9	3.49E+11
182	4-methyl-n-butylpyridinium	Cl	10621	19.18	0.500	N/A	346.7
183	4-methyl-n-butylpyridinium	F	257537	465.12	0.496	N/A	328.9
184	4-methyl-n-butylpyridinium	2-chlorophenol	994	1.80	0.680	218.1	155.3
185	4-methyl-n-butylpyridinium	3-chlorophenol	1026	1.85	0.672	218.6	120.9
186	4-methyl-n-butylpyridinium	4-chlorophenol	1217	2.20	0.635	242.1	127.4
187	4-methyl-n-butylpyridinium	Benzoicacid	1940	3.50	0.570	236.2	503.2
188	4-methyl-n-butylpyridinium	BF_4	655	1.18	0.741	257.0	160.0
189	4-methyl-n-butylpyridinium	Bis((trifluoromethyl)sulfonyl)imide	461	0.83	2.242	261.1	567.9
190	4-methyl-n-butylpyridinium	Butylsulfate	564	1.02	1.078	221.1	507.0
191	4-methyl-n-butylpyridinium	Ethylsulfate	665	1.20	0.840	214.7	213.1
192	4-methyl-n-butylpyridinium	NO_2	2456	4.44	0.517	172.1	59.4
193	4-methyl-n-butylpyridinium	Octylsulfate	485	0.88	1.631	229.6	613.2
194	4-methyl-n-butylpyridinium	PF_6	559	1.01	1.058	330.8	428.1
195	4-methyl-n-butylpyridinium	Toluene-4-sulfonate	663	1.20	0.969	240.8	900.5
196	Aniline	SO_4	378043	682.76	0.002	139.6	1.59E+12
197	Aniline	Cl	71009	128.24	0.005	N/A	234.0
198	Aniline	F	317924	574.18	0.002	N/A	216.2
199	Aniline	2-chlorophenol	61382	110.86	0.186	202.4	787.4
200	Aniline	3-chlorophenol	61414	110.92	0.177	202.3	613.3
201	Aniline	4-chlorophenol	61605	111.26	0.141	232.2	645.8
202	Aniline	Benzoicacid	62328	112.57	0.075	228.6	2560.2
203	Aniline	BF_4	61042	110.24	0.247	270.8	718.8
204	Aniline	Bis((trifluoromethyl)sulfonyl)imide	60849	109.89	1.748	266.3	455.2
205	Aniline	Butylsulfate	60952	110.08	0.583	209.8	1927.5
206	Aniline	Ethylsulfate	61053	110.26	0.345	203.7	1056.2
207	Aniline	NO_2	62844	113.50	0.023	152.8	246.5
208	Aniline	Octylsulfate	60873	109.94	1.137	218.2	500.5
209	Aniline	PF_6	60946	110.07	0.563	408.8	315.4
210	Aniline	Toluene-4-sulfonate	61050	110.26	0.475	233.3	4807.4
211	n-butyl-isoquinolinium	SO_4	317636	573.66	0.656	132.1	4.33E+11
212	n-butyl-isoquinolinium	Cl	10602	19.15	0.660	N/A	392.0
213	n-butyl-isoquinolinium	F	257518	465.08	0.656	N/A	374.2
214	n-butyl-isoquinolinium	2-chlorophenol	975	1.76	0.840	221.4	186.6
215	n-butyl-isoquinolinium	3-chlorophenol	1007	1.82	0.832	221.8	145.3
216	n-butyl-isoquinolinium	4-chlorophenol	1198	2.16	0.795	245.6	153.1
217	n-butyl-isoquinolinium	Benzoicacid	1921	3.47	0.730	240.2	604.3
218	n-butyl-isoquinolinium	BF_4	636	1.15	0.901	259.7	198.9
219	n-butyl-isoquinolinium	Bis((trifluoromethyl)sulfonyl)imide	442	0.80	2.402	266.3	613.2
220	n-butyl-isoquinolinium	Butylsulfate	545	0.98	1.238	224.1	552.4
221	n-butyl-isoquinolinium	Ethylsulfate	646	1.17	1.000	217.4	257.7
222	n-butyl-isoquinolinium	NO_2	2437	4.40	0.678	173.3	75.5
223	n-butyl-isoquinolinium	Octylsulfate	466	0.84	1.791	232.8	658.5
224	n-butyl-isoquinolinium	PF_6	540	0.98	1.218	336.0	473.5
225	n-butyl-isoquinolinium	Toluene-4-sulfonate	644	1.16	1.129	245.0	573.5
226	Pyridine	SO_4	319831	577.63	0.033	124.8	2.34E+11
227	Pyridine	Cl	12797	23.11	0.036	N/A	207.0
228	Pyridine	F	259712	469.05	0.032	N/A	189.2
229	Pyridine	2-chlorophenol	3170	5.72	0.216	184.8	120.9
230	Pyridine	3-chlorophenol	3202	5.78	0.208	185.3	94.2
231	Pyridine	4-chlorophenol	3393	6.13	0.171	212.5	99.1
232	Pyridine	Benzoicacid	4116	7.43	0.106	205.8	393.5
233	Pyridine	BF_4	2831	5.11	0.277	240.8	105.6
234	Pyridine	Bis((trifluoromethyl)sulfonyl)imide	2637	4.76	1.778	243.1	428.1
235	Pyridine	Butylsulfate	2740	4.95	0.614	192.3	299.4
236	Pyridine	Ethylsulfate	2841	5.13	0.376	184.5	160.8
237	Pyridine	NO_2	4632	8.37	0.054	130.5	110.25
238	Pyridine	Octylsulfate	2661	4.81	1.168	203.2	473.5
239	Pyridine	PF_6	2735	4.94	0.594	366.2	288.4
240	Pyridine	Toluene-4-sulfonate	2839	5.13	0.505	211.8	751.8

Table S2. COSMO-RS predicted liquid-liquid equilibria screened with Distribution coefficient (> 1)

Combination No	Cation	Anion	Distribution Coefficient (gsolute/g solute)	Selectivity (gsolute/g carrier)	Solvent Loss (g_{lt})	Melting Point (K)	Viscosity (cP)
1	1-heptyl-3-methyl-imidazolium	SO_4	317641	573.67	0.629	107.0	7.36E+11
2	1-heptyl-3-methyl-imidazolium	Cl	10606	19.16	0.632	N/A	407.9
3	1-heptyl-3-methyl-imidazolium	F	257522	465.09	0.629	N/A	390.1
4	1-heptyl-3-methyl-imidazolium	2-chlorophenol	979	1.77	0.813	218.2	314.6
5	1-heptyl-3-methyl-imidazolium	3-chlorophenol	1012	1.83	0.805	218.6	244.8
6	1-heptyl-3-methyl-imidazolium	4-chlorophenol	1203	2.17	0.768	238.3	258.1
7	1-heptyl-3-methyl-imidazolium	Benzoicacid	1926	3.48	0.703	233.2	1018.3
8	1-heptyl-3-methyl-imidazolium	BF_4	640	1.16	0.874	246.1	338.7
9	1-heptyl-3-methyl-imidazolium	Bis((trifluoromethyl)sulfonyl)imide	447	0.81	2.375	255.1	629.1
10	1-heptyl-3-methyl-imidazolium	Butylsulfate	550	0.99	1.211	221.7	568.2
11	1-heptyl-3-methyl-imidazolium	Ethylsulfate	650	1.17	0.973	215.1	435.3
12	1-heptyl-3-methyl-imidazolium	NO_2	2442	4.41	0.650	177.0	129.4
13	1-heptyl-3-methyl-imidazolium	Octylsulfate	471	0.85	1.764	230.5	674.4
14	1-heptyl-3-methyl-imidazolium	PF_6	544	0.98	1.191	301.4	489.3
15	1-heptyl-3-methyl-imidazolium	Toluene-4-sulfonate	648	1.17	1.102	238.3	589.4
16	1-octyl-3-methyl-imidazolium	SO_4	317626	573.64	0.716	105.1	9.08E+11
17	1-octyl-3-methyl-imidazolium	Cl	10591	19.13	0.719	N/A	435.9
18	1-octyl-3-methyl-imidazolium	F	257507	465.07	0.715	N/A	418.1
19	1-octyl-3-methyl-imidazolium	2-chlorophenol	964	1.74	0.899	220.2	381.9
20	1-octyl-3-methyl-imidazolium	3-chlorophenol	997	1.80	0.891	220.6	297.3
21	1-octyl-3-methyl-imidazolium	4-chlorophenol	1188	2.14	0.854	239.5	313.4
22	1-octyl-3-methyl-imidazolium	Benzoicacid	1910	3.45	0.789	234.6	1235.7
23	1-octyl-3-methyl-imidazolium	BF_4	625	1.13	0.960	246.0	418.4
24	1-octyl-3-methyl-imidazolium	Bis((trifluoromethyl)sulfonyl)imide	432	0.78	2.461	255.5	657.1
25	1-octyl-3-methyl-imidazolium	Butylsulfate	534	0.97	1.297	223.5	596.2
26	1-octyl-3-methyl-imidazolium	Ethylsulfate	635	1.15	1.059	217.1	543.2
27	1-octyl-3-methyl-imidazolium	NO_2	2427	4.38	0.737	180.2	161.7
28	1-octyl-3-methyl-imidazolium	Octylsulfate	455	0.82	1.850	232.3	702.4
29	1-octyl-3-methyl-imidazolium	PF_6	529	0.96	1.277	297.5	517.3
30	1-octyl-3-methyl-imidazolium	Toluene-4-sulfonate	633	1.14	1.188	239.8	617.4
31	Pyrrolidine	SO_4	322417	582.30	0.015	124.6	3.87E+11
32	Pyrrolidine	Cl	15383	536.08	0.018	N/A	206.6
33	Pyrrolidine	F	262298	978.47	0.014	N/A	188.8
34	Pyrrolidine	2-chlorophenol	5756	401.83	0.198	184.3	200.2
35	Pyrrolidine	3-chlorophenol	5788	1.81	0.190	185.0	155.9
36	Pyrrolidine	4-chlorophenol	5979	2.29	0.153	212.4	164.1
37	Pyrrolidine	Benzoicacid	6702	3.53	0.088	203.9	651.6
38	Pyrrolidine	BF_4	5417	1.41	0.259	229.7	174.7
39	Pyrrolidine	Bis((trifluoromethyl)sulfonyl)imide	5223	0.84	1.760	240.5	427.7
40	Pyrrolidine	Butylsulfate	5326	1.07	0.596	194.1	495.9
41	Pyrrolidine	Ethylsulfate	5427	1.20	0.358	185.6	266.2
42	Pyrrolidine	NO_2	7218	113.50	0.036	133.3	118.12
43	Pyrrolidine	Octylsulfate	5247	0.84	1.149	205.4	473.1
44	Pyrrolidine	PF_6	5321	4.94	0.576	346.0	288.0
45	Pyrrolidine	Toluene-4-sulfonate	5425	0.65	0.487	210.9	388.1
46	H_3O	SO_4	601898	1087.05	0.000	N/A	157.7
47	H_3O	Cl	294863	532.53	0.004	N/A	107.6
48	H_3O	F	541779	978.47	0.000	N/A	89.8
49	H_3O	2-chlorophenol	285236	515.15	0.184	N/A	234.8
50	H_3O	3-chlorophenol	285269	515.20	0.176	N/A	235.2
51	H_3O	4-chlorophenol	285460	515.55	0.139	N/A	234.4
52	H_3O	Benzoicacid	286183	516.85	0.074	N/A	237.8
53	H_3O	BF_4	284897	514.53	0.245	N/A	151.8
54	H_3O	Bis((trifluoromethyl)sulfonyl)imide	284704	514.18	1.746	N/A	328.7
55	H_3O	Butylsulfate	284806	514.37	0.582	N/A	267.9
56	H_3O	Ethylsulfate	284907	514.55	0.344	N/A	214.9
57	H_3O	NO_2	286699	517.79	0.021	N/A	119.6
58	H_3O	Octylsulfate	284728	514.23	1.135	N/A	374.1
59	H_3O	PF_6	284801	514.36	0.562	N/A	189.0
60	H_3O	Toluene-4-sulfonate	284905	514.55	0.473	N/A	289.1
61	NH_4	SO_4	603860	1090.59	0.000	N/A	163.4
62	NH_4	Cl	296826	536.08	0.003	N/A	113.3
63	NH_4	F	543741	982.01	0.000	N/A	95.5
64	NH_4	2-chlorophenol	287199	518.69	0.184	N/A	240.5
65	NH_4	3-chlorophenol	287231	518.75	0.176	N/A	240.9
66	NH_4	4-chlorophenol	287422	519.09	0.139	N/A	240.2
67	NH_4	Benzoicacid	288145	520.40	0.074	N/A	243.5
68	NH_4	BF_4	286860	518.08	0.245	N/A	157.6
69	NH_4	Bis((trifluoromethyl)sulfonyl)imide	286666	517.73	1.746	N/A	334.5
70	NH_4	Butylsulfate	286769	517.91	0.582	N/A	273.6
71	NH_4	Ethylsulfate	286870	518.10	0.344	N/A	220.6
72	NH_4	NO_2	288661	521.33	0.021	N/A	125.4
73	NH_4	Octylsulfate	286690	517.77	1.135	N/A	379.8
74	NH_4	PF_6	286763	517.90	0.562	N/A	194.7
75	NH_4	Toluene-4-sulfonate	286867	518.09	0.473	N/A	294.8
76	Na	SO_4	539154	973.73	0.000	N/A	151.1
77	Na	Cl	232120	419.22	0.004	N/A	100.9
78	Na	F	479036	865.15	0.000	N/A	83.1
79	Na	2-chlorophenol	222493	401.83	0.184	N/A	228.1
80	Na	3-chlorophenol	222525	401.89	0.176	N/A	228.5
81	Na	4-chlorophenol	222716	402.23	0.139	N/A	227.8
82	Na	Benzoicacid	223439	403.54	0.074	N/A	231.1
83	Na	BF_4	222154	401.22	0.245	N/A	145.2
84	Na	Bis((trifluoromethyl)sulfonyl)imide	221960	400.87	1.746	N/A	322.1
85	Na	Butylsulfate	222063	401.05	0.582	N/A	261.3
86	Na	Ethylsulfate	222164	401.24	0.344	N/A	208.3
87	Na	NO_2	223955	404.47	0.021	N/A	113.0
88	Na	Octylsulfate	221984	400.91	1.135	N/A	367.4
89	Na	PF_6	222058	401.04	0.562	N/A	182.4
90	Na	Toluene-4-sulfonate	222162	401.23	0.473	N/A	282.4
91	1-butyl-2,3-dimethyl-imidazolium	SO_4	317632	573.65	0.549	121.6	3.54E+11

92	1-butyl-2,3-dimethyl-imidazolium	Cl	10597	19.14	0.552	N/A	353.0
93	1-butyl-2,3-dimethyl-imidazolium	F	257513	465.08	0.549	N/A	335.2
94	1-butyl-2,3-dimethyl-imidazolium	2-chlorophenol	970	1.75	0.733	223.9	156.5
95	1-butyl-2,3-dimethyl-imidazolium	3-chlorophenol	1003	1.81	0.725	224.4	121.8
96	1-butyl-2,3-dimethyl-imidazolium	4-chlorophenol	1194	2.16	0.688	248.6	128.4
97	1-butyl-2,3-dimethyl-imidazolium	Benzoicacid	1916	3.46	0.623	242.5	507.2
98	1-butyl-2,3-dimethyl-imidazolium	BF_4	631	1.14	0.794	265.9	162.1
99	1-butyl-2,3-dimethyl-imidazolium	Bis((trifluoromethyl)sulfonyl)imide	438	0.79	2.295	267.5	574.2
100	1-butyl-2,3-dimethyl-imidazolium	Butylsulfate	540	0.98	1.131	226.5	513.3
101	1-butyl-2,3-dimethyl-imidazolium	Ethylsulfate	641	1.16	0.893	220.4	215.0
102	1-butyl-2,3-dimethyl-imidazolium	NO_2	2433	4.39	0.570	178.8	60.4
103	1-butyl-2,3-dimethyl-imidazolium	Octylsulfate	461	0.83	1.684	234.3	619.5
104	1-butyl-2,3-dimethyl-imidazolium	PF_6	535	0.97	1.111	341.5	434.4
105	1-butyl-2,3-dimethyl-imidazolium	Toluene-4-sulfonate	639	1.15	1.022	246.8	534.5
106	1-butyl-3-methyl-imidazolium	SO_4	317708	573.79	0.392	113.6	3.63E+11
107	1-butyl-3-methyl-imidazolium	Cl	10674	19.28	0.395	N/A	324.3
108	1-butyl-3-methyl-imidazolium	F	257589	465.21	0.392	N/A	306.5
109	1-butyl-3-methyl-imidazolium	2-chlorophenol	1047	1.89	0.576	210.8	164.1
110	1-butyl-3-methyl-imidazolium	3-chlorophenol	1079	1.95	0.567	211.3	127.8
111	1-butyl-3-methyl-imidazolium	4-chlorophenol	1270	2.29	0.531	234.0	134.7
112	1-butyl-3-methyl-imidazolium	Benzoicacid	1993	3.60	0.465	228.0	532.2
113	1-butyl-3-methyl-imidazolium	BF_4	708	1.28	0.637	247.1	166.0
114	1-butyl-3-methyl-imidazolium	Bis((trifluoromethyl)sulfonyl)imide	514	0.93	2.138	253.7	545.5
115	1-butyl-3-methyl-imidazolium	Butylsulfate	617	1.11	0.973	214.9	390.8
116	1-butyl-3-methyl-imidazolium	Ethylsulfate	718	1.30	0.735	208.1	224.4
117	1-butyl-3-methyl-imidazolium	NO_2	2509	4.53	0.413	165.5	60.9
118	1-butyl-3-methyl-imidazolium	Octylsulfate	538	0.97	1.527	223.9	590.8
119	1-butyl-3-methyl-imidazolium	PF_6	612	1.10	0.953	318.4	405.7
120	1-butyl-3-methyl-imidazolium	Toluene-4-sulfonate	716	1.29	0.865	233.1	959.7
121	1-ethyl-2,3-dimethyl-imidazolium	SO_4	317671	573.72	0.393	129.1	2.21E+11
122	1-ethyl-2,3-dimethyl-imidazolium	Cl	10637	19.21	0.396	N/A	296.3
123	1-ethyl-2,3-dimethyl-imidazolium	F	257553	465.15	0.393	N/A	278.5
124	1-ethyl-2,3-dimethyl-imidazolium	2-chlorophenol	1010	1.82	0.577	218.3	102.2
125	1-ethyl-2,3-dimethyl-imidazolium	3-chlorophenol	1042	1.88	0.568	218.8	79.6
126	1-ethyl-2,3-dimethyl-imidazolium	4-chlorophenol	1233	2.23	0.532	245.8	83.9
127	1-ethyl-2,3-dimethyl-imidazolium	Benzoicacid	1956	3.53	0.467	239.0	331.7
128	1-ethyl-2,3-dimethyl-imidazolium	BF_4	671	1.21	0.638	270.1	100.7
129	1-ethyl-2,3-dimethyl-imidazolium	Bis((trifluoromethyl)sulfonyl)imide	477	0.86	2.139	267.3	517.5
130	1-ethyl-2,3-dimethyl-imidazolium	Butylsulfate	580	1.05	0.974	221.1	245.1
131	1-ethyl-2,3-dimethyl-imidazolium	Ethylsulfate	681	1.23	0.736	215.0	139.1
132	1-ethyl-2,3-dimethyl-imidazolium	NO_2	2472	4.47	0.414	169.7	36.3
133	1-ethyl-2,3-dimethyl-imidazolium	Octylsulfate	501	0.91	1.528	229.0	562.8
134	1-ethyl-2,3-dimethyl-imidazolium	PF_6	575	1.04	0.955	365.9	377.8
135	1-ethyl-2,3-dimethyl-imidazolium	Toluene-4-sulfonate	679	1.23	0.866	242.9	604.4
136	1-ethyl-3-methyl-imidazolium	SO_4	317781	573.92	0.260	119.1	2.15E+11
137	1-ethyl-3-methyl-imidazolium	Cl	10746	19.41	0.263	N/A	269.0
138	1-ethyl-3-methyl-imidazolium	F	257662	465.35	0.260	N/A	251.2
139	1-ethyl-3-methyl-imidazolium	2-chlorophenol	1119	2.02	0.444	204.3	102.4
140	1-ethyl-3-methyl-imidazolium	3-chlorophenol	1152	2.08	0.435	204.8	109.72
141	1-ethyl-3-methyl-imidazolium	4-chlorophenol	1343	2.42	0.399	230.1	103.97
142	1-ethyl-3-methyl-imidazolium	Benzoicacid	2066	3.73	0.334	223.4	332.4
143	1-ethyl-3-methyl-imidazolium	BF_4	780	1.41	0.505	299.21	97.8
144	1-ethyl-3-methyl-imidazolium	Bis((trifluoromethyl)sulfonyl)imide	587	1.06	2.006	252.6	490.1
145	1-ethyl-3-methyl-imidazolium	Butylsulfate	689	1.25	0.841	208.8	247.5
146	1-ethyl-3-methyl-imidazolium	Ethylsulfate	790	1.43	0.603	202.0	138.5
147	1-ethyl-3-methyl-imidazolium	NO_2	2582	4.66	0.281	155.6	34.6
148	1-ethyl-3-methyl-imidazolium	Octylsulfate	611	1.10	1.395	218.0	535.5
149	1-ethyl-3-methyl-imidazolium	PF_6	684	1.24	0.822	339.2	350.4
150	1-ethyl-3-methyl-imidazolium	Toluene-4-sulfonate	788	1.42	0.733	228.3	613.0
151	1-hexyl-3-methyl-imidazolium	SO_4	317659	573.70	0.547	109.1	5.92E+11
152	1-hexyl-3-methyl-imidazolium	Cl	10624	19.19	0.550	N/A	380.1
153	1-hexyl-3-methyl-imidazolium	F	257540	465.13	0.546	N/A	362.3
154	1-hexyl-3-methyl-imidazolium	2-chlorophenol	997	1.80	0.730	216.2	257.3
155	1-hexyl-3-methyl-imidazolium	3-chlorophenol	1030	1.86	0.722	216.6	200.3
156	1-hexyl-3-methyl-imidazolium	4-chlorophenol	1221	2.20	0.686	237.2	211.1
157	1-hexyl-3-methyl-imidazolium	Benzoicacid	1944	3.51	0.620	231.9	833.2
158	1-hexyl-3-methyl-imidazolium	BF_4	658	1.19	0.792	246.6	271.9
159	1-hexyl-3-methyl-imidazolium	Bis((trifluoromethyl)sulfonyl)imide	465	0.84	2.292	254.8	601.3
160	1-hexyl-3-methyl-imidazolium	Butylsulfate	567	1.02	1.128	219.8	540.4
161	1-hexyl-3-methyl-imidazolium	Ethylsulfate	668	1.21	0.890	213.2	354.8
162	1-hexyl-3-methyl-imidazolium	NO_2	2460	4.44	0.568	173.8	102.7
163	1-hexyl-3-methyl-imidazolium	Octylsulfate	489	0.88	1.682	228.7	646.6
164	1-hexyl-3-methyl-imidazolium	PF_6	562	1.02	1.108	306.3	461.5
165	1-hexyl-3-methyl-imidazolium	Toluene-4-sulfonate	666	1.20	1.019	237.0	561.6
166	1-pentyl-3-methyl-imidazolium	SO_4	317682	573.74	0.466	111.3	4.68E+11
167	1-pentyl-3-methyl-imidazolium	Cl	10647	19.23	0.469	N/A	352.3
168	1-pentyl-3-methyl-imidazolium	F	257563	465.17	0.466	N/A	334.5
169	1-pentyl-3-methyl-imidazolium	2-chlorophenol	1020	1.84	0.650	214.0	207.3
170	1-pentyl-3-methyl-imidazolium	3-chlorophenol	1053	1.90	0.642	214.5	161.4
171	1-pentyl-3-methyl-imidazolium	4-chlorophenol	1243	2.25	0.605	236.1	170.1
172	1-pentyl-3-methyl-imidazolium	Benzoicacid	1966	3.55	0.540	230.5	671.9
173	1-pentyl-3-methyl-imidazolium	BF_4	681	1.23	0.711	247.3	214.6
174	1-pentyl-3-methyl-imidazolium	Bis((trifluoromethyl)sulfonyl)imide	487	0.88	2.212	254.6	573.4
175	1-pentyl-3-methyl-imidazolium	Butylsulfate	590	1.07	1.048	217.8	512.6
176	1-pentyl-3-methyl-imidazolium	Ethylsulfate	691	1.25	0.809	211.1	284.8
177	1-pentyl-3-methyl-imidazolium	NO_2	2483	4.48	0.487	170.2	79.9
178	1-pentyl-3-methyl-imidazolium	Octylsulfate	511	0.92	1.601	226.7	618.8
179	1-pentyl-3-methyl-imidazolium	PF_6	585	1.06	1.028	312.4	433.7
180	1-pentyl-3-methyl-imidazolium	Toluene-4-sulfonate	689	1.24	0.939	235.5	1200.3
181	4-methyl-n-butylpyridinium	SO_4	317655	573.70	0.496	119.9	3.49E+11
182	4-methyl-n-butylpyridinium	Cl	10621	19.18	0.500	N/A	346.7
183	4-methyl-n-butylpyridinium	F	257537	465.12	0.496	N/A	328.9
184	4-methyl-n-butylpyridinium	2-chlorophenol	994	1.80	0.680	218.1	155.3
185	4-methyl-n-butylpyridinium	3-chlorophenol	1026	1.85	0.672	218.6	120.9
186	4-methyl-n-butylpyridinium	4-chlorophenol	1217	2.20	0.635	242.1	127.4

187	4-methyl-n-butylpyridinium	Benzoicacid	1940	3.50	0.570	236.2	503.2
188	4-methyl-n-butylpyridinium	BF_4	655	1.18	0.741	257.0	160.0
189	4-methyl-n-butylpyridinium	Bis((trifluoromethyl)sulfonyl)imide	461	0.83	2.242	261.1	567.9
190	4-methyl-n-butylpyridinium	Butylsulfate	564	1.02	1.078	221.1	507.0
191	4-methyl-n-butylpyridinium	Ethylsulfate	665	1.20	0.840	214.7	213.1
192	4-methyl-n-butylpyridinium	NO_2	2456	4.44	0.517	172.1	59.4
193	4-methyl-n-butylpyridinium	Octylsulfate	485	0.88	1.631	229.6	613.2
194	4-methyl-n-butylpyridinium	PF_6	559	1.01	1.058	330.8	428.1
195	4-methyl-n-butylpyridinium	Toluene-4-sulfonate	663	1.20	0.969	240.8	900.5
196	Aniline	SO_4	378043	682.76	0.002	139.6	1.59E+12
197	Aniline	Cl	71009	128.24	0.005	N/A	234.0
198	Aniline	F	317924	574.18	0.002	N/A	216.2
199	Aniline	2-chlorophenol	61382	110.86	0.186	202.4	787.4
200	Aniline	3-chlorophenol	61414	110.92	0.177	202.3	613.3
201	Aniline	4-chlorophenol	61605	111.26	0.141	232.2	645.8
202	Aniline	Benzoicacid	62328	112.57	0.075	228.6	2560.2
203	Aniline	BF_4	61042	110.24	0.247	270.8	718.8
204	Aniline	Bis((trifluoromethyl)sulfonyl)imide	60849	109.89	1.748	266.3	455.2
205	Aniline	Butylsulfate	60952	110.08	0.583	209.8	1927.5
206	Aniline	Ethylsulfate	61053	110.26	0.345	203.7	1056.2
207	Aniline	NO_2	62844	113.50	0.023	152.8	246.5
208	Aniline	Octylsulfate	60873	109.94	1.137	218.2	500.5
209	Aniline	PF_6	60946	110.07	0.563	408.8	315.4
210	Aniline	Toluene-4-sulfonate	61050	110.26	0.475	233.3	4807.4
211	n-butyl-isoquinolinium	SO_4	317636	573.66	0.656	132.1	4.33E+11
212	n-butyl-isoquinolinium	Cl	10602	19.15	0.660	N/A	392.0
213	n-butyl-isoquinolinium	F	257518	465.08	0.656	N/A	374.2
214	n-butyl-isoquinolinium	2-chlorophenol	975	1.76	0.840	221.4	186.6
215	n-butyl-isoquinolinium	3-chlorophenol	1007	1.82	0.832	221.8	145.3
216	n-butyl-isoquinolinium	4-chlorophenol	1198	2.16	0.795	245.6	153.1
217	n-butyl-isoquinolinium	Benzoicacid	1921	3.47	0.730	240.2	604.3
218	n-butyl-isoquinolinium	BF_4	636	1.15	0.901	259.7	198.9
219	n-butyl-isoquinolinium	Bis((trifluoromethyl)sulfonyl)imide	442	0.80	2.402	266.3	613.2
220	n-butyl-isoquinolinium	Butylsulfate	545	0.98	1.238	224.1	552.4
221	n-butyl-isoquinolinium	Ethylsulfate	646	1.17	1.000	217.4	257.7
222	n-butyl-isoquinolinium	NO_2	2437	4.40	0.678	173.3	75.5
223	n-butyl-isoquinolinium	Octylsulfate	466	0.84	1.791	232.8	658.5
224	n-butyl-isoquinolinium	PF_6	540	0.98	1.218	336.0	473.5
225	n-butyl-isoquinolinium	Toluene-4-sulfonate	644	1.16	1.129	245.0	573.5
226	Pyridine	SO_4	319831	577.63	0.033	124.8	2.34E+11
227	Pyridine	Cl	12797	23.11	0.036	N/A	207.0
228	Pyridine	F	259712	469.05	0.032	N/A	189.2
229	Pyridine	2-chlorophenol	3170	5.72	0.216	184.8	120.9
230	Pyridine	3-chlorophenol	3202	5.78	0.208	185.3	94.2
231	Pyridine	4-chlorophenol	3393	6.13	0.171	212.5	99.1
232	Pyridine	Benzoicacid	4116	7.43	0.106	205.8	393.5
233	Pyridine	BF_4	2831	5.11	0.277	240.8	105.6
234	Pyridine	Bis((trifluoromethyl)sulfonyl)imide	2637	4.76	1.778	243.1	428.1
235	Pyridine	Butylsulfate	2740	4.95	0.614	192.3	299.4
236	Pyridine	Ethylsulfate	2841	5.13	0.376	184.5	160.8
237	Pyridine	NO_2	4632	8.37	0.054	130.5	110.25
238	Pyridine	Octylsulfate	2661	4.81	1.168	203.2	473.5
239	Pyridine	PF_6	2735	4.94	0.594	366.2	288.4
240	Pyridine	Toluene-4-sulfonate	2839	5.13	0.505	211.8	751.8

Table S3. COSMO-RS predicted liquid-liquid equilibria screened with Selectivity (> 1)

Combination No	Cation	Anion	Distribution Coefficient (gsolute/g solute)	Selectivity (gsolute/g carrier)	Solvent Loss (g_{ll})	Melting Point (K)	Viscosity (cP)
1	1-heptyl-3-methyl-imidazolium	SO_4	317641	573.67	0.629	107.0	7.36E+11
2	1-heptyl-3-methyl-imidazolium	Cl	10606	19.16	0.632	N/A	407.9
3	1-heptyl-3-methyl-imidazolium	F	257522	465.09	0.629	N/A	390.1
4	1-heptyl-3-methyl-imidazolium	2-chlorophenol	979	1.77	0.813	218.2	314.6
5	1-heptyl-3-methyl-imidazolium	3-chlorophenol	1012	1.83	0.805	218.6	244.8
6	1-heptyl-3-methyl-imidazolium	4-chlorophenol	1203	2.17	0.768	238.3	258.1
7	1-heptyl-3-methyl-imidazolium	Benzoicacid	1926	3.48	0.703	233.2	1018.3
8	1-heptyl-3-methyl-imidazolium	BF_4	640	1.16	0.874	246.1	338.7
11	1-heptyl-3-methyl-imidazolium	Ethylsulfate	650	1.17	0.973	215.1	435.3
12	1-heptyl-3-methyl-imidazolium	NO_2	2442	4.41	0.650	177.0	129.4
15	1-heptyl-3-methyl-imidazolium	Toluene-4-sulfonate	648	1.17	1.102	238.3	589.4
16	1-octyl-3-methyl-imidazolium	SO_4	317626	573.64	0.716	105.1	9.08E+11
17	1-octyl-3-methyl-imidazolium	Cl	10591	19.13	0.719	N/A	435.9
18	1-octyl-3-methyl-imidazolium	F	257507	465.07	0.715	N/A	418.1
19	1-octyl-3-methyl-imidazolium	2-chlorophenol	964	1.74	0.899	220.2	381.9
20	1-octyl-3-methyl-imidazolium	3-chlorophenol	997	1.80	0.891	220.6	297.3
21	1-octyl-3-methyl-imidazolium	4-chlorophenol	1188	2.14	0.854	239.5	313.4
22	1-octyl-3-methyl-imidazolium	Benzoicacid	1910	3.45	0.789	234.6	1235.7
23	1-octyl-3-methyl-imidazolium	BF_4	625	1.13	0.960	246.0	418.4
26	1-octyl-3-methyl-imidazolium	Ethylsulfate	635	1.15	1.059	217.1	543.2
27	1-octyl-3-methyl-imidazolium	NO_2	2427	4.38	0.737	180.2	161.7
30	1-octyl-3-methyl-imidazolium	Toluene-4-sulfonate	633	1.14	1.188	239.8	617.4
31	Pyrrolidine	SO_4	322417	582.30	0.015	124.6	3.87E+11
32	Pyrrolidine	Cl	15383	536.08	0.018	N/A	206.6
33	Pyrrolidine	F	262298	978.47	0.014	N/A	188.8
34	Pyrrolidine	2-chlorophenol	5756	401.83	0.198	184.3	200.2
35	Pyrrolidine	3-chlorophenol	5788	1.81	0.190	185.0	155.9
36	Pyrrolidine	4-chlorophenol	5979	2.29	0.153	212.4	164.1
37	Pyrrolidine	Benzoicacid	6702	3.53	0.088	203.9	651.6
38	Pyrrolidine	BF_4	5417	1.41	0.259	229.7	174.7
40	Pyrrolidine	Butylsulfate	5326	1.07	0.596	194.1	495.9
41	Pyrrolidine	Ethylsulfate	5427	1.20	0.358	185.6	266.2
42	Pyrrolidine	NO_2	7218	113.50	0.036	133.3	118.12
44	Pyrrolidine	PF_6	5321	4.94	0.576	346.0	288.0
46	H_3O	SO_4	601898	1087.05	0.000	N/A	157.7
47	H_3O	Cl	294863	532.53	0.004	N/A	107.6
48	H_3O	F	541779	978.47	0.000	N/A	89.8
49	H_3O	2-chlorophenol	285236	515.15	0.184	N/A	234.8
50	H_3O	3-chlorophenol	285269	515.20	0.176	N/A	235.2
51	H_3O	4-chlorophenol	285460	515.55	0.139	N/A	234.4
52	H_3O	Benzoicacid	286183	516.85	0.074	N/A	237.8
53	H_3O	BF_4	284897	514.53	0.245	N/A	151.8
54	H_3O	Bis((trifluoromethyl)sulfonyl)imide	284704	514.18	1.746	N/A	328.7
55	H_3O	Butylsulfate	284806	514.37	0.582	N/A	267.9
56	H_3O	Ethylsulfate	284907	514.55	0.344	N/A	214.9
57	H_3O	NO_2	286699	517.79	0.021	N/A	119.6
58	H_3O	Octylsulfate	284728	514.23	1.135	N/A	374.1
59	H_3O	PF_6	284801	514.36	0.562	N/A	189.0
60	H_3O	Toluene-4-sulfonate	284905	514.55	0.473	N/A	289.1
61	NH_4	SO_4	603860	1090.59	0.000	N/A	163.4
62	NH_4	Cl	296826	536.08	0.003	N/A	113.3
63	NH_4	F	543741	982.01	0.000	N/A	95.5
64	NH_4	2-chlorophenol	287199	518.69	0.184	N/A	240.5
65	NH_4	3-chlorophenol	287231	518.75	0.176	N/A	240.9
66	NH_4	4-chlorophenol	287422	519.09	0.139	N/A	240.2
67	NH_4	Benzoicacid	288145	520.40	0.074	N/A	243.5
68	NH_4	BF_4	286860	518.08	0.245	N/A	157.6
69	NH_4	Bis((trifluoromethyl)sulfonyl)imide	286666	517.73	1.746	N/A	334.5
70	NH_4	Butylsulfate	286769	517.91	0.582	N/A	273.6
71	NH_4	Ethylsulfate	286870	518.10	0.344	N/A	220.6
72	NH_4	NO_2	288661	521.33	0.021	N/A	125.4
73	NH_4	Octylsulfate	286690	517.77	1.135	N/A	379.8
74	NH_4	PF_6	286763	517.90	0.562	N/A	194.7
75	NH_4	Toluene-4-sulfonate	286867	518.09	0.473	N/A	294.8
76	Na	SO_4	539154	973.73	0.000	N/A	151.1
77	Na	Cl	232120	419.22	0.004	N/A	100.9
78	Na	F	479036	865.15	0.000	N/A	83.1
79	Na	2-chlorophenol	222493	401.83	0.184	N/A	228.1
80	Na	3-chlorophenol	222525	401.89	0.176	N/A	228.5
81	Na	4-chlorophenol	222716	402.23	0.139	N/A	227.8
82	Na	Benzoicacid	223439	403.54	0.074	N/A	231.1
83	Na	BF_4	222154	401.22	0.245	N/A	145.2
84	Na	Bis((trifluoromethyl)sulfonyl)imide	221960	400.87	1.746	N/A	322.1
85	Na	Butylsulfate	222063	401.05	0.582	N/A	261.3
86	Na	Ethylsulfate	222164	401.24	0.344	N/A	208.3
87	Na	NO_2	223955	404.47	0.021	N/A	113.0
88	Na	Octylsulfate	221984	400.91	1.135	N/A	367.4
89	Na	PF_6	222058	401.04	0.562	N/A	182.4
90	Na	Toluene-4-sulfonate	222162	401.23	0.473	N/A	282.4
91	1-butyl-2,3-dimethyl-imidazolium	SO_4	317632	573.65	0.549	121.6	3.54E+11
92	1-butyl-2,3-dimethyl-imidazolium	Cl	10597	19.14	0.552	N/A	353.0
93	1-butyl-2,3-dimethyl-imidazolium	F	257513	465.08	0.549	N/A	335.2
94	1-butyl-2,3-dimethyl-imidazolium	2-chlorophenol	970	1.75	0.733	223.9	156.5
95	1-butyl-2,3-dimethyl-imidazolium	3-chlorophenol	1003	1.81	0.725	224.4	121.8
96	1-butyl-2,3-dimethyl-imidazolium	4-chlorophenol	1194	2.16	0.688	248.6	128.4
97	1-butyl-2,3-dimethyl-imidazolium	Benzoicacid	1916	3.46	0.623	242.5	507.2
98	1-butyl-2,3-dimethyl-imidazolium	BF_4	631	1.14	0.794	265.9	162.1
101	1-butyl-2,3-dimethyl-imidazolium	Ethylsulfate	641	1.16	0.893	220.4	215.0
102	1-butyl-2,3-dimethyl-imidazolium	NO_2	2433	4.39	0.570	178.8	60.4
105	1-butyl-2,3-dimethyl-imidazolium	Toluene-4-sulfonate	639	1.15	1.022	246.8	534.5
106	1-butyl-3-methyl-imidazolium	SO_4	317708	573.79	0.392	113.6	3.63E+11

107	1-butyl-3-methyl-imidazolium	Cl	10674	19.28	0.395	N/A	324.3
108	1-butyl-3-methyl-imidazolium	F	257589	465.21	0.392	N/A	306.5
109	1-butyl-3-methyl-imidazolium	2-chlorophenol	1047	1.89	0.576	210.8	164.1
110	1-butyl-3-methyl-imidazolium	3-chlorophenol	1079	1.95	0.567	211.3	127.8
111	1-butyl-3-methyl-imidazolium	4-chlorophenol	1270	2.29	0.531	234.0	134.7
112	1-butyl-3-methyl-imidazolium	Benzoicacid	1993	3.60	0.465	228.0	532.2
113	1-butyl-3-methyl-imidazolium	BF_4	708	1.28	0.637	247.1	166.0
115	1-butyl-3-methyl-imidazolium	Butylsulfate	617	1.11	0.973	214.9	390.8
116	1-butyl-3-methyl-imidazolium	Ethylsulfate	718	1.30	0.735	208.1	224.4
117	1-butyl-3-methyl-imidazolium	NO_2	2509	4.53	0.413	165.5	60.9
119	1-butyl-3-methyl-imidazolium	PF_6	612	1.10	0.953	318.4	405.7
120	1-butyl-3-methyl-imidazolium	Toluene-4-sulfonate	716	1.29	0.865	233.1	959.7
121	1-ethyl-2,3-dimethyl-imidazolium	SO_4	317671	573.72	0.393	129.1	2.21E+11
122	1-ethyl-2,3-dimethyl-imidazolium	Cl	10637	19.21	0.396	N/A	296.3
123	1-ethyl-2,3-dimethyl-imidazolium	F	257553	465.15	0.393	N/A	278.5
124	1-ethyl-2,3-dimethyl-imidazolium	2-chlorophenol	1010	1.82	0.577	218.3	102.2
125	1-ethyl-2,3-dimethyl-imidazolium	3-chlorophenol	1042	1.88	0.568	218.8	79.6
126	1-ethyl-2,3-dimethyl-imidazolium	4-chlorophenol	1233	2.23	0.532	245.8	83.9
127	1-ethyl-2,3-dimethyl-imidazolium	Benzoicacid	1956	3.53	0.467	239.0	331.7
128	1-ethyl-2,3-dimethyl-imidazolium	BF_4	671	1.21	0.638	270.1	100.7
130	1-ethyl-2,3-dimethyl-imidazolium	Butylsulfate	580	1.05	0.974	221.1	245.1
131	1-ethyl-2,3-dimethyl-imidazolium	Ethylsulfate	681	1.23	0.736	215.0	139.1
132	1-ethyl-2,3-dimethyl-imidazolium	NO_2	2472	4.47	0.414	169.7	36.3
134	1-ethyl-2,3-dimethyl-imidazolium	PF_6	575	1.04	0.955	365.9	377.8
135	1-ethyl-2,3-dimethyl-imidazolium	Toluene-4-sulfonate	679	1.23	0.866	242.9	604.4
136	1-ethyl-3-methyl-imidazolium	SO_4	317781	573.92	0.260	119.1	2.15E+11
137	1-ethyl-3-methyl-imidazolium	Cl	10746	19.41	0.263	N/A	269.0
138	1-ethyl-3-methyl-imidazolium	F	257662	465.35	0.260	N/A	251.2
139	1-ethyl-3-methyl-imidazolium	2-chlorophenol	1119	2.02	0.444	204.3	102.4
140	1-ethyl-3-methyl-imidazolium	3-chlorophenol	1152	2.08	0.435	204.8	109.72
141	1-ethyl-3-methyl-imidazolium	4-chlorophenol	1343	2.42	0.399	230.1	103.97
142	1-ethyl-3-methyl-imidazolium	Benzoicacid	2066	3.73	0.334	223.4	332.4
143	1-ethyl-3-methyl-imidazolium	BF_4	780	1.41	0.505	299.21	97.8
144	1-ethyl-3-methyl-imidazolium	Bis((trifluoromethyl)sulfonyl)imide	587	1.06	2.006	252.6	490.1
145	1-ethyl-3-methyl-imidazolium	Butylsulfate	689	1.25	0.841	208.8	247.5
146	1-ethyl-3-methyl-imidazolium	Ethylsulfate	790	1.43	0.603	202.0	138.5
147	1-ethyl-3-methyl-imidazolium	NO_2	2582	4.66	0.281	155.6	34.6
148	1-ethyl-3-methyl-imidazolium	Octylsulfate	611	1.10	1.395	218.0	535.5
149	1-ethyl-3-methyl-imidazolium	PF_6	684	1.24	0.822	339.2	350.4
150	1-ethyl-3-methyl-imidazolium	Toluene-4-sulfonate	788	1.42	0.733	228.3	613.0
151	1-hexyl-3-methyl-imidazolium	SO_4	317659	573.70	0.547	109.1	5.92E+11
152	1-hexyl-3-methyl-imidazolium	Cl	10624	19.19	0.550	N/A	380.1
153	1-hexyl-3-methyl-imidazolium	F	257540	465.13	0.546	N/A	362.3
154	1-hexyl-3-methyl-imidazolium	2-chlorophenol	997	1.80	0.730	216.2	257.3
155	1-hexyl-3-methyl-imidazolium	3-chlorophenol	1030	1.86	0.722	216.6	200.3
156	1-hexyl-3-methyl-imidazolium	4-chlorophenol	1221	2.20	0.686	237.2	211.1
157	1-hexyl-3-methyl-imidazolium	Benzoicacid	1944	3.51	0.620	231.9	833.2
158	1-hexyl-3-methyl-imidazolium	BF_4	658	1.19	0.792	246.6	271.9
160	1-hexyl-3-methyl-imidazolium	Butylsulfate	567	1.02	1.128	219.8	540.4
161	1-hexyl-3-methyl-imidazolium	Ethylsulfate	668	1.21	0.890	213.2	354.8
162	1-hexyl-3-methyl-imidazolium	NO_2	2460	4.44	0.568	173.8	102.7
164	1-hexyl-3-methyl-imidazolium	PF_6	562	1.02	1.108	306.3	461.5
165	1-hexyl-3-methyl-imidazolium	Toluene-4-sulfonate	666	1.20	1.019	237.0	561.6
166	1-pentyl-3-methyl-imidazolium	SO_4	317682	573.74	0.466	111.3	4.68E+11
167	1-pentyl-3-methyl-imidazolium	Cl	10647	19.23	0.469	N/A	352.3
168	1-pentyl-3-methyl-imidazolium	F	257563	465.17	0.466	N/A	334.5
169	1-pentyl-3-methyl-imidazolium	2-chlorophenol	1020	1.84	0.650	214.0	207.3
170	1-pentyl-3-methyl-imidazolium	3-chlorophenol	1053	1.90	0.642	214.5	161.4
171	1-pentyl-3-methyl-imidazolium	4-chlorophenol	1243	2.25	0.605	236.1	170.1
172	1-pentyl-3-methyl-imidazolium	Benzoicacid	1966	3.55	0.540	230.5	671.9
173	1-pentyl-3-methyl-imidazolium	BF_4	681	1.23	0.711	247.3	214.6
175	1-pentyl-3-methyl-imidazolium	Butylsulfate	590	1.07	1.048	217.8	512.6
176	1-pentyl-3-methyl-imidazolium	Ethylsulfate	691	1.25	0.809	211.1	284.8
177	1-pentyl-3-methyl-imidazolium	NO_2	2483	4.48	0.487	170.2	79.9
179	1-pentyl-3-methyl-imidazolium	PF_6	585	1.06	1.028	312.4	433.7
180	1-pentyl-3-methyl-imidazolium	Toluene-4-sulfonate	689	1.24	0.939	235.5	1200.3
181	4-methyl-n-butylpyridinium	SO_4	317655	573.70	0.496	119.9	3.49E+11
182	4-methyl-n-butylpyridinium	Cl	10621	19.18	0.500	N/A	346.7
183	4-methyl-n-butylpyridinium	F	257537	465.12	0.496	N/A	328.9
184	4-methyl-n-butylpyridinium	2-chlorophenol	994	1.80	0.680	218.1	155.3
185	4-methyl-n-butylpyridinium	3-chlorophenol	1026	1.85	0.672	218.6	120.9
186	4-methyl-n-butylpyridinium	4-chlorophenol	1217	2.20	0.635	242.1	127.4
187	4-methyl-n-butylpyridinium	Benzoicacid	1940	3.50	0.570	236.2	503.2
188	4-methyl-n-butylpyridinium	BF_4	655	1.18	0.741	257.0	160.0
190	4-methyl-n-butylpyridinium	Butylsulfate	564	1.02	1.078	221.1	507.0
191	4-methyl-n-butylpyridinium	Ethylsulfate	665	1.20	0.840	214.7	213.1
192	4-methyl-n-butylpyridinium	NO_2	2456	4.44	0.517	172.1	59.4
194	4-methyl-n-butylpyridinium	PF_6	559	1.01	1.058	330.8	428.1
195	4-methyl-n-butylpyridinium	Toluene-4-sulfonate	663	1.20	0.969	240.8	900.5
196	Aniline	SO_4	378043	682.76	0.002	139.6	1.59E+12
197	Aniline	Cl	71009	128.24	0.005	N/A	234.0
198	Aniline	F	317924	574.18	0.002	N/A	216.2
199	Aniline	2-chlorophenol	61382	110.86	0.186	202.4	787.4
200	Aniline	3-chlorophenol	61414	110.92	0.177	202.3	613.3
201	Aniline	4-chlorophenol	61605	111.26	0.141	232.2	645.8
202	Aniline	Benzoicacid	62328	112.57	0.075	228.6	2560.2
203	Aniline	BF_4	61042	110.24	0.247	270.8	718.8
204	Aniline	Bis((trifluoromethyl)sulfonyl)imide	60849	109.89	1.748	266.3	455.2
205	Aniline	Butylsulfate	60952	110.08	0.583	209.8	1927.5
206	Aniline	Ethylsulfate	61053	110.26	0.345	203.7	1056.2
207	Aniline	NO_2	62844	113.50	0.023	152.8	246.5
208	Aniline	Octylsulfate	60873	109.94	1.137	218.2	500.5
209	Aniline	PF_6	60946	110.07	0.563	408.8	315.4
210	Aniline	Toluene-4-sulfonate	61050	110.26	0.475	233.3	4807.4
211	n-butyl-isoquinolinium	SO_4	317636	573.66	0.656	132.1	4.33E+11

212	n-butyl-isoquinolinium	Cl	10602	19.15	0.660	N/A	392.0
213	n-butyl-isoquinolinium	F	257518	465.08	0.656	N/A	374.2
214	n-butyl-isoquinolinium	2-chlorophenol	975	1.76	0.840	221.4	186.6
215	n-butyl-isoquinolinium	3-chlorophenol	1007	1.82	0.832	221.8	145.3
216	n-butyl-isoquinolinium	4-chlorophenol	1198	2.16	0.795	245.6	153.1
217	n-butyl-isoquinolinium	Benzoicacid	1921	3.47	0.730	240.2	604.3
218	n-butyl-isoquinolinium	BF_4	636	1.15	0.901	259.7	198.9
221	n-butyl-isoquinolinium	Ethylsulfate	646	1.17	1.000	217.4	257.7
222	n-butyl-isoquinolinium	NO_2	2437	4.40	0.678	173.3	75.5
225	n-butyl-isoquinolinium	Toluene-4-sulfonate	644	1.16	1.129	245.0	573.5
226	Pyridine	SO_4	319831	577.63	0.033	124.8	2.34E+11
227	Pyridine	Cl	12797	23.11	0.036	N/A	207.0
228	Pyridine	F	259712	469.05	0.032	N/A	189.2
229	Pyridine	2-chlorophenol	3170	5.72	0.216	184.8	120.9
230	Pyridine	3-chlorophenol	3202	5.78	0.208	185.3	94.2
231	Pyridine	4-chlorophenol	3393	6.13	0.171	212.5	99.1
232	Pyridine	Benzoicacid	4116	7.43	0.106	205.8	393.5
233	Pyridine	BF_4	2831	5.11	0.277	240.8	105.6
234	Pyridine	Bis((trifluoromethyl)sulfonyl)imide	2637	4.76	1.778	243.1	428.1
235	Pyridine	Butylsulfate	2740	4.95	0.614	192.3	299.4
236	Pyridine	Ethylsulfate	2841	5.13	0.376	184.5	160.8
237	Pyridine	NO_2	4632	8.37	0.054	130.5	110.25
238	Pyridine	Octylsulfate	2661	4.81	1.168	203.2	473.5
239	Pyridine	PF_6	2735	4.94	0.594	366.2	288.4
240	Pyridine	Toluene-4-sulfonate	2839	5.13	0.505	211.8	751.8

Table S4. COSMO-RS predicted liquid-liquid equilibria screened with solvent loss (SL< 0.5)

Combination No	Cation	Anion	Distribution Coefficient (gsolute/gsolute)	Selectivity (gsolute/gcarrier)	Solvent Loss (g_{II})	Melting Point (K)	Viscosity (cP)
31	Pyrrolidine	SO_4	322417	582.30	0.015	124.6	3.87E+11
32	Pyrrolidine	Cl	15383	536.08	0.018	N/A	206.6
33	Pyrrolidine	F	262298	978.47	0.014	N/A	188.8
34	Pyrrolidine	2-chlorophenol	5756	401.83	0.198	184.3	200.2
35	Pyrrolidine	3-chlorophenol	5788	1.81	0.190	185.0	155.9
36	Pyrrolidine	4-chlorophenol	5979	2.29	0.153	212.4	164.1
37	Pyrrolidine	Benzoicacid	6702	3.53	0.088	203.9	651.6
38	Pyrrolidine	BF_4	5417	1.41	0.259	229.7	174.7
41	Pyrrolidine	Ethylsulfate	5427	1.20	0.358	185.6	266.2
42	Pyrrolidine	NO_2	7218	113.50	0.036	133.3	58.10
46	H_3O	SO_4	601898	1087.05	0.000	N/A	157.7
47	H_3O	Cl	294863	532.53	0.004	N/A	107.6
48	H_3O	F	541779	978.47	0.000	N/A	89.8
49	H_3O	2-chlorophenol	285236	515.15	0.184	N/A	234.8
50	H_3O	3-chlorophenol	285269	515.20	0.176	N/A	235.2
51	H_3O	4-chlorophenol	285460	515.55	0.139	N/A	234.4
52	H_3O	Benzoicacid	286183	516.85	0.074	N/A	237.8
53	H_3O	BF_4	284897	514.53	0.245	N/A	151.8
56	H_3O	Ethylsulfate	284907	514.55	0.344	N/A	214.9
57	H_3O	NO_2	286699	517.79	0.021	N/A	119.6
60	H_3O	Toluene-4-sulfonate	284905	514.55	0.473	N/A	289.1
61	NH_4	SO_4	603860	1090.59	0.000	N/A	163.4
62	NH_4	Cl	296826	536.08	0.003	N/A	113.3
63	NH_4	F	543741	982.01	0.000	N/A	95.5
64	NH_4	2-chlorophenol	287199	518.69	0.184	N/A	240.5
65	NH_4	3-chlorophenol	287231	518.75	0.176	N/A	240.9
66	NH_4	4-chlorophenol	287422	519.09	0.139	N/A	240.2
67	NH_4	Benzoicacid	288145	520.40	0.074	N/A	243.5
68	NH_4	BF_4	286860	518.08	0.245	N/A	157.6
71	NH_4	Ethylsulfate	286870	518.10	0.344	N/A	220.6
72	NH_4	NO_2	288661	521.33	0.021	N/A	125.4
75	NH_4	Toluene-4-sulfonate	286867	518.09	0.473	N/A	294.8
76	Na	SO_4	539154	973.73	0.000	N/A	151.1
77	Na	Cl	232120	419.22	0.004	N/A	100.9
78	Na	F	479036	865.15	0.000	N/A	83.1
79	Na	2-chlorophenol	222493	401.83	0.184	N/A	228.1
80	Na	3-chlorophenol	222525	401.89	0.176	N/A	228.5
81	Na	4-chlorophenol	222716	402.23	0.139	N/A	227.8
82	Na	Benzoicacid	223439	403.54	0.074	N/A	231.1
83	Na	BF_4	222154	401.22	0.245	N/A	145.2
86	Na	Ethylsulfate	222164	401.24	0.344	N/A	208.3
87	Na	NO_2	223955	404.47	0.021	N/A	113.0
90	Na	Toluene-4-sulfonate	222162	401.23	0.473	N/A	282.4
106	1-butyl-3-methyl-imidazolium	SO_4	317708	573.79	0.392	113.6	3.63E+11
107	1-butyl-3-methyl-imidazolium	Cl	10674	19.28	0.395	N/A	324.3
108	1-butyl-3-methyl-imidazolium	F	257589	465.21	0.392	N/A	306.5
112	1-butyl-3-methyl-imidazolium	Benzoicacid	1993	3.60	0.465	228.0	532.2
117	1-butyl-3-methyl-imidazolium	NO_2	2509	4.53	0.413	165.5	60.9
121	1-ethyl-2,3-dimethyl-imidazolium	SO_4	317671	573.72	0.393	129.1	2.21E+11
122	1-ethyl-2,3-dimethyl-imidazolium	Cl	10637	19.21	0.396	N/A	296.3
123	1-ethyl-2,3-dimethyl-imidazolium	F	257553	465.15	0.393	N/A	278.5
127	1-ethyl-2,3-dimethyl-imidazolium	Benzoicacid	1956	3.53	0.467	239.0	331.7
132	1-ethyl-2,3-dimethyl-imidazolium	NO_2	2472	4.47	0.414	169.7	36.3
136	1-ethyl-3-methyl-imidazolium	SO_4	317781	573.92	0.260	119.1	2.15E+11
137	1-ethyl-3-methyl-imidazolium	Cl	10746	19.41	0.263	N/A	269.0
138	1-ethyl-3-methyl-imidazolium	F	257662	465.35	0.260	N/A	251.2
139	1-ethyl-3-methyl-imidazolium	2-chlorophenol	1119	2.02	0.444	204.3	102.4
140	1-ethyl-3-methyl-imidazolium	3-chlorophenol	1152	2.08	0.435	204.8	109.72
141	1-ethyl-3-methyl-imidazolium	4-chlorophenol	1343	2.42	0.399	230.1	103.97
142	1-ethyl-3-methyl-imidazolium	Benzoicacid	2066	3.73	0.334	223.4	332.4
147	1-ethyl-3-methyl-imidazolium	NO_2	2582	4.66	0.281	155.6	34.6
166	1-pentyl-3-methyl-imidazolium	SO_4	317682	573.74	0.466	111.3	4.68E+11
167	1-pentyl-3-methyl-imidazolium	Cl	10647	19.23	0.469	N/A	352.3
168	1-pentyl-3-methyl-imidazolium	F	257563	465.17	0.466	N/A	334.5
177	1-pentyl-3-methyl-imidazolium	NO_2	2483	4.48	0.487	170.2	79.9
181	4-methyl-n-butylpyridinium	SO_4	317655	573.70	0.496	119.9	3.49E+11
182	4-methyl-n-butylpyridinium	Cl	10621	19.18	0.500	N/A	346.7
183	4-methyl-n-butylpyridinium	F	257537	465.12	0.496	N/A	328.9
196	Aniline	SO_4	378043	682.76	0.002	139.6	1.59E+12
197	Aniline	Cl	71009	128.24	0.005	N/A	234.0
198	Aniline	F	317924	574.18	0.002	N/A	216.2
199	Aniline	2-chlorophenol	61382	110.86	0.186	202.4	787.4
200	Aniline	3-chlorophenol	61414	110.92	0.177	202.3	613.3
201	Aniline	4-chlorophenol	61605	111.26	0.141	232.2	645.8
202	Aniline	Benzoicacid	62328	112.57	0.075	228.6	2560.2
203	Aniline	BF_4	61042	110.24	0.247	270.8	718.8
206	Aniline	Ethylsulfate	61053	110.26	0.345	203.7	1056.2
207	Aniline	NO_2	62844	113.50	0.023	152.8	246.5
210	Aniline	Toluene-4-sulfonate	61050	110.26	0.475	233.3	4807.4
226	Pyridine	SO_4	319831	577.63	0.033	124.8	2.34E+11
227	Pyridine	Cl	12797	23.11	0.036	N/A	207.0
228	Pyridine	F	259712	469.05	0.032	N/A	189.2
229	Pyridine	2-chlorophenol	3170	5.72	0.216	184.8	120.9
230	Pyridine	3-chlorophenol	3202	5.78	0.208	185.3	94.2
231	Pyridine	4-chlorophenol	3393	6.13	0.171	212.5	99.1
232	Pyridine	Benzoicacid	4116	7.43	0.106	205.8	393.5
233	Pyridine	BF_4	2831	5.11	0.277	240.8	105.6
236	Pyridine	Ethylsulfate	2841	5.13	0.376	184.5	160.8
237	Pyridine	NO_2	4632	8.37	0.054	130.5	35.10

Table S5. COSMO-RS predicted gas capacity of all IL candidates {CO2 + IL} at the initial mass ratio of 1:1

Combination No	Cation	Anion	Gas Capacity (molCO2/mol IL)	Gas Capacity (gCO2/g IL)	Melting Point (K)	Viscosity (cP)
1	1-heptyl-3-methyl-imidazolium	SO_4	4.77	0.458	106.98	7.36E+11
2	1-heptyl-3-methyl-imidazolium	Cl	2.79	0.566	N/A	407.88
3	1-heptyl-3-methyl-imidazolium	F	3.46	0.761	N/A	390.08
4	1-heptyl-3-methyl-imidazolium	2-chlorophenol	3.43	0.488	218.18	314.56
5	1-heptyl-3-methyl-imidazolium	3-chlorophenol	3.40	0.484	218.62	244.85
6	1-heptyl-3-methyl-imidazolium	4-chlorophenol	3.38	0.482	238.28	258.13
7	1-heptyl-3-methyl-imidazolium	Benzoicacid	3.28	0.478	233.17	1018.29
8	1-heptyl-3-methyl-imidazolium	BF_4	2.74	0.449	246.10	338.74
9	1-heptyl-3-methyl-imidazolium	Bis((trifluoromethyl)sulfonyl)imide	3.97	0.379	255.11	629.05
10	1-heptyl-3-methyl-imidazolium	Butylsulfate	3.26	0.429	221.66	568.21
11	1-heptyl-3-methyl-imidazolium	Ethylsulfate	3.03	0.436	215.12	435.31
12	1-heptyl-3-methyl-imidazolium	NO_2	2.80	0.543	177.02	129.44
13	1-heptyl-3-methyl-imidazolium	Octylsulfate	3.70	0.417	230.48	674.38
14	1-heptyl-3-methyl-imidazolium	PF_6	3.36	0.453	301.38	489.31
15	1-heptyl-3-methyl-imidazolium	Toluene-4-sulfonate	3.48	0.435	238.33	589.38
16	1-octyl-3-methyl-imidazolium	SO_4	4.64	0.42	105.10	9.08E+11
17	1-octyl-3-methyl-imidazolium	Cl	2.76	0.526	N/A	435.88
18	1-octyl-3-methyl-imidazolium	F	3.19	0.656	N/A	418.08
19	1-octyl-3-methyl-imidazolium	2-chlorophenol	3.54	0.483	220.20	381.91
20	1-octyl-3-methyl-imidazolium	3-chlorophenol	3.51	0.479	220.63	297.25
21	1-octyl-3-methyl-imidazolium	4-chlorophenol	3.49	0.475	239.45	313.42
22	1-octyl-3-methyl-imidazolium	Benzoicacid	3.36	0.467	234.60	1235.73
23	1-octyl-3-methyl-imidazolium	BF_4	2.93	0.457	245.99	418.39
24	1-octyl-3-methyl-imidazolium	Bis((trifluoromethyl)sulfonyl)imide	4.12	0.382	255.54	657.06
25	1-octyl-3-methyl-imidazolium	Butylsulfate	3.38	0.426	223.54	596.21
26	1-octyl-3-methyl-imidazolium	Ethylsulfate	3.15	0.433	217.07	543.21
27	1-octyl-3-methyl-imidazolium	NO_2	2.86	0.522	180.23	161.67
28	1-octyl-3-methyl-imidazolium	Octylsulfate	3.80	0.414	232.28	702.38
29	1-octyl-3-methyl-imidazolium	PF_6	3.59	0.465	297.51	517.31
30	1-octyl-3-methyl-imidazolium	Toluene-4-sulfonate	3.58	0.43	239.76	617.39
31	Pyrrolidine	SO_4	3.46	0.634	124.56	3.87E+11
32	Pyrrolidine	Cl	1.38	0.566	N/A	206.56
33	Pyrrolidine	F	6.78	3.276	N/A	188.76
34	Pyrrolidine	2-chlorophenol	1.22	0.27	184.29	200.16
35	Pyrrolidine	3-chlorophenol	1.26	0.278	185.03	155.92
36	Pyrrolidine	4-chlorophenol	1.27	0.279	212.39	164.14
37	Pyrrolidine	Benzoicacid	1.29	0.293	203.94	651.58
38	Pyrrolidine	BF_4	0.27	0.075	229.74	174.66
39	Pyrrolidine	Bis((trifluoromethyl)sulfonyl)imide	1.62	0.202	240.52	427.74
40	Pyrrolidine	Butylsulfate	1.14	0.223	194.07	495.95
41	Pyrrolidine	Ethylsulfate	0.84	0.188	185.60	266.22
42	Pyrrolidine	NO_2	0.83	0.311	133.28	58.10
43	Pyrrolidine	Octylsulfate	1.80	0.281	205.42	473.06
44	Pyrrolidine	PF_6	0.67	0.135	345.98	287.99
45	Pyrrolidine	Toluene-4-sulfonate	1.37	0.248	210.90	388.07
46	H_3O	SO_4	2.33E+11	76600000000.0	N/A	157.70
47	H_3O	Cl	2.27E+14	183320000000000.0	N/A	107.57
48	H_3O	F	0.53	0.616	N/A	89.77
49	H_3O	2-chlorophenol	1.69	0.507	N/A	234.77
50	H_3O	3-chlorophenol	1.59	0.477	N/A	235.19
51	H_3O	4-chlorophenol	1.37	0.41	N/A	234.42
52	H_3O	Benzoicacid	0.48	0.151	N/A	237.78
53	H_3O	BF_4	14981.09	6230.003	N/A	151.82
54	H_3O	Bis((trifluoromethyl)sulfonyl)imide	1.76	0.259	N/A	328.74
55	H_3O	Butylsulfate	1.07	0.275	N/A	267.89
56	H_3O	Ethylsulfate	0.75	0.228	N/A	214.89
57	H_3O	NO_2	6.78E+05	458518.481	N/A	119.61
58	H_3O	Octylsulfate	1.69	0.327	N/A	374.07
59	H_3O	PF_6	245.45	65.873	N/A	189.00
60	H_3O	Toluene-4-sulfonate	0.77	0.177	N/A	289.07
61	NH_4	SO_4	1.63E+14	54341000000000.0	N/A	163.44
62	NH_4	Cl	4.04E+10	33261000000.0	N/A	113.31
63	NH_4	F	1.66E+18	##################	N/A	95.52
64	NH_4	2-chlorophenol	0.96	0.289	N/A	240.52
65	NH_4	3-chlorophenol	1.03	0.313	N/A	240.93
66	NH_4	4-chlorophenol	0.89	0.269	N/A	240.17
67	NH_4	Benzoicacid	0.25	0.079	N/A	243.52
68	NH_4	BF_4	6775.05	2843.919	N/A	157.57
69	NH_4	Bis((trifluoromethyl)sulfonyl)imide	1.14	0.168	N/A	334.49
70	NH_4	Butylsulfate	0.41	0.106	N/A	273.64
71	NH_4	Ethylsulfate	0.19	0.058	N/A	220.64
72	NH_4	NO_2	7513.72	5163.258	N/A	125.36
73	NH_4	Octylsulfate	0.87	0.169	N/A	379.82
74	NH_4	PF_6	158.76	42.865	N/A	194.74
75	NH_4	Toluene-4-sulfonate	0.32	0.075	N/A	294.82
76	Na	SO_4	1.58E+18	##################	N/A	151.06
77	Na	Cl	2.94E+16	##################	N/A	100.92
78	Na	F	3.33E+29	##################	N/A	83.13
79	Na	2-chlorophenol	3.10	0.906	N/A	228.13
80	Na	3-chlorophenol	2.64	0.773	N/A	228.55
81	Na	4-chlorophenol	2.24	0.654	N/A	227.78
82	Na	Benzoicacid	0.67	0.204	N/A	231.13
83	Na	BF_4	6.58E+04	26357.84	N/A	145.18
84	Na	Bis((trifluoromethyl)sulfonyl)imide	2.88	0.418	N/A	322.10
85	Na	Butylsulfate	1.64	0.411	N/A	261.25
86	Na	Ethylsulfate	1.86	0.553	N/A	208.25
87	Na	NO_2	1.15E+08	73417000.0	N/A	112.97
88	Na	Octylsulfate	2.15	0.408	N/A	367.43
89	Na	PF_6	593.25	155.451	N/A	182.35
90	Na	Toluene-4-sulfonate	1.07	0.242	N/A	282.43
91	1-butyl-2,3-dimethyl-imidazolium	SO_4	8.31	0.909	121.60	3.54E+11
92	1-butyl-2,3-dimethyl-imidazolium	Cl	4.65	1.086	N/A	352.99
93	1-butyl-2,3-dimethyl-imidazolium	F	6.57	1.678	N/A	335.19
94	1-butyl-2,3-dimethyl-imidazolium	2-chlorophenol	3.72	0.583	223.94	156.52
95	1-butyl-2,3-dimethyl-imidazolium	3-chlorophenol	3.66	0.574	224.42	121.85

96	1-butyl-2,3-dimethyl-imidazolium	4-chlorophenol	3.68	0.576	248.56	128.42
97	1-butyl-2,3-dimethyl-imidazolium	Benzoicacid	3.88	0.622	242.54	507.20
98	1-butyl-2,3-dimethyl-imidazolium	BF_4	3.01	0.551	265.91	162.12
99	1-butyl-2,3-dimethyl-imidazolium	Bis((trifluoromethyl)sulfonyl)imide	3.97	0.403	267.46	574.16
100	1-butyl-2,3-dimethyl-imidazolium	Butylsulfate	3.68	0.528	226.48	513.32
101	1-butyl-2,3-dimethyl-imidazolium	Ethylsulfate	3.57	0.565	220.45	215.00
102	1-butyl-2,3-dimethyl-imidazolium	NO_2	4.07	0.898	178.77	60.40
103	1-butyl-2,3-dimethyl-imidazolium	Octylsulfate	4.05	0.492	234.27	619.49
104	1-butyl-2,3-dimethyl-imidazolium	PF_6	3.15	0.465	341.46	434.42
105	1-butyl-2,3-dimethyl-imidazolium	Toluene-4-sulfonate	4.03	0.546	246.75	534.49
106	1-butyl-3-methyl-imidazolium	SO_4	6.34	0.745	113.63	3.63E+11
107	1-butyl-3-methyl-imidazolium	Cl	3.43	0.865	N/A	324.30
108	1-butyl-3-methyl-imidazolium	F	5.65	1.572	N/A	306.51
109	1-butyl-3-methyl-imidazolium	2-chlorophenol	3.02	0.499	210.80	164.13
110	1-butyl-3-methyl-imidazolium	3-chlorophenol	2.99	0.494	211.28	127.79
111	1-butyl-3-methyl-imidazolium	4-chlorophenol	3.00	0.495	233.98	134.66
112	1-butyl-3-methyl-imidazolium	Benzoicacid	3.08	0.521	228.00	532.22
113	1-butyl-3-methyl-imidazolium	BF_4	2.18	0.424	247.06	165.99
114	1-butyl-3-methyl-imidazolium	Bis((trifluoromethyl)sulfonyl)imide	3.42	0.359	253.65	545.48
115	1-butyl-3-methyl-imidazolium	Butylsulfate	2.92	0.439	214.86	390.79
116	1-butyl-3-methyl-imidazolium	Ethylsulfate	2.73	0.455	208.11	224.45
117	1-butyl-3-methyl-imidazolium	NO_2	2.94	0.7	165.54	60.89
118	1-butyl-3-methyl-imidazolium	Octylsulfate	3.38	0.426	223.90	590.81
119	1-butyl-3-methyl-imidazolium	PF_6	2.50	0.387	318.40	405.73
120	1-butyl-3-methyl-imidazolium	Toluene-4-sulfonate	3.21	0.454	233.06	959.69
121	1-ethyl-2,3-dimethyl-imidazolium	SO_4	14.14	1.796	129.09	2.21E+11
122	1-ethyl-2,3-dimethyl-imidazolium	Cl	7.43	2.035	N/A	296.34
123	1-ethyl-2,3-dimethyl-imidazolium	F	13.25	4.045	N/A	278.54
124	1-ethyl-2,3-dimethyl-imidazolium	2-chlorophenol	3.42	0.595	218.26	102.21
125	1-ethyl-2,3-dimethyl-imidazolium	3-chlorophenol	3.34	0.582	218.77	79.59
126	1-ethyl-2,3-dimethyl-imidazolium	4-chlorophenol	3.39	0.591	245.82	83.85
127	1-ethyl-2,3-dimethyl-imidazolium	Benzoicacid	3.87	0.692	238.98	331.68
128	1-ethyl-2,3-dimethyl-imidazolium	BF_4	2.84	0.59	270.11	100.67
129	1-ethyl-2,3-dimethyl-imidazolium	Bis((trifluoromethyl)sulfonyl)imide	3.45	0.375	267.28	517.51
130	1-ethyl-2,3-dimethyl-imidazolium	Butylsulfate	3.43	0.543	221.11	245.13
131	1-ethyl-2,3-dimethyl-imidazolium	Ethylsulfate	3.51	0.617	215.04	139.08
132	1-ethyl-2,3-dimethyl-imidazolium	NO_2	5.50	1.413	169.65	36.29
133	1-ethyl-2,3-dimethyl-imidazolium	Octylsulfate	3.74	0.493	228.96	562.84
134	1-ethyl-2,3-dimethyl-imidazolium	PF_6	2.44	0.398	365.87	377.77
135	1-ethyl-2,3-dimethyl-imidazolium	Toluene-4-sulfonate	3.88	0.576	242.89	604.41
136	1-ethyl-3-methyl-imidazolium	SO_4	11.63	1.607	119.06	2.15E+11
137	1-ethyl-3-methyl-imidazolium	Cl	5.81	1.745	N/A	268.96
138	1-ethyl-3-methyl-imidazolium	F	12.82	4.336	N/A	251.17
139	1-ethyl-3-methyl-imidazolium	2-chlorophenol	2.66	0.491	204.33	102.37
140	1-ethyl-3-methyl-imidazolium	3-chlorophenol	2.62	0.483	204.83	109.72
141	1-ethyl-3-methyl-imidazolium	4-chlorophenol	2.66	0.491	230.12	103.97
142	1-ethyl-3-methyl-imidazolium	Benzoicacid	2.99	0.567	223.44	332.43
143	1-ethyl-3-methyl-imidazolium	BF_4	1.91	0.425	299.21	97.85
144	1-ethyl-3-methyl-imidazolium	Bis((trifluoromethyl)sulfonyl)imide	2.89	0.325	252.63	490.14
145	1-ethyl-3-methyl-imidazolium	Butylsulfate	2.64	0.44	208.82	247.49
146	1-ethyl-3-methyl-imidazolium	Ethylsulfate	2.59	0.482	201.98	138.50
147	1-ethyl-3-methyl-imidazolium	NO_2	4.03	1.128	155.56	34.59
148	1-ethyl-3-methyl-imidazolium	Octylsulfate	3.08	0.423	218.03	535.46
149	1-ethyl-3-methyl-imidazolium	PF_6	1.73	0.298	339.18	350.39
150	1-ethyl-3-methyl-imidazolium	Toluene-4-sulfonate	3.00	0.468	228.29	613.00
151	1-hexyl-3-methyl-imidazolium	SO_4	5.04	0.515	109.05	5.92E+11
152	1-hexyl-3-methyl-imidazolium	Cl	2.89	0.626	N/A	380.12
153	1-hexyl-3-methyl-imidazolium	F	3.88	0.916	N/A	362.32
154	1-hexyl-3-methyl-imidazolium	2-chlorophenol	3.30	0.493	216.18	257.27
155	1-hexyl-3-methyl-imidazolium	3-chlorophenol	3.28	0.489	216.63	200.26
156	1-hexyl-3-methyl-imidazolium	4-chlorophenol	3.27	0.488	237.24	211.10
157	1-hexyl-3-methyl-imidazolium	Benzoicacid	3.21	0.491	231.86	833.23

158	1-hexyl-3-methyl-imidazolium	BF_4	2.55	0.442	246.58	271.91
159	1-hexyl-3-methyl-imidazolium	Bis((trifluoromethyl)sulfonyl)imide	3.81	0.375	254.84	601.29
160	1-hexyl-3-methyl-imidazolium	Butylsulfate	3.15	0.433	219.80	540.44
161	1-hexyl-3-methyl-imidazolium	Ethylsulfate	2.93	0.441	213.20	354.76
162	1-hexyl-3-methyl-imidazolium	NO_2	2.79	0.575	173.78	102.65
163	1-hexyl-3-methyl-imidazolium	Octylsulfate	3.60	0.421	228.66	646.62
164	1-hexyl-3-methyl-imidazolium	PF_6	3.10	0.437	306.29	461.55
165	1-hexyl-3-methyl-imidazolium	Toluene-4-sulfonate	3.39	0.441	236.98	561.62
166	1-pentyl-3-methyl-imidazolium	SO_4	5.44	0.595	111.27	4.68E+11
167	1-pentyl-3-methyl-imidazolium	cl	3.05	0.71	N/A	352.26
168	1-pentyl-3-methyl-imidazolium	F	4.45	1.138	N/A	334.47
169	1-pentyl-3-methyl-imidazolium	2-chlorophenol	3.17	0.496	214.01	207.33
170	1-pentyl-3-methyl-imidazolium	3-chlorophenol	3.14	0.492	214.48	161.41
171	1-pentyl-3-methyl-imidazolium	4-chlorophenol	3.14	0.491	236.12	170.12
172	1-pentyl-3-methyl-imidazolium	Benzoicacid	3.14	0.503	230.47	671.87
173	1-pentyl-3-methyl-imidazolium	BF_4	2.36	0.433	247.32	214.63
174	1-pentyl-3-methyl-imidazolium	Bis((trifluoromethyl)sulfonyl)imide	3.63	0.369	254.61	573.44
175	1-pentyl-3-methyl-imidazolium	Butylsulfate	3.04	0.436	217.76	512.59
176	1-pentyl-3-methyl-imidazolium	Ethylsulfate	2.83	0.447	211.12	284.78
177	1-pentyl-3-methyl-imidazolium	NO_2	2.80	0.619	170.24	79.94
178	1-pentyl-3-methyl-imidazolium	Octylsulfate	3.49	0.424	226.66	618.77
179	1-pentyl-3-methyl-imidazolium	PF_6	2.82	0.417	312.35	433.69
180	1-pentyl-3-methyl-imidazolium	Toluene-4-sulfonate	3.30	0.447	235.52	1200.28
181	4-methyl-n-butylpyridinium	SO_4	6.33	0.703	119.88	3.49E+11
182	4-methyl-n-butylpyridinium	cl	3.64	0.864	N/A	346.71
183	4-methyl-n-butylpyridinium	F	4.81	1.25	N/A	328.91
184	4-methyl-n-butylpyridinium	2-chlorophenol	3.42	0.542	218.10	155.25
185	4-methyl-n-butylpyridinium	3-chlorophenol	3.37	0.534	218.56	120.86
186	4-methyl-n-butylpyridinium	4-chlorophenol	3.37	0.534	242.06	127.38
187	4-methyl-n-butylpyridinium	Benzoicacid	3.47	0.563	236.22	503.16
188	4-methyl-n-butylpyridinium	BF_4	2.77	0.514	256.99	160.01
189	4-methyl-n-butylpyridinium	Bis((trifluoromethyl)sulfonyl)imide	3.82	0.39	261.09	567.88
190	4-methyl-n-butylpyridinium	Butylsulfate	3.41	0.494	221.11	507.03
191	4-methyl-n-butylpyridinium	Ethylsulfate	3.25	0.52	214.66	213.06
192	4-methyl-n-butylpyridinium	NO_2	3.38	0.759	172.11	59.42
193	4-methyl-n-butylpyridinium	Octylsulfate	3.81	0.467	229.59	613.21
194	4-methyl-n-butylpyridinium	PF_6	3.06	0.456	330.81	428.13
195	4-methyl-n-butylpyridinium	Toluene-4-sulfonate	3.69	0.506	240.76	900.47
196	Aniline	SO_4	0.49	0.076	139.64	1.59E+12
197	Aniline	Cl	0.23	0.077	N/A	234.00
198	Aniline	F	0.88	0.341	N/A	216.21
199	Aniline	2-chlorophenol	1.29	0.256	202.42	787.41
200	Aniline	3-chlorophenol	1.38	0.273	202.33	613.27
201	Aniline	4-chlorophenol	1.34	0.266	232.19	645.82
202	Aniline	Benzoicacid	0.98	0.2	228.58	2560.20
203	Aniline	BF_4	0.56	0.135	270.82	718.82
204	Aniline	Bis((trifluoromethyl)sulfonyl)imide	1.79	0.21	266.27	455.18
205	Aniline	Butylsulfate	1.05	0.186	209.77	1927.48
206	Aniline	Ethylsulfate	0.69	0.138	203.72	1056.17
207	Aniline	NO_2	0.25	0.078	152.78	246.49
208	Aniline	Octylsulfate	1.68	0.244	218.22	500.51
209	Aniline	PF_6	2.29	0.422	408.77	315.43
210	Aniline	Toluene-4-sulfonate	1.10	0.183	233.27	4807.36
211	n-butyl-isoquinolinium	SO_4	5.85	0.549	132.06	4.33E+11
212	n-butyl-isoquinolinium	Cl	3.39	0.672	N/A	392.03
213	n-butyl-isoquinolinium	F	4.33	0.929	N/A	374.23
214	n-butyl-isoquinolinium	2-chlorophenol	3.61	0.506	221.37	186.61
215	n-butyl-isoquinolinium	3-chlorophenol	3.57	0.501	221.79	145.26
216	n-butyl-isoquinolinium	4-chlorophenol	3.56	0.499	245.62	153.13
217	n-butyl-isoquinolinium	Benzoicacid	3.55	0.508	240.17	604.26
218	n-butyl-isoquinolinium	BF_4	2.92	0.471	259.67	198.87
219	n-butyl-isoquinolinium	Bis((trifluoromethyl)sulfonyl)imide	4.10	0.387	266.28	613.20
220	n-butyl-isoquinolinium	Butylsulfate	3.53	0.458	224.09	552.35
221	n-butyl-isoquinolinium	Ethylsulfate	3.33	0.47	217.40	257.73
222	n-butyl-isoquinolinium	NO_2	3.26	0.618	173.29	75.48
223	n-butyl-isoquinolinium	Octylsulfate	3.96	0.441	232.82	658.53
224	n-butyl-isoquinolinium	PF_6	3.41	0.453	336.00	473.46
225	n-butyl-isoquinolinium	Toluene-4-sulfonate	3.77	0.464	245.02	573.53
226	Pyridine	SO_4	11.33	1.946	124.78	2.34E+11
227	Pyridine	Cl	3.63	1.383	N/A	206.95
228	Pyridine	F	38.46	17.079	N/A	189.16
229	Pyridine	2-chlorophenol	1.18	0.25	184.79	120.87
230	Pyridine	3-chlorophenol	1.22	0.258	185.26	101.90
231	Pyridine	4-chlorophenol	1.24	0.262	212.53	108.20
232	Pyridine	Benzoicacid	1.29	0.283	205.75	393.47
233	Pyridine	BF_4	0.27	0.071	240.79	105.55
234	Pyridine	Bis((trifluoromethyl)sulfonyl)imide	1.66	0.202	243.08	428.13
235	Pyridine	Butylsulfate	1.11	0.209	192.27	299.44
236	Pyridine	Ethylsulfate	0.83	0.178	184.52	160.79
237	Pyridine	NO_2	1.28	0.445	130.53	35.10
238	Pyridine	Octylsulfate	1.75	0.266	203.22	473.46
239	Pyridine	PF_6	0.60	0.117	366.21	288.38
240	Pyridine	Toluene-4-sulfonate	1.30	0.228	211.81	751.81

Table S6. COSMO-RS predicted gas capacity screened with capacity (> 0.023)

Combination No	Cation	Anion	Gas Capacity (molCO2/mol IL)	Gas Capacity (gCO2/g IL)	Melting Point (K)	Viscosity (cP)
1	1-heptyl-3-methyl-imidazolium	SO_4	4.77	0.458	106.98	7.36E+11
2	1-heptyl-3-methyl-imidazolium	Cl	2.79	0.566	N/A	407.88
3	1-heptyl-3-methyl-imidazolium	F	3.46	0.761	N/A	390.08
4	1-heptyl-3-methyl-imidazolium	2-chlorophenol	3.43	0.488	218.18	314.56
5	1-heptyl-3-methyl-imidazolium	3-chlorophenol	3.40	0.484	218.62	244.85
6	1-heptyl-3-methyl-imidazolium	4-chlorophenol	3.38	0.482	238.28	258.13
7	1-heptyl-3-methyl-imidazolium	Benzoicacid	3.28	0.478	233.17	1018.29
8	1-heptyl-3-methyl-imidazolium	BF_4	2.74	0.449	246.10	338.74
9	1-heptyl-3-methyl-imidazolium	Bis((trifluoromethyl)sulfonyl)imide	3.97	0.379	255.11	629.05
10	1-heptyl-3-methyl-imidazolium	Butylsulfate	3.26	0.429	221.66	568.21
11	1-heptyl-3-methyl-imidazolium	Ethylsulfate	3.03	0.436	215.12	435.31
12	1-heptyl-3-methyl-imidazolium	NO_2	2.80	0.543	177.02	129.44
13	1-heptyl-3-methyl-imidazolium	Octylsulfate	3.70	0.417	230.48	674.38
14	1-heptyl-3-methyl-imidazolium	PF_6	3.36	0.453	301.38	489.31
15	1-heptyl-3-methyl-imidazolium	Toluene-4-sulfonate	3.48	0.435	238.33	589.38
16	1-octyl-3-methyl-imidazolium	SO_4	4.64	0.42	105.10	9.08E+11
17	1-octyl-3-methyl-imidazolium	Cl	2.76	0.526	N/A	435.88
18	1-octyl-3-methyl-imidazolium	F	3.19	0.656	N/A	418.08
19	1-octyl-3-methyl-imidazolium	2-chlorophenol	3.54	0.483	220.20	381.91
20	1-octyl-3-methyl-imidazolium	3-chlorophenol	3.51	0.479	220.63	297.25
21	1-octyl-3-methyl-imidazolium	4-chlorophenol	3.49	0.475	239.45	313.42
22	1-octyl-3-methyl-imidazolium	Benzoicacid	3.36	0.467	234.60	1235.73
23	1-octyl-3-methyl-imidazolium	BF_4	2.93	0.457	245.99	418.39
24	1-octyl-3-methyl-imidazolium	Bis((trifluoromethyl)sulfonyl)imide	4.12	0.382	255.54	657.06
25	1-octyl-3-methyl-imidazolium	Butylsulfate	3.38	0.426	223.54	596.21
26	1-octyl-3-methyl-imidazolium	Ethylsulfate	3.15	0.433	217.07	543.21
27	1-octyl-3-methyl-imidazolium	NO_2	2.86	0.522	180.23	161.67
28	1-octyl-3-methyl-imidazolium	Octylsulfate	3.80	0.414	232.28	702.38
29	1-octyl-3-methyl-imidazolium	PF_6	3.59	0.465	297.51	517.31
30	1-octyl-3-methyl-imidazolium	Toluene-4-sulfonate	3.58	0.43	239.76	617.39
31	Pyrrolidine	SO_4	3.46	0.634	124.56	3.87E+11
32	Pyrrolidine	Cl	1.38	0.566	N/A	206.56
33	Pyrrolidine	F	6.78	3.276	N/A	188.76
34	Pyrrolidine	2-chlorophenol	1.22	0.27	184.29	200.16
35	Pyrrolidine	3-chlorophenol	1.26	0.278	185.03	155.92
36	Pyrrolidine	4-chlorophenol	1.27	0.279	212.39	164.14
37	Pyrrolidine	Benzoicacid	1.29	0.293	203.94	651.58
38	Pyrrolidine	BF_4	0.27	0.075	229.74	174.66
39	Pyrrolidine	Bis((trifluoromethyl)sulfonyl)imide	1.62	0.202	240.52	427.74
40	Pyrrolidine	Butylsulfate	1.14	0.223	194.07	495.95
41	Pyrrolidine	Ethylsulfate	0.84	0.188	185.60	266.22
42	Pyrrolidine	NO_2	0.83	0.311	133.28	58.10
43	Pyrrolidine	Octylsulfate	1.80	0.281	205.42	473.06
44	Pyrrolidine	PF_6	0.67	0.135	345.98	287.99
45	Pyrrolidine	Toluene-4-sulfonate	1.37	0.248	210.90	388.07
46	H_3O	SO_4	2.33E+11	76600000000.0	N/A	157.70
47	H_3O	Cl	2.27E+14	183320000000000.0	N/A	107.57
48	H_3O	F	0.53	0.616	N/A	89.77
49	H_3O	2-chlorophenol	1.69	0.507	N/A	234.77
50	H_3O	3-chlorophenol	1.59	0.477	N/A	235.19
51	H_3O	4-chlorophenol	1.37	0.41	N/A	234.42
52	H_3O	Benzoicacid	0.48	0.151	N/A	237.78
53	H_3O	BF_4	14981.09	6230.003	N/A	151.82
54	H_3O	Bis((trifluoromethyl)sulfonyl)imide	1.76	0.259	N/A	328.74
55	H_3O	Butylsulfate	1.07	0.275	N/A	267.89
56	H_3O	Ethylsulfate	0.75	0.228	N/A	214.89
57	H_3O	NO_2	6.78E+05	458518.481	N/A	119.61
58	H_3O	Octylsulfate	1.69	0.327	N/A	374.07
59	H_3O	PF_6	245.45	65.873	N/A	189.00
60	H_3O	Toluene-4-sulfonate	0.77	0.177	N/A	289.07
61	NH_4	SO_4	1.63E+14	54341000000000.0	N/A	163.44
62	NH_4	Cl	4.04E+10	33261000000.0	N/A	113.31
63	NH_4	F	1.66E+18	##################	N/A	95.52
64	NH_4	2-chlorophenol	0.96	0.289	N/A	240.52
65	NH_4	3-chlorophenol	1.03	0.313	N/A	240.93
66	NH_4	4-chlorophenol	0.89	0.269	N/A	240.17
67	NH_4	Benzoicacid	0.25	0.079	N/A	243.52
68	NH_4	BF_4	6775.05	2843.919	N/A	157.57
69	NH_4	Bis((trifluoromethyl)sulfonyl)imide	1.14	0.168	N/A	334.49
70	NH_4	Butylsulfate	0.41	0.106	N/A	273.64
71	NH_4	Ethylsulfate	0.19	0.058	N/A	220.64
72	NH_4	NO_2	7513.72	5163.258	N/A	125.36
73	NH_4	Octylsulfate	0.87	0.169	N/A	379.82
74	NH_4	PF_6	158.76	42.865	N/A	194.74
75	NH_4	Toluene-4-sulfonate	0.32	0.075	N/A	294.82
76	Na	SO_4	1.58E+18	##################	N/A	151.06
77	Na	Cl	2.94E+16	##################	N/A	100.92
78	Na	F	3.33E+29	##################	N/A	83.13
79	Na	2-chlorophenol	3.10	0.906	N/A	228.13
80	Na	3-chlorophenol	2.64	0.773	N/A	228.55
81	Na	4-chlorophenol	2.24	0.654	N/A	227.78
82	Na	Benzoicacid	0.67	0.204	N/A	231.13
83	Na	BF_4	6.58E+04	26357.84	N/A	145.18
84	Na	Bis((trifluoromethyl)sulfonyl)imide	2.88	0.418	N/A	322.10
85	Na	Butylsulfate	1.64	0.411	N/A	261.25
86	Na	Ethylsulfate	1.86	0.553	N/A	208.25
87	Na	NO_2	1.15E+08	73417000.0	N/A	112.97
88	Na	Octylsulfate	2.15	0.408	N/A	367.43
89	Na	PF_6	593.25	155.451	N/A	182.35
90	Na	Toluene-4-sulfonate	1.07	0.242	N/A	282.43
91	1-butyl-2,3-dimethyl-imidazolium	SO_4	8.31	0.909	121.60	3.54E+11
92	1-butyl-2,3-dimethyl-imidazolium	Cl	4.65	1.086	N/A	352.99
93	1-butyl-2,3-dimethyl-imidazolium	F	6.57	1.678	N/A	335.19
94	1-butyl-2,3-dimethyl-imidazolium	2-chlorophenol	3.72	0.583	223.94	156.52
95	1-butyl-2,3-dimethyl-imidazolium	3-chlorophenol	3.66	0.574	224.42	121.85

96	1-butyl-2,3-dimethyl-imidazolium	4-chlorophenol	3.68	0.576	248.56	128.42
97	1-butyl-2,3-dimethyl-imidazolium	Benzoicacid	3.88	0.622	242.54	507.20
98	1-butyl-2,3-dimethyl-imidazolium	BF_4	3.01	0.551	265.91	162.12
99	1-butyl-2,3-dimethyl-imidazolium	Bis((trifluoromethyl)sulfonyl)imide	3.97	0.403	267.46	574.16
100	1-butyl-2,3-dimethyl-imidazolium	Butylsulfate	3.68	0.528	226.48	513.32
101	1-butyl-2,3-dimethyl-imidazolium	Ethylsulfate	3.57	0.565	220.45	215.00
102	1-butyl-2,3-dimethyl-imidazolium	NO_2	4.07	0.898	178.77	60.40
103	1-butyl-2,3-dimethyl-imidazolium	Octylsulfate	4.05	0.492	234.27	619.49
104	1-butyl-2,3-dimethyl-imidazolium	PF_6	3.15	0.465	341.46	434.42
105	1-butyl-2,3-dimethyl-imidazolium	Toluene-4-sulfonate	4.03	0.546	246.75	534.49
106	1-butyl-3-methyl-imidazolium	SO_4	6.34	0.745	113.63	3.63E+11
107	1-butyl-3-methyl-imidazolium	Cl	3.43	0.865	N/A	324.30
108	1-butyl-3-methyl-imidazolium	F	5.65	1.572	N/A	306.51
109	1-butyl-3-methyl-imidazolium	2-chlorophenol	3.02	0.499	210.80	164.13
110	1-butyl-3-methyl-imidazolium	3-chlorophenol	2.99	0.494	211.28	127.79
111	1-butyl-3-methyl-imidazolium	4-chlorophenol	3.00	0.495	233.98	134.66
112	1-butyl-3-methyl-imidazolium	Benzoicacid	3.08	0.521	228.00	532.22
113	1-butyl-3-methyl-imidazolium	BF_4	2.18	0.424	247.06	165.99
114	1-butyl-3-methyl-imidazolium	Bis((trifluoromethyl)sulfonyl)imide	3.42	0.359	253.65	545.48
115	1-butyl-3-methyl-imidazolium	Butylsulfate	2.92	0.439	214.86	390.79
116	1-butyl-3-methyl-imidazolium	Ethylsulfate	2.73	0.455	208.11	224.45
117	1-butyl-3-methyl-imidazolium	NO_2	2.94	0.7	165.54	60.89
118	1-butyl-3-methyl-imidazolium	Octylsulfate	3.38	0.426	223.90	590.81
119	1-butyl-3-methyl-imidazolium	PF_6	2.50	0.387	318.40	405.73
120	1-butyl-3-methyl-imidazolium	Toluene-4-sulfonate	3.21	0.454	233.06	959.69
121	1-ethyl-2,3-dimethyl-imidazolium	SO_4	14.14	1.796	129.09	2.21E+11
122	1-ethyl-2,3-dimethyl-imidazolium	Cl	7.43	2.035	N/A	296.34
123	1-ethyl-2,3-dimethyl-imidazolium	F	13.25	4.045	N/A	278.54
124	1-ethyl-2,3-dimethyl-imidazolium	2-chlorophenol	3.42	0.595	218.26	102.21
125	1-ethyl-2,3-dimethyl-imidazolium	3-chlorophenol	3.34	0.582	218.77	79.59
126	1-ethyl-2,3-dimethyl-imidazolium	4-chlorophenol	3.39	0.591	245.82	83.85
127	1-ethyl-2,3-dimethyl-imidazolium	Benzoicacid	3.87	0.692	238.98	331.68
128	1-ethyl-2,3-dimethyl-imidazolium	BF_4	2.84	0.59	270.11	100.67
129	1-ethyl-2,3-dimethyl-imidazolium	Bis((trifluoromethyl)sulfonyl)imide	3.45	0.375	267.28	517.51
130	1-ethyl-2,3-dimethyl-imidazolium	Butylsulfate	3.43	0.543	221.11	245.13
131	1-ethyl-2,3-dimethyl-imidazolium	Ethylsulfate	3.51	0.617	215.04	139.08
132	1-ethyl-2,3-dimethyl-imidazolium	NO_2	5.50	1.413	169.65	36.29
133	1-ethyl-2,3-dimethyl-imidazolium	Octylsulfate	3.74	0.493	228.96	562.84
134	1-ethyl-2,3-dimethyl-imidazolium	PF_6	2.44	0.398	365.87	377.77
135	1-ethyl-2,3-dimethyl-imidazolium	Toluene-4-sulfonate	3.88	0.576	242.89	604.41
136	1-ethyl-3-methyl-imidazolium	SO_4	11.63	1.607	119.06	2.15E+11
137	1-ethyl-3-methyl-imidazolium	Cl	5.81	1.745	N/A	268.96
138	1-ethyl-3-methyl-imidazolium	F	12.82	4.336	N/A	251.17
139	1-ethyl-3-methyl-imidazolium	2-chlorophenol	2.66	0.491	204.33	102.37
140	1-ethyl-3-methyl-imidazolium	3-chlorophenol	2.62	0.483	204.83	109.72
141	1-ethyl-3-methyl-imidazolium	4-chlorophenol	2.66	0.491	230.12	103.97
142	1-ethyl-3-methyl-imidazolium	Benzoicacid	2.99	0.567	223.44	332.43
143	1-ethyl-3-methyl-imidazolium	BF_4	1.91	0.425	299.21	97.85
144	1-ethyl-3-methyl-imidazolium	Bis((trifluoromethyl)sulfonyl)imide	2.89	0.325	252.63	490.14
145	1-ethyl-3-methyl-imidazolium	Butylsulfate	2.64	0.44	208.82	247.49
146	1-ethyl-3-methyl-imidazolium	Ethylsulfate	2.59	0.482	201.98	138.50
147	1-ethyl-3-methyl-imidazolium	NO_2	4.03	1.128	155.56	34.59
148	1-ethyl-3-methyl-imidazolium	Octylsulfate	3.08	0.423	218.03	535.46
149	1-ethyl-3-methyl-imidazolium	PF_6	1.73	0.298	339.18	350.39
150	1-ethyl-3-methyl-imidazolium	Toluene-4-sulfonate	3.00	0.468	228.29	613.00
151	1-hexyl-3-methyl-imidazolium	SO_4	5.04	0.515	109.05	5.92E+11
152	1-hexyl-3-methyl-imidazolium	Cl	2.89	0.626	N/A	380.12
153	1-hexyl-3-methyl-imidazolium	F	3.88	0.916	N/A	362.32
154	1-hexyl-3-methyl-imidazolium	2-chlorophenol	3.30	0.493	216.18	257.27
155	1-hexyl-3-methyl-imidazolium	3-chlorophenol	3.28	0.489	216.63	200.26
156	1-hexyl-3-methyl-imidazolium	4-chlorophenol	3.27	0.488	237.24	211.10
157	1-hexyl-3-methyl-imidazolium	Benzoicacid	3.21	0.491	231.86	833.23

158	1-hexyl-3-methyl-imidazolium	BF_4	2.55	0.442	246.58	271.91
159	1-hexyl-3-methyl-imidazolium	Bis((trifluoromethyl)sulfonyl)imide	3.81	0.375	254.84	601.29
160	1-hexyl-3-methyl-imidazolium	Butylsulfate	3.15	0.433	219.80	540.44
161	1-hexyl-3-methyl-imidazolium	Ethylsulfate	2.93	0.441	213.20	354.76
162	1-hexyl-3-methyl-imidazolium	NO_2	2.79	0.575	173.78	102.65
163	1-hexyl-3-methyl-imidazolium	Octylsulfate	3.60	0.421	228.66	646.62
164	1-hexyl-3-methyl-imidazolium	PF_6	3.10	0.437	306.29	461.55
165	1-hexyl-3-methyl-imidazolium	Toluene-4-sulfonate	3.39	0.441	236.98	561.62
166	1-pentyl-3-methyl-imidazolium	SO_4	5.44	0.595	111.27	4.68E+11
167	1-pentyl-3-methyl-imidazolium	cl	3.05	0.71	N/A	352.26
168	1-pentyl-3-methyl-imidazolium	F	4.45	1.138	N/A	334.47
169	1-pentyl-3-methyl-imidazolium	2-chlorophenol	3.17	0.496	214.01	207.33
170	1-pentyl-3-methyl-imidazolium	3-chlorophenol	3.14	0.492	214.48	161.41
171	1-pentyl-3-methyl-imidazolium	4-chlorophenol	3.14	0.491	236.12	170.12
172	1-pentyl-3-methyl-imidazolium	Benzoicacid	3.14	0.503	230.47	671.87
173	1-pentyl-3-methyl-imidazolium	BF_4	2.36	0.433	247.32	214.63
174	1-pentyl-3-methyl-imidazolium	Bis((trifluoromethyl)sulfonyl)imide	3.63	0.369	254.61	573.44
175	1-pentyl-3-methyl-imidazolium	Butylsulfate	3.04	0.436	217.76	512.59
176	1-pentyl-3-methyl-imidazolium	Ethylsulfate	2.83	0.447	211.12	284.78
177	1-pentyl-3-methyl-imidazolium	NO_2	2.80	0.619	170.24	79.94
178	1-pentyl-3-methyl-imidazolium	Octylsulfate	3.49	0.424	226.66	618.77
179	1-pentyl-3-methyl-imidazolium	PF_6	2.82	0.417	312.35	433.69
180	1-pentyl-3-methyl-imidazolium	Toluene-4-sulfonate	3.30	0.447	235.52	1200.28
181	4-methyl-n-butylpyridinium	SO_4	6.33	0.703	119.88	3.49E+11
182	4-methyl-n-butylpyridinium	cl	3.64	0.864	N/A	346.71
183	4-methyl-n-butylpyridinium	F	4.81	1.25	N/A	328.91
184	4-methyl-n-butylpyridinium	2-chlorophenol	3.42	0.542	218.10	155.25
185	4-methyl-n-butylpyridinium	3-chlorophenol	3.37	0.534	218.56	120.86
186	4-methyl-n-butylpyridinium	4-chlorophenol	3.37	0.534	242.06	127.38
187	4-methyl-n-butylpyridinium	Benzoicacid	3.47	0.563	236.22	503.16
188	4-methyl-n-butylpyridinium	BF_4	2.77	0.514	256.99	160.01
189	4-methyl-n-butylpyridinium	Bis((trifluoromethyl)sulfonyl)imide	3.82	0.39	261.09	567.88
190	4-methyl-n-butylpyridinium	Butylsulfate	3.41	0.494	221.11	507.03
191	4-methyl-n-butylpyridinium	Ethylsulfate	3.25	0.52	214.66	213.06
192	4-methyl-n-butylpyridinium	NO_2	3.38	0.759	172.11	59.42
193	4-methyl-n-butylpyridinium	Octylsulfate	3.81	0.467	229.59	613.21
194	4-methyl-n-butylpyridinium	PF_6	3.06	0.456	330.81	428.13
195	4-methyl-n-butylpyridinium	Toluene-4-sulfonate	3.69	0.506	240.76	900.47
196	Aniline	SO_4	0.49	0.076	139.64	1.59E+12
197	Aniline	Cl	0.23	0.077	N/A	234.00
198	Aniline	F	0.88	0.341	N/A	216.21
199	Aniline	2-chlorophenol	1.29	0.256	202.42	787.41
200	Aniline	3-chlorophenol	1.38	0.273	202.33	613.27
201	Aniline	4-chlorophenol	1.34	0.266	232.19	645.82
202	Aniline	Benzoicacid	0.98	0.2	228.58	2560.20
203	Aniline	BF_4	0.56	0.135	270.82	718.82
204	Aniline	Bis((trifluoromethyl)sulfonyl)imide	1.79	0.21	266.27	455.18
205	Aniline	Butylsulfate	1.05	0.186	209.77	1927.48
206	Aniline	Ethylsulfate	0.69	0.138	203.72	1056.17
207	Aniline	NO_2	0.25	0.078	152.78	246.49
208	Aniline	Octylsulfate	1.68	0.244	218.22	500.51
209	Aniline	PF_6	2.29	0.422	408.77	315.43
210	Aniline	Toluene-4-sulfonate	1.10	0.183	233.27	4807.36
211	n-butyl-isoquinolinium	SO_4	5.85	0.549	132.06	4.33E+11
212	n-butyl-isoquinolinium	Cl	3.39	0.672	N/A	392.03
213	n-butyl-isoquinolinium	F	4.33	0.929	N/A	374.23
214	n-butyl-isoquinolinium	2-chlorophenol	3.61	0.506	221.37	186.61
215	n-butyl-isoquinolinium	3-chlorophenol	3.57	0.501	221.79	145.26
216	n-butyl-isoquinolinium	4-chlorophenol	3.56	0.499	245.62	153.13
217	n-butyl-isoquinolinium	Benzoicacid	3.55	0.508	240.17	604.26
218	n-butyl-isoquinolinium	BF_4	2.92	0.471	259.67	198.87
219	n-butyl-isoquinolinium	Bis((trifluoromethyl)sulfonyl)imide	4.10	0.387	266.28	613.20
220	n-butyl-isoquinolinium	Butylsulfate	3.53	0.458	224.09	552.35
221	n-butyl-isoquinolinium	Ethylsulfate	3.33	0.47	217.40	257.73
222	n-butyl-isoquinolinium	NO_2	3.26	0.618	173.29	75.48
223	n-butyl-isoquinolinium	Octylsulfate	3.96	0.441	232.82	658.53
224	n-butyl-isoquinolinium	PF_6	3.41	0.453	336.00	473.46
225	n-butyl-isoquinolinium	Toluene-4-sulfonate	3.77	0.464	245.02	573.53
226	Pyridine	SO_4	11.33	1.946	124.78	2.34E+11
227	Pyridine	Cl	3.63	1.383	N/A	206.95
228	Pyridine	F	38.46	17.079	N/A	189.16
229	Pyridine	2-chlorophenol	1.18	0.25	184.79	120.87
230	Pyridine	3-chlorophenol	1.22	0.258	185.26	101.90
231	Pyridine	4-chlorophenol	1.24	0.262	212.53	108.20
232	Pyridine	Benzoicacid	1.29	0.283	205.75	393.47
233	Pyridine	BF_4	0.27	0.071	240.79	105.55
234	Pyridine	Bis((trifluoromethyl)sulfonyl)imide	1.66	0.202	243.08	428.13
235	Pyridine	Butylsulfate	1.11	0.209	192.27	299.44
236	Pyridine	Ethylsulfate	0.83	0.178	184.52	160.79
237	Pyridine	NO_2	1.28	0.445	130.53	35.10
238	Pyridine	Octylsulfate	1.75	0.266	203.22	473.46
239	Pyridine	PF_6	0.60	0.117	366.21	288.38
240	Pyridine	Toluene-4-sulfonate	1.30	0.228	211.81	751.81

Table S7. COSMO-RS predicted gas capacity screened with Melting point (< 298.15K)

Combination No	Cation	Anion	Gas Capacity (mol_{CO2}/mol_{IL})	Gas Capacity (gCO_2/g IL)	Melting Point (K)	Viscosity (cP)
1	1-heptyl-3-methyl-imidazolium	SO_4	4.77	0.458	106.98	7.36E+11
4	1-heptyl-3-methyl-imidazolium	2-chlorophenol	3.43	0.488	218.18	314.56
5	1-heptyl-3-methyl-imidazolium	3-chlorophenol	3.40	0.484	218.62	244.85
6	1-heptyl-3-methyl-imidazolium	4-chlorophenol	3.38	0.482	238.28	258.13
7	1-heptyl-3-methyl-imidazolium	Benzoicacid	3.28	0.478	233.17	1018.29
8	1-heptyl-3-methyl-imidazolium	BF_4	2.74	0.449	246.10	338.74
9	1-heptyl-3-methyl-imidazolium	Bis((trifluoromethyl)sulfonyl)imide	3.97	0.379	255.11	629.05
10	1-heptyl-3-methyl-imidazolium	Butylsulfate	3.26	0.429	221.66	568.21
11	1-heptyl-3-methyl-imidazolium	Ethylsulfate	3.03	0.436	215.12	435.31
12	1-heptyl-3-methyl-imidazolium	NO_2	2.80	0.543	177.02	129.44
13	1-heptyl-3-methyl-imidazolium	Octylsulfate	3.70	0.417	230.48	674.38
15	1-heptyl-3-methyl-imidazolium	Toluene-4-sulfonate	3.48	0.435	238.33	589.38
16	1-octyl-3-methyl-imidazolium	SO_4	4.64	0.42	105.10	9.08E+11
19	1-octyl-3-methyl-imidazolium	2-chlorophenol	3.54	0.483	220.20	381.91
20	1-octyl-3-methyl-imidazolium	3-chlorophenol	3.51	0.479	220.63	297.25
21	1-octyl-3-methyl-imidazolium	4-chlorophenol	3.49	0.475	239.45	313.42
22	1-octyl-3-methyl-imidazolium	Benzoicacid	3.36	0.467	234.60	1235.73
23	1-octyl-3-methyl-imidazolium	BF_4	2.93	0.457	245.99	418.39
24	1-octyl-3-methyl-imidazolium	Bis((trifluoromethyl)sulfonyl)imide	4.12	0.382	255.54	657.06
25	1-octyl-3-methyl-imidazolium	Butylsulfate	3.38	0.426	223.54	596.21
26	1-octyl-3-methyl-imidazolium	Ethylsulfate	3.15	0.433	217.07	543.21
27	1-octyl-3-methyl-imidazolium	NO_2	2.86	0.522	180.23	161.67
28	1-octyl-3-methyl-imidazolium	Octylsulfate	3.80	0.414	232.28	702.38
29	1-octyl-3-methyl-imidazolium	PF_6	3.59	0.465	297.51	517.31
30	1-octyl-3-methyl-imidazolium	Toluene-4-sulfonate	3.58	0.43	239.76	617.39
31	Pyrrolidine	SO_4	3.46	0.634	124.56	3.87E+11
34	Pyrrolidine	2-chlorophenol	1.22	0.27	184.29	200.16
35	Pyrrolidine	3-chlorophenol	1.26	0.278	185.03	155.92
36	Pyrrolidine	4-chlorophenol	1.27	0.279	212.39	164.14
37	Pyrrolidine	Benzoicacid	1.29	0.293	203.94	651.58
38	Pyrrolidine	BF_4	0.27	0.075	229.74	174.66
39	Pyrrolidine	Bis((trifluoromethyl)sulfonyl)imide	1.62	0.202	240.52	427.74
40	Pyrrolidine	Butylsulfate	1.14	0.223	194.07	495.95
41	Pyrrolidine	Ethylsulfate	0.84	0.188	185.60	266.22
42	Pyrrolidine	NO_2	0.83	0.311	133.28	58.10
43	Pyrrolidine	Octylsulfate	1.80	0.281	205.42	473.06
45	Pyrrolidine	Toluene-4-sulfonate	1.37	0.248	210.90	388.07
91	1-butyl-2,3-dimethyl-imidazolium	SO_4	8.31	0.909	121.60	3.54E+11
94	1-butyl-2,3-dimethyl-imidazolium	2-chlorophenol	3.72	0.583	223.94	156.52
95	1-butyl-2,3-dimethyl-imidazolium	3-chlorophenol	3.66	0.574	224.42	121.85
96	1-butyl-2,3-dimethyl-imidazolium	4-chlorophenol	3.68	0.576	248.56	128.42
97	1-butyl-2,3-dimethyl-imidazolium	Benzoicacid	3.88	0.622	242.54	507.20
98	1-butyl-2,3-dimethyl-imidazolium	BF_4	3.01	0.551	265.91	162.12
99	1-butyl-2,3-dimethyl-imidazolium	Bis((trifluoromethyl)sulfonyl)imide	3.97	0.403	267.46	574.16
100	1-butyl-2,3-dimethyl-imidazolium	Butylsulfate	3.68	0.528	226.48	513.32
101	1-butyl-2,3-dimethyl-imidazolium	Ethylsulfate	3.57	0.565	220.45	215.00
102	1-butyl-2,3-dimethyl-imidazolium	NO_2	4.07	0.898	178.77	60.40
103	1-butyl-2,3-dimethyl-imidazolium	Octylsulfate	4.05	0.492	234.27	619.49
105	1-butyl-2,3-dimethyl-imidazolium	Toluene-4-sulfonate	4.03	0.546	246.75	534.49
106	1-butyl-3-methyl-imidazolium	SO_4	6.34	0.745	113.63	3.63E+11
109	1-butyl-3-methyl-imidazolium	2-chlorophenol	3.02	0.499	210.80	164.13
110	1-butyl-3-methyl-imidazolium	3-chlorophenol	2.99	0.494	211.28	127.79
111	1-butyl-3-methyl-imidazolium	4-chlorophenol	3.00	0.495	233.98	134.66
112	1-butyl-3-methyl-imidazolium	Benzoicacid	3.08	0.521	228.00	532.22
113	1-butyl-3-methyl-imidazolium	BF_4	2.18	0.424	247.06	165.99
114	1-butyl-3-methyl-imidazolium	Bis((trifluoromethyl)sulfonyl)imide	3.42	0.359	253.65	545.48
115	1-butyl-3-methyl-imidazolium	Butylsulfate	2.92	0.439	214.86	390.79
116	1-butyl-3-methyl-imidazolium	Ethylsulfate	2.73	0.455	208.11	224.45
117	1-butyl-3-methyl-imidazolium	NO_2	2.94	0.7	165.54	60.89
118	1-butyl-3-methyl-imidazolium	Octylsulfate	3.38	0.426	223.90	590.81
120	1-butyl-3-methyl-imidazolium	Toluene-4-sulfonate	3.21	0.454	233.06	959.69
121	1-ethyl-2,3-dimethyl-imidazolium	SO_4	14.14	1.796	129.09	2.21E+11
124	1-ethyl-2,3-dimethyl-imidazolium	2-chlorophenol	3.42	0.595	218.26	102.21
125	1-ethyl-2,3-dimethyl-imidazolium	3-chlorophenol	3.34	0.582	218.77	79.59
126	1-ethyl-2,3-dimethyl-imidazolium	4-chlorophenol	3.39	0.591	245.82	83.85
127	1-ethyl-2,3-dimethyl-imidazolium	Benzoicacid	3.87	0.692	238.98	331.68
128	1-ethyl-2,3-dimethyl-imidazolium	BF_4	2.84	0.59	270.11	100.67
129	1-ethyl-2,3-dimethyl-imidazolium	Bis((trifluoromethyl)sulfonyl)imide	3.45	0.375	267.28	517.51
130	1-ethyl-2,3-dimethyl-imidazolium	Butylsulfate	3.43	0.543	221.11	245.13
131	1-ethyl-2,3-dimethyl-imidazolium	Ethylsulfate	3.51	0.617	215.04	139.08
132	1-ethyl-2,3-dimethyl-imidazolium	NO_2	5.50	1.413	169.65	36.29
133	1-ethyl-2,3-dimethyl-imidazolium	Octylsulfate	3.74	0.493	228.96	562.84
135	1-ethyl-2,3-dimethyl-imidazolium	Toluene-4-sulfonate	3.88	0.576	242.89	604.41
136	1-ethyl-3-methyl-imidazolium	SO_4	11.63	1.607	119.06	2.15E+11
139	1-ethyl-3-methyl-imidazolium	2-chlorophenol	2.66	0.491	204.33	102.37
140	1-ethyl-3-methyl-imidazolium	3-chlorophenol	2.62	0.483	204.83	109.72
141	1-ethyl-3-methyl-imidazolium	4-chlorophenol	2.66	0.491	230.12	103.97
142	1-ethyl-3-methyl-imidazolium	Benzoicacid	2.99	0.567	223.44	332.43
144	1-ethyl-3-methyl-imidazolium	Bis((trifluoromethyl)sulfonyl)imide	2.89	0.325	252.63	490.14
145	1-ethyl-3-methyl-imidazolium	Butylsulfate	2.64	0.44	208.82	247.49
146	1-ethyl-3-methyl-imidazolium	Ethylsulfate	2.59	0.482	201.98	138.50
147	1-ethyl-3-methyl-imidazolium	NO_2	4.03	1.128	155.56	34.59
148	1-ethyl-3-methyl-imidazolium	Octylsulfate	3.08	0.423	218.03	535.46
150	1-ethyl-3-methyl-imidazolium	Toluene-4-sulfonate	3.00	0.468	228.29	613.00

151	1-hexyl-3-methyl-imidazolium	SO_4	5.04	0.515	109.05	5.92E+11
154	1-hexyl-3-methyl-imidazolium	2-chlorophenol	3.30	0.493	216.18	257.27
155	1-hexyl-3-methyl-imidazolium	3-chlorophenol	3.28	0.489	216.63	200.26
156	1-hexyl-3-methyl-imidazolium	4-chlorophenol	3.27	0.488	237.24	211.10
157	1-hexyl-3-methyl-imidazolium	Benzoicacid	3.21	0.491	231.86	833.23
158	1-hexyl-3-methyl-imidazolium	BF_4	2.55	0.442	246.58	271.91
159	1-hexyl-3-methyl-imidazolium	Bis((trifluoromethyl)sulfonyl)imide	3.81	0.375	254.84	601.29
160	1-hexyl-3-methyl-imidazolium	Butylsulfate	3.15	0.433	219.80	540.44
161	1-hexyl-3-methyl-imidazolium	Ethylsulfate	2.93	0.441	213.20	354.76
162	1-hexyl-3-methyl-imidazolium	NO_2	2.79	0.575	173.78	102.65
163	1-hexyl-3-methyl-imidazolium	Octylsulfate	3.60	0.421	228.66	646.62
165	1-hexyl-3-methyl-imidazolium	Toluene-4-sulfonate	3.39	0.441	236.98	561.62
166	1-pentyl-3-methyl-imidazolium	SO_4	5.44	0.595	111.27	4.68E+11
169	1-pentyl-3-methyl-imidazolium	2-chlorophenol	3.17	0.496	214.01	207.33
170	1-pentyl-3-methyl-imidazolium	3-chlorophenol	3.14	0.492	214.48	161.41
171	1-pentyl-3-methyl-imidazolium	4-chlorophenol	3.14	0.491	236.12	170.12
172	1-pentyl-3-methyl-imidazolium	Benzoicacid	3.14	0.503	230.47	671.87
173	1-pentyl-3-methyl-imidazolium	BF_4	2.36	0.433	247.32	214.63
174	1-pentyl-3-methyl-imidazolium	Bis((trifluoromethyl)sulfonyl)imide	3.63	0.369	254.61	573.44
175	1-pentyl-3-methyl-imidazolium	Butylsulfate	3.04	0.436	217.76	512.59
176	1-pentyl-3-methyl-imidazolium	Ethylsulfate	2.83	0.447	211.12	284.78
177	1-pentyl-3-methyl-imidazolium	NO_2	2.80	0.619	170.24	79.94
178	1-pentyl-3-methyl-imidazolium	Octylsulfate	3.49	0.424	226.66	618.77
180	1-pentyl-3-methyl-imidazolium	Toluene-4-sulfonate	3.30	0.447	235.52	1200.28
181	4-methyl-n-butylpyridinium	SO_4	6.33	0.703	119.88	3.49E+11
184	4-methyl-n-butylpyridinium	2-chlorophenol	3.42	0.542	218.10	155.25
185	4-methyl-n-butylpyridinium	3-chlorophenol	3.37	0.534	218.56	120.86
186	4-methyl-n-butylpyridinium	4-chlorophenol	3.37	0.534	242.06	127.38
187	4-methyl-n-butylpyridinium	Benzoicacid	3.47	0.563	236.22	503.16
188	4-methyl-n-butylpyridinium	BF_4	2.77	0.514	256.99	160.01
189	4-methyl-n-butylpyridinium	Bis((trifluoromethyl)sulfonyl)imide	3.82	0.39	261.09	567.88
190	4-methyl-n-butylpyridinium	Butylsulfate	3.41	0.494	221.11	507.03
191	4-methyl-n-butylpyridinium	Ethylsulfate	3.25	0.52	214.66	213.06
192	4-methyl-n-butylpyridinium	NO_2	3.38	0.759	172.11	59.42
193	4-methyl-n-butylpyridinium	Octylsulfate	3.81	0.467	229.59	613.21
195	4-methyl-n-butylpyridinium	Toluene-4-sulfonate	3.69	0.506	240.76	900.47
196	Aniline	SO_4	0.49	0.076	139.64	1.59E+12
199	Aniline	2-chlorophenol	1.29	0.256	202.42	787.41
200	Aniline	3-chlorophenol	1.38	0.273	202.33	613.27
201	Aniline	4-chlorophenol	1.34	0.266	232.19	645.82
202	Aniline	Benzoicacid	0.98	0.2	228.58	2560.20
203	Aniline	BF_4	0.56	0.135	270.82	718.82
204	Aniline	Bis((trifluoromethyl)sulfonyl)imide	1.79	0.21	266.27	455.18
205	Aniline	Butylsulfate	1.05	0.186	209.77	1927.48
206	Aniline	Ethylsulfate	0.69	0.138	203.72	1056.17
207	Aniline	NO_2	0.25	0.078	152.78	246.49
208	Aniline	Octylsulfate	1.68	0.244	218.22	500.51
210	Aniline	Toluene-4-sulfonate	1.10	0.183	233.27	4807.36
211	n-butyl-isoquinolinium	SO_4	5.85	0.549	132.06	4.33E+11
214	n-butyl-isoquinolinium	2-chlorophenol	3.61	0.506	221.37	186.61
215	n-butyl-isoquinolinium	3-chlorophenol	3.57	0.501	221.79	145.26
216	n-butyl-isoquinolinium	4-chlorophenol	3.56	0.499	245.62	153.13
217	n-butyl-isoquinolinium	Benzoicacid	3.55	0.508	240.17	604.26
218	n-butyl-isoquinolinium	BF_4	2.92	0.471	259.67	198.87
219	n-butyl-isoquinolinium	Bis((trifluoromethyl)sulfonyl)imide	4.10	0.387	266.28	613.20
220	n-butyl-isoquinolinium	Butylsulfate	3.53	0.458	224.09	552.35
221	n-butyl-isoquinolinium	Ethylsulfate	3.33	0.47	217.40	257.73
222	n-butyl-isoquinolinium	NO_2	3.26	0.618	173.29	75.48
223	n-butyl-isoquinolinium	Octylsulfate	3.96	0.441	232.82	658.53
225	n-butyl-isoquinolinium	Toluene-4-sulfonate	3.77	0.464	245.02	573.53
226	Pyridine	SO_4	11.33	1.946	124.78	2.34E+11
229	Pyridine	2-chlorophenol	1.18	0.25	184.79	120.87
230	Pyridine	3-chlorophenol	1.22	0.258	185.26	101.90
231	Pyridine	4-chlorophenol	1.24	0.262	212.53	108.20
232	Pyridine	Benzoicacid	1.29	0.283	205.75	393.47
233	Pyridine	BF_4	0.27	0.071	240.79	105.55
234	Pyridine	Bis((trifluoromethyl)sulfonyl)imide	1.66	0.202	243.08	428.13
235	Pyridine	Butylsulfate	1.11	0.209	192.27	299.44
236	Pyridine	Ethylsulfate	0.83	0.178	184.52	160.79
237	Pyridine	NO_2	1.28	0.445	130.53	35.10
238	Pyridine	Octylsulfate	1.75	0.266	203.22	473.46
240	Pyridine	Toluene-4-sulfonate	1.30	0.228	211.81	751.81

Table S8. COSMO-RS predicted liquid-liquid equilibria screened with melting Point (T<298.15K)

Combination No	Cation	Anion	Coefficient (gsolute/g solute)	Selectivity (gsolute/g carrier)	Solvent Loss (g_{ll})	Melting Point (K)	Viscosity (cP)
31	Pyrrolidine	SO_4	322417	582.30	0.015	124.6	3.87E+11
34	Pyrrolidine	2-chlorophenol	5756	401.83	0.198	184.3	200.2
35	Pyrrolidine	3-chlorophenol	5788	1.81	0.190	185.0	155.9
36	Pyrrolidine	4-chlorophenol	5979	2.29	0.153	212.4	164.1
37	Pyrrolidine	Benzoicacid	6702	3.53	0.088	203.9	651.6
38	Pyrrolidine	BF_4	5417	1.41	0.259	229.7	174.7
41	Pyrrolidine	Ethylsulfate	5427	1.20	0.358	185.6	266.2
42	Pyrrolidine	NO_2	7218	113.50	0.036	133.3	118.12
106	1-butyl-3-methyl-imidazolium	SO_4	317708	573.79	0.392	113.6	3.63E+11
112	1-butyl-3-methyl-imidazolium	Benzoicacid	1993	3.60	0.465	228.0	532.2
117	1-butyl-3-methyl-imidazolium	NO_2	2509	4.53	0.413	165.5	60.9
121	1-ethyl-2,3-dimethyl-imidazolium	SO_4	317671	573.72	0.393	129.1	2.21E+11
127	1-ethyl-2,3-dimethyl-imidazolium	Benzoicacid	1956	3.53	0.467	239.0	331.7
132	1-ethyl-2,3-dimethyl-imidazolium	NO_2	2472	4.47	0.414	169.7	36.3
136	1-ethyl-3-methyl-imidazolium	SO_4	317781	573.92	0.260	119.1	2.15E+11
139	1-ethyl-3-methyl-imidazolium	2-chlorophenol	1119	2.02	0.444	204.3	102.4
140	1-ethyl-3-methyl-imidazolium	3-chlorophenol	1152	2.08	0.435	204.8	109.72
141	1-ethyl-3-methyl-imidazolium	4-chlorophenol	1343	2.42	0.399	230.1	103.97
142	1-ethyl-3-methyl-imidazolium	Benzoicacid	2066	3.73	0.334	223.4	332.4
147	1-ethyl-3-methyl-imidazolium	NO_2	2582	4.66	0.281	155.6	34.6
166	1-pentyl-3-methyl-imidazolium	SO_4	317682	573.74	0.466	111.3	4.68E+11
177	1-pentyl-3-methyl-imidazolium	NO_2	2483	4.48	0.487	170.2	79.9
181	4-methyl-n-butylpyridinium	SO_4	317655	573.70	0.496	119.9	3.49E+11
196	Aniline	SO_4	378043	682.76	0.002	139.6	1.59E+12
199	Aniline	2-chlorophenol	61382	110.86	0.186	202.4	787.4
200	Aniline	3-chlorophenol	61414	110.92	0.177	202.3	613.3
201	Aniline	4-chlorophenol	61605	111.26	0.141	232.2	645.8
202	Aniline	Benzoicacid	62328	112.57	0.075	228.6	2560.2
203	Aniline	BF_4	61042	110.24	0.247	270.8	718.8
206	Aniline	Ethylsulfate	61053	110.26	0.345	203.7	1056.2
207	Aniline	NO_2	62844	113.50	0.023	152.8	246.5
210	Aniline	Toluene-4-sulfonate	61050	110.26	0.475	233.3	4807.4
226	Pyridine	SO_4	319831	577.63	0.033	124.8	2.34E+11
229	Pyridine	2-chlorophenol	3170	5.72	0.216	184.8	120.9
230	Pyridine	3-chlorophenol	3202	5.78	0.208	185.3	94.2
231	Pyridine	4-chlorophenol	3393	6.13	0.171	212.5	99.1
232	Pyridine	Benzoicacid	4116	7.43	0.106	205.8	393.5
233	Pyridine	BF_4	2831	5.11	0.277	240.8	105.6
236	Pyridine	Ethylsulfate	2841	5.13	0.376	184.5	160.8
237	Pyridine	NO_2	4632	8.37	0.054	130.5	35.10

Table S9. COSMO-RS predicted gas capacity screened with Viscosity (< 100cP)

Combination No	Cation	Anion	Gas Capacity (mol_{CO2}/mol_{IL})	Gas Capacity (gCO2/g IL)	Melting Point (K)	Viscosity (cP)
102	1-butyl-2,3-dimethyl-imidazolium	NO_2	4.07	0.898	178.77	60.40
117	1-butyl-3-methyl-imidazolium	NO_2	2.94	0.7	165.54	60.89
125	1-ethyl-2,3-dimethyl-imidazolium	3-chlorophenol	3.34	0.582	218.77	79.59
126	1-ethyl-2,3-dimethyl-imidazolium	4-chlorophenol	3.39	0.591	245.82	83.85
132	1-ethyl-2,3-dimethyl-imidazolium	NO_2	5.50	1.413	169.65	36.29
147	1-ethyl-3-methyl-imidazolium	NO_2	4.03	1.128	155.56	34.59
177	1-pentyl-3-methyl-imidazolium	NO_2	2.80	0.619	170.24	79.94
192	4-methyl-n-butylpyridinium	NO_2	3.38	0.759	172.11	59.42
222	n-butyl-isoquinolinium	NO_2	3.26	0.618	173.29	75.48
230	Pyridine	3-chlorophenol	1.22	0.258	185.26	94.2
231	Pyridine	4-chlorophenol	1.24	0.262	212.53	99.1

Table S10. COSMO-RS predicted liquid-liquid equilibria screened with viscosity (<100cP)

Combination No	Cation	Anion	Coefficient (gsolute/g solute)	Selectivity (gsolute/g carrier)	Solvent Loss (g_{IL})	Melting Point (K)	Viscosity (cP)
42	Pyrrolidine	NO_2	7218	113.50	0.036	133.3	58.12
117	1-butyl-3-methyl-imidazolium	NO_2	2509	4.53	0.413	165.5	60.9
132	1-ethyl-2,3-dimethyl-imidazolium	NO_2	2472	4.47	0.414	169.7	36.3
140	1-ethyl-3-methyl-imidazolium	3-chlorophenol	1152	2.08	0.435	204.8	79.7
141	1-ethyl-3-methyl-imidazolium	4-chlorophenol	1343	2.42	0.399	230.1	84.0
147	1-ethyl-3-methyl-imidazolium	NO_2	2582	4.66	0.281	155.6	34.6
177	1-pentyl-3-methyl-imidazolium	NO_2	2483	4.48	0.487	170.2	79.9
230	Pyridine	3-chlorophenol	3202	5.78	0.208	185.3	94.2
231	Pyridine	4-chlorophenol	3393	6.13	0.171	212.5	99.1
237	Pyridine	NO_2	4632	8.37	0.054	130.5	35.10

Table S11. Separation performance of the mixture (solute + ILs) with operating conditions

Components	Feed (mol frac)	Liquid (mol frac)	Vapor (mol frac)
	Mixture 1 at 0.33bar and 150^{o}C		
Methanol	0.24	6.50E-04	0.28
Formic acid	0.17	1.10E-03	0.19
Water	0.43	1.80E-04	0.5
$BMIMNO_2$	0.17	0.99	0.02
	Mixture 2 at 0.11bar and 150^{o}C		
Methanol	0.24	4.50E-04	0.29
Formic acid	0.17	8.20E-04	0.19
Water	0.43	9.00E-05	0.51
$PMIMNO_2$	0.16	0.99	3.10E-03
	Mixture 3 at 0.11bar and 150^{o}C		
Methanol	0.23	4.90E-04	0.28
Formic acid	0.16	9.40E-04	0.19
Water	0.41	1.00E-04	0.49
$EMIMNO_2$	0.19	0.99	0.03
	Mixture 4 at 0.11bar and 150^{o}C		
Methanol	0.24	2.90E-04	0.29
Formic acid	0.16	5.10E-04	0.2
Water	0.42	6.00E-05	0.51
$EDMIMNO_2$	0.18	0.99	1.00E-05
	Mixture 5 at 0.11bar and 150^{o}C (Benchmark)		
Methanol	0.19	0.02	0.19
Formic acid	0.13	0.33	0.13
Water	0.34	0.06	0.34
Dimethylformamide	0.34	0.59	0.34

Table S12. ILs pre-selected by the three thermodynamic criteria from mass-based LLE calculated at 298.15 K and 1 bar

Combination No	Cation	Anion	Distribution Coefficient	Selectivity	Solvent Loss(gIL)
42	pyrrolidine	NO_2^-	7218	114	0.04
117	1-butyl-3-methyl-imidazolium	NO_2^-	2509	4.53	0.41
132	1-ethyl-2,3-dimethyl-imidazolium	NO_2^-	2472	4.47	0.41
140	1-ethyl-3-methyl-imidazolium	3-chlorophenol	1152	2.08	0.44
141	1-ethyl-3-methyl-imidazolium	4-chlorophenol	1343	2.42	0.4
147	1-ethyl-3-methyl-imidazolium	NO_2^-	2582	4.66	0.28
177	1-pentyl-3-methyl-imidazolium	NO_2^-	2483	4.48	0.49
230	pyridine	3-chlorophenol	3202	5.78	0.21
231	pyridine	4-chlorophenol	3393	6.13	0.17
237	pyridine	NO_2^-	4632.18	8.37	0.05
	Dimethylformamide		1.007	1	0.5

Table S13. ILs pre-selected by the CO2 capacity at 298.15K and 1bar

Combination Number	Cation	Anion	Gas Capacity (mol_{CO2}/mol_{IL})	Gas Capacity (g_{CO2}/g_{IL})
102	1-butyl-2,3-dimethyl-imidazolium	NO_2	4.07	0.898
117	1-butyl-3-methyl-imidazolium	NO_2	2.94	0.7
125	1-ethyl-2,3-dimethyl-imidazolium	3-chlorophenol	3.34	0.582
126	1-ethyl-2,3-dimethyl-imidazolium	4-chlorophenol	3.39	0.591
132	1-ethyl-2,3-dimethyl-imidazolium	NO_2	5.50	1.413
147	1-ethyl-3-methyl-imidazolium	NO_2	4.03	1.128
177	1-pentyl-3-methyl-imidazolium	NO_2	2.80	0.619
192	4-methyl-n-butylpyridinium	NO_2	3.38	0.759
222	n-butyl-isoquinolinium	NO_2	3.26	0.618
230	Pyridine	3-chlorophenol	1.22	0.258
231	Pyridine	4-chlorophenol	1.24	0.262